Development and Application of Chemically Grafted Polymer/Quantum Dot Hybrids

Dissertation

zur Erlangung des Grades “Doktor der Naturwissenschaften”
im Promotionsfach Chemie

am Fachbereich Chemie, Pharmazie und Geowissenschaften
an der Johannes Gutenberg-Universität Mainz

vorgelegt von

Ana Fokina

geboren in Kaliningrad

Mainz 2015

Die vorliegende Dissertation wurde, unter der Betreuung von [redacted], in der Zeit von November 2012 bis Dezember 2015 am Institut für Organische Chemie der Johannes Gutenberg-Universität Mainz und an der Seoul National University durchgeführt. Diese Version wurde am 10.02.2015 modifiziert.

Dekan: Prof. [redacted]

1. Berichterstatter: Prof. [redacted]

2. Berichterstatter: Prof. [redacted]

Tag der mündlichen Prüfung: 28.01.2016

Abstract

Chemical grafting of polymer chains to quantum dots (QDs) leads to the fabrication of polymer/QD hybrids. Due to their combined properties hybrids are appealing systems for applications in various fields, e.g. electronic devices and cellular imaging. This dissertation is focused on two aspects: the development and applications of semiconducting/QD polymer hybrids in lighting applications and the development of new multidentate anchor systems.

Good color purity, ease of color tunability, simple fabrication process and applicability in flexible and transparent displays led to the increased interest in quantum dot light emitting diodes (QLEDs). In this work, semiconducting polymer/QD hybrids were investigated as the active layer in QLEDs. The factors affecting the performance of the hybrid devices were deduced and optimized. To study the correlation between device performance and the HOMO level of the polymer used three carbazole-based side-chain conjugated polymers with different electrochemical properties were developed. A low HOMO level proved to be a requirement for efficient hole injection into QDs and thus the fabrication of devices with good performances. Furthermore, to investigate the influence of active layer morphology on device performance hybrid QLEDs were compared to devices with physically mixed active layers. It was discovered that the homogeneous distribution of the QDs within the semiconducting polymer is essential for the fabrication of the devices with improved charge injection balance and suppressed QD photoluminescence quenching. Additionally, QD to polymer ratios were varied to obtain the ratio which led to the optimized electronic properties and thus to the device with the best performance.

A requirement for the fabrication of stable QD/polymer hybrids is the strong coordination of polymer chains (ligands) to QD surfaces. The presence of multiple anchor groups is generally necessary to facilitate strong binding between the polymers and the QD surfaces. In this work, bidentate and tridentate lipoic acid-based anchor compounds which allow precise control of the quantity of the incorporated anchor groups were developed. The presence of amine and azide groups enabled the efficient introduction of anchor compounds to semiconducting and hydrophilic polymers using reactive ester and azide-alkyne chemistries. Finally, the successful synthesis of water-soluble QDs verified the anchoring ability of the new polymeric ligands.

моим родителям

Table of Content

1 Introduction 1

1.1 Polymer/QD Hybrids 1

1.2 Quantum Dots (QDs) 1

1.3 Polymers 3

1.3.1 Semiconducting Polymers 3

1.3.2 Polysarcosine 7

1.4 Ligand Exchange 8

1.5 Quantum Dot-Based Light Emitting Diodes (QLEDs) 10

1.5.1 QLED Operating Mechanisms 11

1.5.2 Optimization of the Charge Carrier Injection Balance in QLEDs 13

1.5.3 QD Photoluminescence Quenching in QLEDs 14

1.5.4 Hybrid Semiconducting Polymer/QD Light Emitting Diodes 14

1.6 Hybrid Organic Semiconducting Polymer/Inorganic Semiconducting Nanocrystals Solar Cells 15

1.7 Hydrophilic QD Composites for Use in Bio-Applications 17

1.8 Reversible Addition Fragmentation Chain Transfer (RAFT) Polymerization 18

1.9 Reactive Esters 20

1.10 Azide-Alkyne Cycloaddition 21

2 Aims and Objectives 24

3 Results and Discussion 26

3.1 Hybrid QLEDs Based on Hybrid Semiconducting Polymer/QD Active Layers 26

3.1.1 Synthesis of Semiconducting Monomers with Carbazole Cores 28

3.1.2 Side-Chain Conjugated Polymers for the Use in the Active Layers of Hybrid QLEDs 39

3.1.3 Polymer HOMO Level Influence on the Performance of Hybrid QLEDs 48

3.1.4 The Role of the Active Layer Morphology in the Enhanced Performance of Hybrid QLEDs 57

3.1.5 Conclusion 76

3.2 Polymers with Lipoic Acid-Based Multidentate Anchor Groups 77

3.2.1 Synthesis of Lipoic Acid-Based Multidentate Anchor Compounds 79

3.2.2 Multidentate Electroactive Polymeric Ligands with Lipoic Acid-Based Anchor Groups 81

3.2.3 Multidentate P3HT-Based Ligands with Lipoic Acid-Based Anchor Groups 84

3.2.4 Multidentate Polysarcosine-Based Ligands for Water-Soluble Quantum Dots 88

3.2.5 Water Soluble QDs with PSar-Based Polymeric Ligands 93

3.2.6 Conclusion 95

4 Summary 97

5 Publications 103

6 Experimental Part 105

6.1 Materials and Methods 105

6.2 Synthesis of the Semiconducting Monomers 106

6.3 Synthesis of the Side-Chain Conjugated Polymers 113

6.4 Synthesis and Characterization of Polymer/Quantum Dot Systems 117

6.5 Device Fabrication and Characterization 119

6.6 Synthesis of Lipoic Acid-Based Anchor Compounds 119

6.7 Synthesis of PCarb-based Multidentate Polymeric Ligands. 124

6.8 Synthesis of P3HT-Based Multidentate Polymeric Ligands. 124

6.9 Synthesis of Polysarcosine-Based Multidentate Polymeric Ligands 125

6.10 Synthesis of Water Soluble QDs with PSar-Based Ligands 125

7 References 127

8 List of Abbreviations 137

9 Appendix. ^{1}H NMR Spectra 139

1 Introduction

1.1 Polymer/QD Hybrids

Polymers have become a hardly replaceable part of people's life around the globe. Food, personal care articles, clothes, electronics, medicine, furniture all contain synthetically or naturally produced macromolecules. Quantum dots (QDs) which are less well known for the public, however, already gained wide scientific acknowledgement in the fields of optoelectronics and biological imaging. The combination of organic (polymer) and inorganic materials (QDs) opens new horizons as it has the ability to create systems whose properties will surpass that of their constituents. While QDs contribute to the superior optical and electric properties, polymers are accountable for hybrid system solubility and processability. Moreover, depending on the application field and the polymer structure polymers can also contribute with more specific properties, for example, charge conductivity. The word hybrid emphasizes the chemical grafting of the polymers onto the QD surfaces *via* anchor groups. Chemical grafting is necessary to provide a strong and stable connection between the QDs and polymers and identify their combined properties. For applications in electronics QD/semiconducting polymer hybrids are investigated, while for biological applications QD/hydrophilic polymer hybrids are of interest.[1,2]

1.2 Quantum Dots (QDs)

Quantum dots are colloidal semiconductor nanocrystals consisting of hundreds to several thousands of atoms. QDs possess broadband absorptions, easily tunable emissions, particularly narrow emission profiles, high stabilities and high quantum yields (Figure 1.2.1 a).[3] These remarkable qualities have encouraged QD applications as fluorophores in optoelectronics and biological imaging (sections 1.5 and 1.6). Moving from bulk semiconductors to the nanocrystal scale a quantum confinement effect takes place and discrete electron and hole states are created (Figure 1.2.1 b).[4] Upon QD excitation (absorption of a photon with the energy larger than the semiconductor band gap) an exciton (electron and hole pair) is created which later recombines and emits a photon. The energy of the emitted photon is equal to the energy gap between the highest occupied and the lowest unoccupied states. The position of highest occupied and lowest unoccupied states and thus the absorptions and the emissions can be easily tuned by varying the size of the

nanocrystals. Therefore, QDs made from the same chemical species but with different sizes can emit light of various wavelengths (Figure 1.2.1 c).[2]

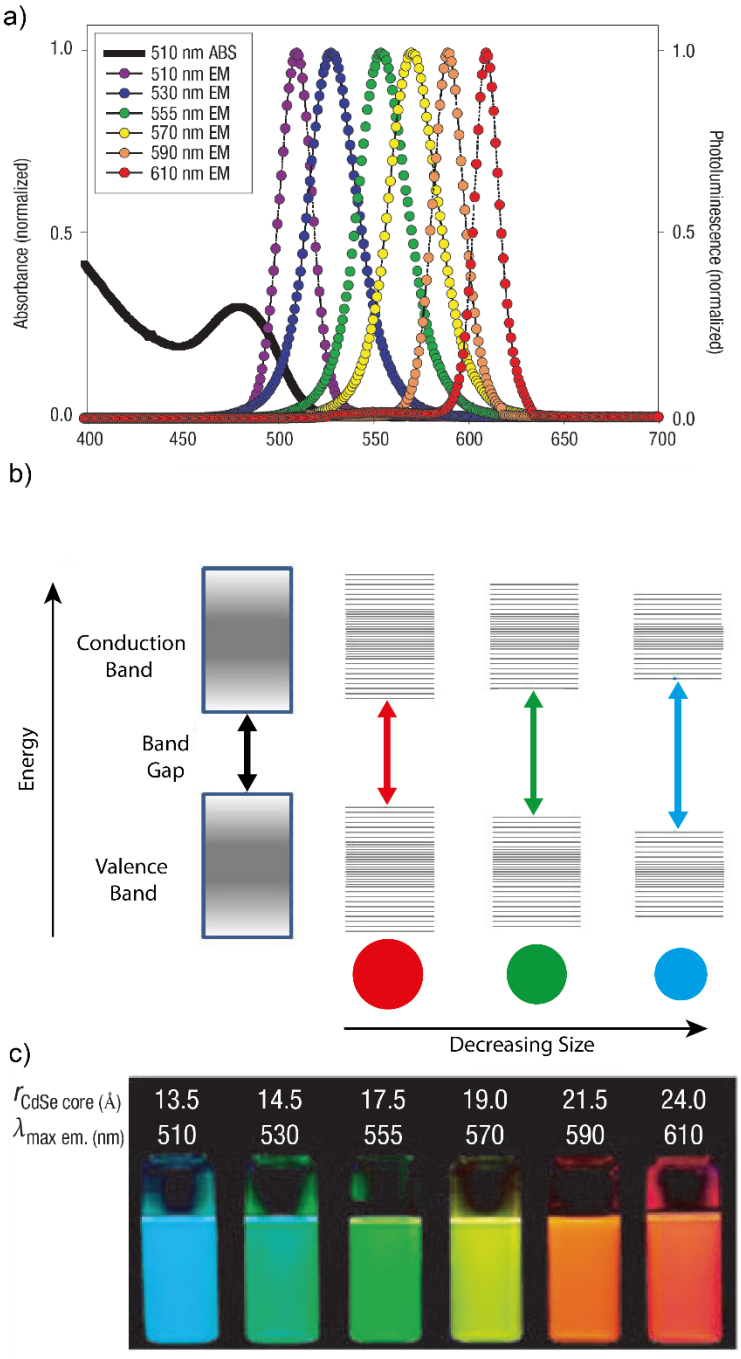

Figure 1.2.1. QD absorption and emission spectra (a), splitting of energy levels in quantum dots due to the quantum confinement effect, semiconductor band gap decreases with increase in size of the quantum dot (b), Size-dependent change of the emission color from the solutions of CdSe QDs. Modified from www.sigmaaldrich.com and Ref. 2 with the permission from Macmillan Publishers Ltd: [Nature Materials], copyright (2005).

For example, the emission color of QDs containing CdSe cores varies from blue for the nanocrystals with a diameter of approximately 2.7 nm to red for the nanocrystals with a diameter of approximately 4.8 nm.[2] Moreover, the use of various semiconducting materials, CdS, CdTe, InP, InS and PbSe, further extends the accessible emission range and allows for additional adjustment of the positions of valence and conducting bands.[5]

High quality, crystalline QDs with narrow core size distribution are produced at high temperatures using metal salt precursors (e. g. CdO, Cd-acetate) and high-temperature solvent/ligand mixtures.[6,7] Furthermore, modern QDs exhibit a core-shell morphology (e.g. CdSe core and ZnS shell).[8,9] The core-shell structure was developed to improve the stability of QDs and to eliminate the non-radiative exciton recombination pathways on the core surface leading to QDs with brighter and more stable luminescence. QDs with CdSe cores and CdZnS shells is an example of type-I heterostructures, where the band edges of the core lie inside the band gap of the outer shell.[10] The exciton recombination in type-I QDs occurs in the QD core, meaning that the absorption and photoluminescence (PL) properties of the QDs are determined largely by the size of core. In type-II QDs the valence and the conduction bands of the outer shell material are lower or higher than that of the core.[11] During excitation of type-II heterostuctures the hole migrates to the material with a valence band with a higher edge energy, while the electron migrates to the material with the lower edge energy conduction band. In this case exciton recombination occurs at the interface between core and shell and thus the PL properties are dependent on both materials. To prevent aggregation of the individual particles QD surfaces are covered with organic ligands.[12] Since the synthesis of QDs typically is performed in nonpolar solvent, the ligands have long aliphatic side chains. One of the most widely used ligands is oleic acid. The acid functionality serves as the anchor and coordinates to the QD surface while the aliphatic chain enables particle solubility. Alongside the acid group, phosphines, phosphine oxides, amines, imidazole, thioles and disulfides functionalities can serve as anchor groups for QDs.

1.3 Polymers

1.3.1 Semiconducting Polymers

The discovery of organic semiconducting materials has enabled the development of organic electronic devices, such as organic photovoltaics (OPVs), organic light emitting diodes (OLEDs) and organic field effect transistors (OFETs).[13–17] Organic electronics exploit the

ability of organic molecules with an extended π-conjugated systems to conduct charge carriers, holes and/or electrons.[18] Organic semiconducting materials can be divided into two major groups, semiconducting small molecules and semiconducting (main chain conjugated) polymers.

Semiconducting polymers were discovered by A. L. Heeger, A. G. MacDiarmid and H. Shirakawa in 1977.[19,20] Carbon atoms and, if applicable, incorporated heteroatoms of the conjugated polymer backbone are sp_2p_x hybridized. p_x orbitals of successive carbon atoms overlap, forming an extended π-conjugated system. This extended π-conjugated system enables electron delocalization along the polymer backbone and provides a pathway for charge carriers. In their undoped state, conjugated polymers are typically semiconductors, thus the name, semiconducting polymers. The essential characteristics of semiconducting polymers are the energies of the highest occupied molecular orbitals (HOMOs) and the lowest unoccupied molecular orbitals (LUMOs) and the charge carrier mobilities. Charge carrier transport in semiconducting polymers is governed by an intramolecular pathway along the π-conjugated system (high charge carrier mobilities) and by an intermolecular hopping along the π-π overlaps of the face-to-face stacked polymer backbones (low charge carrier mobilities).[21,22] While intrachain charge transport is dependent on the chemical composition of the polymer, interchain transport is strongly dependent on the polymer chain orientation in the polymer film. To enable efficient charge transport polymer backbones should be as co-planar as possible, which can be achieved with polymers possessing high level of crystallinity. The position of the HOMO and the LUMO determines the polymers applications, for example polymers with low lying LUMO levels are used as n-type semiconductors (e.g. electron transport materials in LEDs, electron acceptor materials in OPVs), while polymers with relatively high HOMO levels are used as p-type semiconductors (e.g. hole transport materials in LEDs, hole acceptor materials in OPVs). HOMO and LUMO energies are dependent on the chemical structure of the polymer and can be synthetically adjusted to fit the applications needs. Over the years a huge variety of different semiconducting polymers with various optical and electronic properties have been synthesized and tested in optoelectronic devices.[15,23] Relevant examples are shown in Figure 1.3.1. One of the mostly studied semiconducting polymers is poly(3-hexylthiophene) (P3HT). Utilizing the Grignard metatheses (GRIM) polymerization method developed by the McCullough research group P3HT can be synthesized in highly regioregular manner.[24,25] The regioregular P3HT forms highly

crystalline films with high hole carrier mobility up to 0.1 $cm^2V^{-1}s^{-1}$. Due to its remarkable crystallinity, P3HT has been excessively studied in OPVs and OFETs.[26–28] Poly(N-9′-heptadecanyl-2,7-carbazole-alt-5,5-(4′,7′-di-2-thienyl-2′,1′,3′-benzothiadiazole))
PCDTBT is an example of a low band gap polymer, in which an electron deficient unit alternates with an electron rich unit leading to a band gap contraction.[29] Low band gap polymers can absorb more light than P3HT and thus are appealing materials for photovoltaic applications.[30,31]
Poly(2-methoxy-5-(2-ethylhexyloxy)-1,4-phenylenevinylene)) (MEH-PPV) and other poly(1,4-phenylenevinylene)s have been intensively studied as the materials for polymer-based LEDs (PLEDs) due to their notable fluorescence properties.[32,33]

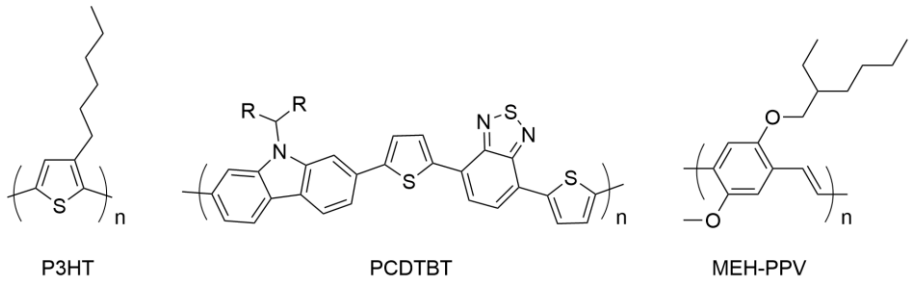

Figure 1.3.1. Main chain conjugated semiconducting polymers P3HT, PCDTBT, MEH-PPV.

Semiconducting polymers, however, exhibit one major drawback, batch-to-batch variation as it is practically impossible to produce exactly the same polymer twice. To overcome this issue small semiconducting molecules have been developed (Figure 1.3.2).[34]

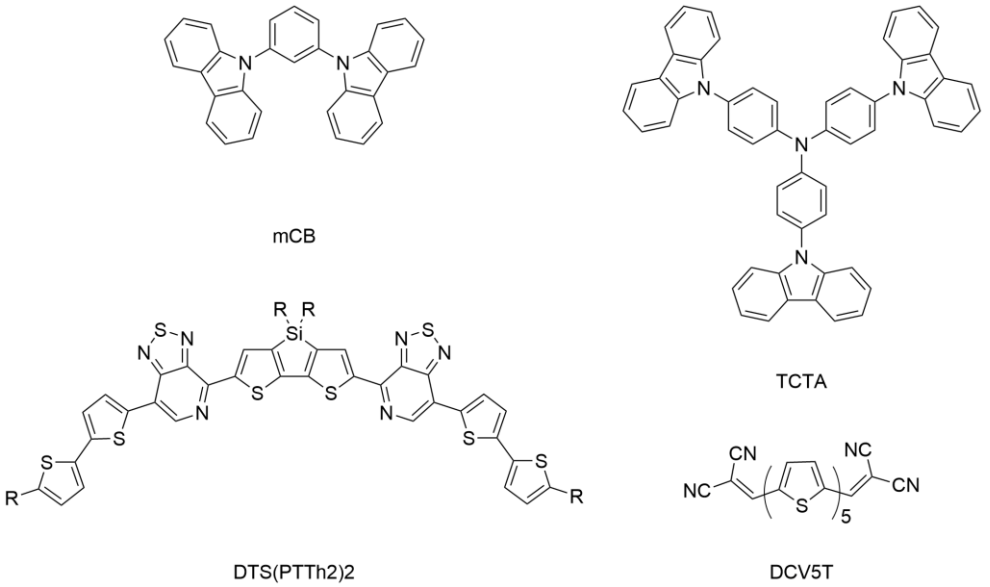

Figure 1.3.2. Semiconducting small molecules mCB, TCTA, DTS(PTTh$_2$)$_2$ and DCV5T.

During the synthesis of such molecules, common purification methods used in organic synthesis are utilized (e.g. column chromatography, sublimation) to obtain the same molecule in a highly reproducible fashion. Various carbazole and triphenyl amine-based molecules (e.g. 1,3-bis(N-carbazolyl)benzene (mCP), tris(4-carbazoyl-9-ylphenyl)amine (TCTA)) are used as hole transport materials in OLEDs,[35] while thiophene-based as well as donor/acceptor structures such as DTS(PTTh$_2$)$_2$* and DCV5T* are used as donor materials in the active layers of OPVs.[36,37]

Once the conjugated small molecules are used as the side chain of a monomer unit (vinyl, methacrylate, styrene, norbornene) side-chain conjugated polymers can be synthesized.[38–45] The most prominent example of a side chain conjugated polymer is poly(9-vinylcarbazole) (PVK) (Figure 1.3.3). PVK is widely used as the hole transport layer in OLEDs. However, carbazole based conjugated systems with unprotected 3 and 6 positions are known to be unstable under oxidative conditions and can be easily dimerized (Scheme 1.3.1).[46,47] Further example of polymers with conjugated side chains are shown in Figure 1.3.3 (**A**-**D**).[48–51]

* The abbreviation was given by the author of the corresponding paper

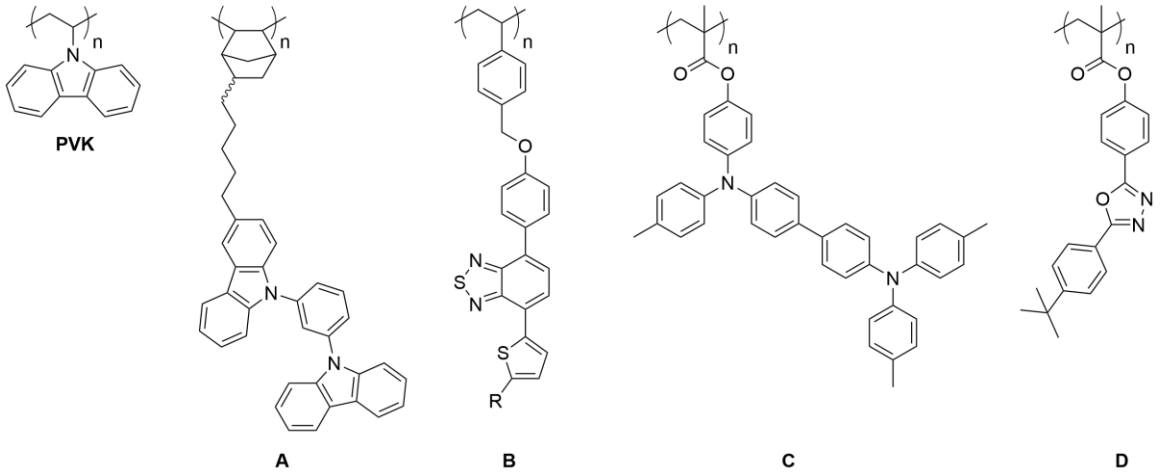

*Figure 1.3.3. Side-chain conjugated polymers **A**-**D** and PVK.*

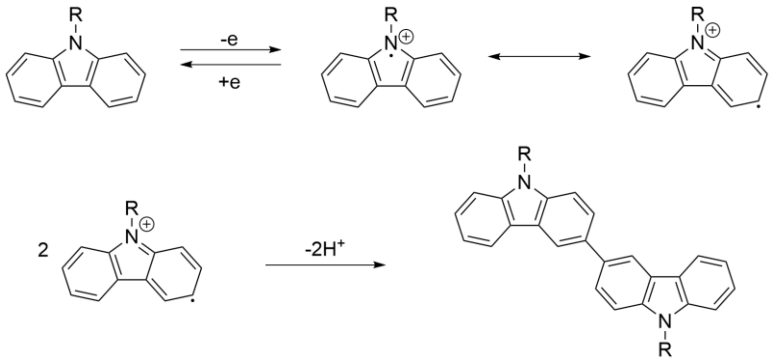

Scheme 1.3.1. Electrochemical oxidation of the carbazole unit.

1.3.2 Polysarcosine

Polysarcosine (poly(N-methyl glycine), PSar) belongs to the polypeptoids class of polymers. The characteristic feature of polypeptoids is attachment of a side chain to the nitrogen atom and not to the α-carbon, as is the case of polypeptides. Polysarcosine possesses stealth-like properties, is hydrophilic, an exclusively hydrogen-bond acceptor without hydrogen-donor properties and it does not possess a net charge. Thus, it is a promising candidate for applications in drug-delivery systems and bio-imaging.[52]

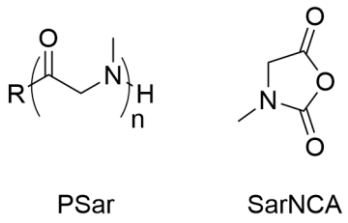

Figure 1.3.4. Structure of polysarcosine (PSar) and N-methyl glycine N-carboxyanhydride (SarNCA).

Polysarcosine with a low molecular weight distribution can be synthesized from N-methyl glycine N-carboxyanhydride (SarNCA) *via* ring opening polymerization. It is soluble in many common organic solvent (e.g. chloroform, DMSO, DMF) and aqueous solutions.[52] *Via* diligent choice of the polymerization initiating amine, various functional groups (R) can be installed in the beginning of each polymer chain and subsequently used in post-polymerization modification reactions.[53,54] A secondary amine group at the end of the polymer chain provides an additional group for further polymer functionalization.

1.4 Ligand Exchange

Depending on the future applications the QD surface must be modified for better adaptation to the surrounding medium. When QDs are used for optoelectronic or biological applications intimate contact between the QDs and the surrounding medium is essential for the development of an effective system.[2] To enable the use of QDs in the active layers of hybrid light emitting diodes or hybrid solar cells, QDs are mixed with semiconducting polymers. In the case of hybrid LEDs, QDs have to be well dispersed in the surrounding polymer matrix to prepare a device with defect-free, uniform luminesce over the entire pixel area.[55] Intimate contact between the semiconducting polymers (hole transport media) and the QDs (electron transport media) is also necessary for efficient exciton separation in hybrid solar cells.[56] However, physical mixing of QDs bearing nonpolar, short, hydrophilic ligands with polymers leads to phase separation and severe QD aggregation. Therefore, chemical grafting techniques have to be applied to produces QDs with polymeric ligands which can be well dispersed in polymer matrices (Figure 1.4.1). Similarly, a chemical grafting approach is necessary to produce water-soluble QDs bearing hydrophilic polymeric ligands for the use in biological applications.

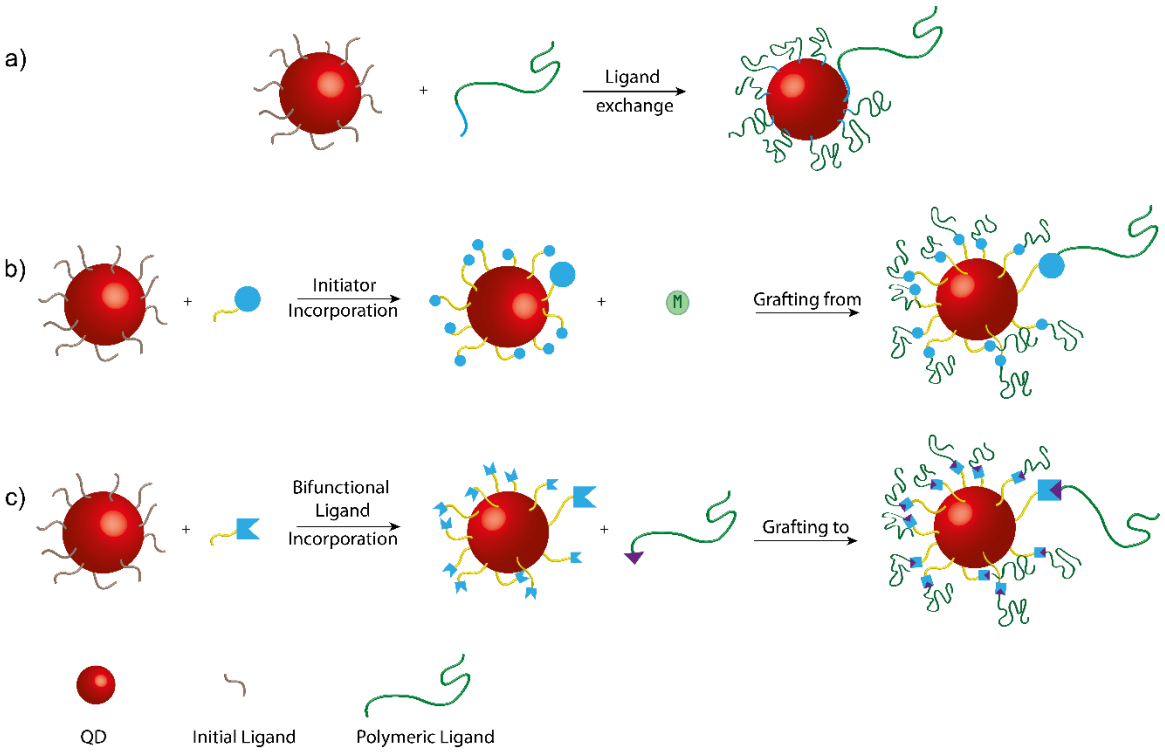

Figure 1.4.1. Schematic illustration of chemical grafting techniques for the synthesis of the polymer/QD hybrids. Ligand exchange (a), grafting from (b) and grafting to(c) approaches.

Ligand exchange procedures enable the easy synthesis of a large variety of polymer/QD hybrids.[57] To synthesize polymer/QD hybrids by the ligand exchange procedure, the initial small molecule ligands are replaced with new polymeric ligands. Polymers participating in the ligand exchange have to possess anchor groups, which are able to coordinate to the QD surfaces. While grafting from and grafting to approaches usually require two modification steps the ligand exchange is executed in one step (Figure 1.4.1). During the "grafting from" process the QD surface is first modified with the polymerization initiator, which subsequently initiates the polymerization. During the "grafting to" approach the QD surface is first modified with bifunctional ligands followed by the introduction of the polymer chains.

The ligand exchange procedure is possible due to the dynamic character of ligand coordination to a QD surface.[58,59] The dynamic equilibrium can be defined by adsorption/desorption processes.[60] The rate of the absorption and desorption processes depends on the binding strength of the ligands. Ligands weakly bound to the QD surface can easily desorb from the surface and provide space for a new ligand. The absorption rate can be increased if the ligands used are present in excess and possess a strong affinity to

the QD surface. When ligands with multiple anchor groups are used, the rate of the ligand desorption decreases significantly due to the chelate effect. If the situation is considered in which ligands of two kinds are present (Equation (1) and Scheme 1.4.1), as is the case of the ligand exchange, the formation of QDs functionalized with new ligands $QD - L_n$ is successful if:

- the binding strength of the new ligand L_n is higher than that of the initial ligand L_i ($k_{a,n}>k_{a,i}$, $k_{d,n}<k_{d,i}$)
- initial ligand is weakly bound to the QD surface

And can be performed more efficiently if

- the new ligand is present in excess (i)
- the free initial ligand is removed from the system (ii)

In the special case when the new ligand is a polymer the steric repulsion effects must to be taken into account. The bound polymeric ligands requires larger space than the small initial ligands and thus can hinder the adsorption of further polymeric ligands.[61,62]

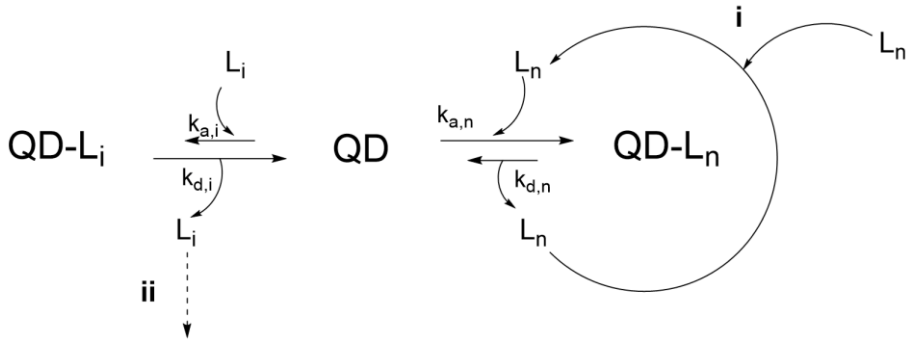

Scheme 1.4.1. Schematic illustration of the ligand exchange procedure.

$$[QD - L_n] = K\frac{[QD-L_i][L_n]}{[L_i]}, K = const \cdot \frac{k_{a,n}\cdot k_{d,i}}{k_{d,n}\cdot k_{a,i}} \quad (1)$$

1.5 Quantum Dot-Based Light Emitting Diodes (QLEDs)

In quantum dot-based light emitting diodes (QLEDs) the electric current is used to excite QDs and generate electroluminescence (EL).[63,64]

The first report of QLEDs was by Colvin *et al.* in 1994.[65] In the early devices QDs played the dual role of light emission and charge (electron) conduction. External quantum efficiencies (EQEs), the ratio between the photons emitted and the charge carriers injected,

of the early QLEDs were very low (0.001-0.01 %) due to the poor quality of the QDs used and the imbalanced charge carrier injection into the QDs.[66] Moreover, the EL spectra combined light emission from the QDs and the neighboring organic charge transport layers negatively affecting the purity of the emitted light. In 2002 Coe *et al.* reported QLEDs where the QD emitting layer was sandwiched between organic hole and electron transport layers resembling the device architecture of organic light emitting diodes (OLEDs).[67] Since 2002 a tremendous amount of work has been performed to improve device performance from EQEs of 0.5 % to 5 %.[68,69] However, the great breakthrough in QLED performance came with the introduction of the device architecture with hybrid charge transport layers (CTL) (organic hole transport layer (HTL) and inorganic electron transport layer (ETL)) by Prof. C. Lee group at the Seoul National University in 2012.[70] In the QLEDs presented the ETL was comprised of ZnO nanoparticle and holes were injected through the small molecule HTL and exhibited EQEs of 7.3 %, 5.8 %, 1.7 % for red, green and blue emitting devices respectively. Further development of the device architecture alongside improvements in the QDs properties lead to devices with the peak EQE of 18 % and luminescence intensities greater than 100,000 cd m^{-2}.[10,71]

1.5.1 QLED Operating Mechanisms

QLED can be separated into two classes, QLEDs with a conventional device configuration and with an inverted configuration (Figure 1.5.1).[70–72] In the conventional device structure (ITO/HTL/active layer/ETL/Al), holes are injected from the indium tin oxide (ITO), which serves as the anode, while electrons are injected from the aluminum (or other metal) cathode. In devices with an inverted structure (ITO/ETL/active layer/ETL/Al), electrons are injected from the ITO, which now serves as the cathode. The metal is evaporated on top of the HTL and serves as the anode.

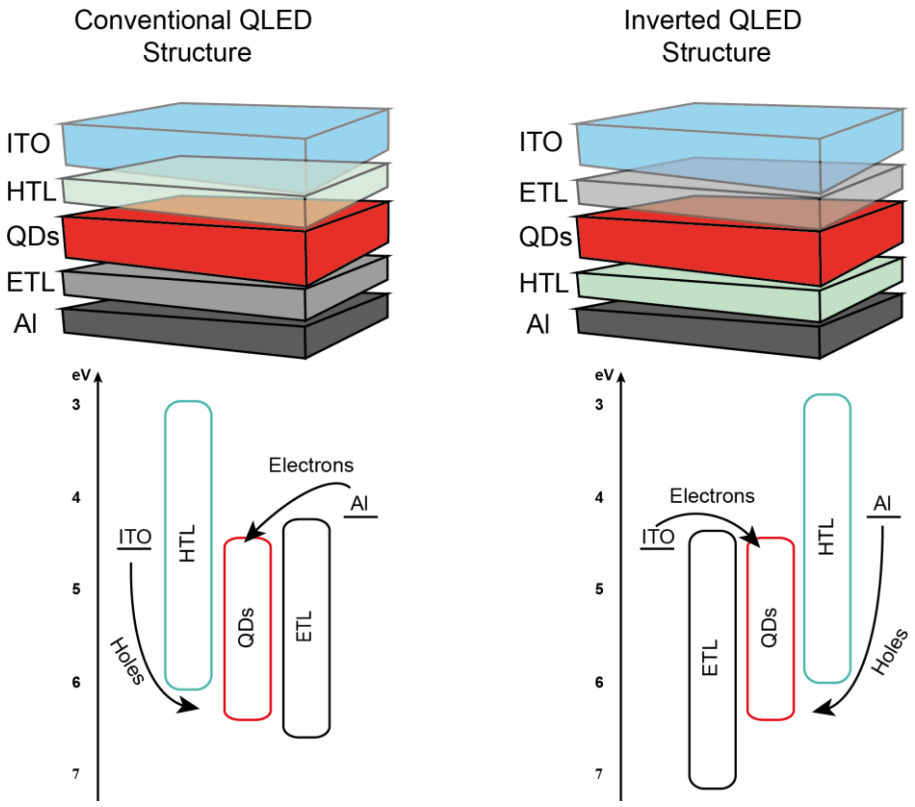

Figure 1.5.1. Schematic images and energy diagrams of QLEDs in conventional and inverted configurations.

In state-of-the-art inverted QLEDs the HTL is composed of organic semiconducting material, while the ETL is made of ZnO nanoparticles. In some cases multiple HTLs are used to enable cascade-like hole transport. Charges travel through the CTLs to the active layer, which is, in the case of QLEDs, composed of QDs, where they recombine leading to photon emission. The EQE of a device describes how efficiently an LED transforms electrons to photons and allows them to escape. EQE can be separated into the injection efficiency, the internal quantum efficiency and the extraction efficiency.[13] The injection efficiency describes the amount of charge carriers which reach the active layer. The internal quantum efficiency is defined by the number of electron-hole recombinations which result in the radiation of a photon. The extraction efficiency is the ratio between photons generated in the active layer and photons which escape the device. There are multiple factors which influence the efficiency. The choice of the compounds for the HTL and the ETL layers significantly influences the injection efficiency, while modifications to the QD structure will result in a change to the internal quantum efficiency.[10,73] The architecture of the device has an influence on all of processes described above, however, the extraction efficiency is especially influenced by the architecture.[74,75]

QDs emit light as the result of electron-hole pair (exciton) recombination. When the light emission is triggered *via* an electric field it is referred to as electroluminescence. There are two primary routes to generate excitons in QDs in operational QLEDs, direct charge injection and energy transfer (Figure 1.5.2).[76–78] During the direct charge injection process, holes and electrons are injected into QDs from the adjacent CTLs forming excitons which recombine *via* emission of photons. During the energy transfer process, the exciton is formed in the neighboring layer and subsequently transferred to the QD *via* Förster resonant energy transfer. To determin the relative contribution of each process is challenging and varies depending on the device architecture.[79,80]

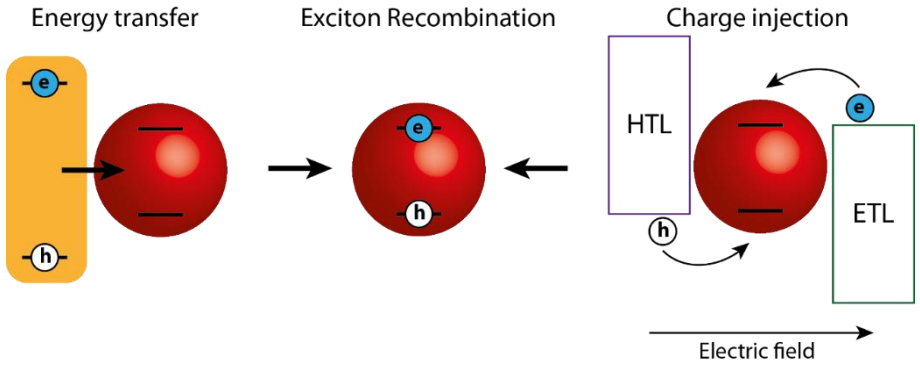

Figure 1.5.2. Quantum dot excitation mechanisms.

1.5.2 Optimization of the Charge Carrier Injection Balance in QLEDs

Recently the optimization of the charge carrier injection balance in the active layer has been intensively pursued.[73,81–84] Facilitated hole injection as well as suppressed electron injection were shown to lead to enhanced device performance. As commonly used QDs possess low lying valence bands, the hole injection from commercially available hole transport materials (HTMs) is rather challenging due to the large energy offset between the HOMO of HTMs and the valence band of QDs. The comparative study by Kwak *et al.* showed that utilizing HTMs with lower HOMO levels provided a smaller energy barrier for hole injection from HTM into QDs and led to LED devices with improved performance.[73] Additionally, Cho *et al.* showed that a reduced band offset between the QDs and the hole transport layer could be achieved by an increase in the QD valance band energy *via* the crosslinking of the QD layer.[81] The nearly energy barrier free injection of electrons into QDs from the electron transport layer leads to a constant presence of an excess of electrons in the active layer (i.e. electron overcharge problem). An excess of electrons leads to non-emissive exciton recombinations and thus efficiency decay. Bae *et al*. proposed a

new QD structure with a modified shell which provided an energetic barrier between the emissive QD core and the electron transport layer leading to partial elimination of the excess electrons and suppression of non-emissive Auger recombination.[82] Additionally, device architecture modification has proven to be a successful strategy in addressing the problem of electron overcharge. Leck *et al.* were able to suppress the amount of injected electrons by the incorporation of a QD layer between the hole transporting layers.[83] Furthermore, Dai *et al.* showed that the incorporation of an insulating polymer (polymethylmethacrylate) layer between the electron transport layer and the QDs can reduce the quantity of injected electrons thus preventing an excess of electrons.[84]

1.5.3 QD Photoluminescence Quenching in QLEDs

QD films exhibit significantly lower photoluminescence PL lifetimes compared to their corresponding solutions. The observed decrease in the PL lifetimes may be attributed to more efficient energy transfer processes between the QDs due to short distances between the individual QD cores in the films. Enhanced energy transfer leads to the observed decrease in radiative emissions and thus drop in the device efficiency.[10] Additionally, contact between the QDs and the adjacent charge transport layers serves to promote even more significant PL decay.[82,84]

1.5.4 Hybrid Semiconducting Polymer/QD Light Emitting Diodes

In hybrid semiconducting polymer/QD light emitting diodes the active layer consists of two components, semiconducting polymer and QDs. The polymers previously studied as the polymeric components of the hybrid active layers are shown in Figure 1.5.3. Two-component active layers were initially used as a pathway to obtain white LEDs with one emission layer.[85–88] Fluorescent semiconducting polymers have been employed as encapsulating polymers resulting in combined QD and polymer emissions. The emission intensity of each compound can be tuned by either varying the component ratios or controlling the applied bias. If the amount of incorporated QDs is significantly increased, LEDs with pure QD emission can be manufactured.[55,89–92] For the incorporation of a large amount of QDs within a polymer matrix while maintaining a homogeneous distribution of the QDs the physical blending of the two components is usually insufficient and phase separation typically occurs in physically blended films. Therefore, to avoid phase separation polymers chemically grafted to the QD surfaces have to be developed.[92] Ideally the role of the polymer in the QLEDs with pure QD emission should be limited to charge

transport from the adjacent CTLs to the QDs. Analogous to the QD only devices hybrid QLEDs can be prepared using a conventional or an inverted device architecture.

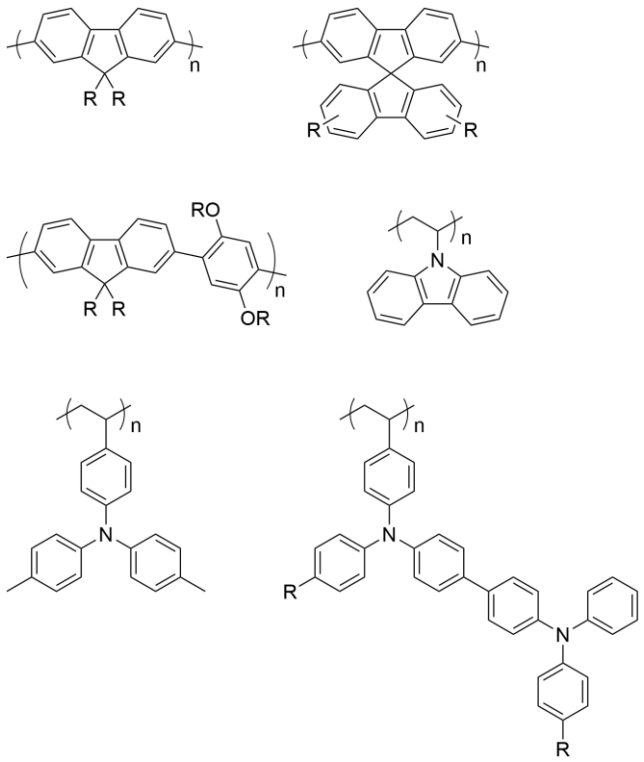

Figure 1.5.3. Polymers used in QLEDs with hybrid active layers.

1.6 Hybrid Organic Semiconducting Polymer/Inorganic Semiconducting Nanocrystals Solar Cells

In hybrid organic /inorganic solar cell the acceptor material is composed of inorganic nanocrystals (eg. CdSe, CdS) and the donor material is made of organic semiconducting polymer or a semiconducting small molecule.[3,56,93] The working principle of a hybrid solar cell is similar to the working principle of an organic bulk heterojunction solar cell (Figure 1.6.1).[13] Upon excitation (photon absorption) an exciton (electron-hole pair) is formed in the active layer (in the acceptor and/or donor material). The formed exciton travels to the donor/acceptor interface where it is separated into an electron and a hole. Holes are transferred to the donor material, while electrons are transferred to the acceptor materials. Following this the charge carriers travel through the respective materials and charge transport layers to the electrodes and an electric current is generated. The EQE of a solar cell is the product of four efficiencies: absorption efficiency, exciton diffusion efficiency, charge separation efficiency and charge collection efficiency.[13]

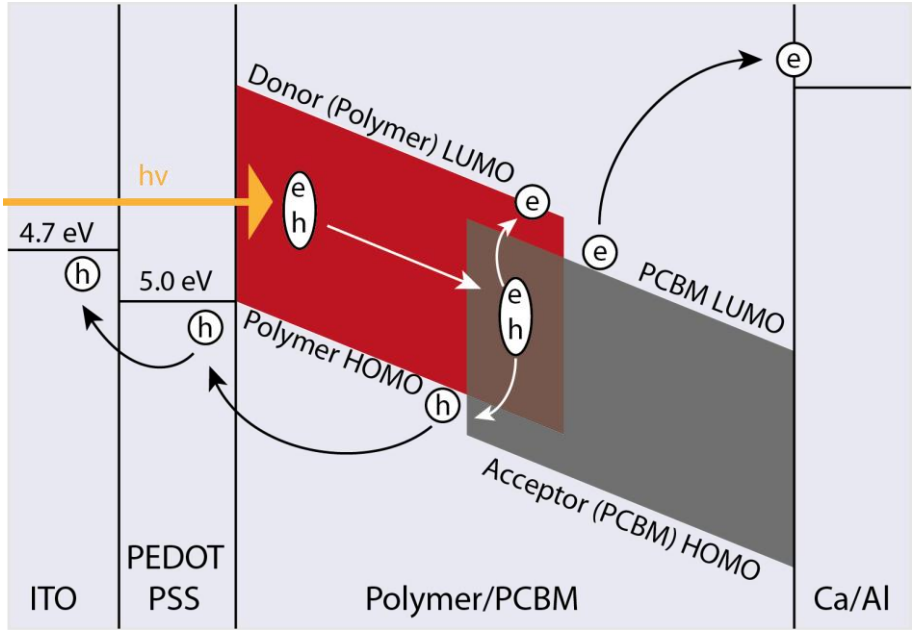

Figure 1.6.1. The operating mechanism of organic solar cell with polymeric donor and PCBM acceptor.[13]

There are several theoretical reasons why the utilization of inorganic acceptor materials should improve the performance of solar cells.[56] First, semiconducting inorganic nanocrystals are good absorbers and can significantly contribute to photon absorption. This is in contrast to the situation in organic solar cells, when the majority of the excitons are formed in the donor material as the commonly used acceptor materials are based on C_{60} molecules which only absorb a small fraction of the sun light emission spectrum.[94,95] The absorption profile of nanocrystals can, furthermore, be easily altered by a change of the nanocrystal size and thus adjusted to compliment the absorption spectrum of the donor material. Second, inorganic materials are environmentally more stable than their organic counterparts. Finally, inorganic nanocrystals exhibit high electron mobility. After additional surface treatment the electron mobility in CdSe/CdS nanocrystals achieves 16 $cm^2V^{-1}S^{-1}$.[96] However, despite the theoretical advantages, the currently reported hybrid devices show efficiencies below the efficiencies of the organic solar cells with C_{60}-based acceptor materials.[56] The complex chemistry of the organic/inorganic interface and the challenging control of the nano morphology of the hybrid active layer contribute to the poor device performance. Conditions for the formation of a locally demixed but macroscopically homogeneous morphology must be obtained.[60] While local phase separation should facilitate the creation of a percolated system and thus enable efficient charge carrier transport to the electrodes, the macroscopically homogeneous distribution of the

nanocrystals in the organic material should create a large interface area for efficient exciton separation. Furthermore, for efficient charge separation, close contact between the nanocrystals and the donor material is required. The morphology of the active layer and the interface interactions can be modified *via* surface modification of the QDs.[90,97–99] For example, the hybrid P3HT/CdSe nanorod solar cell performance was improved once the unfunctionalized P3HT was replaced with an amine-functionalized P3HT.[100] Amine-functionalized P3HT coordinated to the nanorods surface and improved their miscibility with the free polymer. This increased miscibility led to homogeneous nanorod distribution within the polymer matrix and subsequently to more efficient exciton dissociation. Other factors influencing the morphology of the active layers include solvent, annealing temperature, nanocrystal shape (QD, nanorod, tetrapod) and donor/acceptor ratio.[101–106] The efficiency of the hybrid solar cell can furthermore be increased by using low band gap polymers as the donor component and metal oxides as an intermediate electron transport layer.[107–109]

1.7 Hydrophilic QD Composites for Use in Bio-Applications

Hydrophilic composites have been utilized as fluorophores in cellular labelling, *in vivo* and deep tissue imaging.[2,110–112] QDs are responsible for the optical properties, while hydrophilic ligands enable the QDs compatibility with the biological medium. Compared to organic fluorophores QDs exhibit long-term stability, reduced photobleaching, broader absorption, narrower emission and higher molar extinction coefficients.[113] Especially useful for bio-imaging is the ability to excite the mixture of different color QDs with one wavelength; a feature which results from the QD broad absorption profiles combined with the narrow emission profiles and the large Stokes shifts. QDs used in biological applications should fulfill multiple criteria: - colloidal stability across a wide range of pH and at high salt concentrations, - small hydrodynamic radius, - minimal non-specific interactions with biological environment, - presence of functional groups for specific interaction with target biomolecules.[114]

After the commonly used high-temperature synthesis the QD surface is covered by hydrophobic ligands leading to QDs, which are insoluble in aqueous media. As a result, an additional surface modification step is required to obtain water-soluble, biocompatible QDs. There are two main approaches to introduce a hydrophilic shell: the replacement of the hydrophobic shell with a hydrophilic one (by ligand exchange) and the encapsulation

of the QDs with the initial hydrophobic shell by amphiphilic systems (synthesis of micelle-like structures).[2,115] The preservation of the initial shell during the encapsulation method helps to maintain the optical properties of the QDs unchanged, however it mostly leads to a significant increase in the hydrodynamic radius of QDs. The ligand exchange procedure is often associated with a slight shift in the QD emission profile and with a decrease in quantum yield. Ligands used to synthesize QDs for biological applications should possess an anchoring group (or groups) to facilitate a strong coordination to the QD surface, a hydrophilic part, which enables the QDs solubility in aqueous media and an additional functional group to enable specific biologic interactions (Figure 1.7.1).[114,116]

Figure 1.7.1. Schematic image of the ligand used in the fabrication of QDs for biological applications.[114]

Due to the dynamic nature of ligand-QD surface interactions multidentate ligands (e.g. dihydrolipoic acid) are suggested to lead to the formation of more stable QDs and improve QD long term stability.[117–119] Dihydrolipoic acid functionalized QDs are, however, soluble only in basic pHs.[118] To provide stability over a broader pH range zwitterionic, oligomeric and polymeric ligands have been developed.[120–123] Furthermore, the introduction of multiple anchor units to the polymers (e.g. anchor block, anchor brush) enables strong coordination of polymeric ligands to inorganic nanocrystal surfaces.[116,121,124–128]

1.8 Reversible Addition Fragmentation Chain Transfer (RAFT) Polymerization

Controlled radical polymerization (CRP) techniques enable the synthesis of polymers with low molecular weight distributions, polymers with defined end groups and block copolymers. The major CRP techniques include reversible addition fragmentation chain transfer (RAFT) polymerization,[129] nitroxide-mediated polymerization (NMP) and atom-transfer radical polymerization (ATRP).[130] The key feature of all CRP techniques is the presence of the specific compound (a nitroxide radical in NMP,[131] a transition metal catalyst in ATRP and a thiocarbonyl-based chain transfer agent in RAFT) which enables a reversible blocking of active polymeric radicals. With the majority of the active radicals

blocked, their concentration decreases significantly leading to the diminishing of undesired transfer and termination reactions. Furthermore, the initiation step in CRP occurs significantly faster than the polymer growth step, thus leading to a nearly simultaneous initiation of all polymer chains. The simultaneous initiation together with the low number of transfer and termination reactions leads to the synthesis of polymers with narrow molecular weight distributions.

Due to the tolerance towards a wide variety of functionalities and reaction conditions RAFT is in all probability the most versatile CRP technique. Monomers containing styrene, vinyl ester, methacrylate, acrylate and acrylamide functionalities can be polymerized *via* the RAFT process.[132] In Scheme 1.8.1 the generally accepted mechanism for RAFT polymerization is shown.[133] During the initiation step a radical is produced (step a). Subsequently the created oligomeric radicals react with the RAFT agent (i). Previous studies provide convincing evidence that all RAFT agents are consumed in this step before any chain propagation occurs.[134] The reason for this is the highly reactive thiocarbonyl bond of the RAFT agent, which makes the radical addition to the chain transfer agent favorable over the radical addition to the double bonds of monomers. The radical intermediate (ii) can fragment into oligomeric RAFT agent (iii) and a reinitiating $R^{\cdot}$ radical which reinitiates the next polymer chain (step c). Once all the R groups are released the polymer chain growth takes place. The growing polymer chains are rapidly added to the species capped with a thiocarbonylthio group (iii, step d) to form the intermediate compound (iv). The fragmentation of compound (iv) leads to the formation of deactivated polymer chains (iii and iv), which are inactive towards any reactions and the active polymeric radicals $P_n^{\cdot}$ and $P_m^{\cdot}$ which participate in the chain growth step. The equilibrium state (d) leads to the presence of only a small amount of the active radicals and thus to the very limited number of termination reactions. At the end of the polymerization process most of the polymer chains still bear the reactive chain-transfer group (iii) which enables, for example, the synthesis of block copolymers *via* the RAFT technique.

The essential component of the RAFT polymerization is the chain transfer agent (CTA) (i), a thiocarbonylthio-based compound, e.g dithioesters, dithiocarbamates, trithiocarbonates, xanthates.[135–137] Through the choice of side group R various functional groups can be introduced in the beginning of the polymer chain. Additionally, the R group should enable a quick fragmentation of the intermediate (ii) and efficient polymer reinitiation (step c).

The Z group controls the thiocarbonyl group reactivity and influences the rate of the addition and fragmentation reactions.

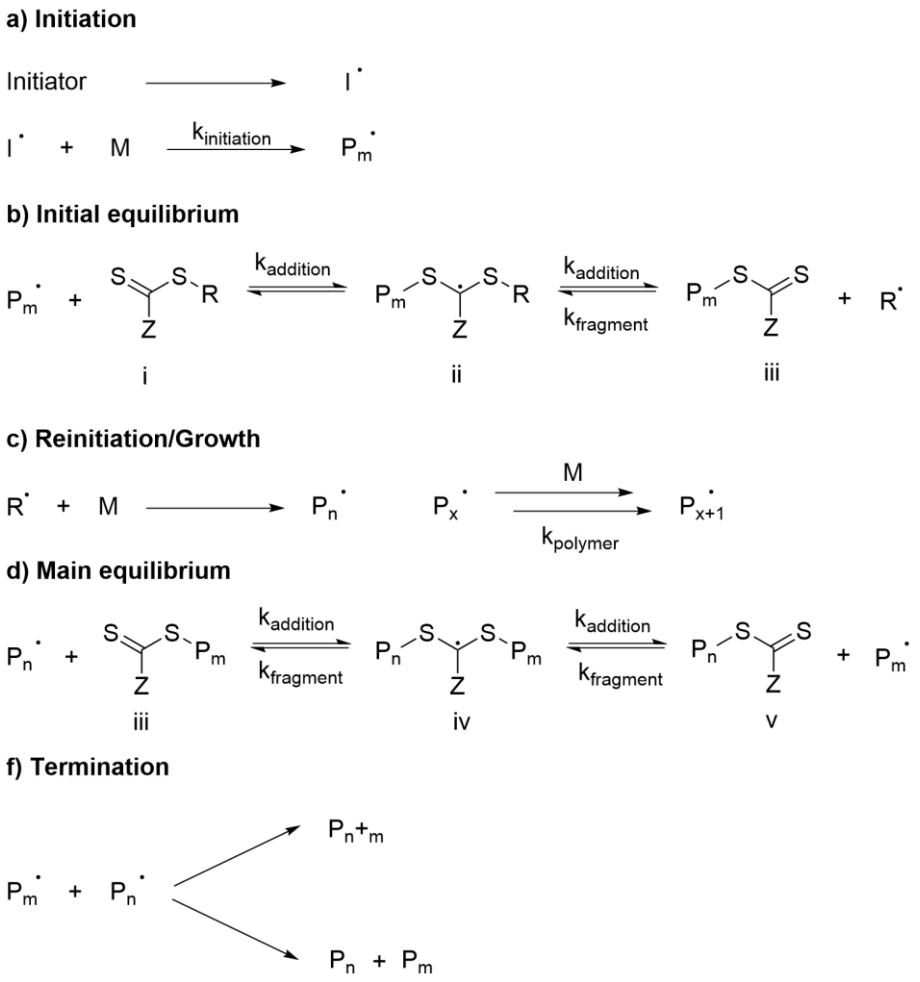

Scheme 1.8.1. RAFT polymerization mechanism.[133]

1.9 Reactive Esters

The reaction between reactive esters and amines presents an efficient way for the synthesis of the respective amides in high yields under mild reaction conditions.[138] The reactive (activated) esters are carboxylic acid derivatives which are less reactive than the respective chlorides (and thus more stable) but more reactive than the respective aliphatic esters. The group X (e.g. N-hydroxysuccinimide, pentafluorophenyl, pentachlorophenyl) in the case of the reactive ester (RCOOX) possess an electron withdrawing character leading to the increase in the partial positive charge on the carbon atom of the carboxyl group thus the increased electrophilicity of the ester (Figure 1.9.1).[139]

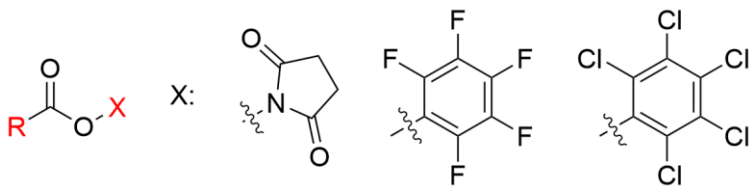

Figure 1.9.1. Reactive ester groups.

While the reactive ester approach was initially developed for the synthesis of peptides and small organic molecules it was successfully adopted to the polymer chemistry by the groups of Ferruti and Ringsdorf in 1972.[140–142] N-Hydroxysuccinimide modified acrylate and methacrylate monomers were synthesized and subsequently polymerized *via* radical polymerization to yield polymers with multiple activated ester units. The polymers were shown to be resistant to hydrolysis but readily reacted with primary and secondary amines. Pentafluorophenyl ester containing polymers gained their popularity due to their enhanced solubility in most organic solvents compared to the N-hydroxysuccinimide based polymers.[143,144] The incorporation of the reactive esters into polymers enables the introduction of the functional groups which are not compatible with the radical polymerization procedure (e.g. thioles, disulfides).[139] To introduce such groups the reactive ester units are subjected to the post-polymerization modification reaction with the respective amines. The high efficiency of the nucleophilic substitution reaction and the absence of side reactions leads to the quantitative conversion of reactive ester groups to the desired amides. With the correct choice of the groups X and R the reactivity of the ester can be precisely adjusted. For example the poly(pentafluorophenyl methacrylate) selectively reacts with primary aliphatic amines but not with alcohols. Such selectivity enables the selective synthesis of the poly(N-(2-hydroxypropyl) methacrylamide) from poly(pentafluorophenyl methacrylate) and 2-hydroxypropyl amine.[145] The reactivity of the pentafluorophenyl ester can be further increased by the modification of the R group. For instance, while the poly(pentafluorophenyl methacrylate) does not necessarily react with aromatic amines, its aromatic derivative poly(pentafluorophenyl 4-vinylbenzoate) readily undergoes the reaction with aniline under the same reaction conditions.[146]

1.10 Azide-Alkyne Cycloaddition

The azide-alkyne cycloaddition is a 1,3-dipolar cycloaddition between a terminal or an internal alkyne and an azide to yield 1,2,3-triazoles. The uncatalyzed cycloaddition leads to an isomeric mixture of 1,4 and 1,5 substituted triazoles (Scheme 1.10.1 a). The copper-

catalyzed version (CuAAC), however, enables a selective synthesis of the 1,4 substituted species (Scheme 1.10.1 b).[147,148] The CuAAC is the leading example of a click reaction and presents a straightforward, high yielding way to link two molecules together.[149] Its high tolerance towards other functional groups made it highly popular in various fields of chemistry and material science. However, in the field of life science the use of CuAAC is limited due to the cell toxicity of Cu(I) ions. A non-toxic alternative is provided by the catalyst-free strain-promoted azide-alkyne cycloaddition (SPAAC, Scheme 1.10.1 c).[150]

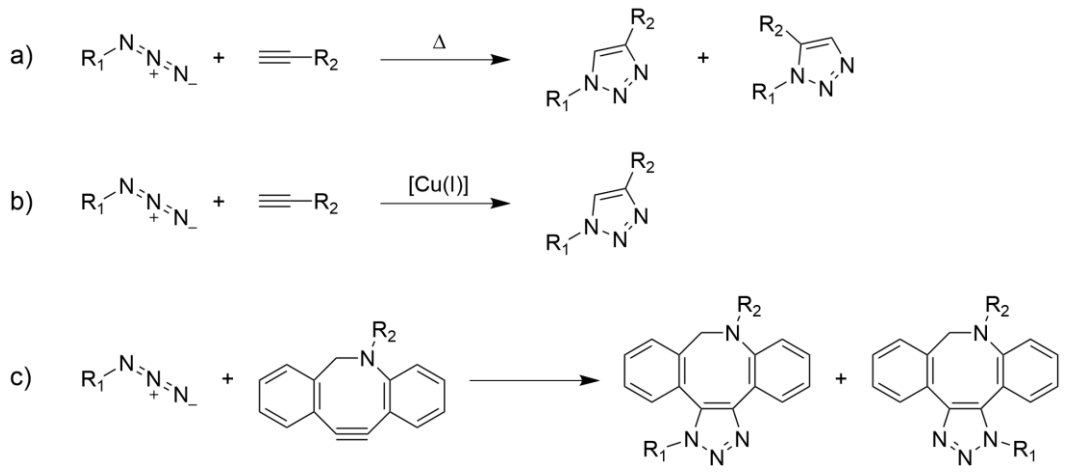

Scheme 1.10.1. Reaction equations for thermally activated (a), copper-catalized (b) and strain promotend (c) azide-alkyne cycloadditions.

In SPAAC the alkyne component is represented *via* strained cyclooctyne moiety. The great bond angle deformation of 163° of the acetylene bonds leads to the reaction rates which are significantly higher than these of the unstrained alkynes.[151,152] Therefore, the SPAAC can be performed under ambient temperatures in the absence of auxiliary reagents. To further increase the SPAAC reaction rate heteroatoms, e.g. nitrogen, were incorporated into the ring and various side groups were introduced, e.g. phenyl rings.[153,154]

While uncatalyzed reactions proceed in a cyclic matter, the mechanism of the Cu-catalyzed reaction has been the subject of multiple discussions. The mechanism shown in Scheme 1.10.2 was suggested by the groups of K. B. Sharpless and G. Bertrand.[147,155] The catalytic cycle shown on the left side was proposed by the K. B. Sharpless group in 2002 and includes mono-copper catalyst. It starts with the formation of the copper (I) acetylide **A**. The five-membered ring **D** is, however, not formed *via* the concerted cycloaddition but *via* the stepwise reactions through the intermediates **B** and **C**. Additionally, in 2015 the

Bertrand group provided evidence that the bis-copper species **E** and **F** also participate in the reaction and even lead to the pathway which is kinetically favored (right catalytic circle).

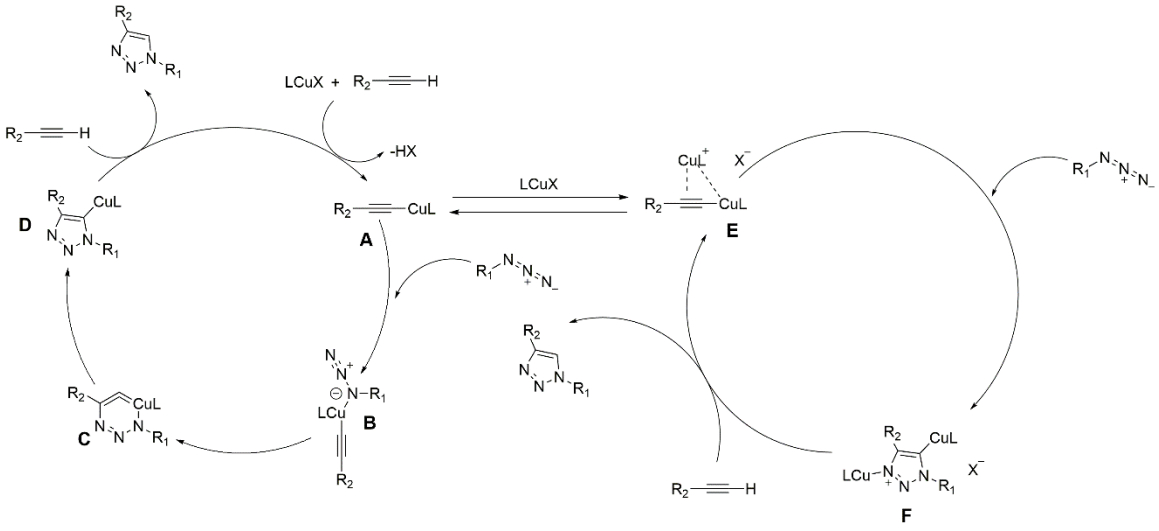

Scheme 1.10.2. Copper catalyzed azide-alkyne reaction mechanism.

2 Aims and Objectives

Quantum dot light-emitting diodes (QLEDs) have attracted attention due to their numerous advantages, such as good color purity, ease of color tunability, simple fabrication processes and viability for flexible and transparent displays. Despite the advances made in improving device performances and in understanding the mechanism of QD luminescence, the issue of imbalanced charge transport and diminished quantum dot (QD) photoluminescence remains. Devices containing hybrid active layers, in which QDs are distributed in a semiconducting matrix, could provide a solution to these problems. Section 3.1 of this dissertation will focus on the study of factors which affect the performance of QLEDs with hybrid semiconducting polymer/quantum dot active layers. First, the development of new side-chain conjugated polymers is presented. The polymers were then tested in devices in order to determine the dependence of device performance on the properties of the polymers used. Second, the device performance is correlated with the morphology and composition of the active layer. QLEDs with different QD/polymer ratios were tested to investigate how the quantity of the incorporated polymer influences the devices characteristics. Furthermore, the influence of the active layer morphology on the charge career transport balance and on the quenching of QD photoluminescence is discussed.

The premise for the synthesis of stable QD/polymer hybrids is the strong coordination of polymer chains to QD surfaces. To facilitate the strong coordination the presence of multiple anchor groups is sometimes necessary. Section 3.2 will focus on the development of anchor compounds which enable an efficient and reproducible introduction of multiple anchor groups to polymer chains. The synthesis and the incorporation of bidentate and tridentate lipoic acid-based ligands to semiconducting and hydrophilic polymers is shown. Additionally, to test the anchoring ability of the new compounds, the modified polymers were tested as hydrophilic ligands to fabricate water-soluble QDs.

3 Results and Discussion

3.1 Hybrid QLEDs Based on Hybrid Semiconducting Polymer/QD Active Layers

Quantum dot based light emitting diodes (QLEDs) are competitive alternatives to organics light emitting diodes (OLEDs) in terms of color purity, luminescence intensities and external quantum efficiencies (EQEs).[71,84,156] Since the first report in 1994 by Colvin *et al*. a tremendous amount of work has been performed to understand how QLEDs work as well as how to improve device performance.[65,70–72,77,156,157] However, there is still need for improvement in terms of the charge transport balance and the photoluminescence quenching (PL) of the QDs as described in detail in sections 1.5.2 and 1.5.3.

An interesting alternative to thin QD-only active layers which are sandwiched between electron and hole transport layers is provided by an active layer consisting of QDs distributed in a semiconducting matrix (section 1.5.4). If one uses a semiconducting polymer to surround the QDs the polymer would serve as an electron blocking layer thus leading to the improvement in the charge balance and simultaneously increase the distance between the individual QDs leading to suppression of fluorescence quenching. A recent study by Bae *et al.* shows that the distribution of QDs within a semiconducting polymer matrix leads to better charge balance within the active layer and to the efficient distribution of charge carriers and excitons through the active layer. [158] Moreover, the efficiency of the hole injection into the QDs can be tuned through diligent choice of the semiconducting polymer used.[159]

While many semiconducting polymers and small molecules have been intensively investigated as host materials in the active layers of fluorescent and phosphorescent organic LEDs [160–162], only a few polymers have been tested as a component of an active layer in hybrid semiconducting polymer/QD-based LEDs. [85–87,89,90,92,159,163] In order to address the issue of charge injection balance polymers with high lying lowest unoccupied molecular orbitals (LUMOs) and low lying HOMOs should be developed. High LUMO levels are important for reducing electron injection into the QDs (i.e. electron overcharge problem), while low HOMOs and a hole conducting ability should enable sufficient hole injection into the QDs. Side-chain conjugated polymers are promising candidates to fulfill the above

mentioned criteria and have been previously successfully investigated as host materials in organic LEDs.[38,39,49,51,164]

To produce QLEDs with pure QD emission the homogeneous distribution of a large amount of QDs within a polymer matrix is required.[55] Uniform QD distribution can be efficiently achieved by the chemical blending of QDs and polymers (i.e. polymers grafted onto QDs).[55,165] An effective route to the fabrication of chemically grafted QD/polymer hybrids is the ligand exchange procedure (section 1.4).[60] Polymers used in the ligand exchange must possess functional groups which can effectively coordinate to the surface of QDs and substitute the initial small molecule ligands. Following the ligand exchange procedure, the QD surface is functionalized with polymer chains which will impart the properties of the ligands. The modified QDs may now be easily homogenized with an excess of free polymer chains preventing phase separation in films and thus leading to defect-free, uniform electroluminescence over the entire pixel area.

In the following sections the synthesis of new carbazole-based monomers and their corresponding side-chain conjugated polymers is described (sections 3.1.1and 3.1.2). The polymers synthesized possess one or multiple anchor groups to enable chemical grafting with QDs *via* ligand exchange. Furthermore, the polymers are subsequently investigated as components of the active layers in hybrid QLEDs. Moreover, the influence of the HOMO level of the polymers (section 3.1.3) and of the active layer morphologies (section 3.1.4) on the device performance is determined and the implications considered.

3.1.1 Synthesis of Semiconducting Monomers with Carbazole Cores

The efficiency of QLED performance is highly dependent on the choice of hole transport materials and specifically on the HOMO levels of hole transport layers as explicitly discussed in the section 1.5.2. The performance of hybrid semiconducting polymer/QD QLED devices in previous studies have been found to be notably below the efficiencies of the contemporary QD-only QLEDs.[10,71,84,92,156,159] The low performance of hybrid QLEDs has been attributed to impeded hole injection from the polymer into QDs due to the large energy offset between the HOMO of the polymer and the valence band of the QDs.[70,159] Therefore, semiconducting polymers with low lying HOMO levels should be developed. As mentioned in the introduction of the section 3.1 side-chain conjugated polymers are promising candidates. In the case of side-chain conjugated polymers, the electrochemical properties of the polymer are already determined by the monomer. Thus, the monomers with low lying HOMO levels have to be synthesized.

In this study the carbazole functionality was chosen as the basis of all monomers investigated. The carbazole core is a promising choice for the electroactive unit as carbazole-based small molecules and polymers possess relatively low HOMO levels and are widely known hole conducting materials.[35,166] Additionally, the carbazole core may provide polymers with HOMO levels lower than that of triphenylamine-based structures previously studied in our group (e.g. **PTPDF** Figure 3.1.1).[159] A styrene group was chosen as the precursor for the chemically and electrochemically inert polystyrene backbone of the resulting polymers.

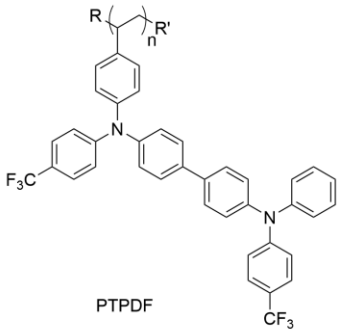

*Figure 3.1.1. Structure of the **PTPDF** polymer.*

To confirm that carbazole-based monomers will provide materials with HOMO levels lower than that of the **PTPDF** polymer theoretical calculations were performed prior to the

synthesis. Table 3.1.1 shows the calculated values of the HOMO and LUMO levels, and energy band gaps of various carbazole containing molecules (Figure 3.1.2). It should be noted that the values in Table 3.1.1 are obtained by computational calculations and should only be compared among each other and not with the experimentally obtained data. The calculated HOMO values of the carbazole-based structures **CBP**, **CTP** and **CTPF** were determined to be lower than the HOMO of **TPDF** which reflects the basis of **PTPDF** polymer. Therefore, the acquired results motivated us to proceed with efforts to develop synthetic protocols for our proposed structures.

Table 3.1.1. Calculated values of HOMO und LUMO levels of structures shown in Figure 3.1.2. The calculations were carried out with the Turbomole program using B3LYP/def2-SVP with the help of [redacted] *and* [redacted] *(Department of Physical Chemistry JGU Mainz).*

	TPDF	**CBP**	**CTP**	**CTPF**
HOMO (eV)	-5.2	-5.5	-5.3	-5.7
LUMO (eV)	-1.4	-1.5	-0.9	-1.4
Gap (eV)	3.8	4.0	4.4	4.3

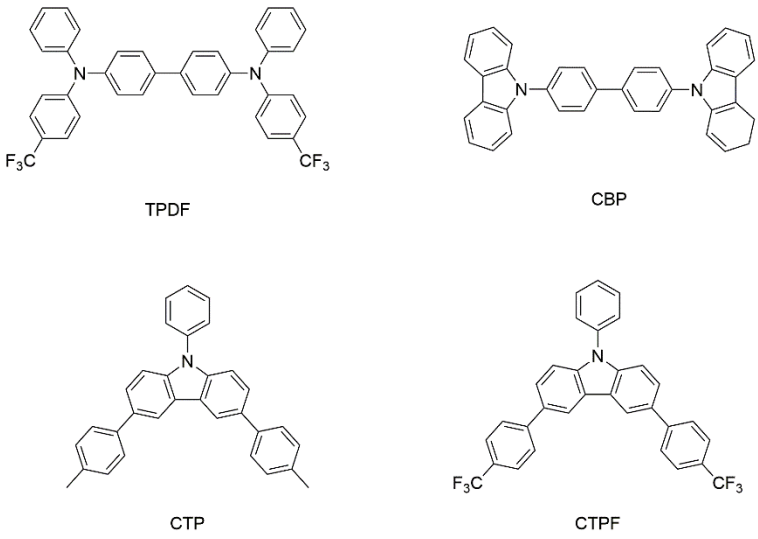

Figure 3.1.2. Structures used in the theoretical calculations summarized in Table 3.1.1.

3.1.1.1 Monomer **M1**

Kwak *et al*. reported that the morphological and electrochemical stability of the carbazole can be increased by the introduction of the phenyl groups in 3, 6 and 9 positions of the carbazole.[167] These results inspired the design of the monomer **M1**. The monomer **M1** was

synthesized in five steps (Scheme 3.1.1) starting with a copper catalyzed Ullmann coupling reaction between carbazole and 4-iodoanisole in *o*-chlorobenzene which led to the formation of 9-(4-methoxyphenyl)carbazole **1**. Following this the bromination of **1** with 4 eq. of N-bromosuccinimide in DMF quantitatively produced 3,6-dibromo-9-(4-methoxyphenyl) carbazole **2** which was precipitated into water and used in the next step without any further purification. 3,6-bis(4-methylphenyl)-9(4-methoxyphenyl) carbazole **3** was synthesized from **2** and *p*-tolylboronic acid using palladium-catalyzed Suzuki coupling with $Pd(PPh_3)_4$ in a toluene / 2M aqueous Na_2CO_3 solution / ethanol mixture. The subsequent highly efficient deprotection of the hydroxyl group with boron tribromide in dry dichloromethane was followed by a nucleophilic substitution reaction between 3,6-bis(4-methylphenyl)-9(4-hydroxyphenyl) carbazole **4** and 4-vinylbenzyl chloride in a acetonitrile/DMF mixture to yield monomer **M1** as a colorless crystalline powder.

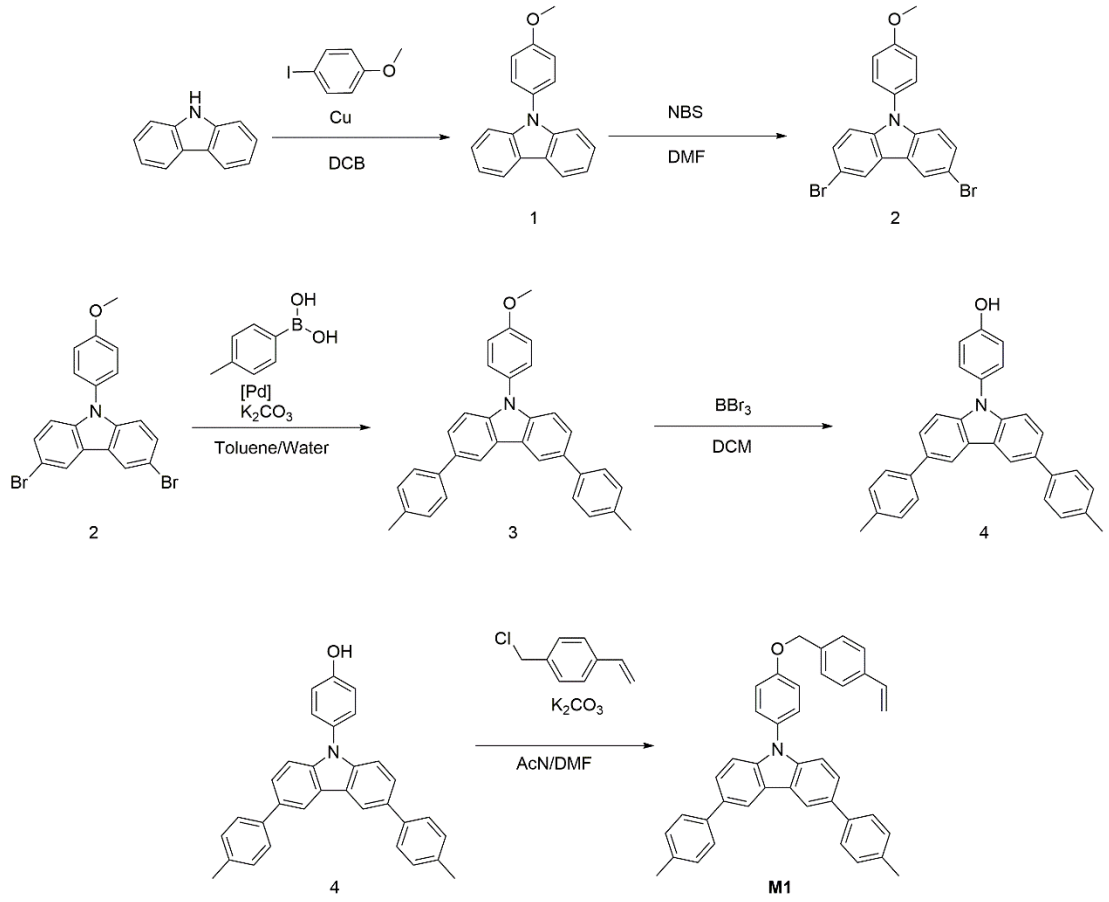

*Scheme 3.1.1. Synthesis of monomer **M1**.*

The successful synthesis of the desired compounds during each step was verified *via* HRMS (ESI$^+$), ^{1}H NMR and ^{13}C NMR spectroscopies. Highlighted below are specific proton signals in ^{1}H NMRs which provide clear indications for the formation of the desired compounds (Figure 3.1.3).

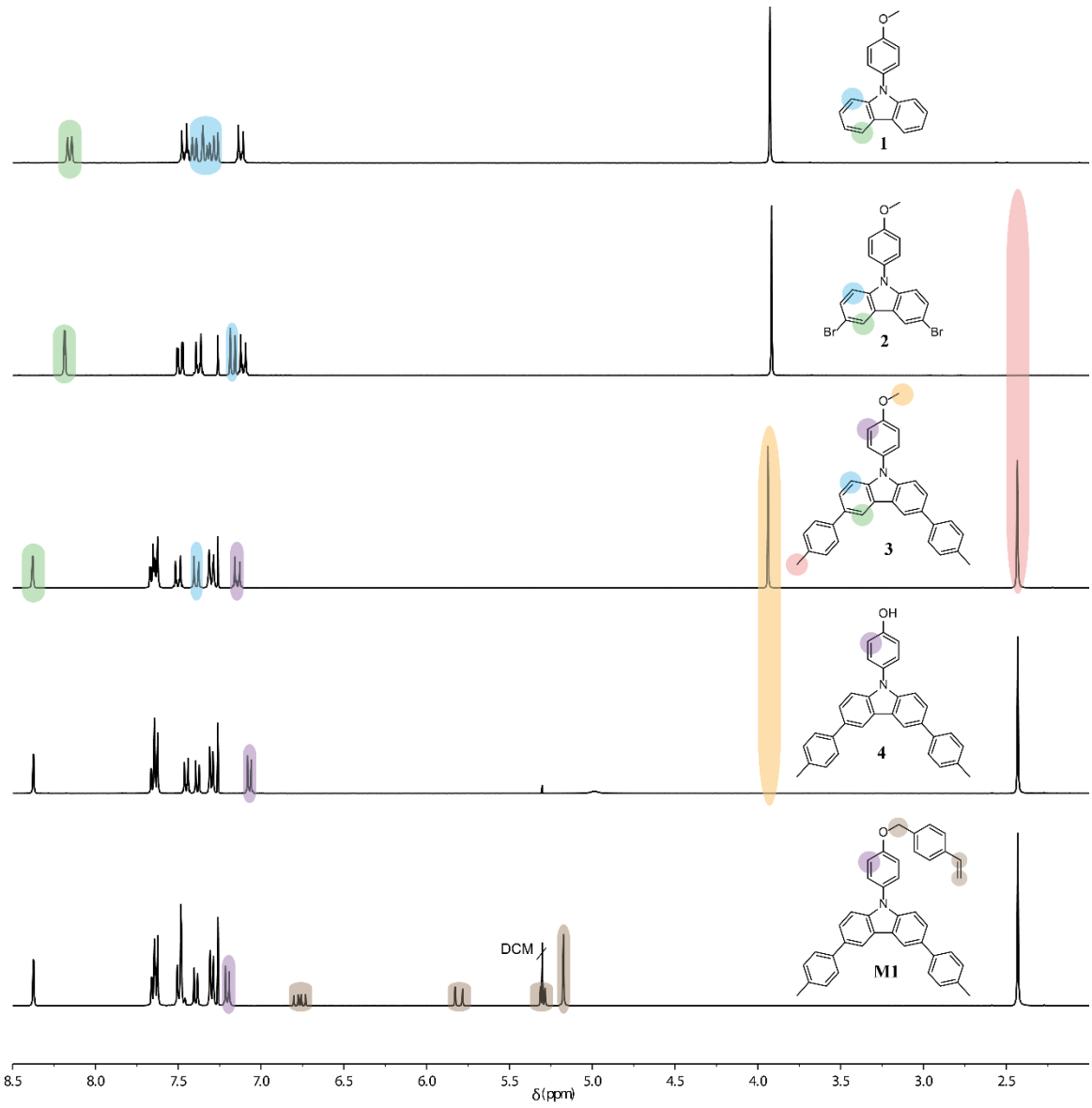

*Figure 3.1.3. Stacked ^{1}H NMR spectra of compounds **1-4** and **M1**. ^{1}H NMR spectra with all protons assigned can be found in section 9.*

The introduction of the Br atoms and the 4-methylphenyl rings in the 3 and 6 positions of the carbazole ring leads to a shift of the signal attributed to the protons at 4 and 5 positions from 8.16 ppm to 8.19 ppm and 8.38 ppm for compounds **1**, **2** and **3** respectively (green). While the signal shift following the formation of compound **2** is insignificant, a substantial

change in the signal shape from a doublet of triplets with a large ^{3}J coupling constant of 7.7 Hz to a doublet of doublets with a ^{3}J of 2.0 Hz can be observed. The formation of compounds **2** and **3** can, furthermore, be verified by the change in the resonance of protons in the 1 and 8 positions of the carbazole ring (blue). In the NMR spectrum of compound **1** the signal of the above mentioned protons is incorporated into the multiplet at 7.42-7.28 ppm and shifts to 7.17 ppm and 7.39 ppm for compounds **2** and **3** respectively. Moreover, in the spectrum of compound **3** the new singlet at 2.43 ppm appears corresponding to the methyl groups of the newly incorporated 4-methylphenyl rings (red). Deprotection of the hydroxyl group leads to the disappearance of the singlet corresponding to the methoxy group at 3.94 ppm (orange) in the spectrum of compound **4**. Additionally, the formation of compound **4** and monomer **M1** can be monitored by a change in the resonance of the signal attributed to the aromatic protons adjacent to the methoxy group (violet). In the spectrum of compound **3** the signal of the above mentioned protons appears at 7.15 ppm and shifts to 7.07 ppm and 7.20 ppm for compound **4** and monomer **M1** respectively. In the spectrum of monomer **M1** the presence of the signals at 6.77, 5.81, 5.30 and 5.17 ppm indicates the successful introduction of the styrene functionality (brown).

X-ray crystallography unambiguously confirmed the synthesis of the monomer **M1**. (Figure 3.1.4). Due to the steric demand of phenyl rings monomer **M1** reveals a twisted structure with torsion angles of 42°, 34° and 47° between the carbazole unit and the phenyl rings in the third, sixth and ninth position respectively.

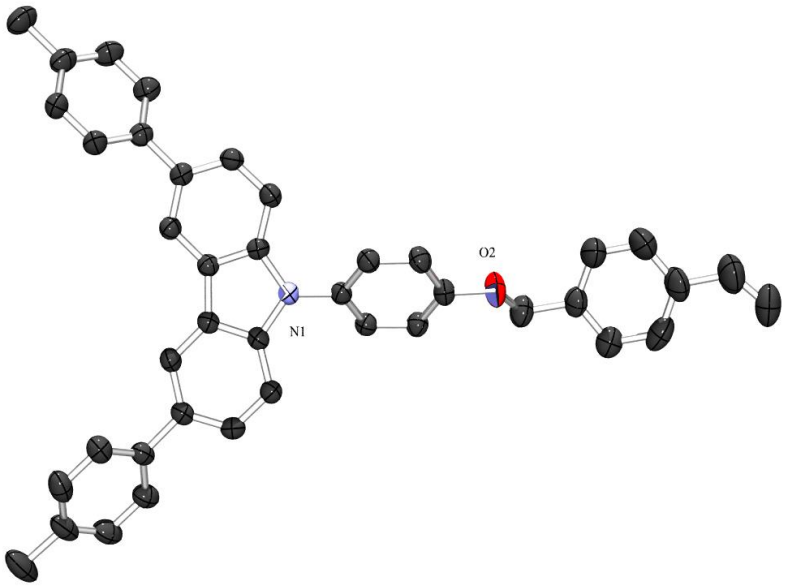

*Figure 3.1.4. Single crystal structure of monomer **M1** (ORTEP plot, hydrogen atoms are omitted for clarity).*

The introduction of aromatic rings in the 3, 6 and 9 positions of the carbazole unit was undertaken to expand the size of conjugated system and to increase the solubility of the monomer and thus the future polymer. Additionally, the methyl groups in the para positions of phenyl rings prevent irreversible oxidation under electrolytic conditions.[47,168] The prevention of the irreversible oxidation can be ascertained by the cyclic voltammetry (CV) measurements. As only the electrochemical behavior of the semiconducting core should be investigated, the intermediate structure **3** is used in CV experiments. The repeated oxidation cycling of the first oxidation peak of compound **3** in DCM/TBAPF$_6$ (Figure 3.1.5 a) does not lead to any changes in the CV profile indicating a fully reversible oxidation process. However, if the electrochemical window is extended, a second oxidation peak is observed, which is responsible for an irreversible oxidation process (Figure 3.1.5 b).

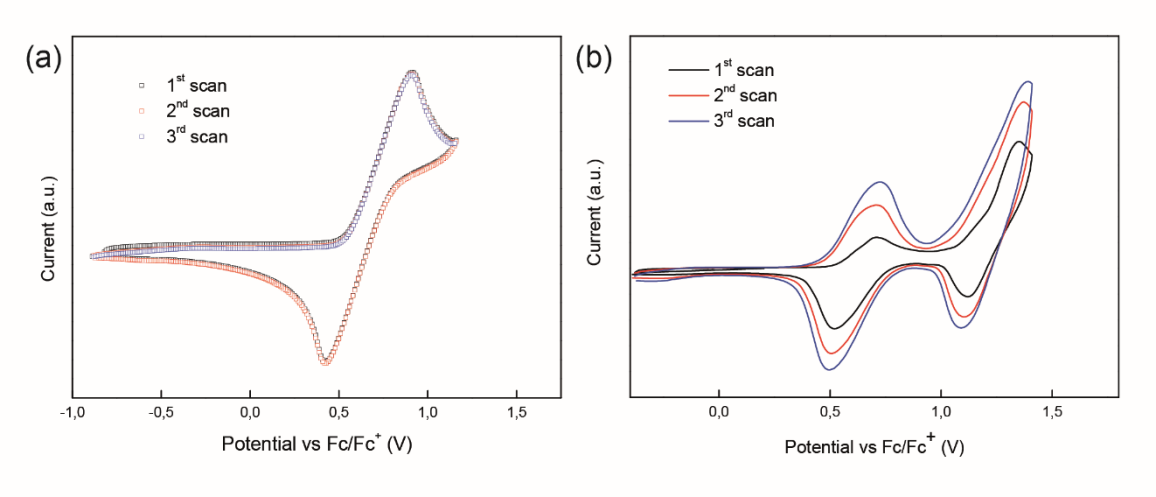

*Figure 3.1.5. CV voltammograms of the compound **3** in DCM/TBAPF$_6$. The repeated cycling of the first oxidation peak (a) and of the extended electroactive region (b).*

The chosen synthetic route allows for the simple modification of the substituents in the 3 and 6 positions of the carbazole and thus for variation of the electrochemical properties. The *p*-tolyl groups can be substituted by electron rich 2-methylthiophene or by electron deficient trifluoromethylphenyl groups leading to compounds **5** and **6** respectively (Scheme 3.1.2). Cyclic voltammetry experiments reveal the significant shifts in the onsets of the oxidation peaks of compound **3**, **5** and **6** und thus in their HOMO levels (Figure 3.1.6). Compound **5** is oxidized first with an oxidation onset at 0.54 V vs. Fc/Fc$^+$, meaning that it possesses the highest HOMO level, followed by **3** and **6** with oxidation onsets at 0.51 V and 0.67 V respectively. The electron donating character of the thiophene rings leads to the higher HOMO level of compound **5** compared to **3** while the electron withdrawing character of the trifluoromethyl groups leads to the lower HOMO level of compound **6** compared to **3**. Based on the positions of the oxidation peaks in the cyclic voltammetry measurements compounds **3** and **6** feature HOMO levels which are lower than the HOMO of **PTBDF**.

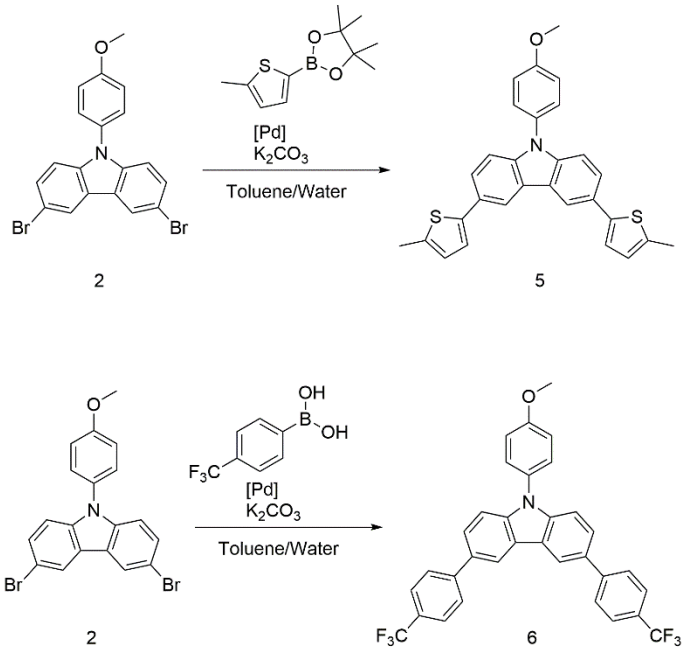

*Scheme 3.1.2. Synthesis of compounds **5** and **6**.*

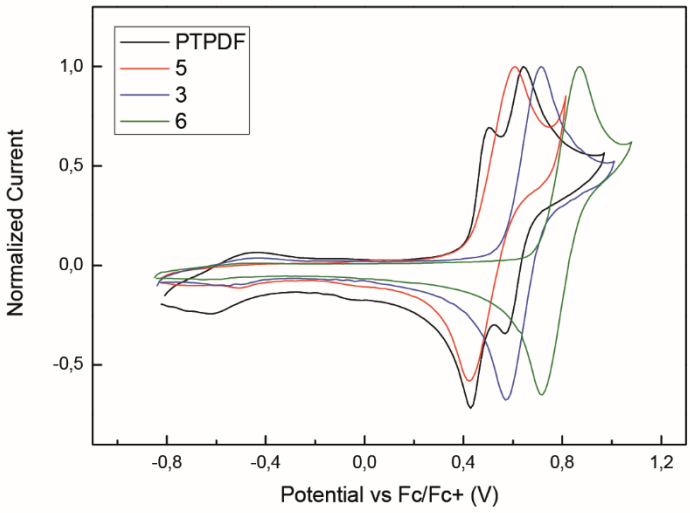

*Figure 3.1.6. CV voltammograms of compounds **PTPDF**, **3**, **5** and **6** in DCM/TBAPF$_6$.*

3.1.1.2 Monomer **M2**

The choice of the monomer **M2** was motivated by the widely and successfully used semiconducting polymer poly(9-vinylcarbazole) (PVK) with HOMO level of approximately 5.8 eV.[169] Monomer **M2** was synthesized in one step by the nucleophilic substitution reaction between carbazole and 4-vinylbenzyl chloride in DMF and subsequently was recrystallized from acetone to yield highly crystalline colorless needles

(Scheme 3.1.3). The successful synthesis of the monomer **M2** was verified *via* HRMS (ESI^+), ^1H NMR and ^{13}C NMR spectroscopies. The ^1H NMR spectrum with the assigned protons can be found in section 9.

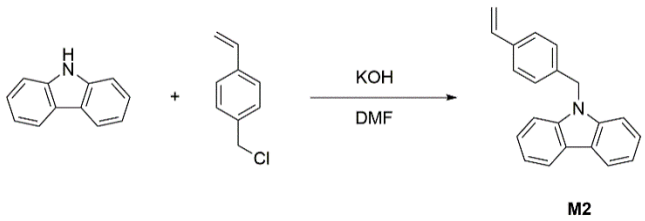

*Scheme 3.1.3. Synthesis of the monomer **M2**.*

3.1.1.3 Monomer **M3**

4,4′-Bis(N-carbazolyl)-1,1′-biphenyl (CBP) is commonly used as the host material in phosphorescent LEDs and as the hole transport layer in the state-of-the-art QLEDs. Due to its low HOMO level of approximatively 6 eV CBP was chosen as the basis of the monomer **M3**. The synthesis of the monomer **M3** was carried out in five steps (Scheme 3.1.4). The mono formylation of 4,4'-bis(N-carbazolyl)-1,1'-biphenyl was carried out with tin(IV) chloride and dichloromethyl methyl ether in dry dichloromethane, followed by an aqueous work-up. The Knoevenagel-Doebner condensation of **5** with malonic acid in pyridine resulted in the formation of the α,ß-unsaturated carboxylic acid derivative **6**. In order to reconstitute to the π-system of the CBP unit, the hydrogenation of the side chain double bond was performed in dry THF with palladium on charcoal producing compound **7**. Subsequent reduction of the acid group with $LiAlH_4$ led to the formation of hydroxypropyl-CBP **8**. Finally, the nucleophilic substitution reaction between **8** and 4-vinylbenzyl chloride gave the monomer **M3** as colorless crystalline solid. The incorporated alkyl spacer between the styrene backbone unit and the CBP functionality facilitates the easy accessibility of vinyl double bonds during polymerization and improves monomer solubility. The successful synthesis of the desired compounds during each step was verified *via* HRMS (ESI^+), ^1H NMR and ^{13}C NMR spectroscopies.

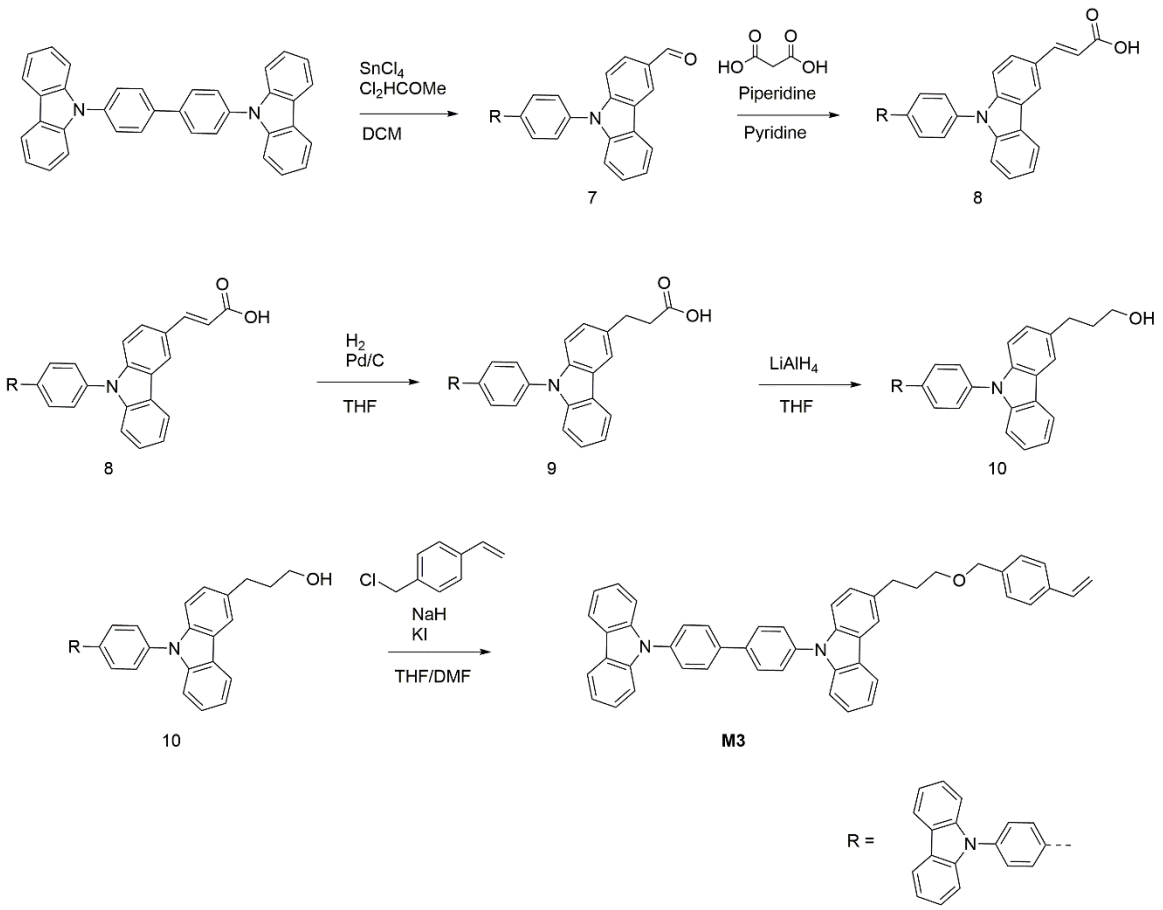

*Scheme 3.1.4. Synthesis of the monomer **M3**.*

Indication for the formation of the desired compounds are provided by some specific proton signals which are highlighted in Figure 3.1.7. The formation of compounds **8** and **9** is suggested by the shift of the signal corresponding to the carbazole proton adjacent to the side chain from 8.71 ppm to 8.37 ppm and 8.02 ppm, respectively (green). Furthermore, the formation of compound **8** is indicated by the disappearance of the singlet at 10.15 ppm corresponding to the aldehyde group (blue) and the appearance of signals which correlate to the newly created double bond at 8.05 ppm and 6.55 ppm (orange). The selective hydrogenation of the double bond leads to the disappearance of the double bond signals and the appearance of two new signals at 3.20 ppm and 2.82 ppm in the spectrum of compound **9**. Following this, the reduction of the acid group to an alcohol during the synthesis of compound **10** leads to the appearance of a new triplet at 3.76 ppm (violet). Furthermore, the signals at 3.20 ppm and 2.82 ppm shift to 2.94 ppm and 2.03 ppm, respectively. The triplet signal at 3.76 ppm (compound **10**) shifts to 3.56 ppm during the synthesis of the monomer **M3** as the result of the ether formation. Finally, the introduction

of the styrene functionality leads to the appearance of signals at 6.73 ppm, 5.76 ppm, 5.25 ppm and 4.54 ppm (red).

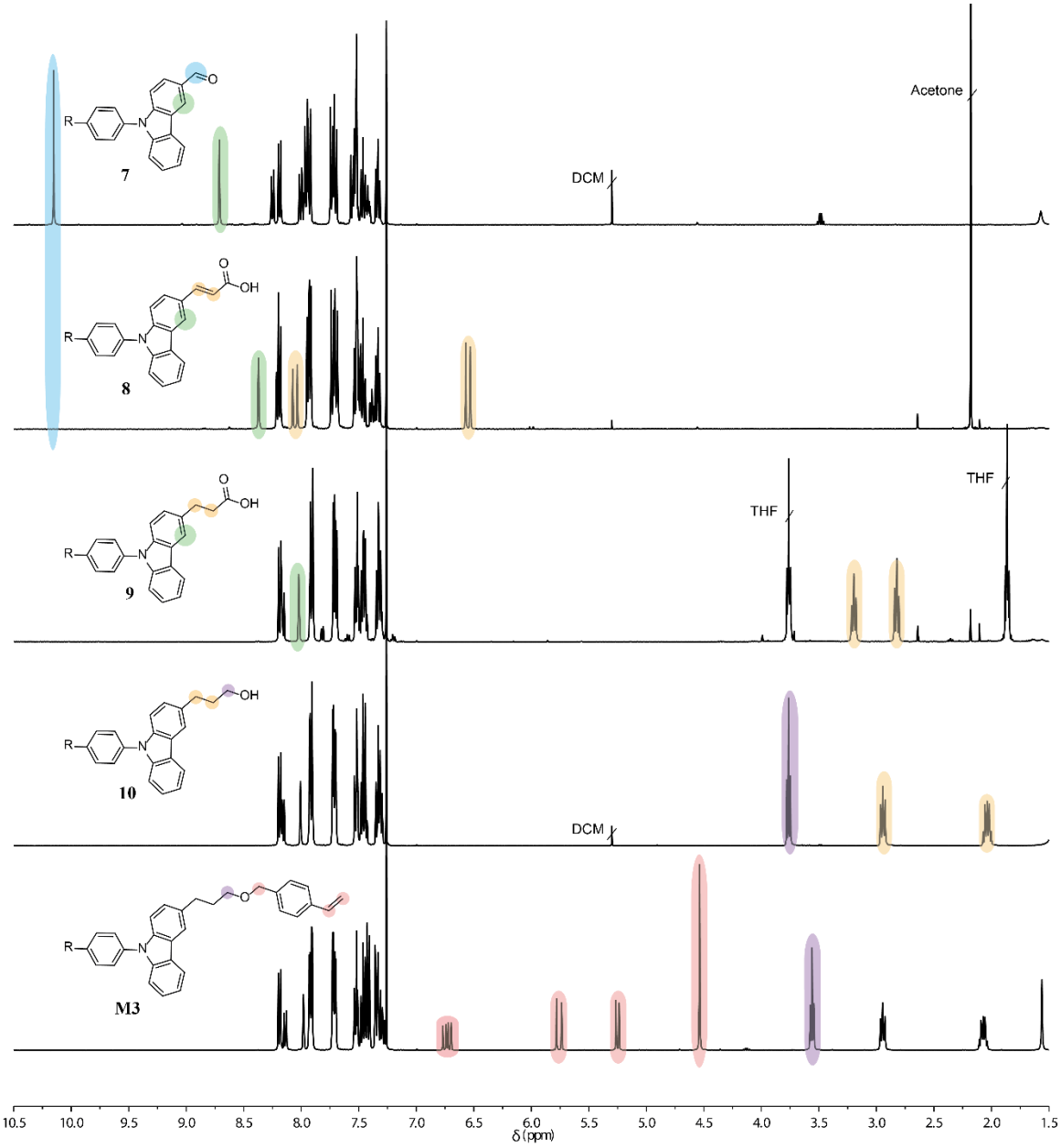

*Figure 3.1.7. Stacked ^{1}H NMR spectra of compounds **7-10** and **M3**. ^{1}H NMR spectra with all protons assigned can be found in section 9.*

3.1.2 Side-Chain Conjugated Polymers for the Use in the Active Layers of Hybrid QLEDs

3.1.2.1 Synthesis of Side-Chain Conjugated Polymers with One Anchor Group

Reversible addition-fragmentation chain transfer (RAFT) radical polymerization was employed for polymerization of monomers **M1**-**M3** (Scheme 3.1.5). RAFT enables to produce polymers with narrow molecular weight distribution and defined endgroups, qualities which are necessary for polymer applications in hybrid QLEDs.

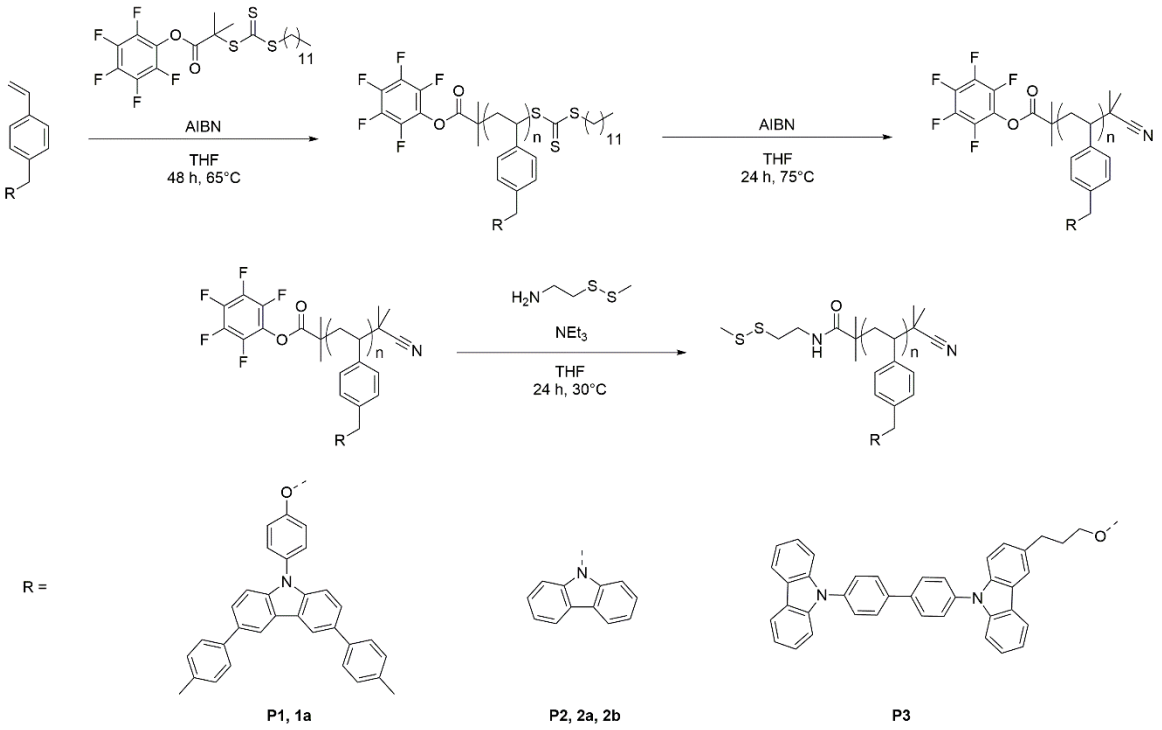

*Scheme 3.1.5. RAFT polymerization and post-polymerization modification reactions of **P1**, **P1a**, **P2**, **P2a**, **P2b** and **P3**.*

S-1-dodecyl-S′-(α,α′-dimethyl-α″-pentafluorophenyl acetate) trithiocarbonate was chosen as the RAFT chain transfer agent because trithiocarbonates have previously been reported as efficient agents in polymerization of bulky styrene derivatives.[170] Moreover, the reactive pentaflouorophenyl ester group, which can be later replaced with other desired functionalities, was incorporated at the beginning of each polymer chain. Relevant ratios of monomer, RAFT agent, and initiator (2,2′-azibis(2-methylpropionitrile) (AIBN)) were dissolved in dry THF and degassed *via* three freeze-pump-thaw cycles. The polymerization was carried out under a nitrogen atmosphere at 65°C, in a sealed Schlenk flask for 48 hours.

Afterwards, the reaction solutions were cooled down to room temperature and the polymers were precipitated into hexanes. For purification, the polymers were repeatedly redissolved in THF and precipitated into suitable solvents. The successful polymerization was confirmed by gel permeation chromatography (GPC) and ^{1}H NMR spectroscopy. As an example the comparison of ^{1}H NMR spectra of monomer **M3** and polymer **P3** is shown in Figure 3.1.8. The formation of polymer can be verified by the disappearance of double bond signals at 5.25 and 5.76 ppm and by the, for polymer characteristic, peak broadening in the polymer spectrum.

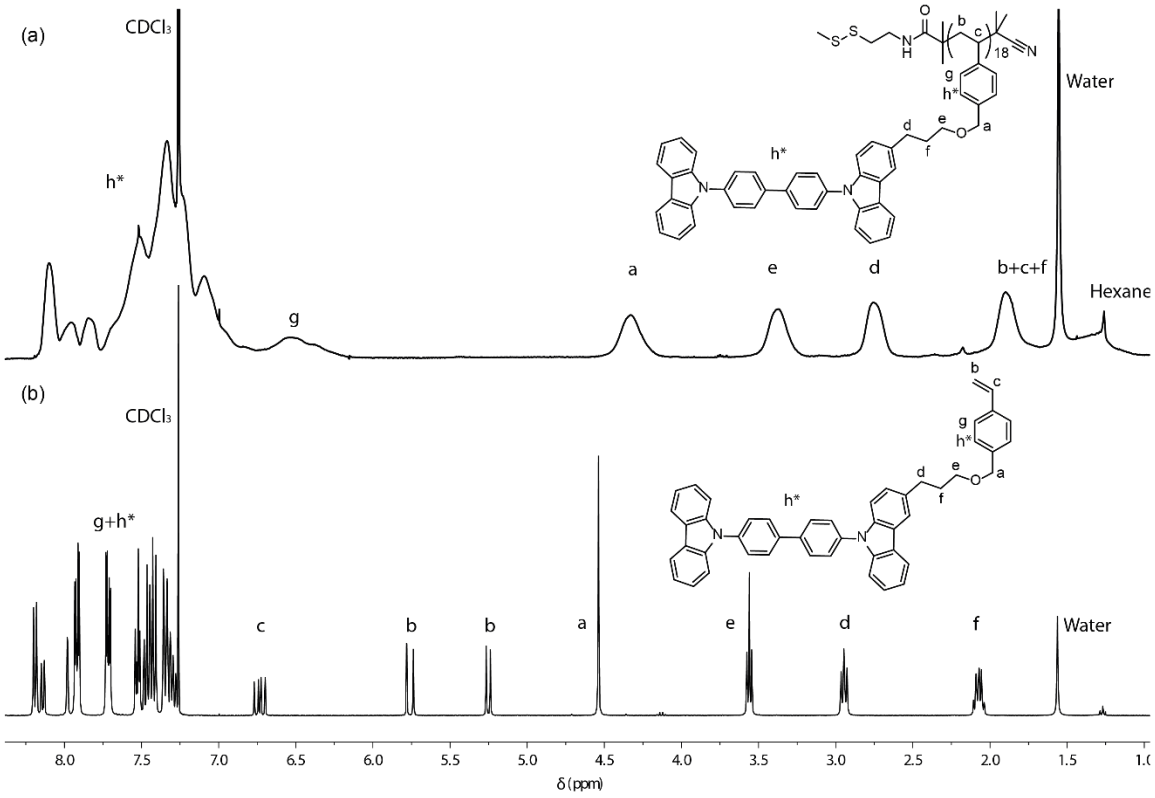

*Figure 3.1.8. ^{1}H NMR spectra of polymer **P3** (a) and monomer **M3** (b). h* represents all the aromatic peaks of CBP moiety and in case of monomer also the styrene peaks. The exact peak assignment can be found in the experimental section and section 9.*

Depending on the applied monomer ratios polymers with different chain lengths were synthesized and the experimental conditions are summarized in Table 3.1.2.

Table 3.1.2. Summary of the side-chain conjugated polymers with one anchor group. a: obtained by GPC measurements in THF with polystyrene as standard.

Polymer	M_n	P_n	PDI	Monomer	Monomer eq	CTA eq	AIBN eq	Solvent
P1	10900	20	1.1	M1	60	1	0.143	THF
P1a	19600	35	1.2	M1	120	1	0.143	THF
P2	5300	19	1.2	M2	60	1	0.143	THF
P2a	8100	29	1.1	M2	120	1	0.143	THF
P2b	13600	48	1.2	M2	240	1	0.143	THF
P3	11600	18	1.1	M3	60	1	0.143	THF

In the next step the reactive trithiocarbonate polymer end group was replaced with an inert 2-cyanoisopropyl functionality by reaction with an excess of AIBN in THF. Finally, the reaction of 2-methyldithio-ethylamine with pentaflourophenyl ester in THF at 30°C for 24 hours led to the quantitative replacement of the pentaflourophenyl groups with 2-methyldithio-ethylamine. The disappearance of the C=O band of the pentafluorophenyl ester at 1772 cm^{-1} and the presence of C=O band of the amide at 1663 cm^{-1} in IR spectroscopy indicated the formation of the amide (Figure 3.1.9 a). Additionally, the substitution was confirmed by the disappearance of the pentafluorophenyl peaks in ^{19}F NMR spectroscopy (Figure 3.1.9 b).

The incorporated disulfide moieties enable polymers to graft onto a CdSe@$Cd_xZn_{1-x}S$ QD surface due to the preferred disulfides affinity to the unsaturated Zn-centers. The introduction of the anchor groups is a necessary step in the synthesis of the polymers which are utilized in hybrid polymer/QD systems as the polymer grafting onto QD surface is required for the uniform dispersion of QDs within polymer matrices. The 2-methyldithio-ethylamine was used instead of cysteamine, a group widely used for QD functionalization, to prevent interchain cross-coupling reactions between individual polymer chains thus retaining the low polydispersity of the samples.[92]

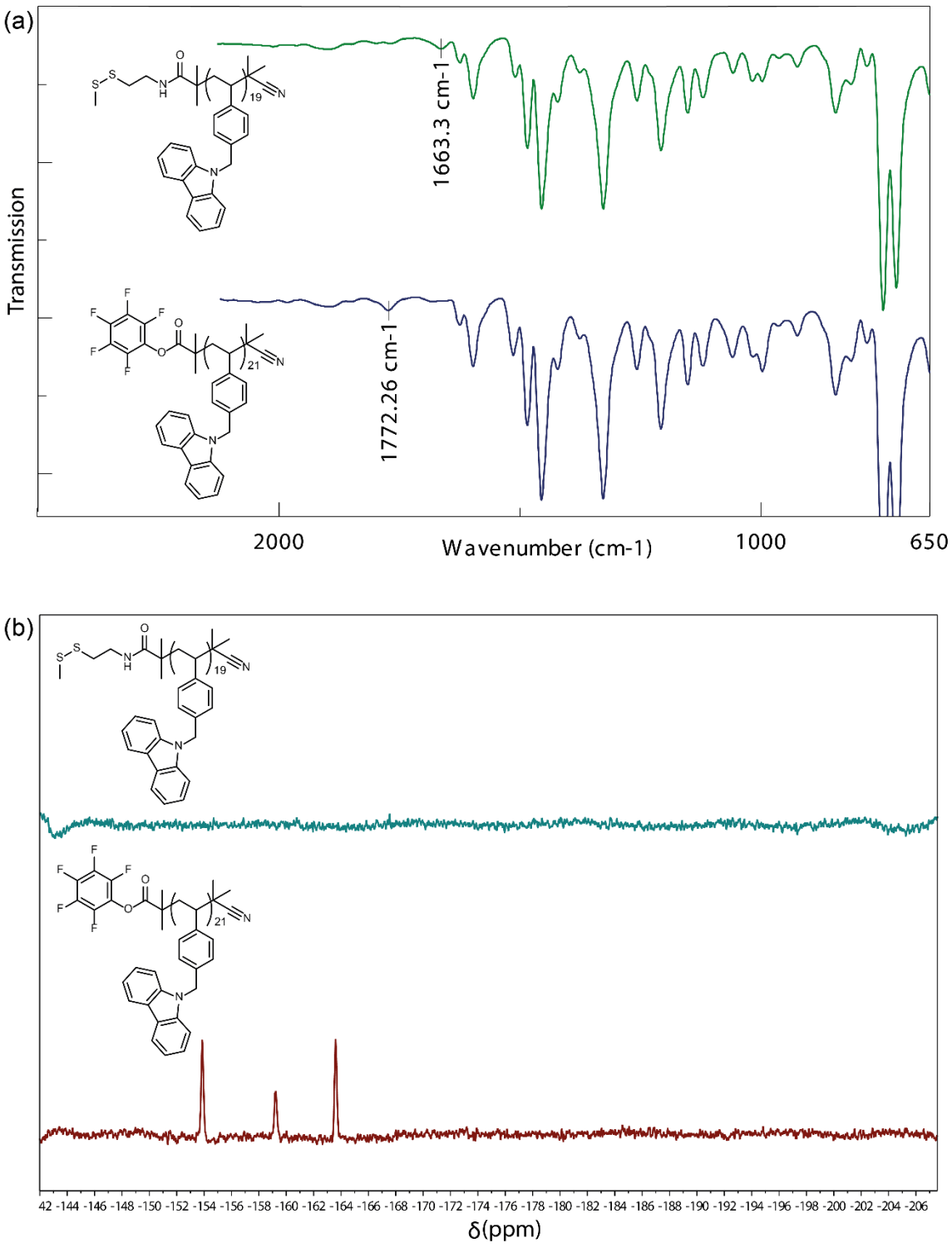

*Figure 3.1.9. IR spectra (a) and ^{19}F NMR spectra (b) of polymer **P2** before and after the post-polymerization modification reaction.*

3.1.2.2 Synthesis of Side-Chain Conjugated Polymers with an Anchor Block

The presence of the multiple anchor groups (anchor block) instead of only one anchor group facilitates the formation of more stable polymer functionalized QDs.[2] Therefore block copolymers containing an electroactive block and an anchor block were synthesized. The electroactive homopolymers were synthesized by RAFT polymerization using the chain transfer agent 2-cyano-2-propyl dodecyl trithiocarbonate and monomers **M1** and **M2** (Scheme 3.1.6). Varying the ratio of the monomers, polymers with different chain lengths were produced. (Table 3.1.3).

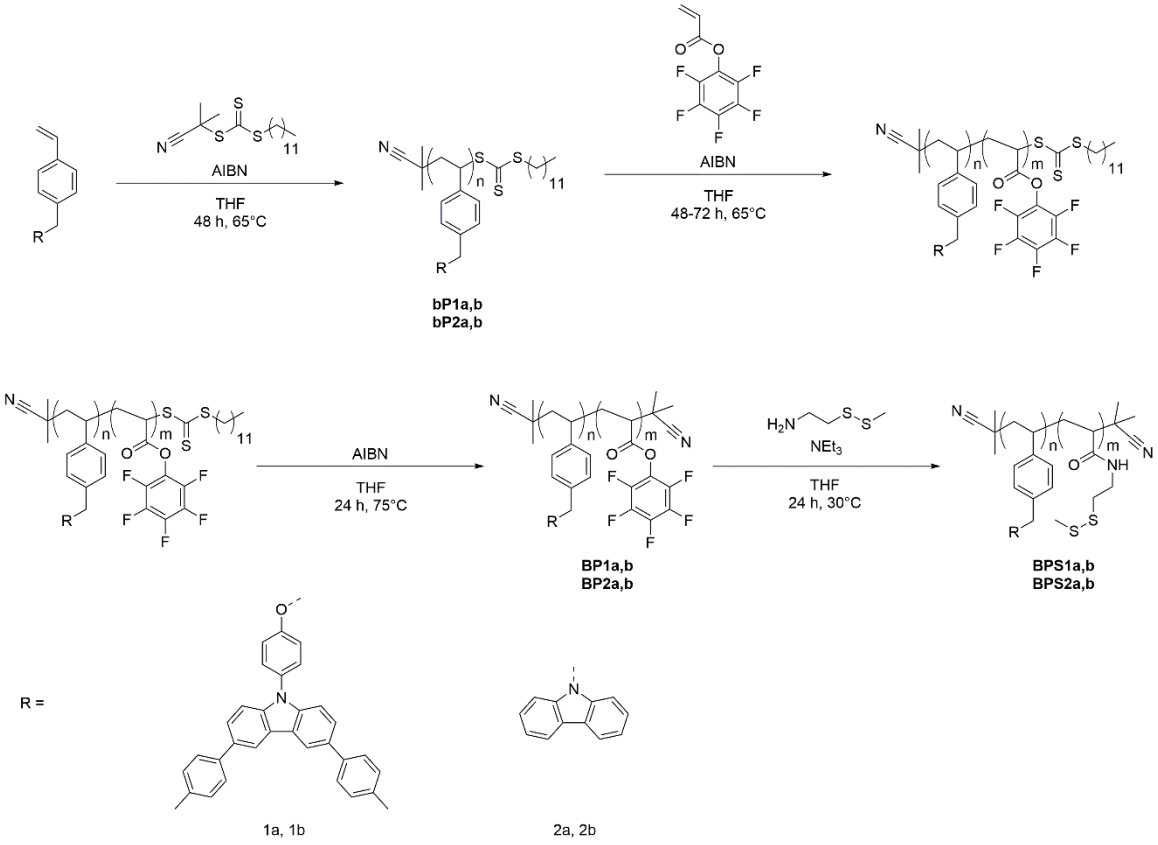

*Scheme 3.1.6. RAFT polymerization and post-polymerization modification reactions of blockcopolymers **BPS1a, b** and **BPS2a, b**.*

Table 3.1.3. Summary of the electroactive homopolymers. a: obtained by GPC measurements in THF with polystyrene as standard.

Polymer	M_n[a]	P_n	PDI[a]	Monomer	Monomer eq	CTA eq	AIBN eq	Solvent
bP1a	11200	20	1.1	M1	80	1	0.143	THF
bP1b	23700	43	1.2	M1	120	1	0.143	THF
bP2a	5900	21	1.2	M2	90	1	0.167	THF
bP2b	11300	40	1.2	M2	240	1	0.143	THF

Subsequently, the homopolymers were used as the macrochain-transfer agents and second blocks containing pentafluorophenyl ester groups were synthesized (Table 3.1.4). The successful polymerization of the second block was confirmed by the presence of C=O band in IR spectroscopy and the presence of pentafluorophenyl signals in ^{19}F NMR spectroscopy analogous to the polymers **P1**-**P2** in section 3.1.2.1. The intensity of the C=O band at 1784 cm^{-1}) for **BP2a** with a pentafluorophenyl ester block is higher than the peak intensity of polymer **P2** which has an equal number of electroactive groups but only one pentafluorophenyl ester functionality (Figure 3.1.10). The difference in intensities indicates the successful incorporation of multiple pentafluorophenyl ester groups in **BP2a**.

Table 3.1.4. Summary of the blockcopolymers consisting of the electroactive block and the pentafluorophenyl containing block. a: obtained by GPC measurements in THF with polystyrene as standard, b: determined by ^1H NMR spectroscopy. c: could not be determined due to the low intensity of the signals of poly (pentafluorophenylacrylate) block.

Polymer	M_n[a]	PDI[a]	1st Block	m/n[b]	PFPA eq	CTA eq	AIBN eq	Solvent
BP1a	11100	1.1	bP1a	-[c]	60	1	0.125	THF
BP1b	23300	1.2	bP1b	-[c]	100	1	0.125	THF
BP2a	6300	1.2	bP2a	0.25	80	1	0.125	THF
BP2b	11500	1.2	bP2b	0.08	80	1	0.125	THF

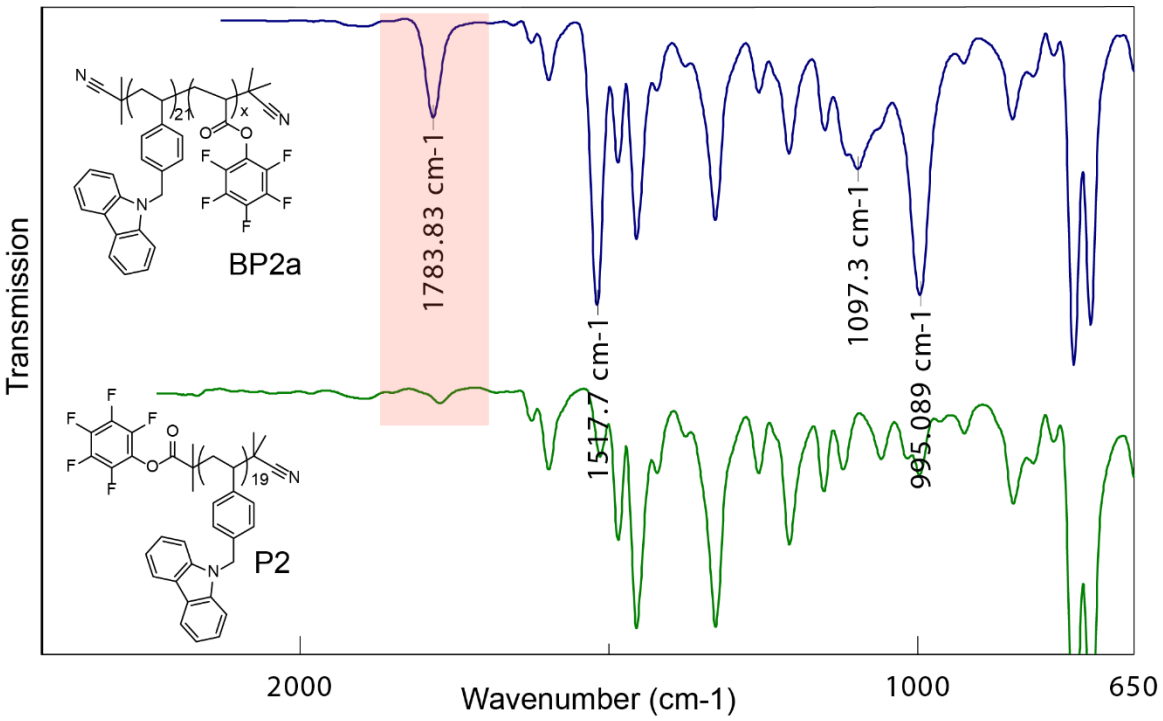

*Figure 3.1.10. IR spectra of polymers **BP2a** and **P2**.*

Additionally, the peaks at 1518, 1097 and 995 cm^{-1} corresponding to pentafluorophenyl groups become clearly visible. Similar characteristics were obtained for other block copolymers. Moreover, the presence of polyacrylate backbone signals at 2.13, 2.53, 2.87 and 3.09 ppm in ^{1}H NMR spectra verifies the formation of the poly(pentafluorophenylacrylate) block (Figure 3.1.11 b). The comparison of the integral ratios of the aromatic signals of carbazole groups with the signals of the polyacrylate backbone enables the estimation of the ratio between the two blocks. However, in case of **BP1a** and **BP1b** the intensities of the signals of the poly(pentafluorophenylacrylate) block were too low for quantitative analysis. For the polymer **BP2a** the polymerization of the second block was furthermore confirmed by the shift of the polymer signal in GPC to higher molecular weight values (smaller elution volume) (Figure 3.1.12). A difference of the M_n of 400 mg ml^{-1} was detected. However, due to the different solubility of the blocks in THF and subsequent variation of polymer coil shape and size, the change in M_n cannot be directly correlated with the number of incorporated pentafluorophenyl repeat units. Due to the higher molecular weights of the polymers **BP1a**, **BP1b** and **BP2b** the relative change in the polymer size after the polymerization of the second block is less significant than in the case of polymer **BP1**. Therefore, no significant changes in the position of GPC peaks for polymers **BP1a**, **BP1b** and **BP2b** were obtained.

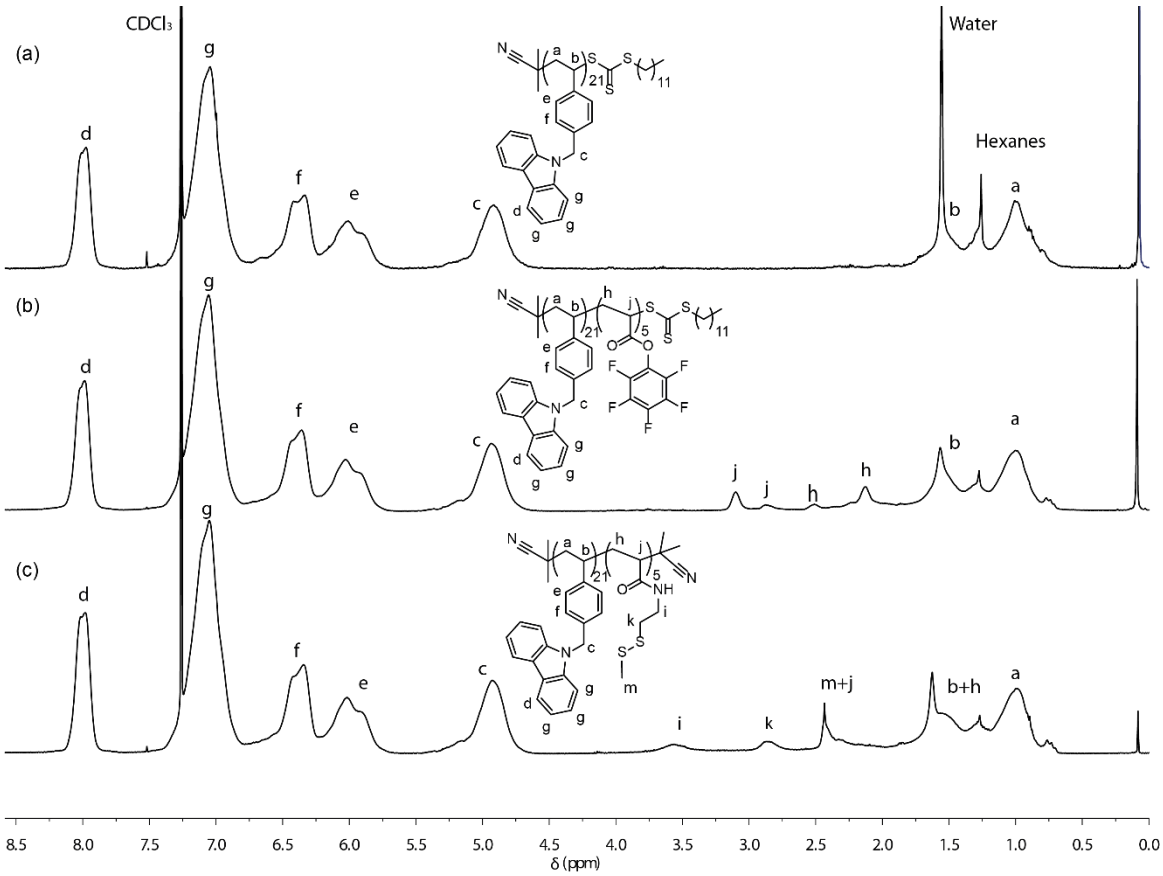

*Figure 3.1.11. ^{1}H NMR spectra of homopolymer **bP2a** (a), block copolymer **BP2a** with poly(pentafluorophenylacrylate) block (b) and block copolymer **BPS2a** with the anchor block (c).*

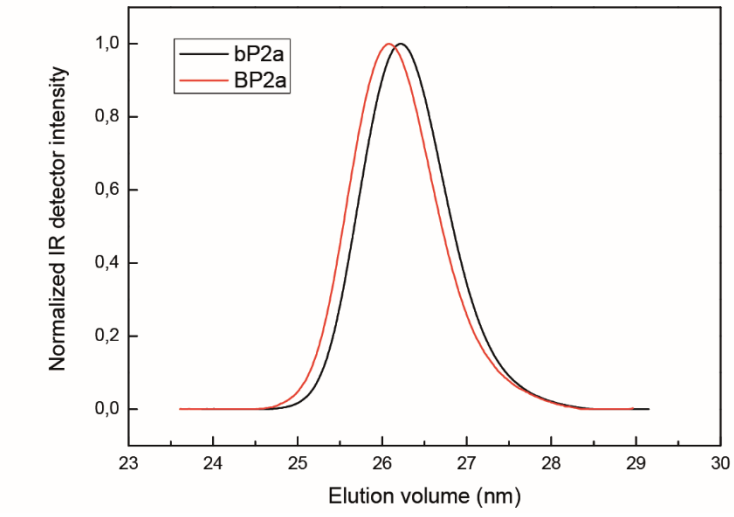

*Figure 3.1.12. GPC IR detector traces of the polymers **bP2a** and **BP2a**.*

Moreover, the change in the shape of the polymer coil leads to M_n values which are smaller than the ones measured for the homopolymers **bP1a** and **bP1b.** Nevertheless, the presence

of C=O bands in IR spectroscopy and the presence of pentafluorophenyl signals in ^{19}F NMR spectroscopy verified the polymerization of the second block.

After the substitution of the reactive trithiocarbonate polymer end groups with an inert 2-cyanoisopropyl functionality the reaction of 2-methyldithio-ethylamine with the reactive pentrafluorophenyl ester groups led to block copolymers with disulfide anchor blocks **BPS1a, b** and **BPS2a, b**. For the complete conversion of ester groups to amides 100 eq. of 2-methyldithio-ethylamine (relative to the polymer) and 200 eq. of triethylamine were used. The formation of amides during the post-polymerization modification step was confirmed by ^{19}F NMR and IR spectroscopies analogous to the polymers **P1**-**P2** in section 3.1.2.1. Furthermore, the signals corresponding to the disulfide groups at 3.57, 2.86 and 2,43 ppm are present in the ^{1}H NMR spectra of block copolymers (Figure 3.1.11 c).

3.1.3 Polymer HOMO Level Influence on the Performance of Hybrid QLEDs

3.1.3.1 Semiconducting Polymers **P1-P3** as the Polymeric Components of the Hybrid Active Layers

The polymer comprised of monomers **M1**-**M3** were tested as the semiconducting polymers within the active layers of hybrid QLEDs (Figure 3.1.13).[171] To facilitate simplified comparison of properties of the produced QD/polymer hybrids and devices, the polymers used in the hybrid synthesis should have a similar number of electrochemically active groups (i.e. repeat units). Therefore, for the synthesis of hybrids **QH1**-**QH3** polymers with chain lengths of approximately 20 repeat units were chosen. (Table 3.1.5 Figure 3.1.14). Polymers **P1**-**P3** were synthesize from monomers **M1**-**M3** respectively. Prior to hybrid fabrication polymers were thoroughly characterized in terms of thermal, optical and electrochemical properties.

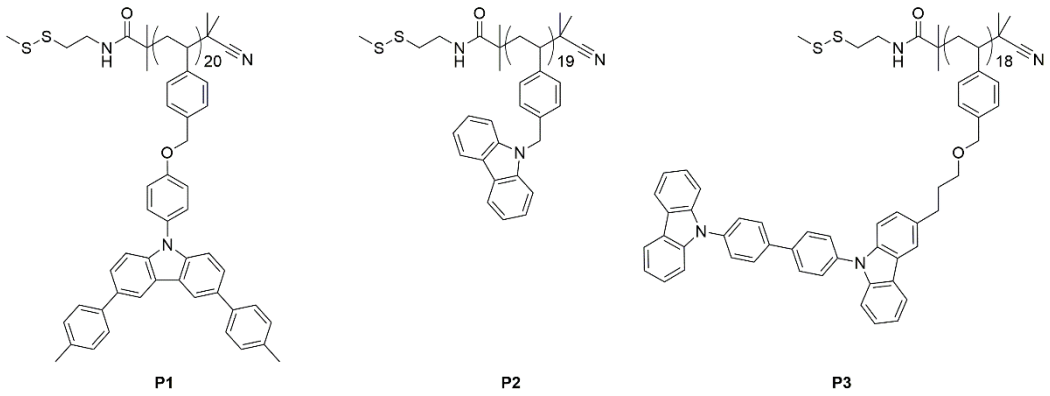

*Figure 3.1.13. Polymers **P1**, **P2** and **P3**.*

*Table 3.1.5. Summary of the properties of polymer **P1**, **P2** and **P3**. a. obtained by GPC measurements in THF with polystyrene as standard, b. decomposition temperature at 5% weight loss, c: glass transition temperature calculated with software fit, d: values obtained from UPS measurements, e: calculated as HOMO minus optical band gap, f: optical band gap.*

Polymer	**M_n (D)[a]**	**PDI[a]**	**P_n[a]**	**T_{d5} (°C)[b]**	**T_g (°C)[c]**	**HOMO (eV)[d]**	**LUMO (eV)[e]**	**Gap (eV)[f]**
P1	10900	1.1	20	400	190	5.52	2.24	3.28
P2	5300	1.2	19	380	155	5.78	2.32	3.46
P3	11600	1.1	18	390	160	5.82	2.45	3.37

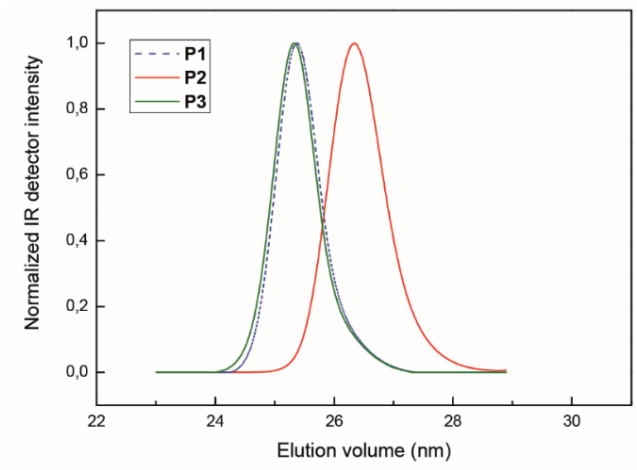

*Figure 3.1.14. GPC IR detector traces of polymers **P1**, **P2** and **P3**.*

3.1.3.1.1 Thermal Properties of Polymers **P1**-**P3**

The thermal properties of the polymers prepared in the present study were characterized using thermo-gravimetric analysis (TGA) and differential scanning calorimetry (DSC) (Figure 3.1.15).

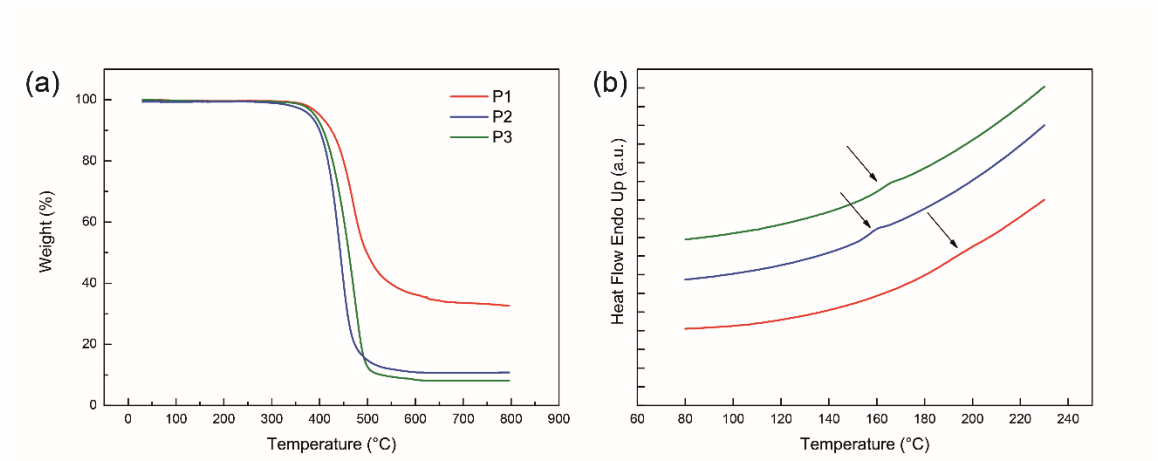

*Figure 3.1.15. Thermal properties of polymers **P1-P3**. Thermogravimetric analysis (a) and differential scanning calorimetry with arrows indication glass transition area (b). While the glass transition area of **P1** is barely visible on the graph, it was recognized by the DSC software.*

All three polymers **P1**, **P2** and **P3** possess high thermal stability with decomposition temperatures T_{d5} (temperature at which 5% of weight loss accrues) above 380°C with the highest thermal stability for **P1** with T_{d5} at 400°C (Table 3.1.5). **P1** also exhibits the highest glass transition temperature at 190°C along with 155°C and 160°C for **P2** and **P3**

respectively. We note that these T_g values are higher than the glass transition temperatures of hole transport layer materials based on carbazole-based small molecules.[40,172]

3.1.3.1.2 Optical Properties of Polymer **P1**-**P3**

The normalized solution and fluorescence spectra of the polymers are shown in Figure 3.1.16. The solution absorption spectrum of **P1** in toluene exhibits a broad absorption with a maximum centered at 295 nm along with a weak shoulder with the absorption onset at 378 nm. Upon excitation of the **P1** solution at 315 nm photoluminescence (PL) spectrum with the maximum at 397 nm is observed. The absorption spectrum of **P2** is consistent with previous reports of polymers containing carbazoles as side groups and exhibits the typical absorption pattern of the carbazole unit with maxima at 345, 331 and 295 nm and the absorption onset at 355 nm. The red-shifted absorption onset of **P1** compared to **P2** reflects the larger conjugated system of semiconducting side groups of the former polymer. The PL spectrum of **P2** shows two maxima at 365 and 352 nm (with λ_{ex} 310 nm). The absorption and PL spectra of **P3** exhibit only slight deviation from the characteristics of molecular CBP with the onset of absorption at 360 nm and two absorption maxima at 325 and 295 nm and the emission maximum at 390 nm (with λ_{ex} 315 nm).[47] From the onsets of thin film absorption spectra, the optical band gaps of **P1**, **P2** and **P3** were estimated to be 3.28, 3.46 and 3.37 eV, respectively.

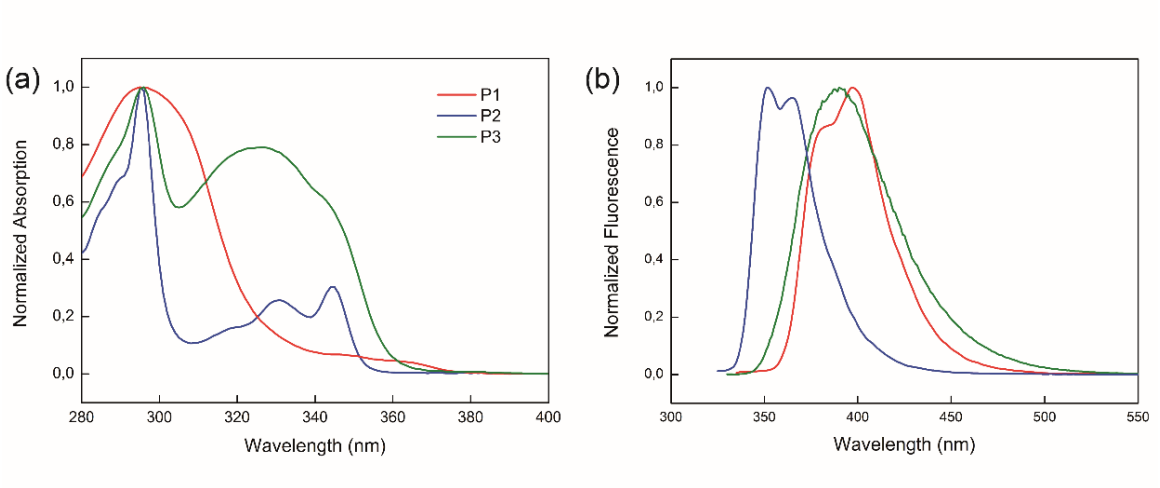

*Figure 3.1.16. Optical properties of polymers **P1**-**P3**. Normalized absorption in toluene (a) and normalized fluorescence in toluene (b).*

3.1.3.1.3 Electrochemical Properties of Polymers **P1**-**P3**

The HOMO levels of the polymers **P1**-**P3** were determined by ultraviolet photoelectron spectroscopy (UPS) measurements and estimated to be 5.52, 5.78 and 5.82 eV for **P1**, **P2**, and **P3**, respectively. Additionally, the electrochemical behavior of the polymers was studied *via* cyclic voltammetry in dichloromethane (Figure 3.1.17). The onset positions of the first polymer oxidation peaks are in agreement with the values obtained by UPS measurements with **P1** having the lowest oxidation potential, followed by **P2** and **P3**.

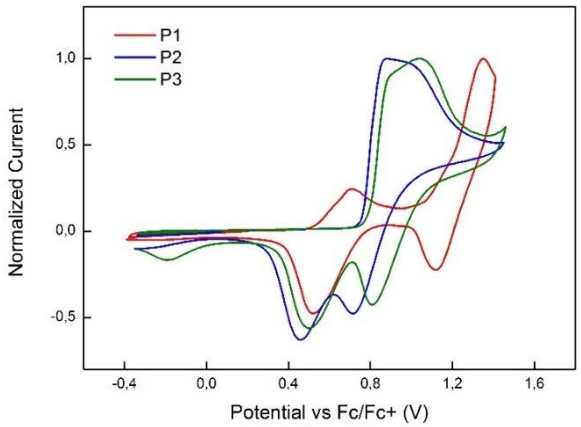

*Figure 3.1.17. Cyclic voltammogram of polymers **P1**-**P3** in DCM/TBAPF$_6$.*

In the analyzed electrochemical window **P2** exhibited one broad irreversible oxidation peak which is typical for carbazole structures with unprotected 3 and 6 positions (Figure 3.1.18 a).[47] In the second cycle a new oxidation peak with the onset potential of approximately 0.4 V is visible, indicating the formation of the new dimerized species with an extended π-system (section 1.3.1, Scheme 1.3.1).

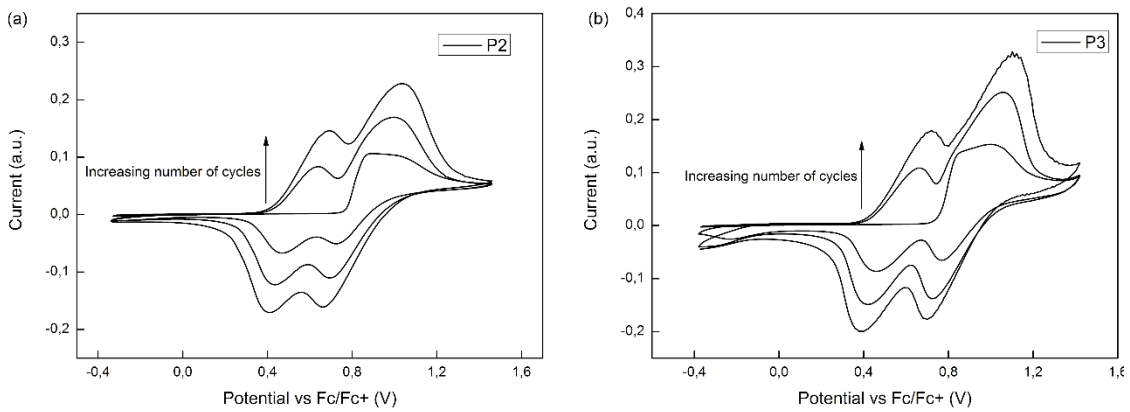

*Figure 3.1.18. Three consecutive cycles of cyclic voltammogram of polymers **P2** (a) and **P3** (b).*

The species with the extended π-system possess the HOMO level which is higher than that of the carbazole unit and thus oxidize at the lower potential. Similar electrochemical behavior is observed for the polymer **P3** (Figure 3.1.18 b). However, in the same voltage range **P1** with methyl protected 3 and 6 positions shows two distinct oxidation peaks with the first oxidation process being reversible and the second irreversible (section 3.1.1.1, Figure 3.1.5).

3.1.3.2 Synthesis of the Polymer/QD Hybrids **QH1**-**QH3**

The QD/polymer hybrids **QH1**, **QH2**, and **QH3** were prepared using CdSe/$Cd_xZn_{1-x}S$ red QDs (core 4 nm, total diameter 16 nm, synthesized in the group of [redacted], KIST, Seoul) and polymers **P1**, **P2** and **P3** respectively. The utilized QDs are type-I heterostructures which possess almost core-localized hole and electron wave functions, meaning that the absorption and PL properties of the QDs are determined by the size of CdSe core. In order to prevent inorganic/organic phase separation and to obtain films with a uniform QD distribution within the polymer matrices the QDs were functionalized with polymer chains by the ligand exchange procedure.[55] During ligand exchange the polymer disulfide end groups coordinate to the QD surface, substituting the oleic acid ligands initially coordinated and thus leading to the formation of polymer-modified QDs.[158,159,173] QDs with weakly bond oleic acid ligands are used in the ligand exchange as the initial small molecule ligands should possess weaker affinity to QD surfaces than the disulfide functionalities.

For the ligand exchange polymer and QDs were separately dissolved in small amount of toluene and subsequently combined. The reaction mixture was sonicated for one hour and ethanol was added. The formed sediment was dispersed in a small amount of toluene, sonicated for one additional hour and left at room temperature for 18 hours. Afterwards ethanol was added and the formed sediment was again dispersed in toluene and sonicated for one hour. After addition of ethanol the sediment was dried and dispersed in toluene to obtain QD/polymer 1 wt% polymer, 1 wt% QDs hybrid solution. The polymer ratio was deliberately kept high in the hybrid solutions in order to emphasize the impact of the polymer on the device performance. The ligand exchange procedure has only a minor impact on QDs optical properties, with PL profile remaining nearly unchanged (Figure 3.1.19 a). The course of the ligand exchange can be monitored by the solubility change of the QDs. The solubility change of QDs is governed by the types of ligands on the surface,

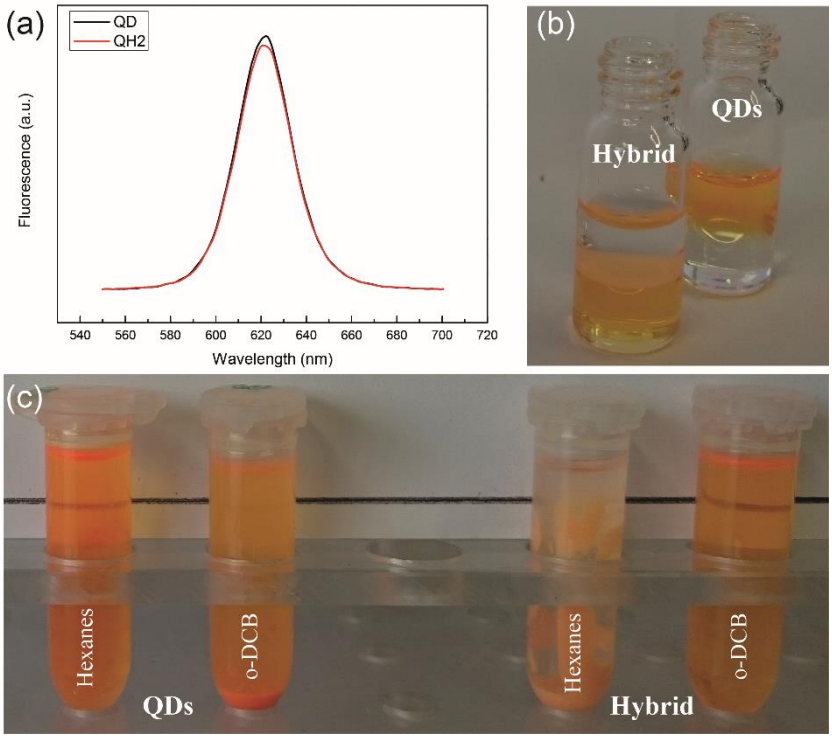

*Figure 3.1.19. Photoluminescence spectra of pristine QD solution and **QH2** QD/polymer hybrid solution in toluene with excitation wavelength of 425 nm (a). In (b) two phase system hexanes and o-dichlorobenzene and the respective solubility of pristine QDs with oleic acid ligands in hexanes and the hybrid **QH2** in o-dichlorobenzene is shown. In (c) hexane and o-dichlorobenzene were added to toluene solutions of initial **QD**s, and QD/**P2** polymer hybrid **QH2** (after the ligand exchange procedure). The initial QDs are well soluble in hexanes and only poorly soluble in o-dichlorobenzene. Due to the polymer chains grafted on the surface of QDs in the case of **QH2**, QD in **QH2** acquire the solubility properties of the polymer used and become insoluble in hexanes and well soluble in o-dichlorobenzene.*

thus after the ligand exchange procedure QDs acquire the solubility properties of the polymers grafted on their surface (Figure 3.1.19 b and c).

Polymers **P1**-**P3** are well soluble in *o*-dichlorobenzene and are not soluble in hexanes. While the pristine QDs with initial oleic acid ligands are well soluble in hexanes and only partly soluble in *o*-dichlorobenzene, the modified QDs with polymeric ligands become well soluble in *o*-dichlorobenzene and are no longer soluble in hexanes. Furthermore, the modified QDs can now be efficiently dispersed in the polymer matrices leading to films with improved QD distribution within the polymer compared with physically blended QD/polymer systems (Figure 3.1.20)[55,159].

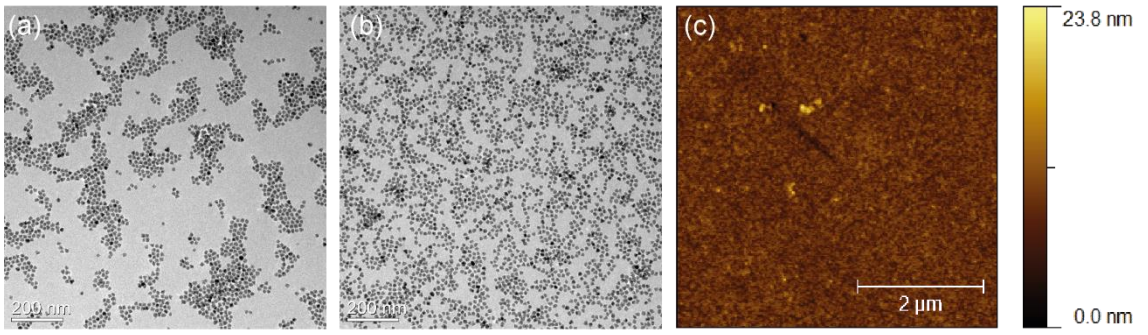

*Figure 3.1.20. An example of the influence of chemical grafting of a polymer onto a QD surface. TEM images (scale bar 200 nm) of spin cast films of (a) physically blended QD/polymer **P2** solution and (b) **QH2** QD/polymer hybrid prepared by ligand exchange procedure. The AFM image (scale bar 2 µm)of the spin cast film of **QH2** on glass substrate.*

3.1.3.3 Hybrid QLEDs with **QH1**-**QH3** Active Layers

To examine the impact of different polymers on QLED performance, devices with **QH1**, **QH2**, and **QH3** films as the active layers were fabricated in the inverted structure configuration: ITO(150 nm)//ZnO nanoparticles (40 nm)// QD@polymer hybrids (30 nm) // CBP (40 nm)//MoOx (10 nm)//Al (100 nm) (Figure 3.1.21, fabricated by [redacted], Department of Electrical Engineering, SNU). In the inverted architecture ZnO layer provides the electron transport from the ITO cathode, while CBP and MoOx layers are responsible for the hole transport from the aluminum anode.

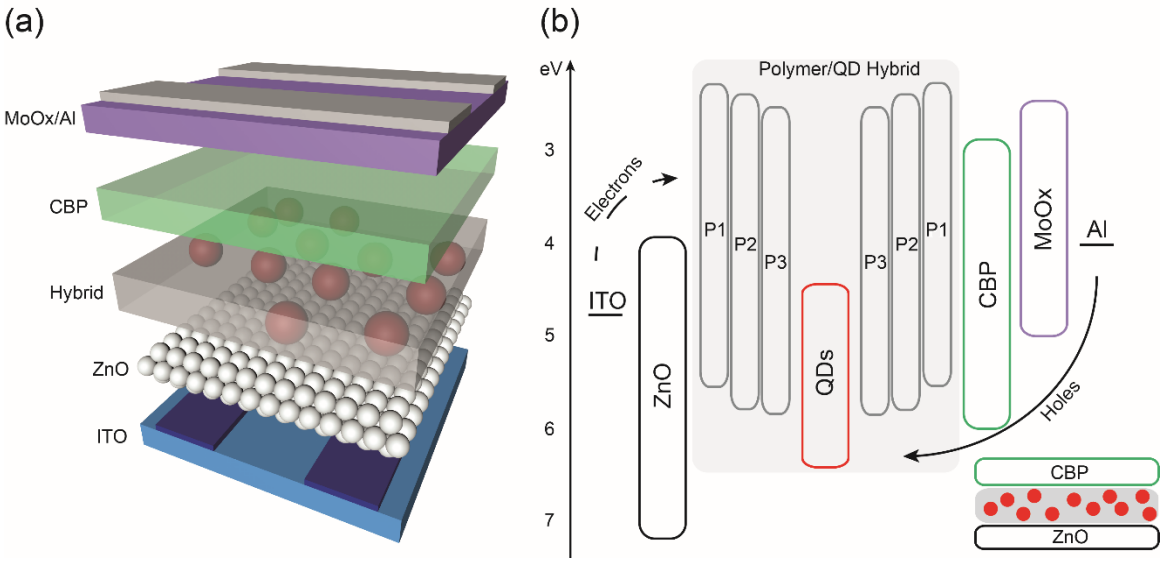

Figure 3.1.21. Schematic 3D device image (a) and schematic device energy diagram (b).

Figure 3.1.22 shows the characteristics (electroluminescence spectra, external quantum efficiency, current-voltage (J-V) and luminance-voltage (L-V) curves) of the devices fabricated in the present study. The results obtained show that the polymers synthesized can be successfully used in the active layer of QD/polymer hybrid LEDs leading to devices with good efficiencies while retaining the superior electroluminescence properties of QDs. As shown in Figure 3a all the devices tested show narrow electroluminescence spectra with Gaussian fits (λ_{max}= 630 nm, FWHM = 35 nm), indicating that light emission is solely originating from the quantum dots without parasitic emissions from the hybridized polymers or neighboring hole transport layers. A maximum external quantum efficiency (EQE) of 6.09% is achieved with the device containing the **QH3** active layer. An EQE of 6.09 % is, to the best of our knowledge, the highest reported EQE for LEDs with mixed QD/polymer active layers. The devices with **QH2** and **QH1** exhibit efficiencies of 5.05% and 2.14% respectively (Figure 3.1.22 b). Furthermore, the device with **QH3** also shows better performance in terms of both driving voltage and luminance in a wide range of applied voltages followed by **QH2** and **QH1** (Figure 3.1.22 b and c). This tendency is in agreement with the results previously published suggesting that polymers with low lying HOMO levels provide a reduced barrier for hole injection into QDs and lead to devices with improved characteristics.[159] Hybrid QLED performance is typically dependent on several factors including QD/polymer ratio, active layer morphology, charge carrier mobility and charge carrier injection into QDs. The results presented here indicate that among many other factors the HOMO energy of the polymer has a significant influence on device performance. As a consequence, polymers with appropriately low HOMO levels should be used in the active layers of hybrid polymer/QD QLEDs in order to fabricate efficient devices. Polymers **P2** and **P3** with HOMO levels of 5.78 eV and 5.82 eV, respectively, led to devices with high efficiencies which are comparable to the efficiencies of QD only devices fabricated utilizing analogous architectures.[10] However, a HOMO level of 5.52 eV determined for polymer **P1** is thought to be too high and led to a device with diminished performance.

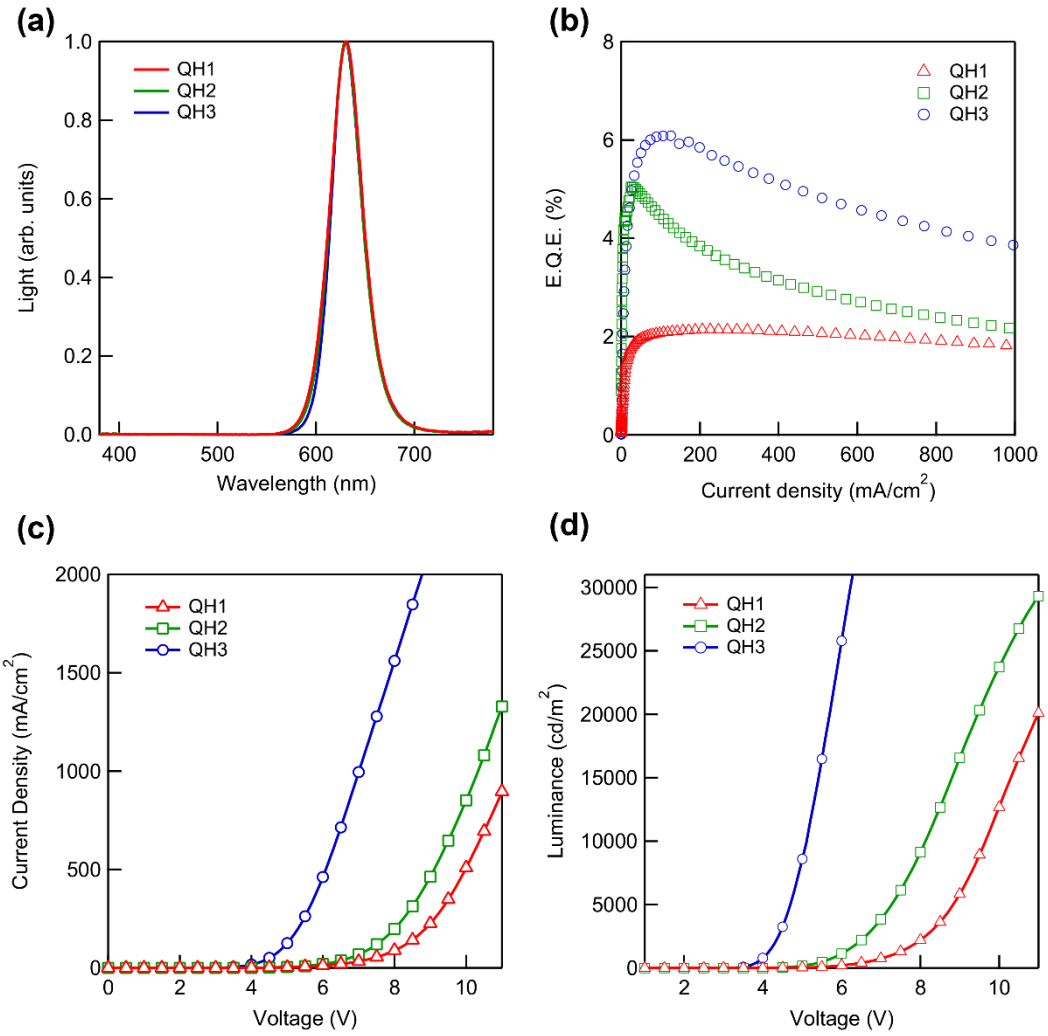

*Figure 3.1.22. Device characteristics with QD/polymer hybrids **QH1-QH3** as the active layer. a) Normalized electroluminescence intensity versus emission wavelength b) external quantum efficiency versus current density c) J-V characteristic d) luminance versus voltage characteristics.*

3.1.4 The Role of the Active Layer Morphology in the Enhanced Performance of Hybrid QLEDs

In this section the origin of the enhanced performance in hybrid QLEDs is investigated. Characteristics of hybrid devices with active layers comprised of polymers chemically grafted onto QDs are compared to conventional QD-only devices (hereafter referred to as reference) and to devices with physically blended polymer/QD active layer (hereafter referred to as blend). The morphologies of the active layer films are investigated by transmission electron microscopy (TEM) and atomic force microscopy (AFM). Furthermore, the device characteristics and photoluminescence properties are correlated with the morphology of the active layers.

3.1.4.1 Synthesis and Morphology Properties of Hybrids **H1**-**H4**

The QD/polymer hybrids **H1**-**H4** were prepared using red CdSe/$Cd_xZn1_{1-x}S$ QDs (core 4 nm, total diameter 9 nm, synthesized in the group of Dr. W. K. Bae, KIST, Seoul) and the block copolymer **BPS2a** containing an electroactive block and a disulfide-based anchor block (Figure 3.1.23). The utilized QDs are type-I heterostructures analogous to the QDs used in section 3.1.3.2. However, the shell of the QDs used for hybrids **H1**-**H4** is twice as thin as the shell of the QDs used in section 3.1.3.2. QDs with thinner outer shells lead to diminished devices performances once used as the active layers in QD-only QLEDs.[10] Therefore, the ability to enhance the performance of the devices utilizing QDs with thin shells is more lucrative.

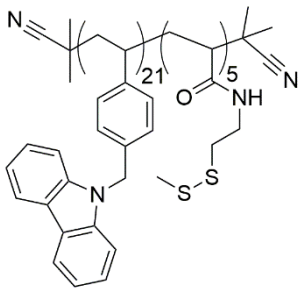

*Figure 3.1.23. Polymer **BPS2a**.*

The QD/polymer hybrids **H1**-**H4** were fabricated by the ligand exchange procedure during which the oleic acid ligands initially coordinated to the QD surfaces were replaced with **BPS2a** polymer chains. Moving from **H1** to **H4** the quantity of polymer in the hybrid was continuously decreased from 33.3 wt % to 11.1 wt % (Table 3.1.6).

*Table 3.1.6. Characteristics of hybrids **H1**-**H4**.a: RMS (root-mean-squared) roughness obtained by AFM measurements.*

	H1	H2	H3	H4	QDs
QD/Polymer ratio	1:0.5	1:0.375	1:0.25	1:0.125	-
RMS roughness[a]	1.24	1.44	1.34	1.31	2.60

Polymer and quantum dots were separately dissolved in small amount of chlorobenzene and subsequently combined. The reaction mixture was sonicated for one hour and ethanol was added. The formed residue was dispersed in a small amount of chlorobenzene, sonicated for one additional hour and left at room temperature for 18 hours. Afterwards ethanol was added and the formed residue was again dispersed in chlorobenzene and sonicated for one hour. After addition of ethanol the residue was dried and dispersed in toluene to obtain QD/polymer hybrid solution with total concentration of 19.8 mg ml^{-1}. During preparation the QD quantity was kept constant while the polymer quantity was varied, leading to the hybrids with various QD to polymer ratios. The hybrids prepared in this study contain polymer functionalized QDs as well as the free polymer.

In Figure 3.1.25 TEM and AFM images of the spin cast **H1**-**H4** films show that in all four hybrids QDs are evenly distributed within the polymer. The values of root-mean-squared (RMS) roughness of the hybrid films obtained from AFM measurements are lower than the RMS roughness of the film made solely from QDs. The decrease in the RMS roughness indicates the smoother surface of the hybrid films compared to the QD-only film. For comparison, TEM and AFM images of QD-only film are shown in Figure 3.1.24.

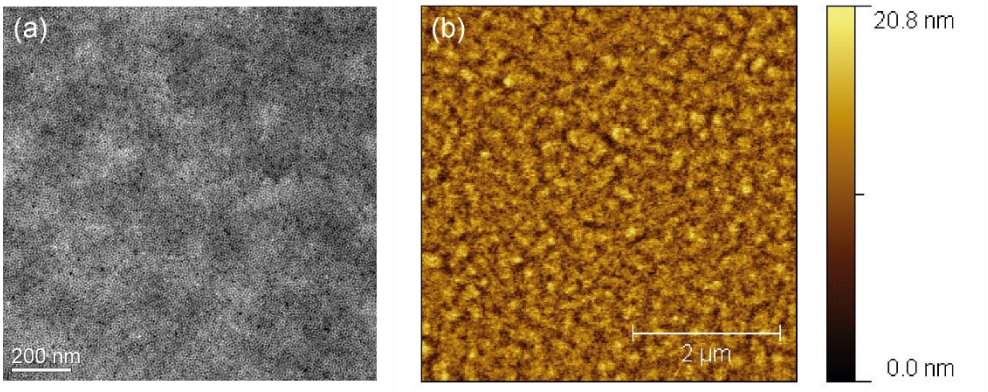

Figure 3.1.24. TEM images (a) and AFM height images (b) of QD-only films.

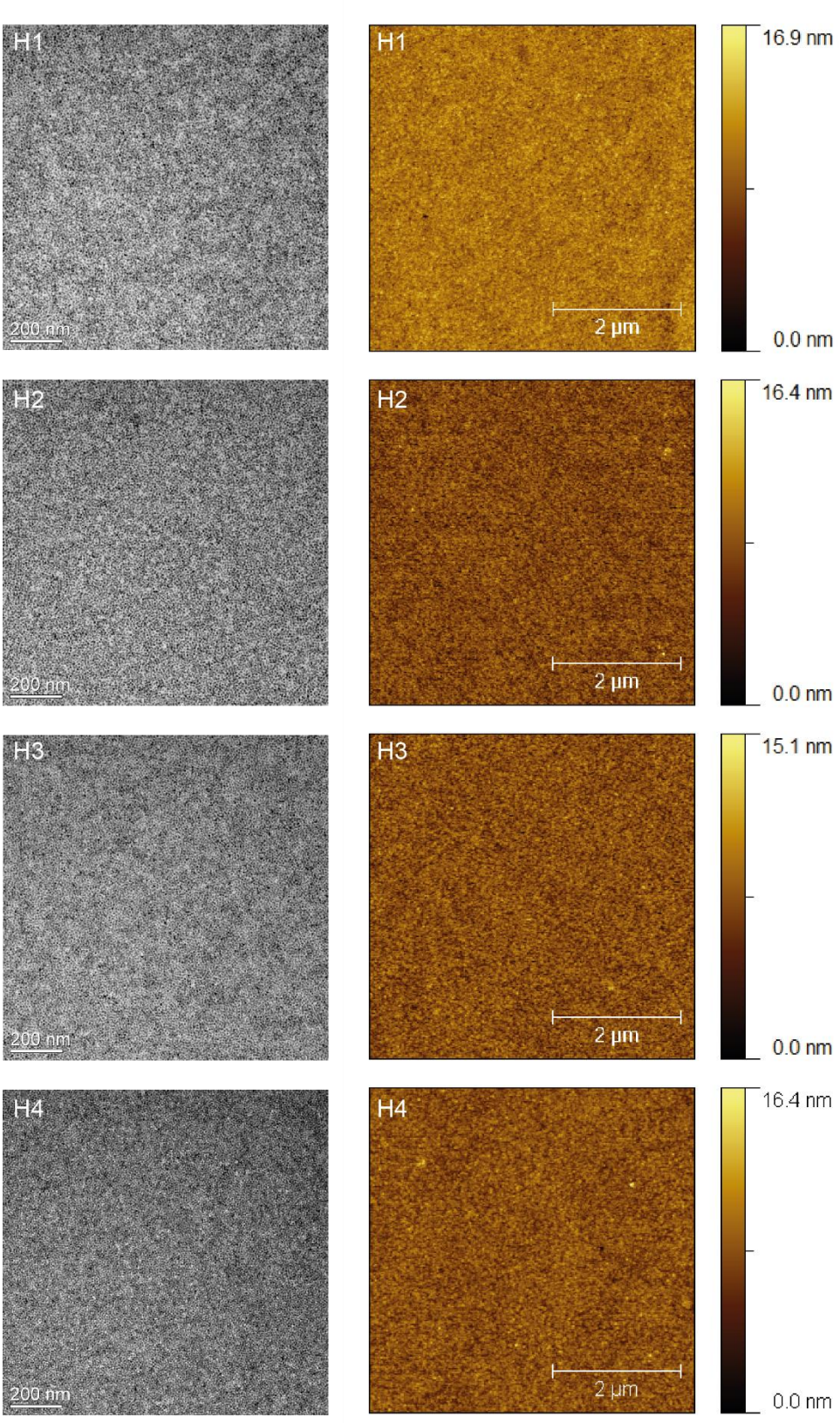

*Figure 3.1.25. TEM images (left, scale bar 200 nm) and AFM height images (right, scale bar 2 µm) of spin cast hybrid **H1**-**H4** films.*

The variation in the amount of polymer incorporated in different hybrids was verified *via* solid state absorption measurements of hybrid films. (Figure 3.1.26). The hybrids were spin cast onto quartz glass substrates and exhibited approximately constant thickness of 30 nm. The decrease in the absorption intensity of the peaks at 345 nm, 331 nm and 295 nm (which correspond to polymer **BPS2a** absorption) moving from **H1** to **H4** demonstrates the lessening polymer content.

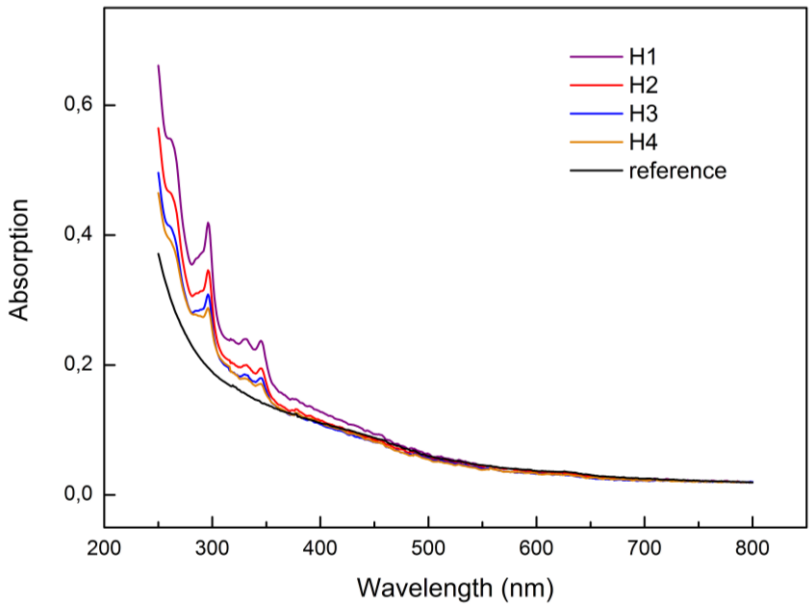

*Figure 3.1.26. Absorption of QD–only (reference) and hybrid **H1**-**H4** spin cast films.*

3.1.4.2 Hybrids **H1**-**H4** as the Active Layers in QLEDs

To investigate the electrical and optical characteristics of QLEDs with active layers containing QD/polymer hybrids **H1**-**H4** devices with inverted architecture [ITO (150nm)//ZnO nanoparticles (40nm)//hybrids emission layer (**H1**-**H4**) (30nm)// CBP (40 nm)//MoOx (10 nm)//Al (100 nm)] were studied (Table 3.1.7 and Figure 3.1.27, fabricated by Y. Lee, Department of Electrical Engineering, SNU). In this setup ZnO nanoparticle are responsible for electron transport from cathode to the hybrid emission layer, while CBP and MoO_x layers are employed as hole transport and hole injection layers, respectively. Through the adjustment of the experimental conditions the thickness of the active layer is kept nearly constant in all devices, meaning that moving from **H1** to **H4** the amount of polymer per unit area of the active layer decreases while the number of QDs increases.

*Table 3.1.7. Device characteristic of hybrid **H1-H4**. a: determined by ellipsometry.*

Active layer	**QD/Polymer ratio (wt%)**	**Film thickness[a] (nm)**	**V_{on}(V) (@1cdm^{-2})**	**Peak EQE(%)**	**@1000 cdm^{-2}**	
					V(V)	**J(mAcm^{-2})**
H1	1:0.5	33	3.1	3.3	6	30.27
H2	1:0.375	32	2.7	5.6	5	25.51
H3	1:0.25	31	2.4	4.3	4.7	43.44
H4	1:0.125	32	2.4	3.3	5	51.94

Device characteristics in Figure 3.1.27 show that polymer grafted QDs can be effectively utilized as the emission layer in QLEDs while maintaining electroluminescence characteristics of devices based on QD-only active layers. Regardless of polymer to QD ratios all devices show narrow electroluminescence spectra with Gaussian shape (λ_{max}= 639nm, FWHM = 33 nm) indicating that emission exclusively originates from the QDs without parasitic contributions from surrounding polymers or neighboring charge transport layers. In contrast to the electroluminescence spectra the electrical properties, luminance intensities and external quantum efficiencies (EQEs) are strongly affected by the change in the polymer content of hybrids with **H2** showing the best performance. As the polymer presence in hybrids effects multiple properties at the same time, the trade-off in the polymer quantity has to be found to lead to the device with the best characteristics. On one hand, an increase in the amount of polymer leads to the improvement in the

electron-hole balance as can be seen from the profoundly suppressed leakage current in the case of the **H1** and **H2** compared to **H3** and **H4** (Figure 3.1.27 d, left panel). On the other hand, the lower polymer amount provides devices with lower turn-on voltage. Decreasing the polymer content leads to the less hindered charge transport to the QDs which is reflected in the continuously dropping turn-on voltages, shown in the right panel of the Figure 3.1.27, with **H1** having the highest turn-on voltage of 3.1 V and **H4** having the lowest of 2.4 V.

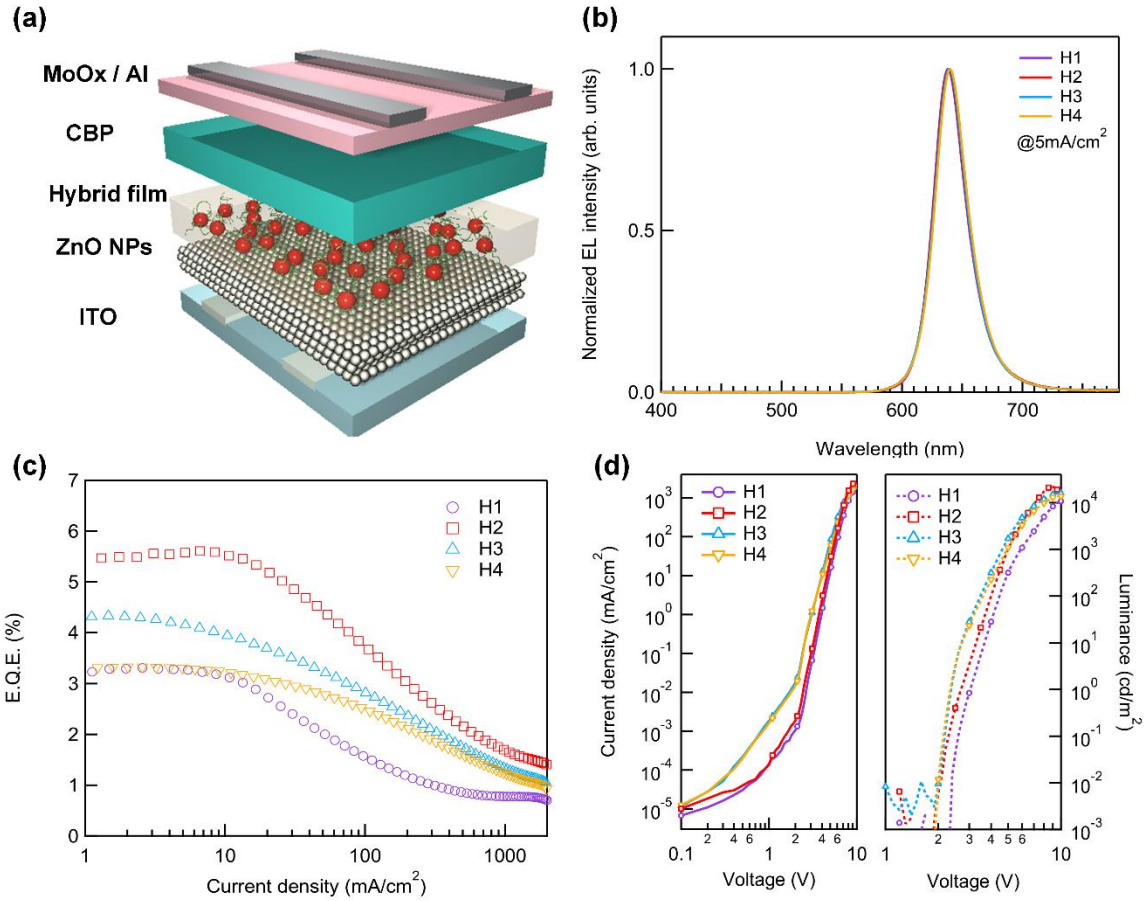

*Figure 3.1.27. Device characteristic of hybrid **H1-H4** QLEDs, 3D schematic device structure (a), normalized EL intensity (b), EQE vs. current density (c) and left: current density vs. voltage, right: luminance vs. voltage (d).*

Hybrid **H2** with the intermediate amount of polymer provides the best balance of electronic properties leading to a device with the best characteristics and an EQE of 5.6 %. It should be noted, that the hybrid devices presented in this study suffer from EQE roll-off in the region of higher applied voltages. The roll-off becomes more severe as the polymer content increases, suggesting that the incorporated polymer is the origin of the roll-off. We infer

that in high electric field regions the charge balance becomes disturbed due to the hole conducting properties of the polymer leading to the efficiency droop.

It is assumed that the improvement in the electron-hole balance of the hybrid devices originates from the electron blocking properties of the polymer **BPS2a**. To verify the electron blocking properties of **BPS2a** electron only devices (EODs) (devices were current flow is solely comprised of electrons) were studied (Figure 3.1.28). The ITO/Al/ZnO/active layer/ZnO/Al configuration of the EOD was used. At low voltages the EOD with QD-only active layer (reference) exhibits higher current density than hybrids, indicating that the presence of polymer suppresses the electron transport. Additionally, a gradual decrease of the leakage current with an increasing amount of polymer is observed further verifying the electron blocking abilities of the polymer incorporated.

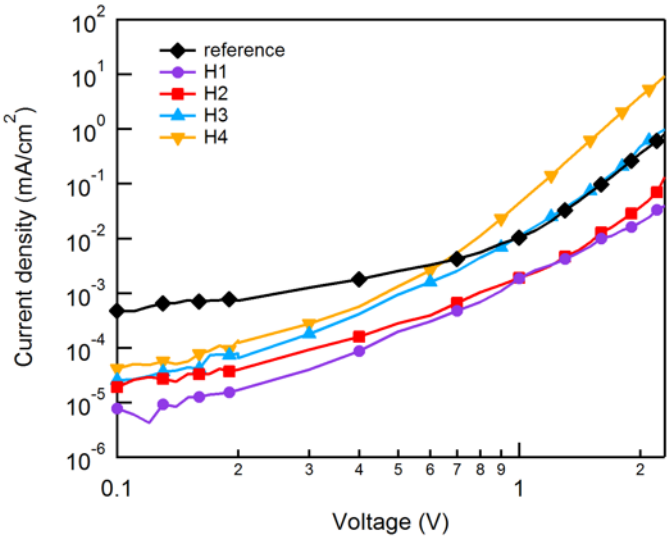

*Figure 3.1.28. Characteristics of electron only devices with QD-only (reference) and **H1**-**H4** active layers.*

3.1.4.3 Synthesis and Morphology Properties of Blends **B1**-**B4**

To compare the properties of QD/polymer hybrids with QD/polymer blends the blends **B1**-**B4** were prepared. **B1**-**B4** have the same QD to polymer ratios as hybrids **H1**-**H4** and consist of physically mixed QDs and the polymer **P2*** (modified **P2** with an inert butyl group instead of the reactive disulfide group) (Figure 3.1.29). The electrochemical properties of **P2*** are alike the polymer **BPS2a** used in hybrids. However, the absence of the anchor groups prevents polymer grafting to the QDs surface thus leading to systems which are only physically mixed.

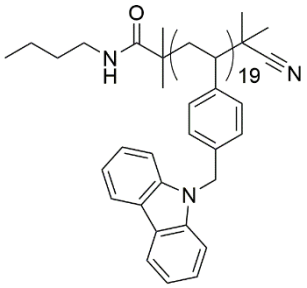

*Figure 3.1.29. Polymer **P2***.*

*Table 3.1.8. Characteristics of blends **B1**-**B4**.*

	B1	**B2**	**B3**	**B4**
QD/Polymer ratio	1:0.5	1:0.375	1:0.25	1:0.125
RMS roughness[a]	1.22	1.50	2.07	2.38

TEM and AFM images of spin cast **B1**-**B4** films in Figure 3.1.30 show QD aggregation. The immiscibility between polymer and QDs with short oleic acid ligands lead to the inorganic/organic phase separation and thus the formation of heterogeneous films. The heterogeneity of the **B1**-**B4** films can be better detected by AFM than TEM. TEM images show the distribution of QDs through the entire film thickness, which complicates the recognition of the phase separation in the vertical direction. With AFM only the surface of the film is investigated leading to the precise detection of the heterogeneous film surface. The phase separation also leads to the increase in the RMS roughness (Table 3.1.8).

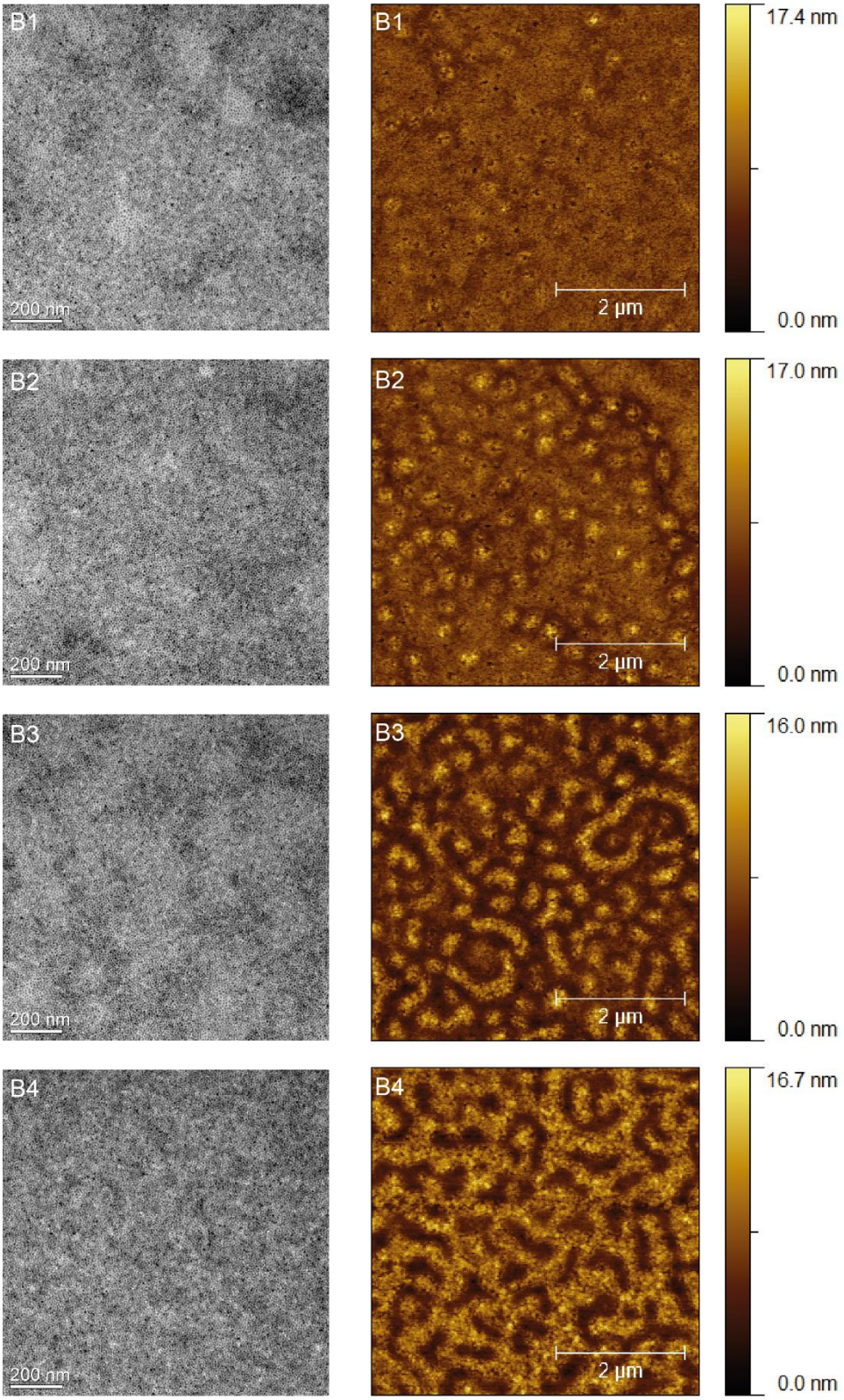

*Figure 3.1.30. TEM images (left, scale bar 200 nm) and AFM height images (right, scale bar 2 µm) of spin cast hybrid **B1**-**B2** films.*

3.1.4.4 Comparison of Hybrid LEDs with QD-Only and Blend Devices

Figure 3.1.31 and Table 3.1.9 show the device characteristics of QLEDs with QD-only (reference), hybrid **H2** and blend **B2** active layers.

*Table 3.1.9. Device characteristics of QD-only (reference) hybrid **H2** and blend **B2** QLEDs.*

Active layer	QD/Polymer ratio (wt%)	Film thickness[a] (nm)	V_{on}(V) (@1cdm^{-2})	Peak EQE(%)	@1000 cdm^{-2}	
					V(V)	J(mAcm^{-2})
reference	-	33	2.9	2.0	5.4	74.13
H2	1:0.375	32	2.7	5.6	5	25.51
B2	1:0.375	-	2.4	1.67	4.8	90.21

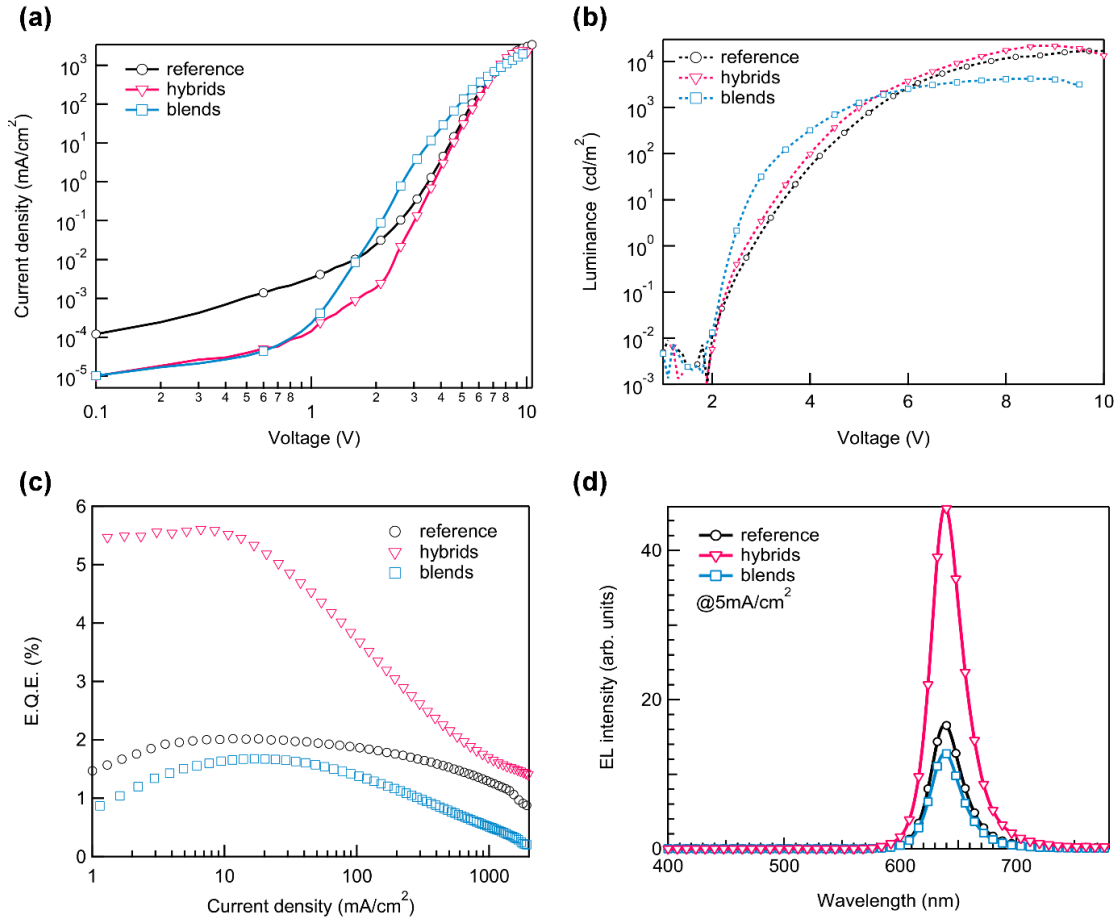

*Figure 3.1.31. Device characteristics of reference, hybrid **H2** and blend **B2** QLEDs. Current density vs. voltage (a), luminance vs. voltage (b), EQE vs. current density (c) and EL intensity (d).*

To provide the best comparison of device performance the device architectures of the hybrid, reference and blend devices were kept consistent. The devices with different active layers exhibit the same narrow electroluminescence emission profiles with the emission maximum at 639 nm, which solely originates from the QDs, however, different electrical properties in each case are observed. The hybrid device achieved an EQE of 5.6 % which is over two times higher than the EQE values of the reference and blend devices with 2.0 % and 1.67 %, respectively. Such a low EQE of the reference device compared to the state of the art QLEDs is not surprising and well in agreement with previously published results if the thin outer shells of the QDs and the thickness of the active layer are considered.[174] Additionally, the maximum luminance was increased from 16843 cd/m^2 and 4207 cd/m^2 for the reference and blend respectively to 21707 cd/m^2 for the hybrid. The improvement of the maximum luminance of the **H2** hybrid device compared to the reference becomes even more significant considering that due to the presence of the polymer the hybrid active layer has a smaller total amount of QDs per area compared to the QD-only film of the same thickness. Hybrid **H2** and blend **B2** were chosen as the representative examples of hybrid and blend devices, however, it should be noted that all hybrid devices (**H1**-**H4**) show higher EQE values and brighter luminance than blend devices with the same QD to polymer ratios (**B1**-**B4**) (Figure 3.1.32). Moreover, while the device with **H2** shows the highest efficiency among the hybrids, all the hybrids **H1**-**H4** regardless of QD to polymer ratios lead to QLEDs with improved device performance compared to the reference.

The enhanced hybrid device performance could be attributed to the improved charge balance in the hybrid devices compared to the reference. The hybrid devices show reduced leakage current compared to the reference indicating the improved charge balance of the devices (Figure 3.1.31 a). The reduction in the leakage current is thought to be the consequence of the incorporation of a semiconducting polymer between the ZnO nanoparticles and the QDs. In the reference device, the QD-only active layer is sandwiched between CBP hole transport layer (HTL) and the electron transport layer (ETL) made of ZnO nanoparticles (Figure 3.1.33 a). Due to the energy barrier free electron injection and the field-assisted hole injection there is a constant presence of an excess of electrons in the QD layer. The presence of excess electron leads to exciton quenching *via* non-radiative Auger recombination and therefore efficiency loss in the QLED. In hybrid devices QDs are covered with the polymer **BPS2a** prohibiting the direct contact between ZnO layer and QDs (Figure 3.1.33 b).

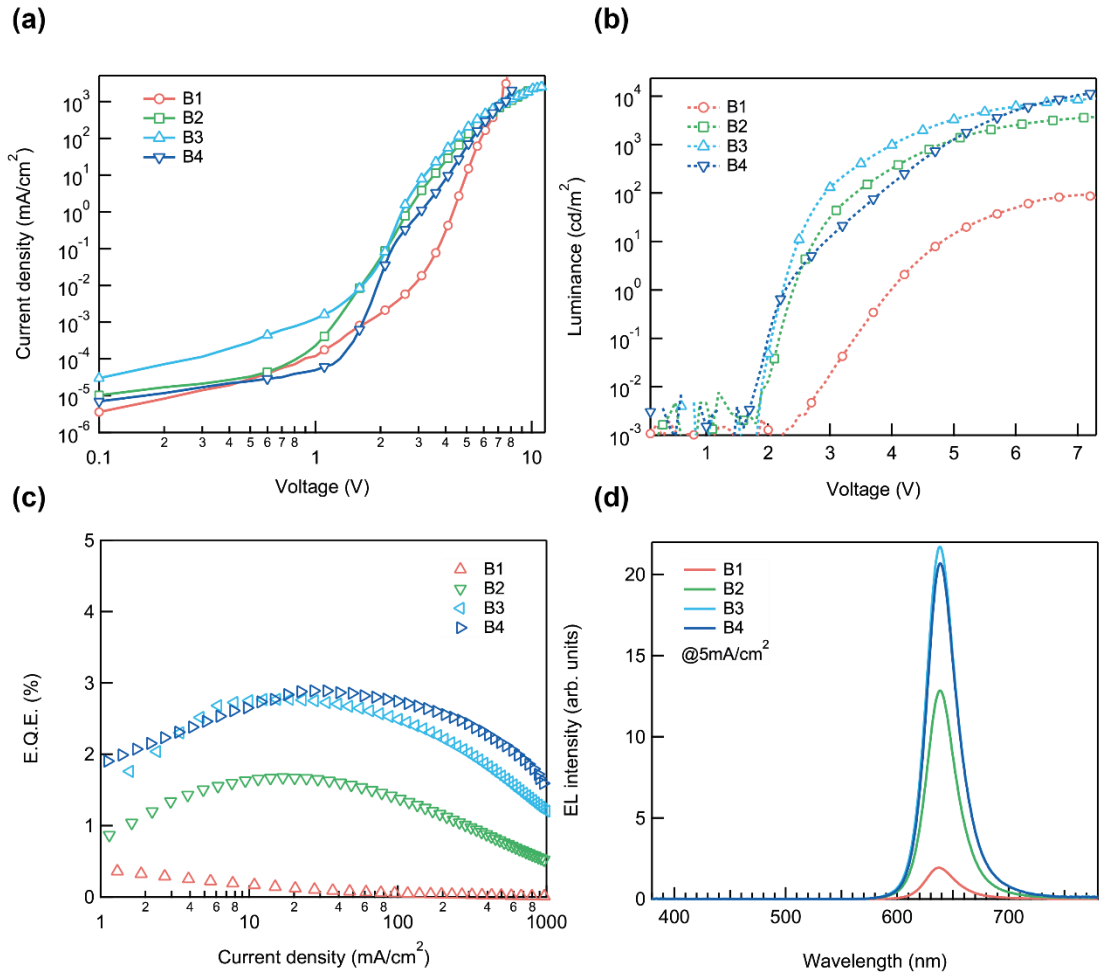

*Figure 3.1.32. Device characteristics of devices with **B1-B4** as the active layers. Current density vs. voltage (a), luminance vs. voltage (b), EQE vs. current density (c) and EL intensity (d).*

The **BPS2a** possesses a relatively high LUMO level of 2.32 eV which enables the suppression of the number of the injected electrons from ZnO into QDs compared to the reference. Additionally, due the hole conducting ability of the **BPS2a**, the polymer does not only provide the electron blocking properties but also enables enhanced hole transport within the active layer. The diminished amount of electrons injected into the QDs and the facilitated hole transport in the hybrid films improves the charge balance of the devices. The improved charge balance leads to the suppression of non-emissive Auger recombinations and thus to the observed increase in the device efficiencies.

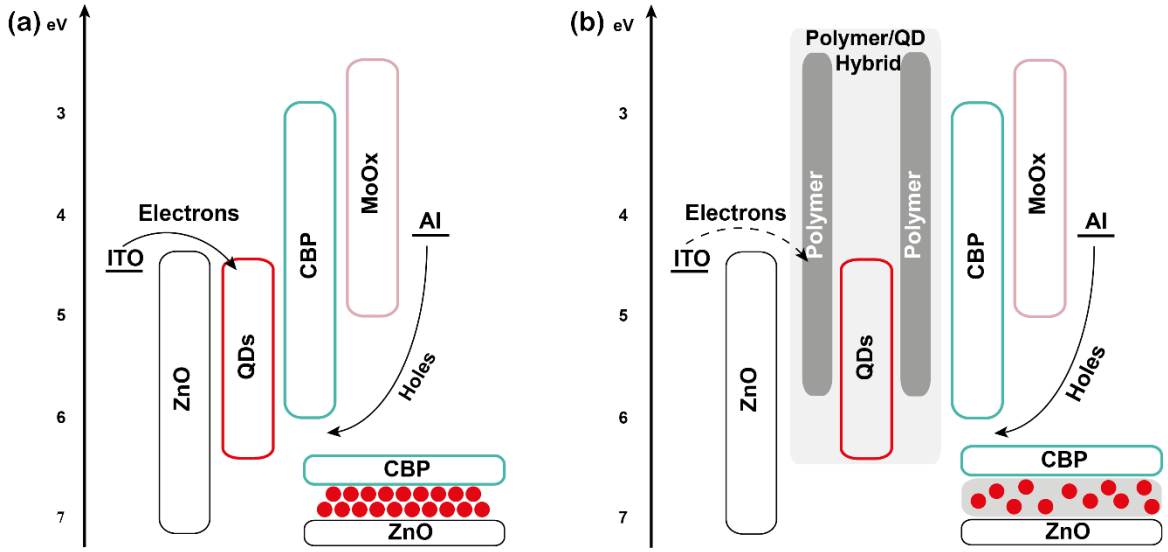

Figure 3.1.33. Energy diagrams of QD-only (reference) (a) and hybrid (b) devices. Inset shows the schematic cross section of the active layer with the adjacent hole and electron transport layers.

The difference in the characteristics of hybrid and blend devices originates from the differences in the morphology of the active layers. While in the hybrid film the QDs are homogeneously distributed within the polymer matrix, a significant phase separation between the organic polymer and inorganic QDs occurs during film formation of physically blended QD/polymer films (Figure 3.1.34). The phase separation leads to the formation of a very heterogeneous active layer film with some areas mostly filled with QDs (bright areas in the dark field scanning transmission electron microscopy (STEM) image of the device cross-section in Figure 3.1.34 c), while other areas consist primarily of polymer (dark areas in the cross-section STEM) with a very thin QD layer on top. The formed heterogeneous polymer interlayer between the QDs and the ZnO ETL still enables partial electron blocking leading to suppression of leakage current compared to the reference. However, the irregular polymer distribution and the varying interlayer thickness results in differing electron blocking abilities compared to the hybrid devices. Additionally, due to the changed morphology, the polymer does not contribute to the improvement of hole transport. Therefore, we believe that the special morphology of the hybrid films is the key to the optimized balance between electron and hole transport and to the associated improved device performance.

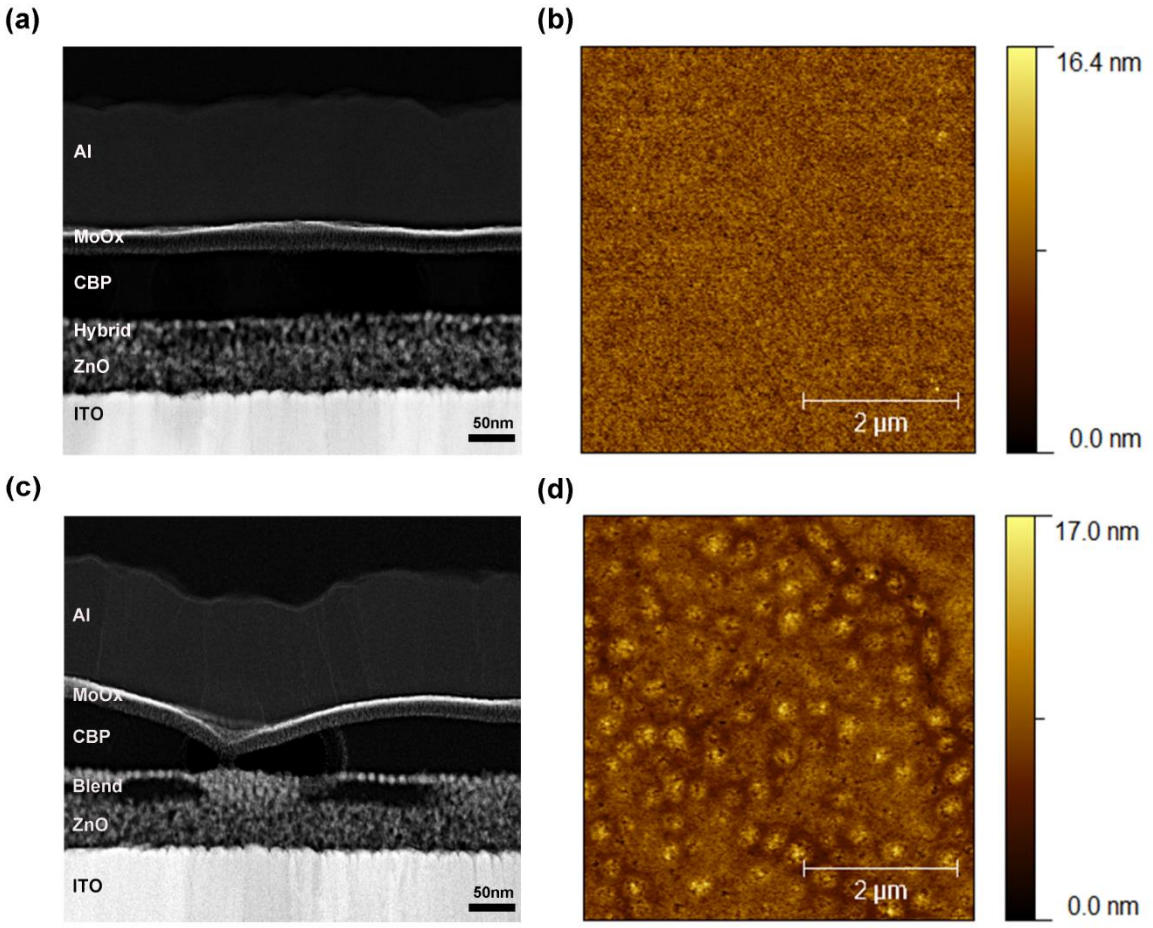

*Figure 3.1.34. The cross-section STEM image of hybrid **H2** QLED, scale bar 50 nm (a), AFM height image of the **H2** hybrid film on the glass substrate, scale bar 2 µm (b), the cross-section STEM image of blend **B2** QLED, scale bar 50 nm (c), AFM height image of the **B2** blend film on the glass substrate, , scale bar 2 µm (d).*

3.1.4.5 QD PL Decay Measurements in Devices

To further elucidate the reasons for the enhanced device performance in the hybrid devices, PL decay dynamics of the active layers were investigated. Photoluminescence (PL) decay measurements in solution (Figure 3.1.35 a) show the QD PL lifetimes of all three systems have a constant value of approximately 25 ns indicating that the exciton decay dynamics are preserved throughout hybridization and blending processes. However, QD PL decay measurements of active layer films within the QLEDs show a different tendency. QD PL lifetimes in all three films are drastically decreased compared to the PL lifetimes in solutions with blend and QD-only films being more affected than the hybrid film (Figure 3.1.35 b).

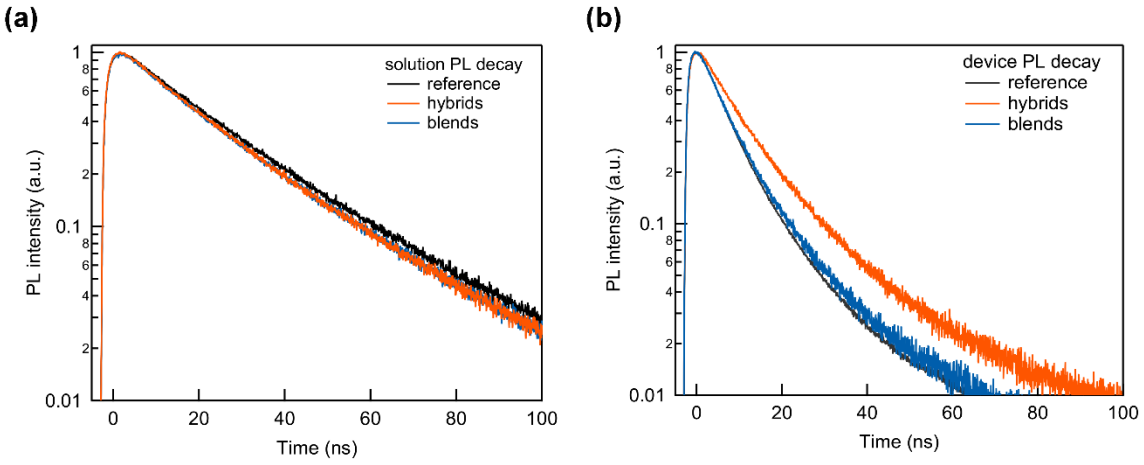

*Figure 3.1.35. QD PL-decay dynamics of QDs with oleic acid ligands (reference), hybrid **H2** and blend **B2** in toluene (a) and as active layer in QLEDs (b).*

QD PL lifetime in the **H2** hybrid device was estimated to be 12.06 ns while in the **B2** blend device and reference lifetimes of 8.84 ns and 8.40 ns respectively were recorded. We believe that such a significant drop in the PL lifetimes is caused by two factors, the closer distance between QDs in solid films compared to solution and the direct contact between QDs and the ETL. In the case of the QD-only devices the QDs are packed closely together with short core to core distances, especially in the case of QDs with thin outer shells such as ones used in this study. In such closely packed systems energy transfer *via* FRET between the individual QDs can take place. FRET leads to exciton recombination through non-radiative decay pathways resulting in reduced PL QY of the affected QDs. Furthermore, due to the energetic proximity of ZnO and QD conduction bands a spontaneous electron injection into the QDs is possible and was previously shown to lead to the additional decay of QD PL.[84] The less profound decrease of PL lifetime in the case of hybrid films arises from the unique morphology of the active layer. The polymer incorporated between evenly distributed QDs increases the distance between individual QD cores leading to less efficient energy transfer and suppressed exciton quenching. The polymer simultaneously provides a separation layer between the QDs and the ZnO ETL preventing direct contact and spontaneous electron injection. Therefore, we conclude that the incorporation of QDs within a polymer matrix leads to suppressed energy transfer, longer PL lifetimes, and associated improved device performance. In the blend devices the loss in PL lifetime remains comparable to the reference due to the significant phase separation between the QDs and the polymer. Here the polymer presence neither leads to increased QD-to-QD distance nor provides an uninterrupted barrier between ZnO and QDs.

3.1.4.6 Morphology and Device Performance of Two-Component Polymer/QD Systems containing Polymers with One Anchor Group

Polymer **P2**/QD two-component systems (**A1**-**A4**) containing the polymer **P2** (Figure 3.1.36) with one disulfide anchor group and red QDs (CdSe core with diameter of 4 nm, $Cd_xZn_{1-x}S$ shell, total diameter 9 nm) were synthesized in the same way as hybrids **H1**-**H4** (section 3.1.4.1). **A1**-**A4** were developed to investigate the influence of the quantity of anchor groups on the hybridization of QDs. **A1**-**A4** have the same QD to polymer ratios as hybrids **H1-H4** (Table 3.1.10).

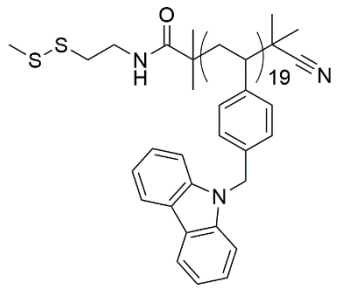

*Figure 3.1.36. Polymer **P2**.*

*Table 3.1.10. Characteristics of **A1**-**A4**.*

	A1	**A2**	**A3**	**A4**
QD/Polymer ratio	1:0.5	1:0.375	1:0.25	1:0.125
RMS roughness[a]	1.10	1.32	1.65	1.32

The aggregation of QDs can be seen in the TEM and AFM images of the spin cast films, resembling the morphologies of the films of the blends **B1**-**B4.** It should be noted that the amount of the aggregation in **A1**-**A4** films is less profound than in **B1**-**B4** films, which is also supported by the lower values of RMS roughness. The phase separation in **A1**-**A4** films is the result of the insufficient hybridization of QDs. In section 3.1.3.2 the use of high polymer ratios (polymer:QD 1:1) and large QDs (diameter 16 nm) with relatively small surface area led to the efficient ligand exchange between QDs and polymers **P1**-**P3** with one achor group. However, due to high QD ratios and high surface area of small QDs in the case of **A1**-**A4** polymer **P2** did not lead to the efficient ligand exchange.

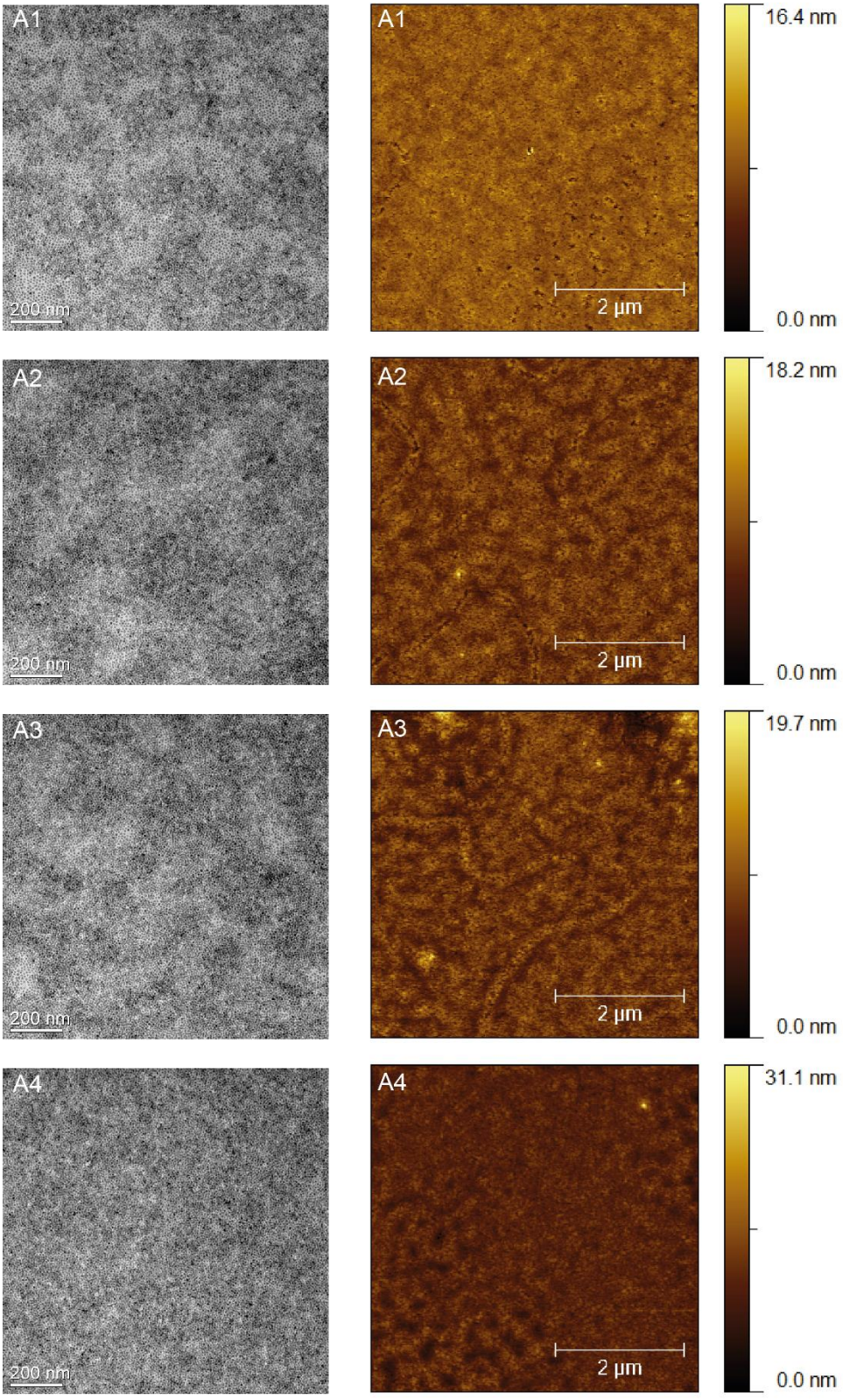

*Figure 3.1.37. TEM images (left, scale bar 200 nm) and AFM height images (right, scale bar 2 µm) of spin cast hybrid **B1**-**B2** films.*

Figure 3.1.38 shows the solubility of **H1**-**H4** and **A1**-**A4** in hexanes. Hybrids **H1** and **H2** are completely insoluble in hexanes, indicating that all QDs possess polymeric ligands. **H3** and **H4** have a very small amount of polymer unfunctionalized QDs which are soluble in hexanes. The unfunctionalized QDs lead to the light orange color of the solution. The bright orange color of the **A1**-**A4** solutions indicates the presents of a large amount of QDs which do not bear polymer ligands. The polymer unfunctionalized QDs aggregate during the film formation and lead to the phase separation observed in **A1**-**A4** films.

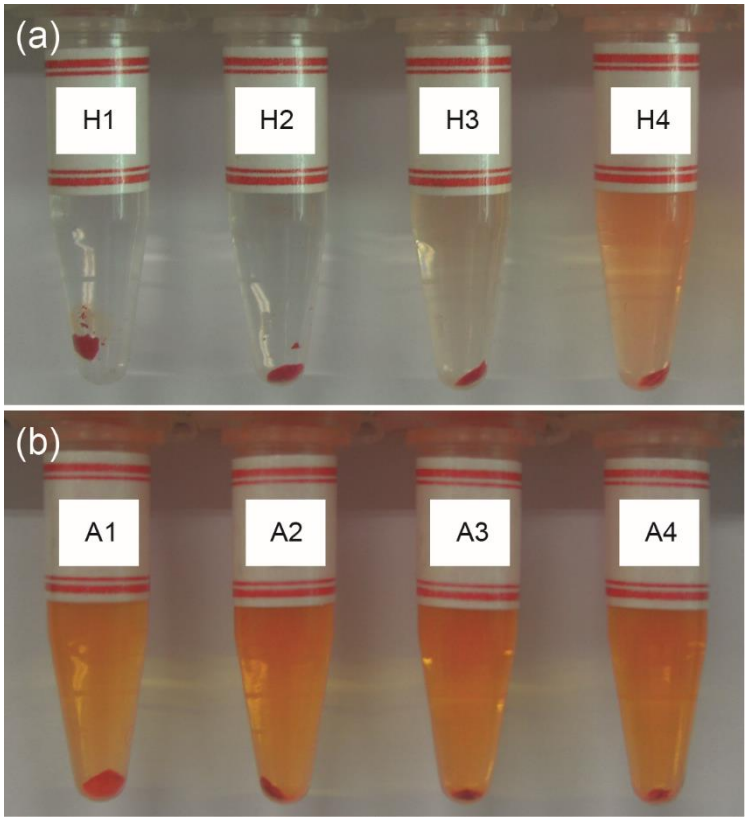

*Figure 3.1.38. Solubility of **H1**-**H4** (a) and **A1**-**A4** (b) in hexanes.*

The performances of the devices fabricated with **A1, A3** and **A4** (inverted device structure described in section 3.1.4.2) are lower than of the devices with **H1, H3** and **H4** (Figure 3.1.39). The attempts to fabricate device with **A2** as the active layer remained unsuccessful. The diminished device performance is not surprising considering the results presented in the section 3.1.4.4, which suggest that homogeneous distribution of QDs within the polymer is required for achieving high EQEs. Moreover, the results in this section even further support the importance of QD hybridization for the fabrication of efficient QLEDs.

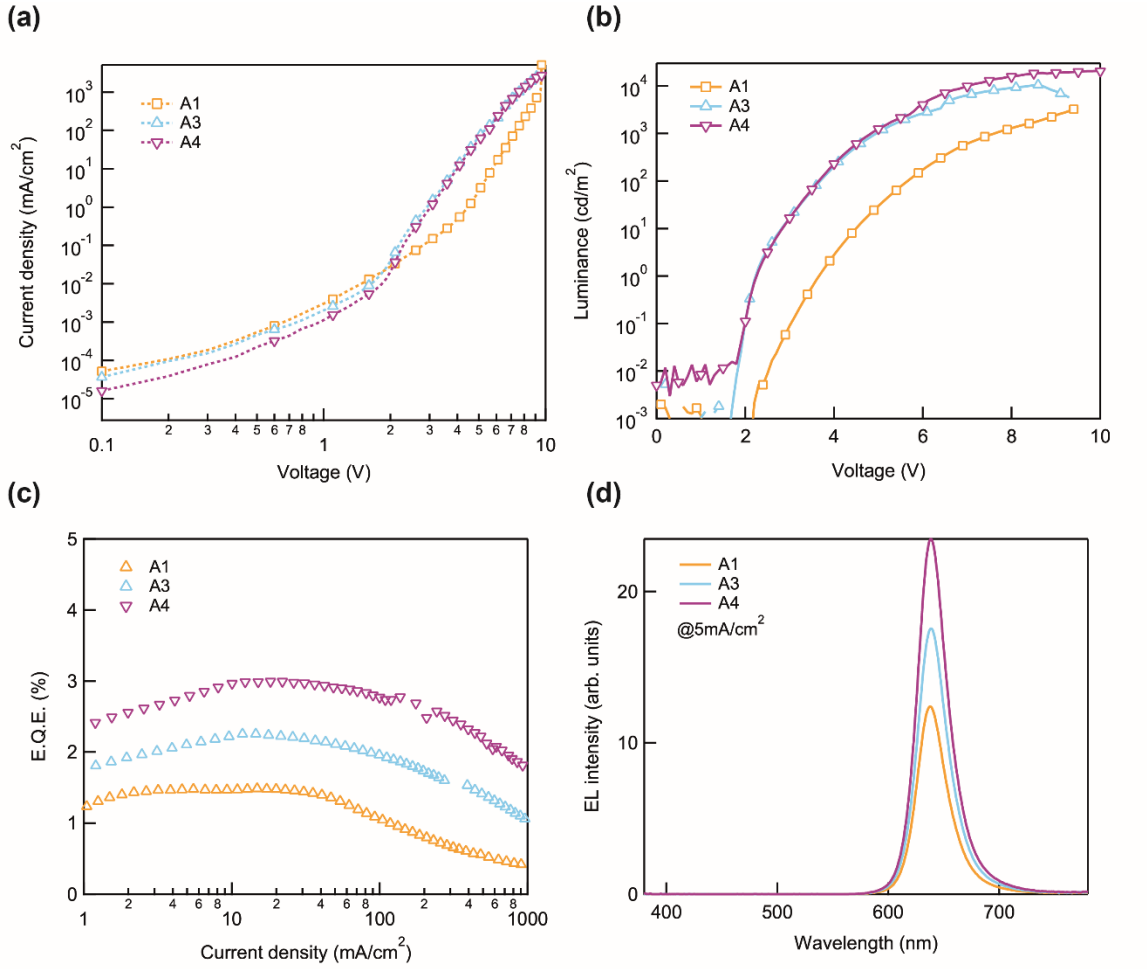

*Figure 3.1.39. Device characteristics of devices with **A1**, **A3** and **A4** as the active layers. Current density vs. voltage (a), luminance vs. voltage (b), EQE vs. current density (c) and EL intensity (d).*

3.1.5 Conclusion

The results presented in the section 3.1 indicate that improvements in QLED performance are possible with the use of hybrid semiconducting polymer/QD active layers. Polymers incorporated lead to the improved charge transport balance and reduced PL quenching of QDs. The application of various combinations of QDs, semiconducting polymers and device architectures will eventually enable the further development of hybrid QLEDs and will open their full potential.

The synthesis of new carbazole-based monomers with low-lying HOMO levels was developed. The monomers were further used in the RAFT polymerization to yield side-chain conjugated polymers for the use in hybrid polymer/QD LEDs. Polymers with defined molecular weights, narrow polydispersities, anchor end groups or anchor blocks were prepared. Depending on the substituents of carbazole unit thermal, optical and, electrochemical properties of the polymers were tuned. The disulfide anchor groups enabled the chemical grafting of the polymers onto a QD surface *via* the ligand exchange procedure leading to the formation of polymer/QD hybrids. Chemically blended QD/polymer hybrids were then tested as the active layers in LED devices and devices with high efficiencies and narrow electroluminescence profiles, solely composed of QD emission, were fabricated. The importance of polymer HOMO level adjustment for the development of efficient hybrid LEDs has been confirmed. The utilization of the polymers with low-lying HOMO levels is a precondition to obtained hybrid QLED with high EQEs. Moreover, it was demonstrated that great attention should be paid to the morphologies of polymer/QD systems as they have an enormous influence on the device characteristics and the improvement opportunities. Hybrid systems where polymers are chemically grafted to the QD surfaces lead to an even distribution of QDs throughout the entire active layer. It was revealed that such morphology is the key to the fabrication of QLEDs with improved charge transport balance and suppressed PL quenching.

3.2 Polymers with Lipoic Acid-Based Multidentate Anchor Groups

Due to their superior optical properties QDs are widely used in optoelectronic and biological applications. Directly after synthesis, the surface of commonly used high quality QDs is covered by small, hydrophobic ligands (e.g. oleic acid), however, for some applications QDs must be further modified with polymeric ligands to become compatible with the application environment. For example, for applications in the field of cellular imaging the initial hydrophobic QD ligands must be exchanged with polymeric hydrophilic ligands to stabilize the QDs in an aqueous medium.[2] Additionally, the strong interactions between the new ligands and nanoparticles is desirable for electronic applications. In the case of hybrid polymer/QD QLEDs the efficient grafting of the polymers onto the QD surface is prerequisite for the formation of the films with homogeneous QD distribution within the polymer matrix.[55] The homogeneous QD distribution is in itself a precondition for the preparation of devices with good performance characteristics. In hybrid organic/inorganic solar cells, the strong coordinating ability of the polymers to the surfaces of the QDs enhances the interaction area between the hole acceptors (polymers) and the electron acceptors (QDs) leading to more efficient exciton dissociation.[100]

The presence of multiple anchoring groups substantially improves the coordination efficiency of the polymer chains to the QD surface.[2] Due to the dynamic behavior of the interactions between the QD surface and the ligand polymeric ligands with one anchor group are significantly more prone to desorption from the QD surface. The chelating nature of polymeric ligands with multiple anchor groups diminishes the desorption probability, leading to a substantial increase in system stability.[116,121,124–128] The synthesis of block copolymers in which one of the blocks consists of anchor groups is a prominent approach for the preparation of polymers with multiple anchor groups. However, the block copolymer approach is not without some disadvantages. The reproducible incorporation of the same quantity of anchor groups to different polymers (different first block) is challenging due to changing experimental conditions. Additionally, the determination of the quantity of the incorporated anchor groups may be difficult. To circumvent this synthetic hurdle we believe that a different approach would allow for the consistent elimination of this problem. Therefore, the bidentate and tridentate anchor compounds **DL-NH_2**, **DL-N_3** and **TL-NH_2**, **TL-N_3**, respectively, were developed to enable a reproducible attachment of multiple, defined numbers of anchor groups to polymers (Figure 3.2.1).

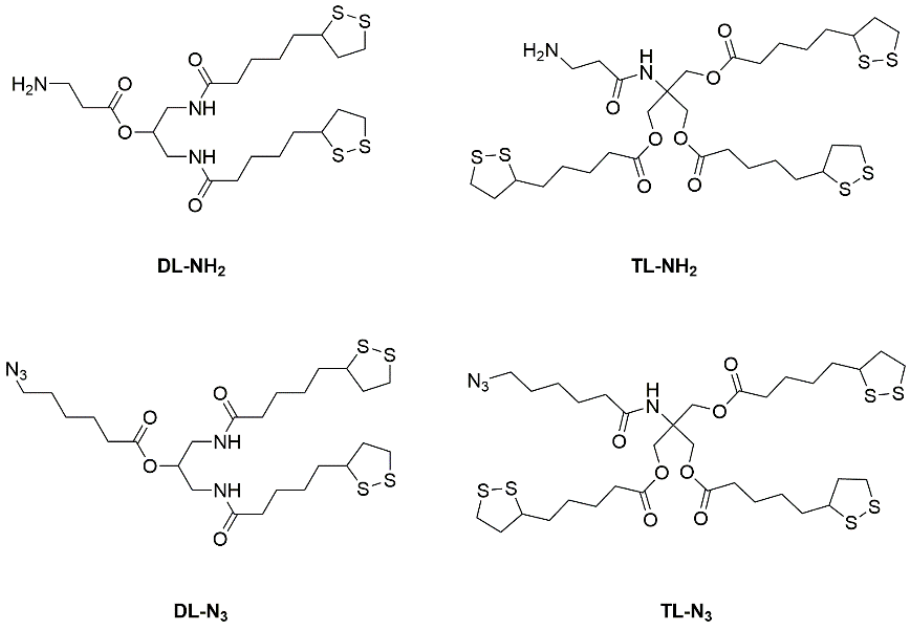

*Figure 3.2.1. Multidentate anchor compounds **DL-NH$_2$**, **TL-NH$_2$**, **DL-N$_3$** and **TL-N$_3$**.*

Lipoic acid (LA) was chosen as the anchor functionality because sulfur-based ligands show high ligand-to-QD (for QDs with Zn-based shell) surface affinity and have been shown to efficiently replace the initial ligands during the ligand exchange procedure.[2] While the LA functionality alone is sufficient to enable ligand attachment to a QD surface, its grafting ability can be enhanced by the reduction of LA to dihydrolipoic acid (DHLA) or as the result of a photo-induced ligation process.[175] It was recently reported that UV light or sunlight-assisted photoligation of QDs provides a highly efficient method for the direct grafting of LA-modified ligands to QD surfaces, thus, eliminating the need of an additional reduction step.[120,176]

Furthermore, the incorporation of the anchor compound to side-chain conjugated, main chain conjugated and hydrophilic (polysarcosine) polymers *via* the amine and azide groups is investigated.

3.2.1 Synthesis of Lipoic Acid-Based Multidentate Anchor Compounds

The lipoic acid-based bidentate (**DL-NH$_2$** and **DL-N$_3$**) and tridentate (**TL-NH$_2$** and **TL-N$_3$**) anchor compounds allow for precise control of the quantity of incorporated anchor groups into the polymer. In addition, the highly reproducible introduction of multiple anchor groups is possible. The amine functionalities of **DL-NH$_2$** and **TL-NH$_2$** enables the efficient addition of these anchor groups to polymers bearing reactive ester groups (e.g. pentafluorophenyl ester, section 1.9). The azide functionalities of **DL-N$_3$** and **TL-N$_3$** facilitates the efficient addition of anchor groups to the polymers *via* click-chemistry which has been widely shown to be a nearly quantitative synthetic step (section 1.10). Furthermore, the presence of multiple anchoring groups facilitates the efficient grafting of the polymer onto the QD surface.

The bidentate anchor **DL-NH$_2$** was obtained in a three step synthesis (Scheme 3.2.1). Two lipoic acid functionalities were coupled to the amine groups of 1,3-diamino-2-propanol *via* a N,N'-dicyclohexylcarbodiimide (DCC) mediated coupling reaction leading to the formation of compound **11**. The following DCC coupling of the hydroxy group of **11** with Boc-β-Alanin-OH yielded compound **12**, which was subsequently deprotected to yield the desired product **DL-NH$_2$**.

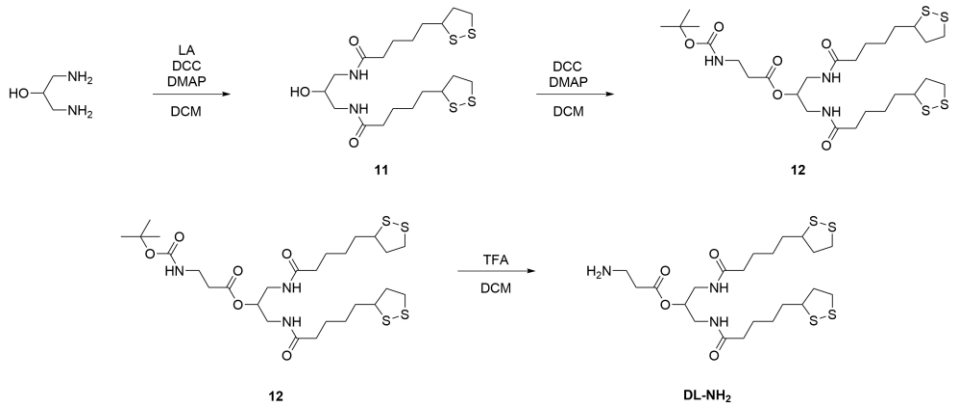

*Scheme 3.2.1. Synthesis of the anchor group **DL-NH$_2$**.*

The tridentate anchor **TL-NH$_2$** was synthesized in five steps (Scheme 3.2.2). First, the amine group of tri(hydroxymethyl)aminomethane was protected with the *tert*-butyloxycarbonyl (BOC) protecting group. The DCC coupling of the three hydroxy groups of compound **13** with lipoic acid was carried out resulting in the formation of triester **14**. Deprotection of the amine led to compound **15**. The amine group of **15** could theoretically

undergo a substitution reaction with polymers bearing reactive ester groups (e.g. pentafluorophenyl groups) leading to the formation of amides. However, the steric shielding of the amine group by the three lipoic acid residues leads to incomplete conversions. Therefore, compound **15** was coupled with Boc-β-alanin-OH and subsequently deprotected to yield the tridentate anchor **TL-NH$_2$** with a less sterically shielded amine group.

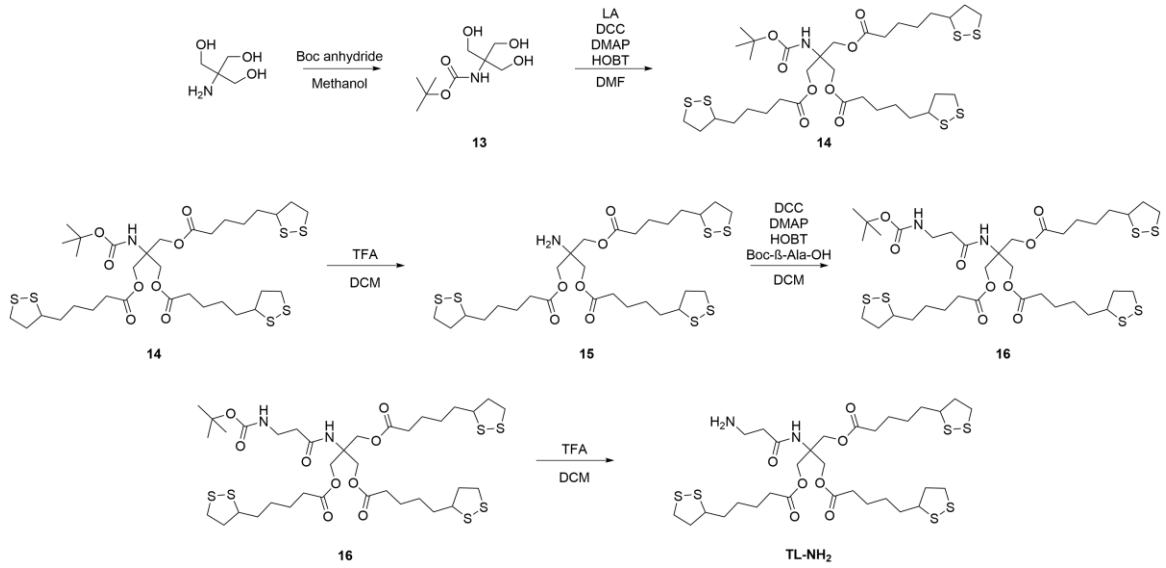

*Scheme 3.2.2. Synthesis of the anchor group **TL-NH$_2$**.*

If 6-azidohexanoic acid is used instead of Boc-β-alanin-OH the anchor groups **DL-N$_3$** and **TL-N$_3$** with azide functionalities can be synthesized (Scheme 3.2.3). **DL-N$_3$** and **TL-N$_3$** enable the functionalization of polymers which contain alkyne functionalities *via* cycloaddition reactions.

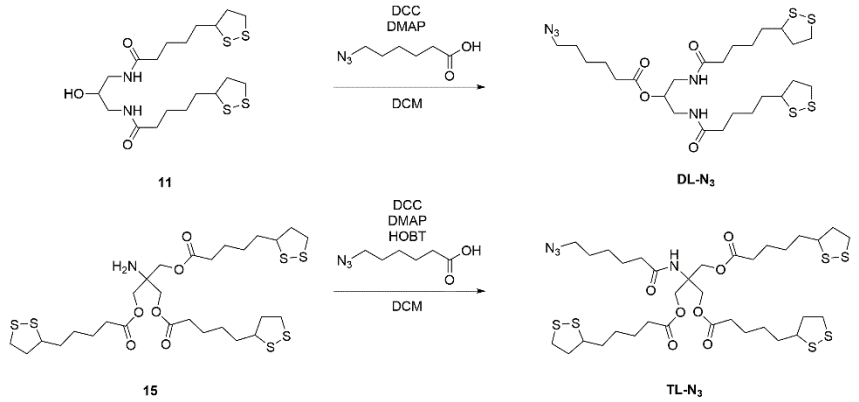

*Scheme 3.2.3. Synthesis of the anchor groups **DL-N$_3$** and **TL-N$_3$**.*

3.2.2 Multidentate Electroactive Polymeric Ligands with Lipoic Acid-Based Anchor Groups

As discussed in section 3.1.4.6 the presence of multiple anchor groups is sometimes necessary to obtain films with QDs homogeneously dispersed within the polymer matrix. In cases where high ratios of QDs with large surface areas are used one disulfide anchor group is insufficient for efficient QD functionalization with polymeric ligands leading to partial phase separation during film formation. An alternative to block copolymers with an anchor block (section 3.1.2.2) is given by the use of multidentate electroactive polymeric ligands **PCarb-DL** and **PCarb-TL**.

PCarb-DL and **PCarb-TL** were synthesized *via* post-polymerization modification reactions of the **PCarb** polymer with anchor compounds **DL-NH$_2$** and **TL-NH$_2$** (Scheme 3.2.4). **PCarb** was synthesized by RAFT polymerization with S-1-dodecyl-S′-(α,α′-dimethyl-α′′-pentafluorophenyl acetate)trithiocarbonate as the CTA agent as previously described in section 3.1.2.1. A M_n of 5100 g mol^{-1} and a PDI of 1.2 were determined by GPC.

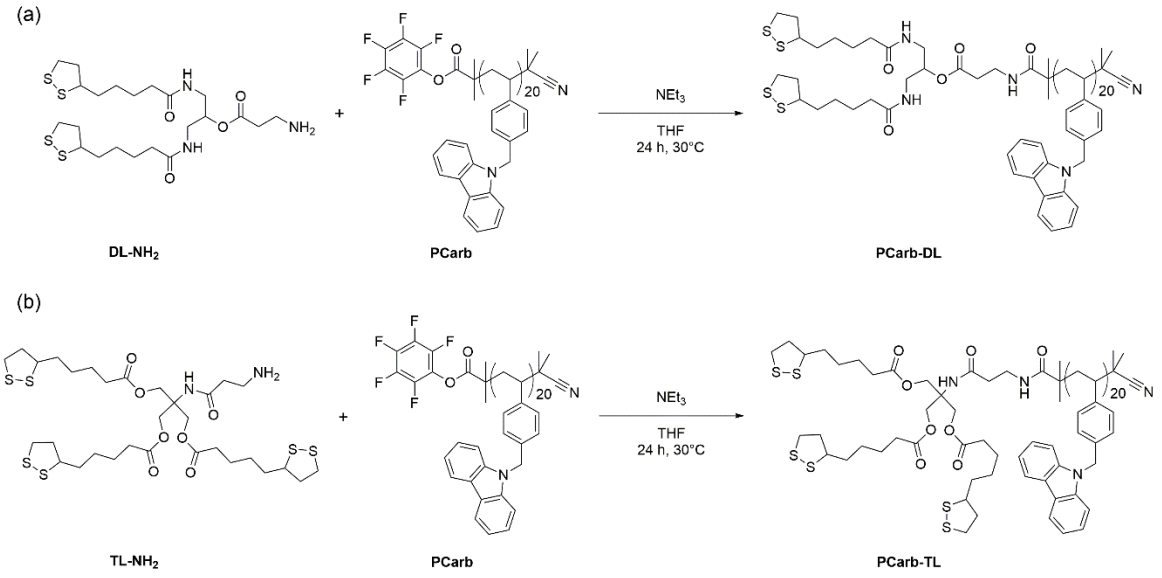

*Scheme 3.2.4. Synthesis of multidentate side-chain conjugated polymeric ligands **PCarb-DL** (a) and **PCarb-TL** (b).*

The successful introduction of anchor functionalities was confirmed by IR, ^{19}F NMR, ^{1}H NMR and DOSY NMR spectroscopies. The IR spectra of **PCarb-DL** and **PCarb-TL** in Figure 3.2.2 demonstrates the disappearance of the C=O band of the pentafluorophenyl

ester at 1773 cm^{-1} and the presence of the C=O amide band at 1673 cm^{-1}. The C=O amide bands correspond not only to the amides formed during the post-polymerization modification step, but also to the amide groups previously present in the **DL-NH2** and **TL-NH2** compounds. Additionally, at 1735 cm^{-1} the C=O bands of the aliphatic esters of the anchor groups are detected. The disappearance of the pentafluorophenyl signals in ^{19}F NMR is analogous to the polymers **P1-P3** described in section 3.1.2.1 and indicate the quantitative conversion of all ester groups to amides.

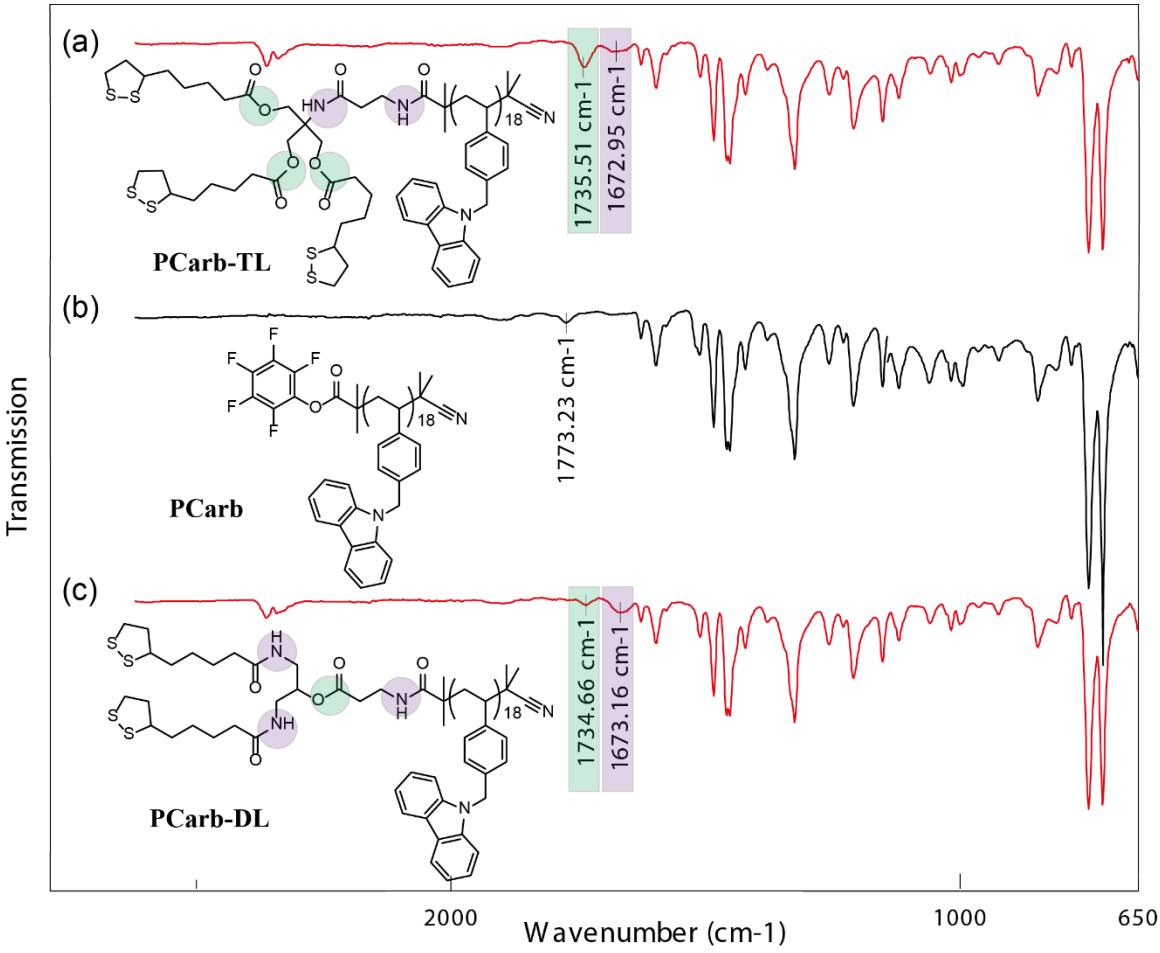

*Figure 3.2.2. IR spectra of **PCar-TL** (a), **PCarb** (b) and **PCarb-DL** (c).*

In DOSY NMR spectra, the signals corresponding to the lipoic acid functionalities (3.61-3.01 ppm and 2.50-2.17 ppm) and the carbazole groups (8.02 ppm, 7.10 ppm) are visible as one diffusing species, indicating the successful polymer functionalization (Figure 3.2.3).

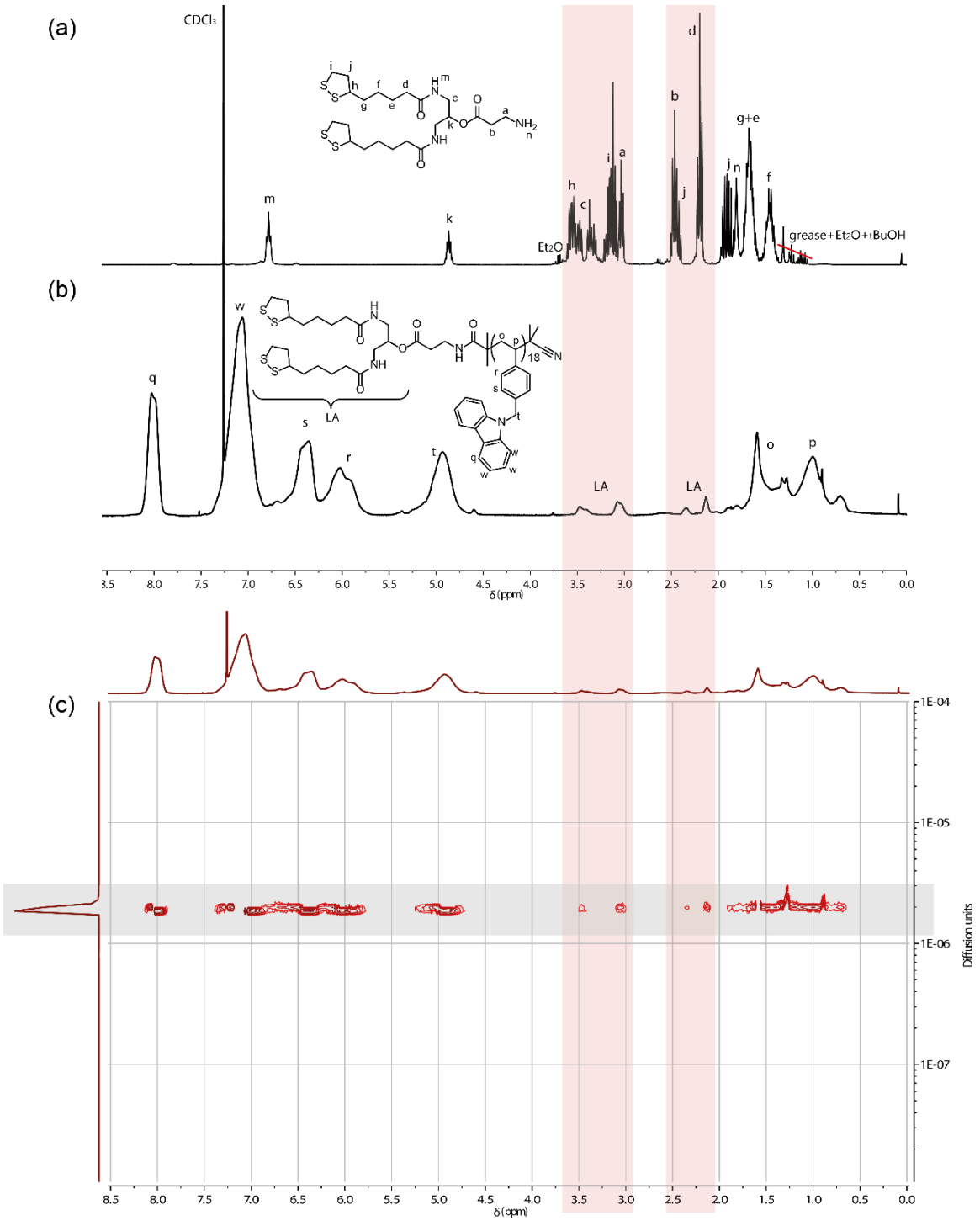

*Figure 3.2.3. ^{1}H NMR spectra of **DL-NH$_2$** (a) and **PCarb-DL** (b). DOSY NMR spectrum of **PCarb-DL**. Red lines mark the area of the signals corresponding to the anchor compound. The grey line marks the diffusion area of **PCarb-DL** (c).*

3.2.3 Multidentate P3HT-Based Ligands with Lipoic Acid-Based Anchor Groups

Poly(3-hexylthiophene) (P3HT) is a widely used polymer in organic and hybrid solar cells (sections 1.3.1 and 1.6). In hybrid organic/inorganic solar cells inorganic nanocrystals (e.g. QDs) facilitate electron transport (electron acceptor), while the polymer (e.g. P3HT) enables hole transport (hole acceptor). The morphology and thus the device performance of the hybrid solar cells is strongly dependent on the anchor groups which coordinate P3HT to the QDs. The morphology requirement of hybrid solar cells are, however, more complicated than in the case of LEDs.[60] On one side, good dispersion of the QDs within the polymer is desired to minimize the exciton diffusion length. On the other side, the presence of a percolated system is required for charge transport through the active layer to the electrodes. The reproducible and easy introduction of a defined number of anchor groups to P3HT could enable the systematic investigation of the anchor group influence on the active layer morphology of hybrid solar cells.

In order to incorporate the anchor compounds **DL-N$_3$** and **TL-N$_3$** into P3HT a polymer with alkyne end groups was first synthesized (Scheme 3.2.5).[177] GRIM polymerization of 2,5-dibromo-3-hexythiophene followed by quenching with ethynylmagnesium bromide led to the formation of ethynyl-terminated P3HT (**P3HT-Ethynyl**).[178]

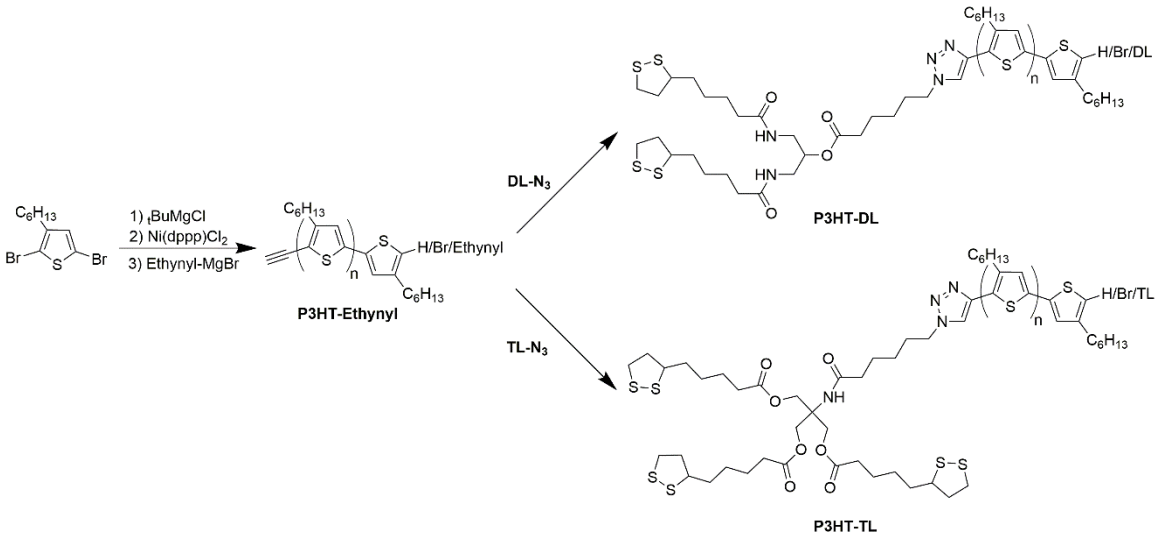

*Scheme 3.2.5. Synthesis of the P3HT-based multidentate **P3HT-DL** and **P3HT-TL** ligands.*

The formation of 85 % mono- and 15 % bifunctional ethynyl-terminated polymer chains was verified using matrix-assisted laser desorption ionization time-of-flight mass

spectrometry (MALDI-TOF MS, Figure 3.2.4). For **P3HT-Ethynyl** the molecular weight of 3428 g ml^{-1} which corresponds to 20 repeat units was determined by MALDI-TOF MS, and a M_n of 5200 mg ml^{-1} and a PDI of 1.2 were obtained by GPC.

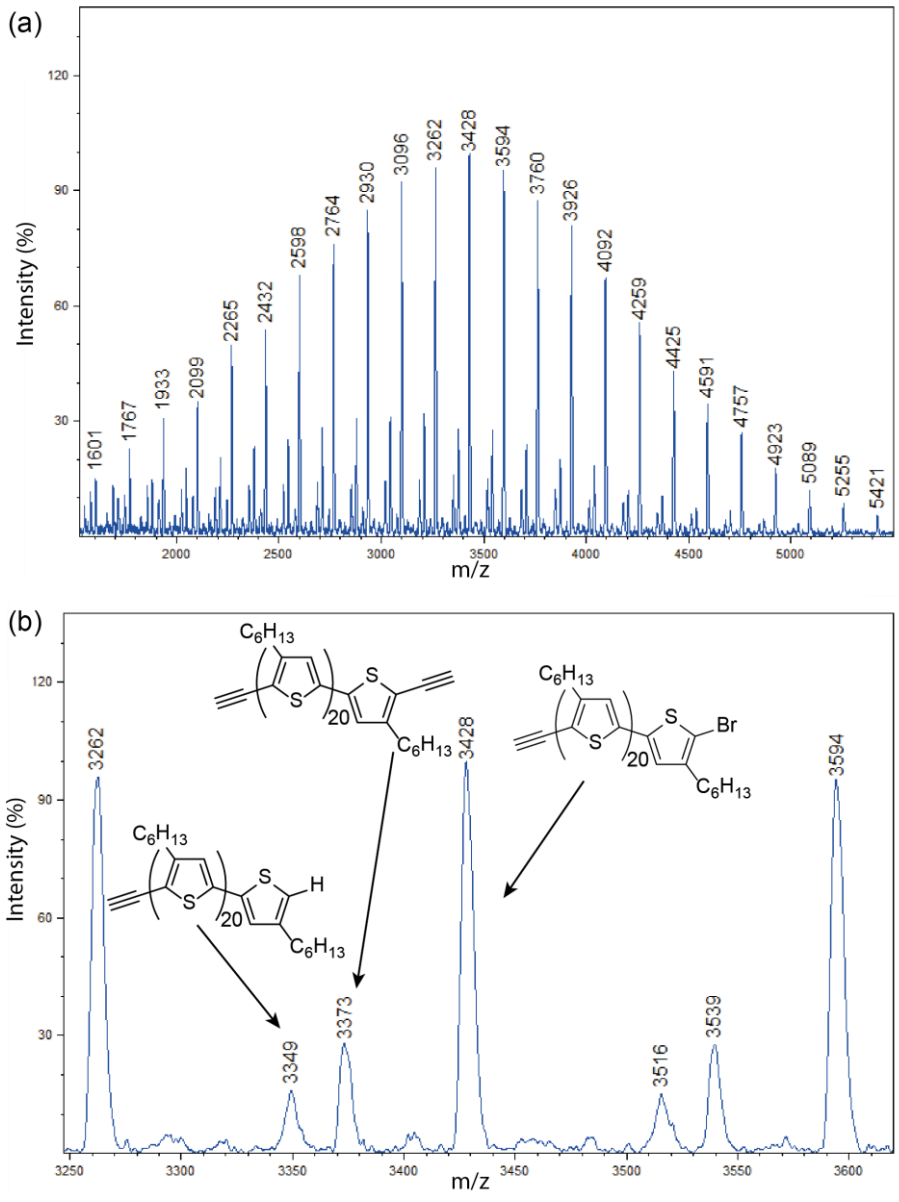

*Figure 3.2.4. MALDI-TOF MS spectra of **P3HT-Ethynyl**. Entire spectrum (a) and the peak assignment in the enlarge segment (b).*

The multidentate P3HT-based ligands **PH3T-DL** and **P3HT-TL** were synthesized *via* copper catalyzed azide-alkyne Huisgen cycloaddition of ethynyl-terminated P3HT (**P3HT-Ethynyl**) with compounds **DL-N$_3$** and **TL-N$_3$** (Scheme 3.2.5). Successful end group modification was verified using ^{1}H-NMR spectroscopy (Figure 3.2.5) and MALDI-TOF MS (Figure 3.2.6). Characteristic signals, which can be assigned to the lipoic acid

functionalities are visible in the ^{1}H NMR spectrum of **P3HT-DL**. Moreover, after the cycloaddition reaction the singlet of the alkyne proton of **P3HT-Ethynyl** at 3.53 ppm disappears and a singlet corresponding to the triazole ring appears at 7.73 ppm. Additionally, the triplet of the methylene group attached to the azide shifts from 3.37 ppm to 4.49 ppm once the triazole ring is formed in **P3HT-DL**.

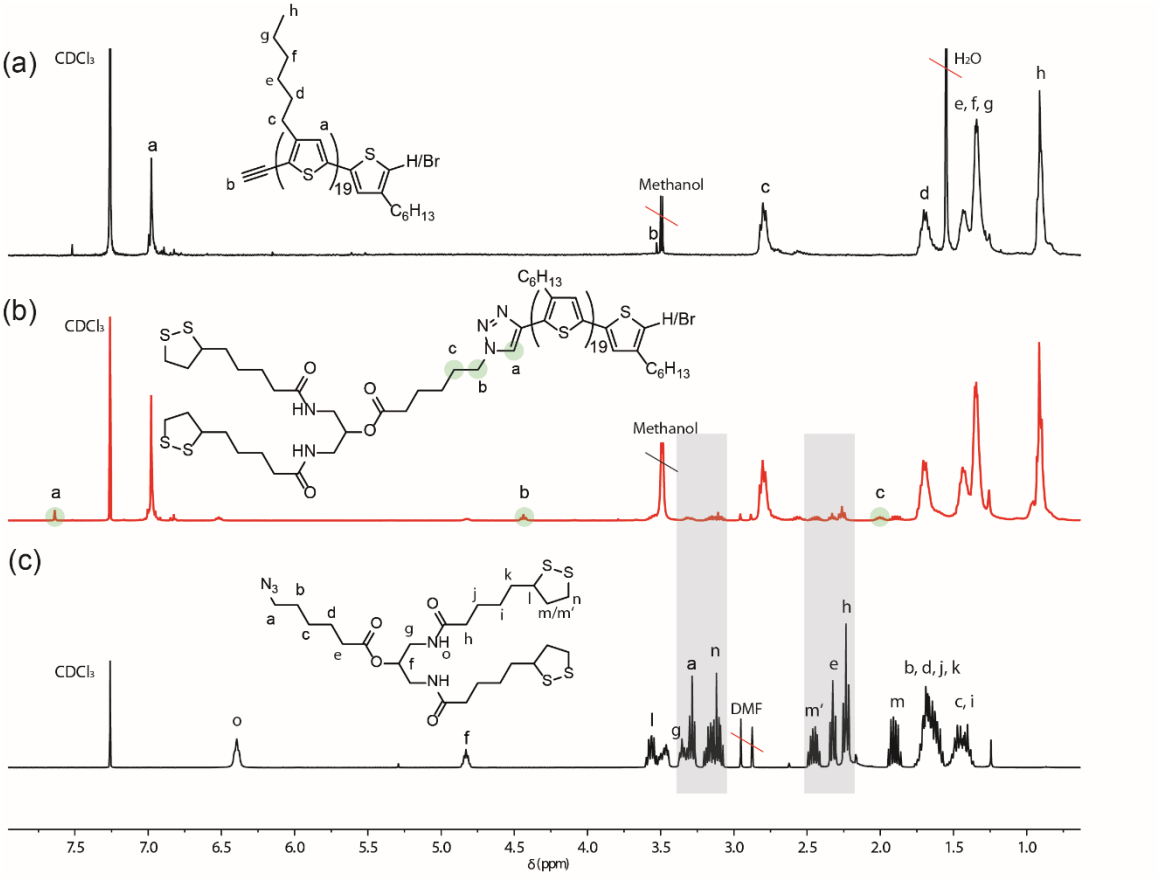

*Figure 3.2.5. 1H NMR of **P3HT-Ethynyl** (a), **P3HT-DL** (b) and **DL-N₃** (c).*

Since the **P3HT-Ethynyl** polymer includes both mono- and bifunctional polymer chains the anchor compounds **DL-N$_3$** and **TL-N$_3$** can be incorporated once or twice. The presence of mono-and bifunctional species in **P3HT-DL** and **P3HT-TL** was confirmed by MALDI-TOF MS (Figure 3.2.6). The bifunctional polymer chains can act as a crosslinker between two inorganic nanoparticles leading to a controlled aggregation. Controlled aggregation might facilitate the formation of a percolated morphology in a film which is desirable for photovoltaic applications. Moreover, no ethynyl-functionalized P3HT was detected in MALDI-TOF MS indicating a quantitative conversion.

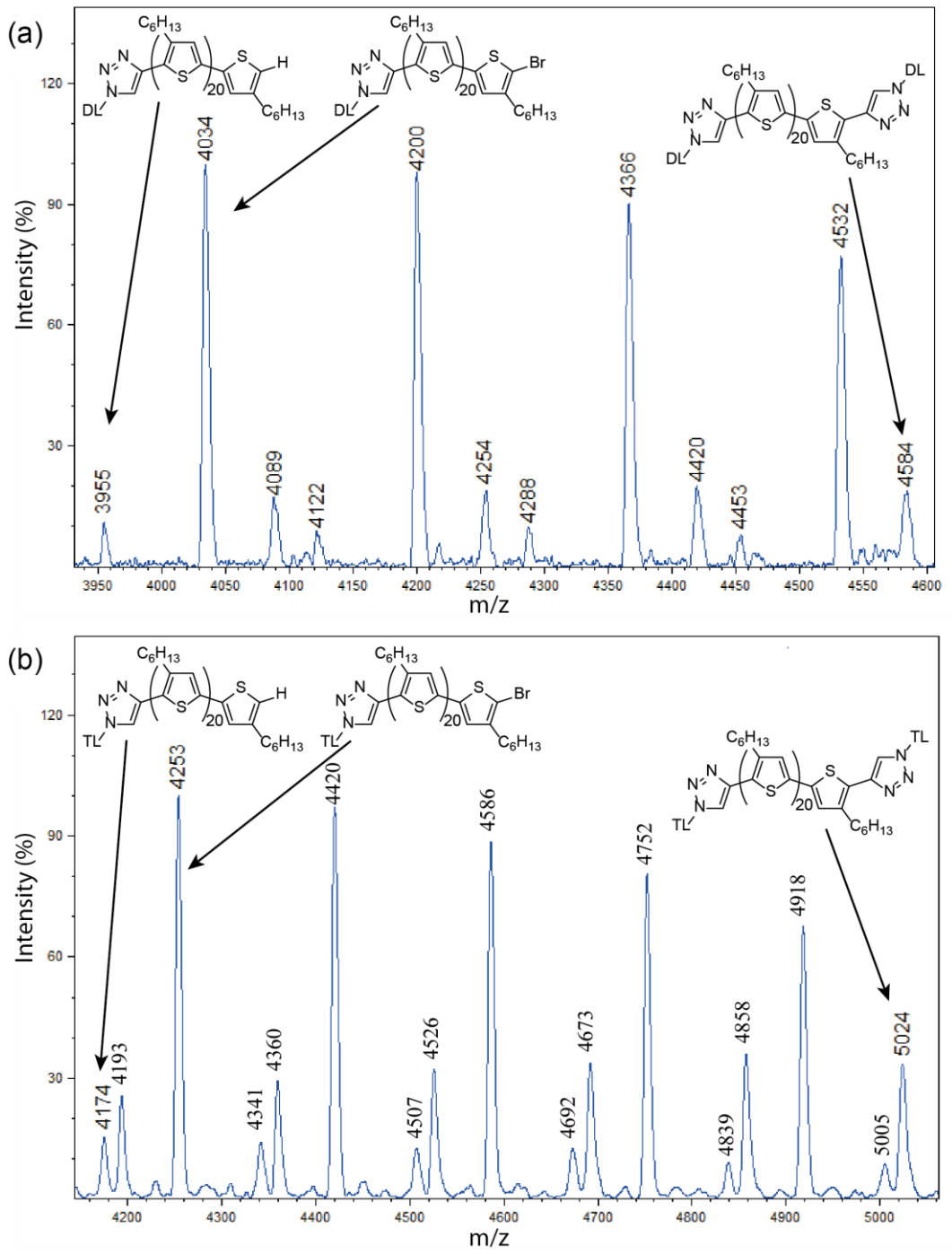

Figure 3.2.6. The enlarge segment of MALDI-TOF MS spectra of polymeric ligands ***P3HT-DL*** *and* ***P3HT-TL****.*

3.2.4 Multidentate Polysarcosine-Based Ligands for Water-Soluble Quantum Dots

A modular approach for the effective and easily variable synthesis of new hydrophilic multidentate polymeric ligands consisting of polysarcosine (poly((N-methyl)glycine)) and **DL-N$_3$** and **TL-N$_3$** anchoring compounds for the preparation of water-soluble QDs was developed. Polysarcosine belongs to the polymer class of polypeptoids and displays stealth-like properties, zero net charge, hydrophilicity and the inability to act as a hydrogen donor.[52] Additionally, polysarcosine consists of the endogeneous amino acid sarcosine and is, thus, expected to be not only biocompatible but also biodegradable. Lipoic acid-based multidentate anchor compounds were covalently linked to the polymer using highly efficient strain-promoted azide-alkyne cycloaddition (SPAAC) (section 1.10). Using this approach, the same amount of anchoring units could be reproducibly attached to various polymers. Moreover, the free secondary amine group of polysarcosine enabled the functionalization of hydrophilic quantum dots with biologically active species. Alternatively, the free amine group was prefunctionalized with the biotine functionality as an example of a target molecule or capped with acetic anhydride to prevent unspecific interactions with either the biological environment or with the QD itself.

The synthesis of dibenzocyclooctyl (DBCO)-functionalized polysarcosine was carried out by the primary amine-initiated ring opening polymerization of N-methyl glycine N-carboxyanhydride (SarNCA) using DBCO amine (Scheme 3.2.6, synthesized by [redacted], Department of Organic Chemistry, JGU Mainz).[53] The polymerization was conducted in absolute DMF at 0°C. Analytical data of the end group functionalized polymer is summarized in (Table 3.2.1).

*Table 3.2.1. Analytical data of **DBCO-PSar**. a):obtained from 1H NMR spectrum, b:obtained from GPC measurement.*

Polymer	**M/I**	**$X_{n(NMR)}$[a]**	**M_n[b]**	**PDI[b]**
DBCO-PSar	200	198	29,000	1.11

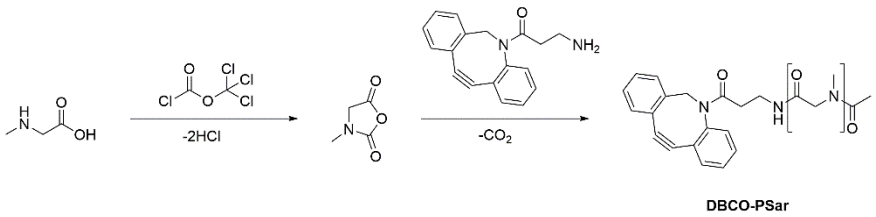

*Scheme 3.2.6. Reaction scheme of **DBCO-PSar**.*

The resulting polymer displayed a narrow dispersity and the degree of polymerization was determined by ^{1}H NMR spectroscopy by comparing the signal originating from the eight aromatic protons of the initiator with the backbone protons of PSar (N-methyl and methylene). The obtained degree of polymerization was close to the calculated one (M/I), which is expected for a controlled ring opening polymerization reaction.

In order to obtain polysarcosine polymeric ligands, orthogonally-functionalized polysarcosine was submitted to post-polymerization modification reactions with azide functionalized anchor compounds **DL-N$_3$** and **TL-N$_3$** (Scheme 3.2.7). First, the amine was capped with acetic anhydride, biotin N-hydroxysuccinimide ester or kept unmodified. For the N-terminus modification the polymer and the corresponding capping agent were dissolved in dry DMF and stirred at room temperature for 24 hours. Second, the SPAAC reaction in dry DMF was carried out between the polymeric dibenzocyclooctyne group and the azide groups of bidentate lipoic acid anchor **DL-N$_3$** or the tridentate anchor **TL-N$_3$** leading to **PL1a-c** and **PL2a-c** respectively.

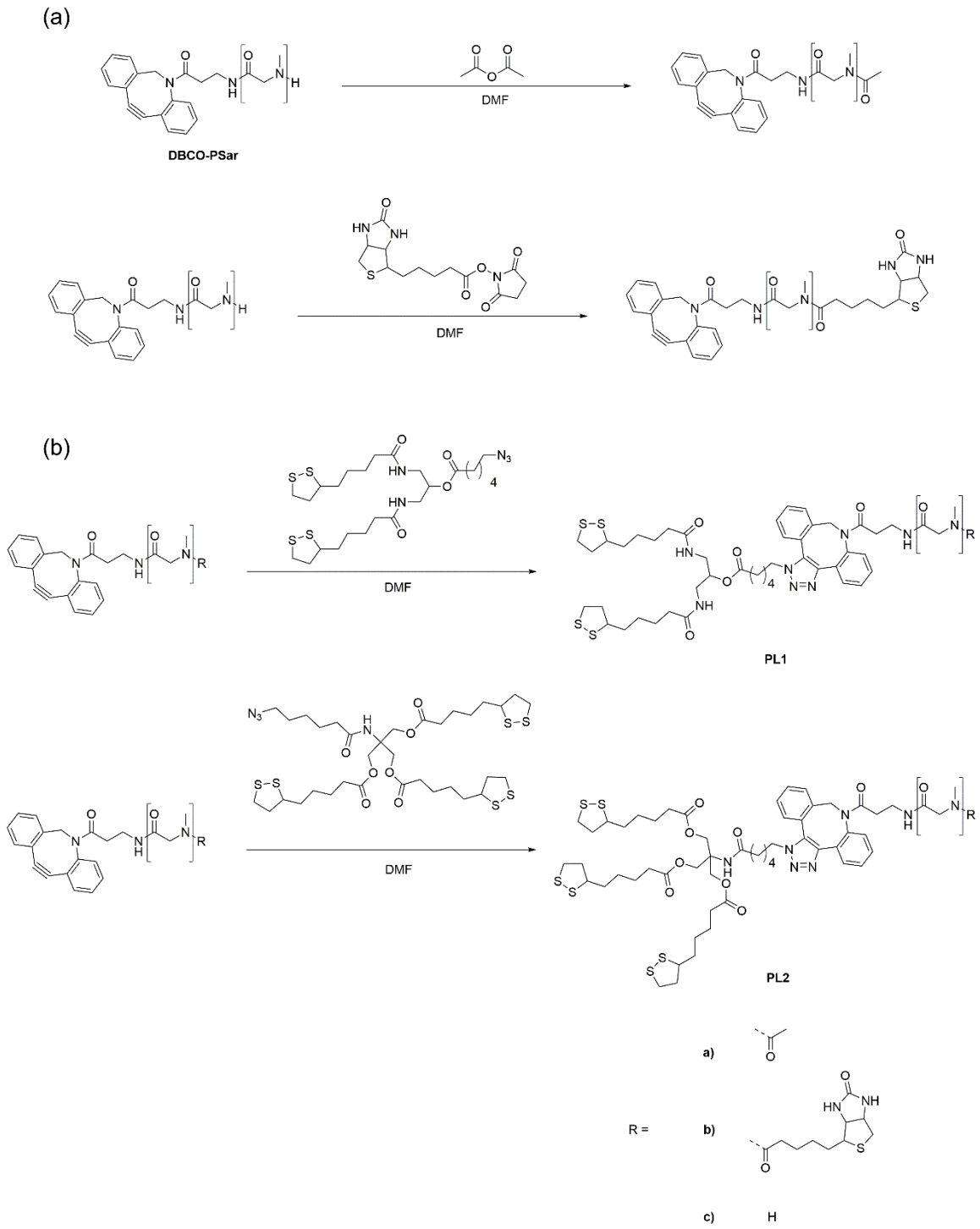

*Scheme 3.2.7. Synthesis of polysarcosine-based polymeric ligands **PL1a-c** and **PL2a-c**. The modification of amine terminus (a) and the DBCO terminus (b).*

Successful polymer functionalization was confirmed by ^{1}H NMR and ^{1}H DOSY NMR spectroscopies (Figure 3.2.7 and Figure 3.2.8). In DOSY NMR spectra, the signals corresponding to the polymer backbone (4.35-4-39 ppm, 2.94-2.74 ppm) and lipoic acid functionalities (2.08 ppm, 1.91-1.82 ppm and 1.71-1.24 ppm) are visible as one diffusing

species, indicating the successful functionalization of the polymer. The negative control consisting of a mixture of **DBCO-PSar** and compound **14** which possess similar solution properties as **TL-N$_3$** clearly shows two well-distinguishable diffusing species. Additionally, according to GPC data, no or only negligible change in the polymer molecular weight occurred, which accounts for successful post-polymerization in absence of side reactions.

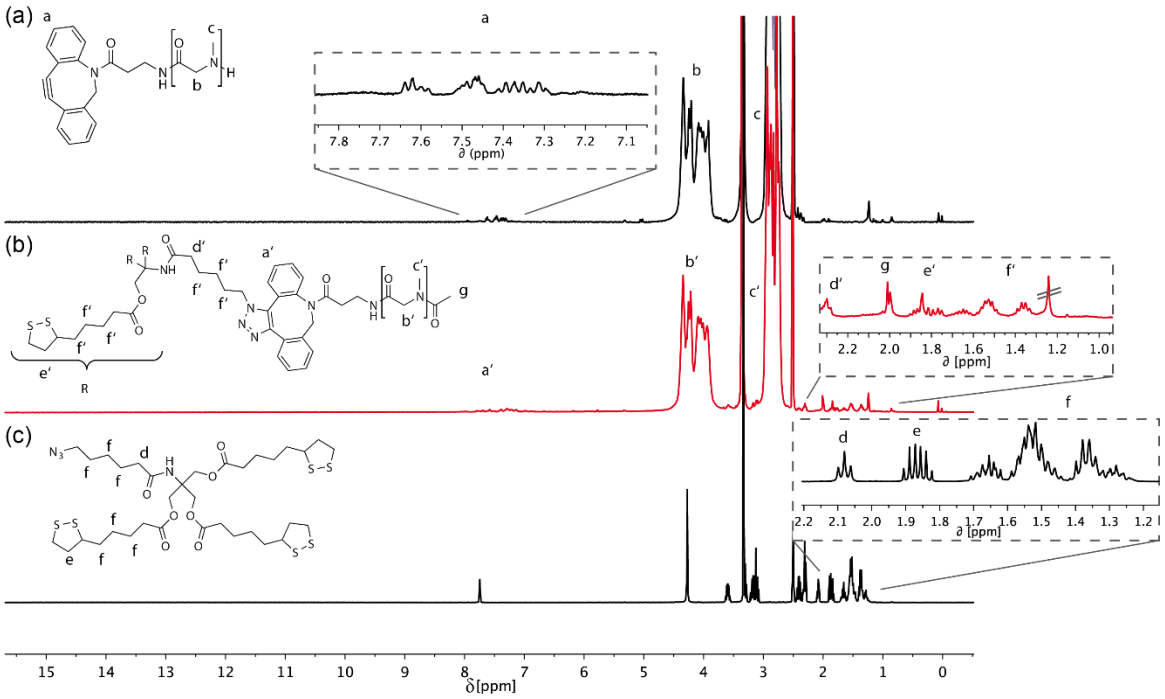

*Figure 3.2.7. ^{1}H NMR in DMSO-d_6 of DBCO-initiated PSar (a), trilipoic acid-functionalized PSar capped with acetyl **PL1a** (b) and anchor group **TL-N$_3$** (c).*

The choice of the reactants in the first post-polymerization reaction step determines the future biological activity of the ligands. The modification of amine group with biotin N-hydroxysuccinimide ester (biotin NHS ester) reflects only one example of a highly efficient way to incorporate of a huge variety of biologically active components to the polysarcosine polymer through the NHS ester coupling method (**PL1b** and **PL2b**). The use of such pre-modified polysarcosine as a ligand would lead to QDs with biologically active surface. On the other hand, the ligands **PL1a** and **PL2a** with the inert acetamide end group are not expected to interact with surrounding biomolecules. Moreover, if the functionalization of the QDs is carried out with polymeric ligands **PL1c** and **PL2c**, the coupling with biologically active components could be performed in a later stage directly on the quantum dot surface.

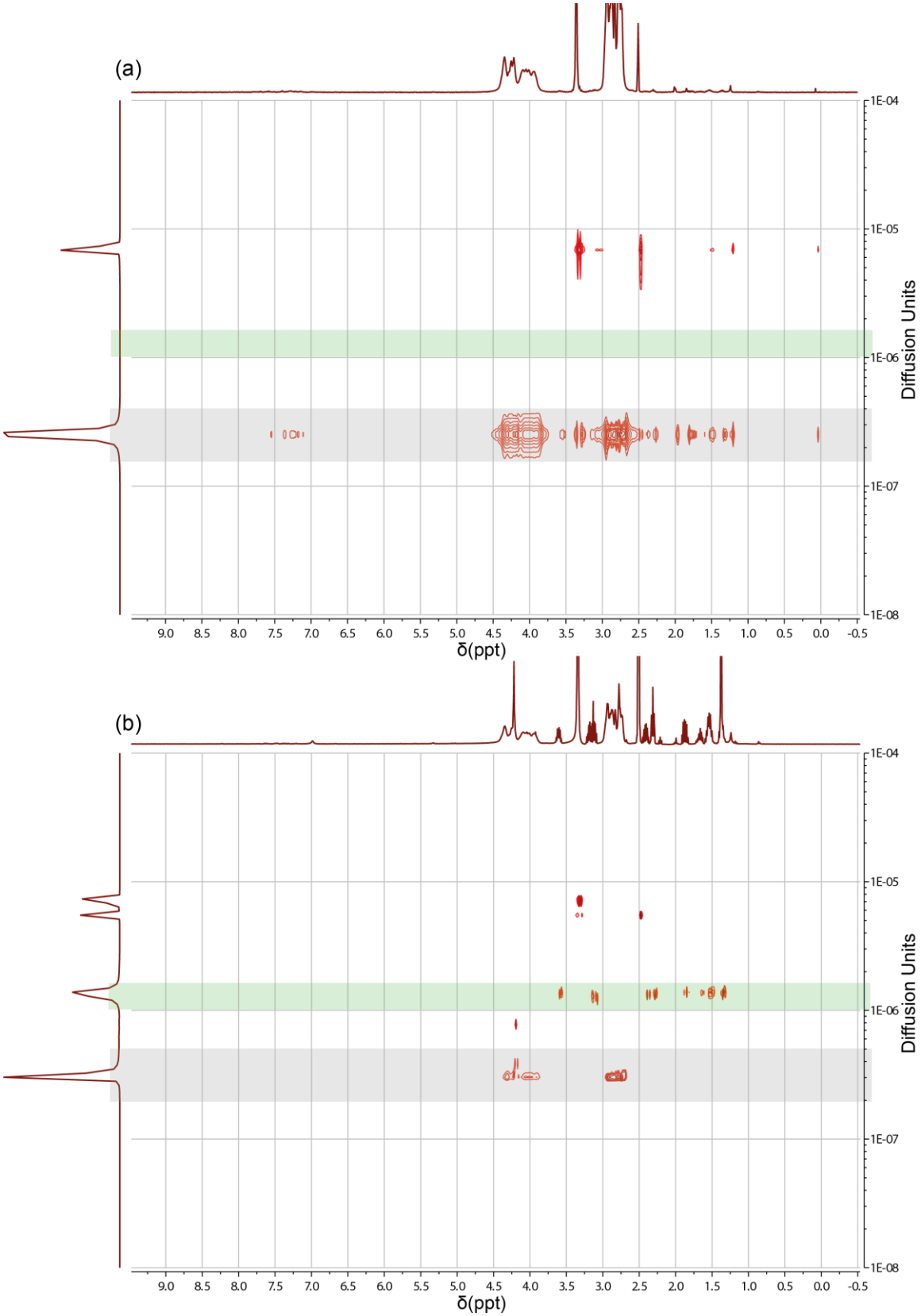

*Figure 3.2.8. ^{1}H DOSY spectra of **PL2a** (a) and a mixture of **DBCO-PSar** and compound **14** (b). The green line marking the diffusion area of compound 14 and the gray line marking the diffusion are of PSar-based **PL2a** and **DBCO-PSar**.*

3.2.5 Water Soluble QDs with PSar-Based Polymeric Ligands

To verify the anchor compounds affinity to QDs the ligand exchange procedure was carried out between CdSe/$Cd_xZn_{1-x}S$ QD (diameter 16 nm) and polysarcosine-based bidentate **PL1a** and tridentate **PL2a** ligand**s**. The polymeric ligands and the QDs were dissolved in chloroform (polymer:QDs 3:1) and submerged into a sonication bath for 60 minutes. Afterwards, the water was added to the reaction mixture and the now water-soluble quantum dots were extracted from the organic to the aqueous phase. The excess polymer was removed by repeated centrifugation with Amicon® Ultra centrifugal filters (100K MWCO). The water-soluble QDs (with **PL1a** and **PL2a** as new hydrophilic ligands) retained the fluorescence properties of the initial oleic acid modified QDs with fluorescence maxima at 623 nm and FWHM of 28 nm (Figure 3.2.9). Moreover, QDs functionalized with ligands **PL1a** and **PL2a** were stable at high salt concentrations (1 M NaCl) and in the pH range from 4.6 to 8.1. AFM and TEM measurements of **PL1a** functionalized QDs further verified the formation of a polymeric shell around the QDs (Figure 3.2.10). While TEM images provide information about the size of the inorganic sphere, during the AFM measurement the polymeric corona of the QDs is also detected. The change in QD size from 16 nm in TEM to 41±5 nm in AFM indicates the formation of a PSar-based polymeric shell.

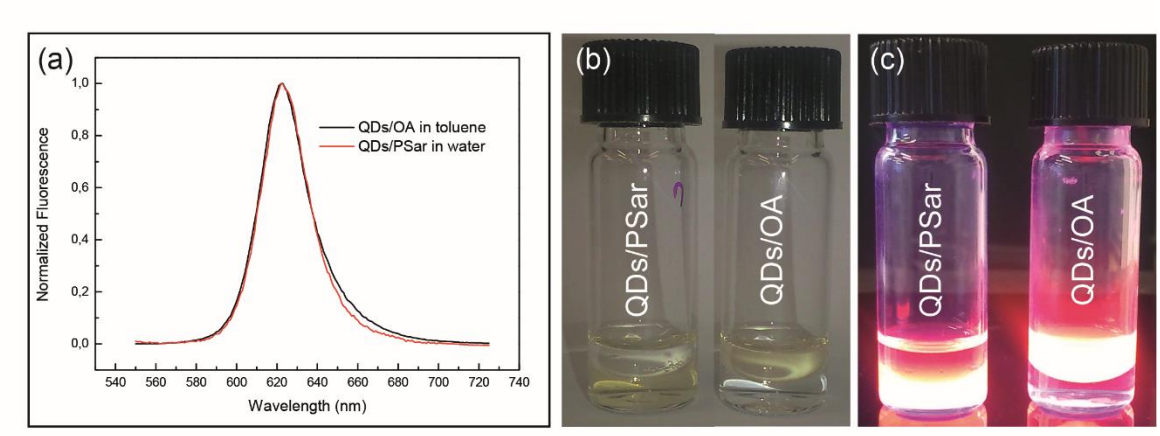

*Figure 3.2.9. Fluorescence spectra of QDs with oleic acid ligands (QDs/OA) in toluene and of QDs functionalized with polysarcosine (**PL1a**) (QDs/PSar) in water (a). QDs/OA and QDs/PSar in water/hexanes mixture under ambient (b) and UV light (c).*

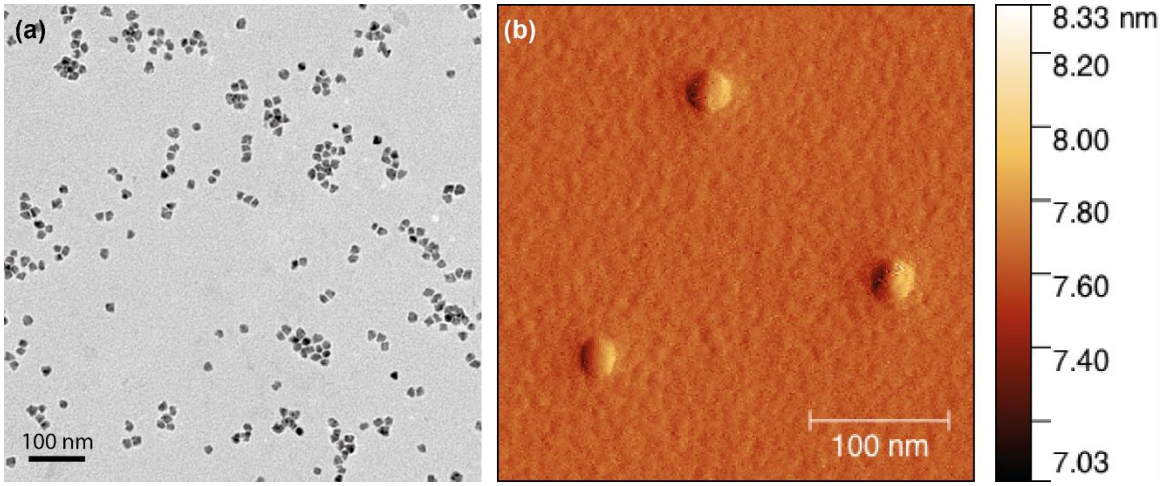

Figure 3.2.10. TEM image (scale bar 100 nm (a)) and AFM amplitude image (scale bare 100 µm (b)) of ***PL1a*** *functionalized QDs.*

3.2.6 Conclusion

The results in the section 3.2 present a new approach for the incorporation of a defined number of multiple lipoic acid anchor groups to various polymers in one reproducible and high yielding step. The only requirement for the polymers to be modified is the presence of reactive ester or alkyne end groups. Besides the need for a particular end group, the introduction of the anchor groups *via* compounds **DL-NH$_2$**, **TL-NH$_2$**, **DL-N$_3$** and **TL-N$_3$** is independent from the polymerization method and the properties of the polymer.

The synthesis of new bidentate and tridentate lipoic acid-based anchor compounds **DL-NH$_2$**, **DL-N$_3$** and **TL-NH$_2$**, **TL-N$_3$** was developed. Lipoic acid functionalities were chosen as anchor groups due to their ability to coordinate to QDs, while azide and amine functionalities enable the attachment of the anchor compounds to the polymers. Polymers with reactive ester end groups can be modified using the amine containing **DL-NH$_2$** and **TL-NH$_2$** compounds. As an example for this reaction, the electroactive polymer with carbazole-based side chains and a pentafluorophenyl ester end group was successfully modified. Furthermore, the azide functionalized compounds **DL-N$_3$** and **TL-N$_3$** can undergo a cycloaddition reaction with alkyne containing polymers. Multiple lipoic acid anchor groups were incorporated into P3HT *via* copper catalyzed azide-alkyne Huisgen cycloaddition using ethynyl functionalized P3HT. Furthermore, the azide-functionalized compounds were used to prepare hydrophilic multidentate polysarcosine-based ligands *via* a catalyst-free strain-promoted azide-alkyne cycloaddition reaction. Finally, polysarcosine-based polymeric ligands containing lipoic acid anchor groups were successfully used in the synthesis of stable water soluble QDs.

4 Summary

Polymer/quantum dot (QD) hybrids are systems where the sum of the properties surpass the properties of the individual compounds and thus open new application possibilities. QDs exhibit remarkable optical and electrical qualities, such as broadband absorption, easily tunable emissions, particularly narrow emission profiles, high quantum yields, good electron conductivity and high stability. Polymers used in the synthesis of hybrids possess both an anchoring and a property defining functionalities. The anchoring functionality enables the chemical grafting of the polymer chains onto the QD surfaces, and thus distinguishes hybrids from their physically mixed counterparts. The desired future application of the hybrid determines the choice of the property defining functionality. Semiconducting polymers are of interest for potential applications of hybrids in photovoltaic and lighting applications. When the property defining functionality consists of hydrophilic polymers hybrids can be used in imaging, labelling and sensing of biological systems.

In Figure 3.2.1 a schematic summary of the hybrids studied in this dissertation is presented.

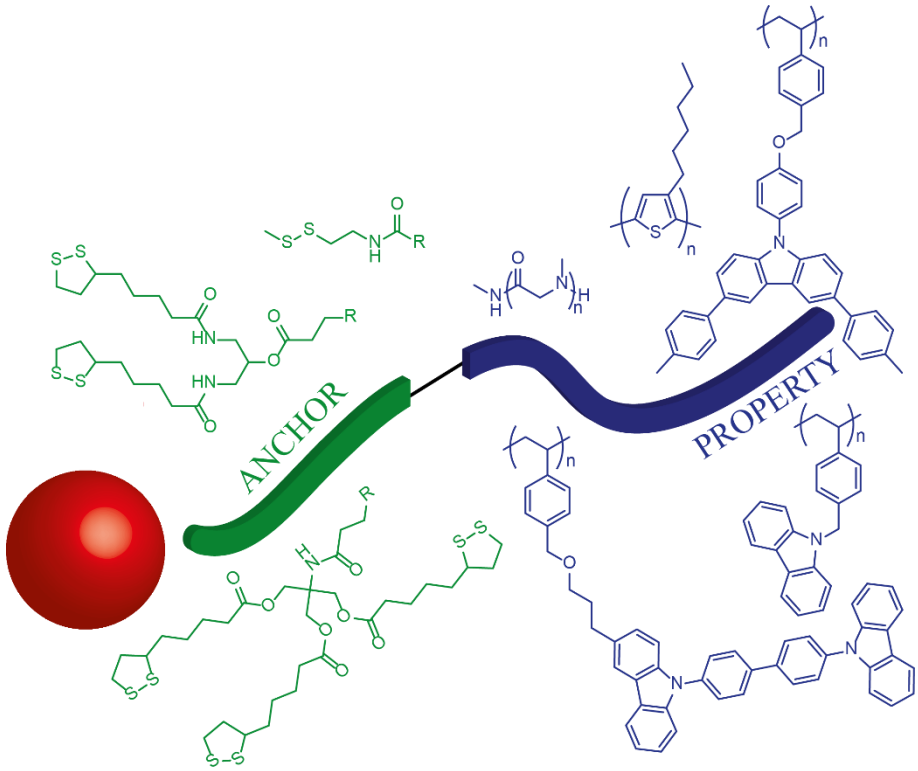

Figure 3.2.1. A schematic summary of anchoring (green) and property defining (blue) functionalities studied in this dissertation.

Significant attention was given to the development of new side-chain conjugated polymers and their application in the active layer of hybrid quantum dot-based light emitting diodes (QLEDs) (section 3.1). Additionally, new well defined multidentate anchor compounds were investigated and their incorporation into different polymers was studied (section 3.2).

The use of semiconducting polymer/QD hybrids as the active layers in QLEDs provides a promising pathway to overcome some intrinsic disadvantages of QD-only devices. Disadvantages of QD-only systems include unbalanced charge injection and QD photoluminescence quenching.[158] As opposed to idealized systems the performance of previously studied hybrid QLEDs have been found to be markedly below the efficiencies of the QD-only devices.[84,92] Hindered hole injection from the polymer into the QDs due to the large energy offset between the HOMO of the polymer and the valence band of the QDs has been suggested to be the reason for the low performances.[70,159] In order to decrease the hole injection barrier side-chain conjugated carbazole-based polymers with low lying HOMO levels were developed. Prior to the synthesis computational calculation were performed to screen for possible lead structures. The calculations confirmed that the HOMO levels of the newly chosen carbazole-based structures are below the previously studied systems. Subsequently, three monomers with differently substituted carbazole cores and a styrene functionality were synthesized (section 3.1.1). Side-chain conjugated polymers possess, as the name implies, an electrochemically inert backbone and conjugated, electrochemically active side-chains. The conjugated systems do not change during the polymerization process therefore the electrochemical properties of the polymer are predetermined by the monomer. A carbazole core was chosen as the electroactive unit due to its relatively low HOMO level and its well-known hole conducting ability. Monomer **M2** is based on an unsubstituted carbazole core while in monomers **M1** and **M3** additional conjugated substituents are introduced to tune their electrochemical properties. Styrene was selected as the basic monomer functionality because of its polymerization characteristics. The polymerization of styrene allows the formation of a chemically and electrically stable polystyrene backbone. Furthermore, styrene can be readily polymerized *via* reversible addition fragmentation chain transfer (RAFT) radical polymerization. The prepared monomers **M1**-**M3** were used in RAFT polymerization experiments to yield polymers with defined molecular weights and narrow polydispersities (section 3.1.2).

To enable the grafting of the polymers to the QDs anchoring disulfide groups have been incorporated into the polymer. Disulfide group are well known for their ability to efficiently graft to the surface of the QDs used in this work. To achieve this perfluorophenyl reactive ester functional groups were first incorporated into the polymers either as a single end group or as a second block. Second, through post-polymerization modification reactions the reactive ester groups were replaced with disulfide containing functionalities. Properties of the polymers (**P1**, **P2** and **P3**) consisting of approximately 20 repeat units (monomer **M1**, **M2** and **M3**, respectively) and one disulfide group were compared and the results showed that thermal, optical and electrochemical properties of the polymers varied depending on the substituents of the carbazole unit. HOMO energies were determined to be 5.52 eV, 5.78 eV and 5.82 eV for the polymer **P1**, **P2** and **P3**, respectively.

The polymers were used to synthesize QD/polymer hybrids with red CdSe@$Cd_xZn_{1-x}S$ QDs (total diameter of 16 nm) *via* a ligand exchange procedure. The prepared hybrids formed films with the QDs homogeneously distributed within the polymer matrix, which confirmed the successful coordination of the polymer chains onto the QD surfaces. The QD/polymer hybrids were then tested as the active layers in LED devices. The devices fabricated had high efficiencies and narrow electroluminescence profiles, solely composed of QD emission. Moreover, the importance of the polymer HOMO level adjustment for the development of efficient hybrid LEDs has been confirmed (section 3.1.3.3). Polymers **P2** and **P3** with HOMO levels of 5.78 eV and 5.82 eV led to devices with high external quantum efficiencies (EQEs) of 5.05 % and 6.09 %, respectively. However, a HOMO level of 5.52 eV determined for polymer **P1** is thought to be too high for efficient hole injection into QDs, and thus led to a device with diminished performance (EQE of 2.14 %). Therefore, from the results obtained it could be asserted that the utilization of polymers with low-lying HOMO levels is a precondition for obtaining hybrid QLEDs with good device performance.

Hybrid QLED performance is dependent on several factors including the QD/polymer ratio, active layer morphology, charge carrier mobility and charge carrier injection into QDs. To investigate the influence of the QD/polymer ratio, hybrids with different polymer content (from 11.1 wt% to 33.3 wt%) were tested in devices (section 3.1.4.2). As the polymer presence in the active layer affects multiple properties simultaneously an optimized polymer quantity had to be found to obtain a device with the best characteristics. On one

hand, an increase in the amount of polymer led to an improvement in the electron-hole balance as was seen from the profoundly suppressed leakage current in devices with a high polymer ratio. On the other hand, a lower polymer content was more favorable to obtain devices with low turn-on voltages. Increasing the polymer percentage led to hindered charge transport to the QDs thus resulting in continuously rising turn-on voltages. The hybrid device with an intermediate polymer content of 27 wt% exhibited the best device performance with an EQE of 5.6 %. This ratio provided optimal electronic conditions which were reflected in both the low turn-on voltage and the suppressed leakage current.

To investigate the influence of active layer morphology the performance of devices comprised of active layers based on only QDs, hybrids (chemically blended system) and blends (physically mixed system) were compared (section 3.1.4.4). The best hybrid device achieved an EQE of 5.6 % which is over two times greater than the EQE values of the QD-only and blend devices with 2.0 % and 1.67 %, respectively. In the QD-only device a densely packed QD-based active layer is directly sandwiched between the hole and electron transport layers. This architecture leads to imbalanced charge injection into the QDs and subsequently QD photoluminescence (PL) quenching.[82] In the active layers based on hybrids the QDs are evenly distributed in the polymer matrix throughout the entire active layer. This homogenous morphology creates a barrier between the QDs and the charge transport layers which, due to the electron blocking properties of the polymer used, leads to the improved charge transport balance observed. Moreover, polymer grafting increases the distance between the individual QDs leading to suppressed PL quenching, and thus improved device performance. Active layers spin coated from blends exhibit, however, inorganic/organic phase separation. The heterogeneity of the blend films prohibits the implementation of the advantages which polymers provide in the hybrid systems and therefore leads to devices with low efficiencies. The results reported herein indicate that the morphology of the active layer has an enormous influence on the improvement opportunities and the device characteristics.

The influence of the quantity of anchor groups on QD hybridization and on hybrid film morphology was investigated (section 3.1.4.6). It was shown that high QD to polymer ratios and the high surface areas of small QDs (total diameter 9 nm) led to the incomplete QD hybridization when a polymer with one anchor group was used. The incomplete functionalization resulted in the presence of unfunctionalized QDs and subsequently led to

the organic/inorganic phase separation in films. The hybridization was, however, successful when the block copolymer with an anchor block (multiple anchor groups) was utilized. The chelating effect of multiple anchoring groups substantially improves coordination of polymer chains to the QD surface, while polymeric ligands with one anchor group are able to easily desorb from a QD surface due to the dynamic character of the ligand coordination to the QD surface. As a result of these observations the synthesis of new lipoic acid-based multidentate compounds was developed (section 3.2.1).

The introduction of multiple anchor groups as an anchor block has some disadvantages. First, the introduction of the same quantity of anchoring groups to different polymers (different first block) is challenging due to changing experimental conditions. Second, the determination of the quantity of the incorporated anchor groups may be problematic. With the lipoic acid-based multidentate anchor compounds **DL-NH$_2$**, **TL-NH$_2$**, **DL-N$_3$** and **TL-N$_3$** a reproducible incorporation of a defined number of anchor groups to different polymers was achieved (sections 3.2.2-3.2.4). Azide and amine functionalities enabled the attachment of the anchor compounds to the polymers with the only requirement for the polymers modified being the presence of the alkyne or reactive ester end groups. The new anchor compounds were successfully incorporated into the carbazole-based side-chain conjugated polymer *via* a reactive ester approach, into ethynyl-terminated poly(3-hexylthiophene) *via* a copper catalyzed azide-alkyne cycloaddition and into cyclooctyne-terminated polysarcosine *via* a catalyst-free strain-promoted azide-alkyne cycloaddition. Finally, the anchoring ability of the compounds was confirmed by the synthesis of stable water soluble QDs (section 3.2.5).

In summary, in this dissertation it is shown that the use of hybrid semiconducting polymer/QD active layer provides an effective way to improve QLED performance. In order to fabricate hybrid QLEDs which surpass the performance of the QD-only devices polymers with low HOMO levels should be used. Furthermore, special attention must be paid to the active layer morphology. Only when QDs are evenly distributed throughout the polymer matrix the enhanced QD photoluminescence and improvement in the charge transport balance can be realized. One pathway towards achieving homogeneous distribution is the application of polymer/QD hybrids where polymer chains are chemically grafted to the QD surfaces. Chemical grafting is achieved *via* the use of anchor groups and is especially successful if the chelate effect of multiple anchor groups is exploited.

Therefore, for the versatile synthesis of multidentate polymeric ligands new bidentate and tridentate lipoic acid-based anchor compounds were developed. The anchor compounds were then easily incorporated into different polymers using efficient reactive ester and azide-alkyne cycloaddition reactions.

5 Publications

The section 3.1 contains work included in the following publications:

Fokina A., Lee Y., Chang J. H., Braun L., Bae W. K., Char K., Lee C., Zentel R. "Side-chain conjugated polymers for the use in the active layers of hybrid semiconducting polymer/quantum dot light emitting diodes", Polym. Chem., (2015), DOI: 10.1039/c5py01492a.

Fokina A.,* Lee Y.*, Chang J. H., Park M., Sung Y., Bae W. K., Char K., Zentel R., Lee C., "The role of the active layer morphology in the enhanced performance of light emitting diodes based on quantum dot/semiconducting polymer hybrids" *in preparation*.

Fokina A. and Lee Y contributed equally to the preparation of this article. Lee. Y performed the fabrication of the QLED devices and the AFM measurements, Chang J. H. performed the synthesis of QDs and PL measurements, Sung. Y. performed the TEM measurements, all authors contributed to the scientific discussions and the preparation of the manuscripts.

The section 3.2 contains work included in the following articles:

Menk F.*, Fokina A.*, Oschmann B.*, Bergmann V. W., Bauer T. A., Nyguist Y., Berger R., Zentel R. "Functionalization of P3HT with Various Mono- and Multidentate Anchor Groups" *in preparation*

Menk F., Fokina A.and Oschmann B. contributed equally to the preparation of this article. Menk F. and Oschamann B. performed the synthesis of the P3HT polymers, Bauer T. A. contributed to the development of the anchor compounds, all authors contributed to the scientific discussions and the preparation of the manuscripts.

Fokina A.*, Klinker K.*, Jeong B. G., Bae W. K., Barz M., Zentel R., "Multidentate Polysarcosine Ligands for Water-Soluble Quantum Dots", *in preparation*

Fokina A and Klinker K. contributed equally to the preparation of this article. Klinker K. performed the synthesis of polysarcosine polymers, Jeong B. G. performed the synthesis of QDs, all authors contributed to the scientific discussions and the preparation of the manuscripts.

6 Experimental Part

6.1 Materials and Methods

Solvents used in the reactions were purchased from Sigma Aldrich and used without further purification unless stated otherwise. Dry DMF was purchased from Acros Organics (99.8 % Extra). THF for polymerization reactions was dried over Na prior to use. Solvents used in column chromatography had technical grade purity and were additionally purified by distillation. Chemicals were purchased from Sigma Aldrich, Acros Organics, Alfa Aesar, or Fluka. 2,2′-Azobis(2-methylpropionitrile) (AIBN) was purchased from Acros Organics, recrystallized from diethylether and stored at -20°C. S-1-Dodecyl-S′-(α,α′-dimethyl-α′′-pentafluorophenyl acetate)trithiocarbonate, cysteaminemethyldisulfide, polysarcosine, tri(hydroxymethyl)aminomethane, ethynyl terminated P3HT and quantum dots with CdSe core, $Cd_xZn_{1-x}S$ shell (core diameter 4 nm, total diameter 16 nm/9 nm with oleic acid surface ligands) were synthesized according to the literature.[10,159,170,178,179]

All NMR spectra were recorded in $CDCl_3$ (Deutero GmbH) with a Bruker AV 400 or Bruker AC 300 spectrometer at room temperature. Chemical shifts are reported in respect to residual solvent signal as internal standards $CDCl_3$ (^1H, ^{13}C): 7.26 ppm and 77.16 ppm and DMSO-d6 (^1H) 2.50 ppm. Polymer molecular weight was determined by gel permeation chromatography (GPC) in THF with polystyrene as external and toluene as internal standard and in HFIP 3 g l^{-1} potassium trifluoroacetate at 40 °C with PMMA as external and toluene as internals standard. A refractive index detector (G 1362A RID, Jasco) and a UV/vis detector (UV-2075 Plus, JASCO) were used to detect the polymer. UV−VIS spectra were recorded on a Varian Cary 5000 spectrometer. Emission spectra were recorded on a Varian Cary Eclipse spectrometer. Infrared spectroscopy was performed on a Jasco FT/IR-4100 with an ATR sampling accessory (MIRacle, Pike Technologies) using 16 scans per measurement. IR spectra were analyzed using Spectra Manager 2.0 (Jasco). DSC measurements were performed with Parkin Elmer DSC 8500 under nitrogen flow at 10 °C min^{-1} heating/cooling rate with three heating cycles (50 °C - 250 °C) and two cooling cycles from (250 °C - 50 °C). TGA measurements were performed with Parkin Elmer Pyris 6 TGA under nitrogen flow at 10 °C min^{-1} heating rate from 30 °C until 800 °C. Cyclic voltammetry experiments were performed with a Biologic SP-50 voltammetric analyzer using platinum wire working and counter electrodes and a 0.01 M $Ag/AgNO_3$ reference electrode with a scan rate of 100 mV s^{-1} with $[^nBu_4N][PF_6]$ as

supporting electrolyte in dichloromethane. Transmission electron microscopy (TEM) images were obtained with Carl Zeiss LIBRA 120 microscope. Scanning electron microscopy (STEM) images were obtained with Jeol JEM-2100F microscope. Atomic force microscopy (AFM) was performed at XE-100 (Park system) microscope in non-contact mode with Nanosensors™ ppp-NCHR tips (320 kHz, 42 N/m) under ambient conditions. Single crystal X-ray crystallographic data was collected using a STOE IPDS 2T diffractometer with Cu-K_α IμS radiation. Intensities were corrected for Lorentz and polarization effects. Structure solved by direct methods, SIR-2004, and refined with a full-matrix algorithm using SHELXL-2014 software package.

6.2 Synthesis of the Semiconducting Monomers

*Synthesis of 9-(4-Methoxyphenyl)carbazole **1***

Carbazole (1.00 g, 5.98 mmol), 4-iodoanisole (1.68 g, 7.18 mmol), pulverized copper (1.52 g, 23.92 mmol), potassium carbonate (6.61 g, 47.84 mmol) and 18-crown-6 ether (0.32 g, 1.20 mmol) were added to a Schlenk flask under a nitrogen atmosphere. Ortho-dichlorobenzene (30 mL) was added and the reaction mixture was heated to 200°C for 18 hours. The hot mixture was then vacuum filtered. The filtrate was distilled in vacuo (20 mbar, 70°C) to remove the solvent. The residue was purified via column chromatography (eluent hexanes/ethyl acetate 9:1) to yield 9-(4-methoxyphenyl)carbazole as colorless powder (1.20 g, 4.39 mmol, 73%). ^{1}H-NMR (300 MHz, $CDCl_3$): δ/ppm 8.16 (dt, *J* = 7.7, 1.0 Hz, 2H), 7.51 - 7.27 (m, 8H), 7.16 - 7.08 (m, 2H), 3.93 (s, 3H). ^{13}C NMR (75.4 MHz, $CDCl_3$) δ/ppm 158.97, 141.48, 130.42, 128.70, 125.96, 123.21, 120.38, 119.76, 115.18, 109.82, 55.74. HRMS (ESI+) m/z calcd 274.1232 [M+H] found 274.1226.

*Synthesis of 3,6-Dibromo-9-(4-methoxyphenyl) carbazole **2***

9-(4-Methoxyphenyl)carbazole (1.00 g, 3.66 mmol) was dissolved in dry DMF (30 mL) in a Schlenk flask under a nitrogen atmosphere. Recrystallized N-bromosuccinimide (2.61 g, 14.64 mmol) was dissolved in a separate Schlenk flask in dry DMF (30 mL) under a nitrogen atmosphere. Both solutions cooled in an ice bath for 10 minutes and the NBS solution was slowly added to the 9-(4-methoxyphenyl)carbazole solution. The mixture was left stirred at room temperature for 48 hours after which it was poured onto an ice/water mixture leading to the precipitation of 3,6-dibromo-9-(4-methoxyphenyl) carbazole. The obtained 3,6-dibromo-9-(4-methoxyphenyl) carbazole was collected via vacuum filtration,

washed several times with cold acetone and dried in vacuum for 24 hours (1.48 g, 3.43 mmol, 94%). ^{1}H-NMR (300 MHz, $CDCl_3$): δ/ppm 8.19 (dd, J = 2.0, 0.6 Hz, 2H), 7.49 (dd, J = 8.7, 2.0 Hz, 2H), 7.41 – 7.33 (m, 2H), 7.17 (dd, J = 8.7, 0.6 Hz, 2H), 7.14 – 7.08 (m, 2H), 3.92 (s, 3H). ^{13}C NMR (75.4 MHz, $CDCl_3$) δ/ppm 159.42, 140.46, 129.43, 129.39, 128.53, 123.81, 123.28, 115.40, 112.93, 111.59, 55.78. HRMS (ESI+) m/z calcd 428.9364 found 428.9345.

*Synthesis of 3,6-Bis(4-methylphenyl)-9(4-methoxyphenyl) carbazole **3***

3,6-Dibromo-9-(4-methoxyphenyl) carbazole (1.21 g, 2.81 mmol), p-tolylboronic acid (985 mg, 7.24 mmol) and tetrakis(triphenylphosphine) palladium(0) (162 mg, 0.14 mmol) were added to a Schlenk flask. Toluene (35 mL) was added to the mixture, followed by the addition of a 2 M aqueous sodium carbonate solution (8.5 mL) and ethanol (4.25 mL). The biphasic mixture was freeze-pump-thawed (3x) and left under a nitrogen atmosphere. A condenser was attached and the mixture was heated at 90°C for 20 hours under a nitrogen atmosphere. The mixture was then cooled to room temperature and the organic phase was separated from the aqueous. The aqueous phase was extracted twice with ethyl acetate and the combined organic phases were washed with water and brine. After drying with magnesium sulfate the solvents were removed by rotary evaporation. The residue was purified via column chromatography (eluent hexanes/dichloromethane) to yield 3.6-bis(4-methylphenyl)-9(4-methoxyphenyl) carbazole (820 mg, 1,81 mmol, 64%). ^{1}H-NMR (300 MHz, $CDCl_3$): δ/ppm 8.38 (dd, J = 1.8, 0.6 Hz, 2H), 7.71 – 7.59 (m, 6H), 7.55 – 7.46 (m, 2H), 7.39 (dd, J = 8.5, 0.6 Hz, 2H), 7.34 – 7.27 (m, 4H), 7.19 – 7.10 (m, 2H), 3.94 (s, 3H), 2.43 (s, 6H). ^{13}C NMR (75.4 MHz, $CDCl_3$) δ/ppm 159.02, 141.25, 139.25, 136.35, 133.41, 130.40, 129.64, 128.55, 127.29, 125.57, 123.89, 118.72, 115.25, 110.14, 110.11, 55.76, 21.24. . HRMS (ESI+) m/z calcd 453.2092 found 453.2103

*Synthesis of 3,6-Bis(4-methylphenyl)-9(4-hydroxyphenyl) carbazole **4***

3,6-Bis(4-methylphenyl)-9(4-methoxyphenyl) carbazole (490 mg, 1.08 mmol) was dissolved in dry dichloromethane (12 mL) and the solution was cooled in a acetone/dry ice bath. Boron tribromide solution (1.5 mL, 1.51 mmol, 1M in dichloromethane) was added dropwise, slowly warmed after 30 minutes and stirred for 22 hours at room temperature. Then water (2mL) was added and the mixture was stirred for additional 30 minutes. The solution was washed twice with water and once with brine and dried with magnesium

sulfate. After removal of dichloromethane by rotary evaporation 3,6-bis(4-methylphenyl)-9(4-hydroxyphenyl) carbazole was obtained as grey powder and was used in the next step without further purification (458 mg, 1.04 mmol, 96%).^{1}H-NMR (400 MHz, $CDCl_3$): δ/ppm 8.37 (dd, J = 1.8, 0.6 Hz, 2H), 7.70 – 7.59 (m, 6H), 7.48 – 7.43 (m, 2H), 7.41 – 7.36 (m, 2H), 7.10 – 7.04 (m, 2H), 2.43 (s, 6H). ^{13}C NMR (100.6 MHz, $CDCl_3$) δ/ppm 155.07, 141.24, 139.25, 136.38, 133.47, 130.66, 129.65, 128.82, 127.30, 125.60, 123.92, 118.74, 116.78, 110.12, 21.24.

*Synthesis of monomer **M1***

3,6-Bis(4-methylphenyl)-9(4-hydroxyphenyl) carbazole (770 mg, 1.75 mmol), 4-vinylbenzyl chloride (0.41 mL, 446 mg, 2.92 mmol), potassium carbonate (1.21 g, 8.76 mmol) and a catalytic amount of potassium iodide were added to the flask. A mixture of acetonitrile (12 mL) and DMF (24 mL) was added. The mixture was heated at 60°C for 3 hours. The mixture was then cooled to the room temperature and poured to of ice/water mixture (250 g). After the ice melted dichloromethane (250 mL) was added to the mixture to extract the organic compounds. The aqueous phase was extracted with dichloromethane two more time and the combined organic phases were washed with brine and dried with magnesium sulfate. Dichloromethane was removed by rotary evaporation and the residue was purified via column chromatography (eluent hexanes/dichloromethane) to yield monomer **M1** (795 mg, 1.44 mmol, 82 %). ^{1}H-NMR (400 MHz, $CDCl_3$): δ/ppm 8.37 (dd, J = 1.8, 0.6 Hz, 2H), 7.69 – 7.60 (m, 6H), 7.53 – 7.45 (m, 6H), 7.39 (d, J = 8.5 Hz, 2H), 7.35 – 7.27 (m, 4H), 7.24 – 7.17 (m, 2H), 6.77 (dd, J = 17.6, 10.9 Hz, 1H), 5.81 (dd, J = 17.6, 0.9 Hz, 1H), 5.30 (dd, J = 10.9, 0.8 Hz, 1H), 5.17 (s, 2H), 2.43 (s, 6H). ^{13}C NMR (100.6 MHz, $CDCl_3$) δ/ppm 158.16, 141.19, 139.24, 137.67, 136.53, 136.35, 136.31, 133.43, 130.65, 129.65, 128.53, 127.91, 127.28, 126.67, 125.57, 123.91, 118.71, 116.17, 114.43, 110.15, 70.29, 21.24. . HRMS (ESI+) m/z calcd 555.2562 found 555.2558. Crystallographic data: space group (crystal system): P 2_1/c (monoclinic); absorption: μ = 0.54 mm^{-1}, transmission: T_{min} = 0.8454, T_{max}= 0.9891, crystal size (color): 0.02 x 0.13 x 0.47 mm^3 (colorless), lattice constants (calculated with 16944 reflexes with 2.43°< θ < 67.72°): a=18.3586(10) Å, b=22.0396(12) Å, ß=97.835(5)°, c=7.6912(5) Å, V = 3082.9(3) $Å^3$, z = 4, F(000) = 1176.0, temperature: -60 °C, density: d_{xray}=1.197 gcm^{-3}.

*Synthesis of 3,6-Bis(4-methylthiophene)-9(4-methoxyphenyl) carbazole **5***

3,6-Dibromo-9-(4-methoxyphenyl) carbazole (1.00 g, 2.32 mmol), p-tolylboronic acid (1.46 mL, 1.37 g, 6.11 mmol) and tetrakis(triphenylphosphine) palladium(0) (134 mg, 0.11 mmol) were added to a Schlenk flask. Toluene (28 mL) was added to the mixture, followed by the addition of a 2 M aqueous sodium carbonate solution (7.0 mL) and ethanol (3.5 mL). The biphasic mixture was freeze-pump-thawed (3x) and left under a nitrogen atmosphere. A condenser was attached and the mixture was heated at 90°C for 20 hours under a nitrogen atmosphere. The mixture was then cooled to room temperature and the organic phase was separated from the aqueous. The aqueous phase was extracted twice with ethyl acetate and the combined organic phases were washed with water and brine. After drying with magnesium sulfate the solvents were removed by rotary evaporation. The residue was purified via column chromatography (eluent hexanes/dichloromethane) to yield 3.6-bis(4-methylphenyl)-9(4-methoxyphenyl) carbazole (781 mg, 1.68 mmol, 72%). ^{1}H-NMR (400 MHz, $CDCl_3$): δ/ppm δ 8.30 (dd, J = 1.8, 0.6 Hz, 2H), 7.61 (dd, J = 8.5, 1.8 Hz, 2H), 7.49-7.41 (m, 2H), 7.29 (dd, J = 8.5, 0.6 Hz, 2H), 7.15 (d, J = 3.4 Hz, 2H), 7.14-7.09 (m, 2H), 6.80-6.73 (m, 2H), 3.93 (s, 3H), 2.55 (s, 6H). ^{13}C NMR (75.4 MHz, $CDCl_3$) δ/ppm 159.08, 143.21, 141.18, 138.60, 130.11, 128.49, 127.23, 126.28, 124.56, 123.61, 122.12, 117.51, 115.26, 110.25, 110.12, 55.76, 15.64.

*Synthesis of 3,6-bis(4-trifluoromethylphenyl)-9(4-methoxyphenyl) carbazole **6***

3,6-Dibromo-9-(4-methoxyphenyl) carbazole (500 mg, 1.16 mmol), 4-(trifluoromethyl) phenylboronic acid (579 mg, 3.05 mmol) and tetrakis(triphenylphosphine) palladium(0) (67 mg, 0.058 mmol) were added to a Schlenk flask. Toluene (15 mL) was added to the mixture, followed by the addition of a 2 M aqueous sodium carbonate solution 3.5 mL) and ethanol (1.75 mL). The biphasic mixture was freeze-pump-thawed (3x) and left under a nitrogen atmosphere. A condenser was attached and the mixture was heated at 90°C for 18 hours under a nitrogen atmosphere. The mixture was then cooled to room temperature and the organic phase was separated from the aqueous. The aqueous phase was extracted twice with ethyl acetate and the combined organic phases were washed with water and brine. After drying with magnesium sulfate the solvents were removed by rotary evaporation. The residue was purified via column chromatography (eluent hexanes/dichloromethane) to yield 3,6-bis(4-trifluoromethylphenyl)-9(4-methoxyphenyl) carbazole **6** (385 mg, 0.69 mmol, 59%). ^{1}H-NMR (400 MHz, $CDCl_3$): δ/ppm δ 8.42 (dd, J = 1.8, 0.6 Hz, 2H),

7.87-7.80 (m, 4H), 7.76-7.71 (m, 4H), 7.69 (dd, J = 8.5, 1.8 Hz, 2H), 7.53-7.47 (m, 2H), 7.43 (dd, J = 8.5, 0.6 Hz, 2H), 7.20-7.10 (m, 2H), 3.95 (s, 3H).

*Synthesis of monomer **M2***

Carbazole (8.5 g, 0.051 mol),potassium hydroxide (4.28 g, 0.076 mol) and DMF (100 mL) were added to a flask and stirred at room temperature for two hours. Then 4-vinylbenzyl chloride (7.9 mL, 8.53 g, 0.056 mol) was added and the ice bath removed. The mixture was stirredat room temperature for 24 hours and then was poured into a ice/water mixture (400 g) and a white precipitation formed. After the ice melted the precipitation was filtered and washed with methanol and hexanes. The residue was then recrystallized from acetone to yield monomer **M2** as colorless needles (12.55 g, 0.044 mol, 87 %). ^{1}H-NMR (400 MHz, $CDCl_3$): δ/ppm 8.15 (dt, J = 7.8, 1.0 Hz, 2H), 7.46-7.42 (m, 2H), 7.37 (dt, J = 8.2, 0.9 Hz, 2H), 7.33 – 7.23 (m, 4H), 7.11 (d, J = 8.0 Hz, 2H), 6.66 (dd, J = 17.6, 10.9 Hz, 1H), 5.69 (dd, J = 17.6, 1.0 Hz, 1H), 5.21 (dd, J = 10.9, 0.9 Hz, 1H). ^{13}C NMR (100.6 MHz, $CDCl_3$) δ/ppm 140.76, 137.01, 136.84, 136.41, 126.75, 126.73, 125.99, 123.17, 120.53, 119.36, 114.06, 109.01, 46.49. HRMS (ESI+) m/z calcd 284.1439 [M+H] found 284.1466.

*Synthesis of formyl- 4,4'-bis(N-carbazolyl)-1,1'-biphenyl (formyl-CBP) **7***

4,4'-Bis(N-carbazolyl)-1,1'-biphenyl (1.25 g, 2.60 mmol) was dissolved in dry dichloromethane (100 mL) in a Schlenk flask under a nitrogen atmosphere. The solution was cooled in an ice bath and a tin(IV) chloride solution (3.9 mL, 1M in dichloromethane) was added slowly. After 25 minutes dichloromethyl methyl ether (0.35 mL, 0.45 g, 0.0039 mmol) was added drop wise. After 2 hours the ice bath was removed and the mixture was stirred at room temperature for three additional hours. Then the mixture was poured onto ice (160 g). After ice melted the phases were separated and the organic phase was extracted once with water and three times with saturated aqueous $NaHCO_3$ solution. $NaHCO_3$ was added to the aqueous phase and the neutralized aqueous phase was extracted twice with dichloromethane. The combined organic phases were washed with water and brine and dried with MgSO4. The solvent was removed by rotary evaporation and the residue purified by column chromatography (eluent hexanes/ethyl acetate) to yield formyl-CBP (693 mg, 1.35 mmol, 52 %). ^{1}H-NMR (400 MHz, $CDCl_3$): δ/ppm 10.15 (s, 1H), 8.71 (dd, J = 1.6, 0.7 Hz, 1H), 8.25 (dt, J = 7.8, 1.1 Hz, 1H), 8.19 (dt, J = 7.7, 1.0 Hz, 2H), 8.03 – 7.90 (m, 5H), 7.76 – 7.67 (m, 4H), 7.58 – 7.39 (m, 8H), 7.40-7.31 (m, 2H). ^{13}C NMR

(100.6 MHz, $CDCl_3$) δ/ppm 191.89, 144.58, 141.94, 140.90, 140.41, 140.10, 139.10, 137.64, 136.56, 136.30, 129.76, 129.71, 128.98, 128.91, 128.72, 127.80, 127.74, 127.67, 127.24, 126.18, 124.06, 123.87, 123.66, 123.50, 121.55, 121.50, 120.90, 120.55, 120.28, 110.61, 110.33, 109.93. . HRMS (ESI+) m/z calcd 513.1967 [M+H] found 513.1948.

Synthesis of acrylic acid- 4,4'-bis(N-carbazolyl)-1,1'-biphenyl (acrylic acid-CBP) ***8***

The compound **5** (1.05 g, 2.05 mmol) and malonic acid (639 mg, 6.15 mmol) were suspended in dry pyridine (100 mL) and piperidine (cat. 20 drops) was added dropwise. The reaction mixture was stirred at 100°C for 19 hours. Upon heating all components dissolved and a clear reaction solution was obtained. The reaction solution was let to cool down to room temperature and slowly added to 600 mL of 3M HCl. The aqueous phase was repeatedly extracted with dichloromethane and the combined organic phases were washed twice with water and twice with brine solution. The solvent was removed by rotary evaporation and the residue purified by column chromatography (eluent dichloromethane/acetone) to yield compound **6** (900 mg, 1.62 mmol, 79 %). ^{1}H-NMR (400 MHz, $CDCl_3$): δ/ppm 8.37 (d, J = 1.6 Hz, 1H), 8.18 – 8.22 (m, 3H), 8.05 (d, J = 15.8 Hz, 1H), 7.97 – 7.90 (m, 4H), 7.77 – 7.66 (m, 5H), 7.58 – 7.30 (m, 10H), 6.55 (d, J = 15.9 Hz, 1H). ^{13}C NMR (100.6 MHz, $CDCl_3$) δ/ppm 172.44, 148.17, 142.41, 141.60, 140.92, 139.99, 139.22, 137.54, 136.69, 128.81, 128.69, 127.65, 127.59, 126.89, 126.52, 126.46, 126.17, 124.11, 123.65, 123.38, 121.65, 121.04, 120.73, 120.54, 120.26, 114.52, 110.51, 110.40, 109.95. . HRMS (ESI+) m/z calcd 554.1994 [M+H] found 554.2001.

Synthesis of propanoic acid- 4,4'-bis(N-carbazolyl)-1,1'-biphenyl (propanoic acid-CBP) ***9***

Compound **6** (817 mg, 1.47 mmol) was dissolved in dry THF in a schlenk flask and palladium on charcoal (82 mg, 10 wt% Pd) was added. The reaction mixture was purged with hydrogen and a balloon filled with hydrogen was attached to the flask via the stopcock. The reaction mixture was shaken at room temperature for 24 hours. The black residue was filtered off and the solvent was removed by rotary evaporation. Compound **7** was used in the next step without further purification. ^{1}H-NMR (400 MHz, $CDCl_3$): δ/ppm 8.20 – 8.15 (m, 3H), 8.05 – 8.00 (m, 1H), 7.95 – 7.88 (m, 4H), 7.75 – 7.67 (m, 4H), 7.55 – 7.42 (m, 7H), 7.37 – 7.29 (m, 4H), 3.20 (t, J = 7.8 Hz, 2H), 2.82 (t, J = 7.8 Hz, 2H). ^{13}C NMR (100.6 MHz, $CDCl_3$) δ/ppm 178.02, 141.19, 140.94, 139.73, 139.41, 139.33, 137.43, 137.37, 132.56, 132.18, 130.21, 129.06, 128.64, 128.41, 127.61, 127.49, 126.65, 126.19, 126.16,

123.86, 123.63, 123.44, 120.52, 120.50, 120.21, 120.18, 119.93, 110.12, 110.04, 109.99, 109.96, 68.11, 36.50, 30.95, 25.75. . HRMS (ESI+) m/z calcd 579.2049 [M+Na] found 579.2057.

Synthesis of propanol- 4,4'-bis(N-carbazolyl)-1,1'-biphenyl (propanol-CBP) ***10***

Compound **7** (780 mg, 1.40 mmol) dissolved in THF (50 mL) was slowly added to a $LiAlH_4$ (53.2 g, 1.4 mmol) suspension in THF (20 mL). The reaction mixture was stirred at room temperature for four hours. The reaction was quenched with ethanol. Afterward 110 mL of 10% H_2SO_4 solution was added and the mixture was repeatedly extracted with diethyl ether. The combined organic phases were washed with water and brine and dried over MgSO4. The solvent was removed by rotary evaporation and the residue purified by column chromatography (eluent dichloromethane/acetone) to yield compound **8** (580 mg, 1.12 mmol, 76 % (two steps)) ^{1}H-NMR (400 MHz, $CDCl_3$): δ/ppm 8.19 (d, J = 7.7 Hz, 2H), 8.16 (d, J = 7.7 Hz, 1H), 8.01 (dd, J = 1.7, 0.7 Hz, 1H), 7.93 – 7.90 (m, 4H), 7.75 – 7.68 (m, 4H), 7.56 – 7.41 (m, 7H), 7.37 – 7.28 (m, 4H), 3.76 (t, J = 6.4 Hz, 2H), 2.94 (t, J = 7.6 Hz, 2H), 2.10 – 1.96 (m, 2H). ^{13}C NMR (100.6 MHz, $CDCl_3$) δ/ppm 141.15, 140.95, 139.52, 139.44, 139.26, 137.53, 137.35, 133.74, 128.63, 127.62, 127.48, 126.86, 126.16, 126.09, 123.81, 123.63, 123.50, 120.52, 120.46, 120.21, 120.10, 119.94, 109.96, 109.88, 62.53, 35.17, 32.26. HRMS (ESI+) m/z calcd 542.2358 found 542.2379.

Synthesis of Monomer ***M3***

Compound **8** (300 mg, 0.55 mmol), NaH (60% in oil, 26.5 mg, 1.11 mmol) and KI (cat.) were added to dry THF (50 mL)/DMF (5 mL). 4-Vinylbenzyl chloride (90%, 0.13 mL, 126 mg, 0.83 mmol) was added and the reaction mixture was stirred at 50°C for 24 hours. After addition of DCM (100 mL) and water (100 mL) the organic phase was separated and washed with water and brine. The solvent was removed by rotary evaporation and the residue purified by column chromatography (eluent hexanes/dichloromethane) to yield monomer **M3** as colorless powder (295 mg, 0.45 mmol, 83 %). ^{1}H-NMR (400 MHz, $CDCl_3$): δ/ppm 8.19 (d, J = 7.7, 2H), 8.14 (d, J = 7.8, 1H), 7.98 (d, J = 1.6 Hz, 1H), 7.95 – 7.89 (m, 4H), 7.75 – 7.68 (m, 4H), 7.56 – 7.27 (m, 16H), 6.73 (dd, J = 17.6, 10.9 Hz, 1H), 5.76 (dd, J = 17.6, 1.0 Hz, 1H), 5.25 (dd, J = 10.9, 0.9 Hz, 1H), 3.56 (t, J = 6.3 Hz, 2H), 2.94 (t, J = 7.6 Hz, 2H), 2.18 – 1.99 (m, 2H). ^{13}C NMR (100.6 MHz, $CDCl_3$) δ/ppm 141.11, 140.94, 139.45, 139.21, 138.40, 137.56, 137.34, 137.05, 136.72, 133.93, 128.63, 128.61,

128.06, 127.61, 127.46, 126.96, 126.38, 126.15, 126.02, 123.74, 123.62, 123.55, 120.52, 120.45, 120.21, 120.07, 120.00, 113.87, 109.97, 109.93, 109.77, 72.84, 69.66, 32.54, 32.32. HRMS (ESI+) m/z calcd 658.2984 found 658.2972.

6.3 Synthesis of the Side-Chain Conjugated Polymers

*General procedure for the RAFT polymerization of polymers **P1**, **P1a**, **P2**, **P2a**, **P2b and P3***

Appropriate amount of monomer (**M1**-**M3**), chain transfer agent (CTA) S-1-Dodecyl-S′-(α,α′-dimethyl-α′′-pentafluorophenyl acetate)trithiocarbonate) and initiator 2,2′-azibis(2-methylpropionitrile) (AIBN) were dissolved in dry THF and degassed *via* three freeze-pump-thaw cycles. At the end the flask was filled with nitrogen and sealed. Afterward the polymerization solution was immerged into preheated oil bath and left to react at 65°C for 48 hours. The reaction solution was rapidly cooled down by immersing the flask into liquid nitrogen for several second. The formed polymer and excess monomer were first precipitated into hexanes. For purification the polymer was repeatedly redissolved in THF and precipitates into suitable solvent. The remaining solutions containing excess of the monomer were collected and the unreacted monomer recovered for the use in future reactions. The collected polymer was dried at 30°C in vacuum for 24 hours. The polymers were analyzed *via* THF-GPC, IR, ^{1}H and ^{19}F NMR spectroscopies. All polymers exhibit the same signals in ^{19}F NMR and the characteristic C=O band of the aromatic ester at approximately 1772 cm^{-1} in IR spectra. ^{19}F-NMR (282 MHz, $CDCl_3$): δ/ppm -154 (2H), -159 (1H), -163 (2H).

*Polymer **P1***

Monomer **M1** (680 mg, 1.22 mmol), CTA (10.8 mg, 0.020 mmol), AIBN (0.44 mg, 0.0029 mmol), THF (4.5 mL). Solvent for purification: methanol/diethyl ether 2/1. 380 mg polymer as a lightly yellow powder (51%). M_n = 10900 g mol^{-1}, PDI 1.1.

*Polymer **P1a***

Monomer **M1** (1.0 g, 1.80 mmol), CTA (7.95 mg, 0.015 mmol), AIBN (0.35 mg, 0.0021 mmol), THF (7.6 mL). Solvent for purification: methanol/diethyl ether 2/1. 560 mg polymer as a lightly yellow powder (56%). M_n = 19600 g mol^{-1}, PDI 1.2

*Polymer **P2***

Monomer **M2** (1.0 g, 3.53 mmol), CTA (30.4 mg, 0.058 mmol), AIBN (1.38 mg, 0.0084 mmol), THF (10 mL). Solvent for purification: hexanes/acetone 4/1. 480 mg of polymer as a lightly yellow powder (48%). M_n = 5300g mol^{-1}, PDI 1.2.

*Polymer **P2a***

Monomer **M2** (1.0 g, 3.53 mmol), CTA (15.5 mg, 0.030 mmol), AIBN (0.69 mg, 0.0042 mmol), THF (10 mL). Solvent for purification: hexanes/acetone 4/1. 420 mg of polymer as a lightly yellow powder (42%). M_n = 8100g mol^{-1}, PDI 1.1.

*Polymer **P2b***

Monomer **M2** (1.0 g, 3.53 mmol), CTA (7.80 mg, 0.015 mmol), AIBN (0.35 mg, 0.0021 mmol), THF (10 mL). Solvent for purification: hexanes/acetone 4/1. 380 mg of polymer as a lightly yellow powder (38%). M_n = 13600g mol^{-1}, PDI 1.2.

*Polymer **P3***

Monomer **M3** (250 mg, 0.379 mmol), CTA (3.36 mg, 0.0062 mmol), AIBN (0.15 mg, 0.0009 mmol), THF (2 mL). Solvent for purification: methanol/acetone 2/1 and hexanes/acetone 3/1. 110 mg of polymer as a lightly yellow powder (44%). M_n = 11600 g mol^{-1}, PDI 1.1.

General procedure for the CTA-end group removal

The polymer and 70 eq. of AIBN were dissolved in dry THF and stirred at 75°C for 24 hours. The reaction solution was cooled down and repeatedly precipitated into hexanes/diethyl ether 3/1. The polymer was obtained as colorless powder and dried at 30°C in vacuum for 24 hours.

General procedure for the post-polymerization modification of pentafluorophenyl ester end group with 2-methyldithio-ethylamine

The polymer, 20 eq. of 2-methyldithio-ethylamine and 40 eq. of triethylamine were dissolved in dry THF and stirred for 24 hours at 30°C. The reaction solution was repeatedly precipitated into methanol and hexanes. The polymer was obtained as colorless powder and

dried at 30°C in vacuum for 24 hours. The successful modification was verified *via* ^{19}F spectroscopy (no signals) and IR spectroscopy. All polymers exhibit the characteristic C=O band of the amide group at approximately 1663 cm^{-1} in IR spectra.

General procedure for the RAFT polymerization of homopolymers ***bP1a***, ***bP1b***, ***bP2a*** *and* ***bP2b***

Appropriate amount of monomer (**M1** or **M2**), chain transfer agent (CTA) 2-cyano-2-propyl dodecyl trithiocarbonate and initiator 2,2′-azibis(2-methylpropionitrile) (AIBN) were dissolved in dry THF and degassed *via* three freeze-pump-thaw cycles. At the end the flask was filled with nitrogen and sealed. Afterward the polymerization solution was immerged into preheated oil bath and left to react at 65°C for 48 hours. The reaction solution was rapidly cooled down by immersing the flask into liquid nitrogen for several second. The formed polymer and excess monomer were first precipitated into hexanes. For purification the polymer was repeatedly redissolved in THF and precipitates into suitable solvent. The remaining solutions containing excess of the monomer were collected and the unreacted monomer recovered for the use in future reactions. The collected polymer was dried at 30°C in vacuum for 24 hours. The polymers were analyzed *via* THF-GPC.

Polymer ***bP1a***

Monomer **M1** (600 mg, 1.08 mmol), CTA (4.67 mg, 0.014 mmol), AIBN (0.32 mg, 0.0019 mmol), THF (4.5 mL). Solvent for purification: methanol/diethyl ether 2/1. 320 mg polymer as a lightly yellow powder (53%). M_n = 11200 g mol^{-1}, PDI 1.1.

Polymer ***bP1b***

Monomer **M1** (1.0 g, 1.80 mmol), CTA (5.18 mg, 0.015 mmol), AIBN (0.35 mg, 0.0021 mmol), THF (7.5 mL). Solvent for purification: methanol/diethyl ether 2/1. 535 mg polymer as a lightly yellow powder (54%). M_n = 23700 g mol^{-1}, PDI 1.2.

Polymer ***bP2a***

Monomer **M2** (1.0 g, 3.53 mmol), CTA (13.55 mg, 0.039 mmol), AIBN (1.08 mg, 0.0065 mmol), THF (15 mL). Solvent for purification: hexanes/acetone 4/1. 310 mg of polymer as a lightly yellow powder (31%). M_n = 5900g mol^{-1}, PDI 1.2.

*Polymer **bP2b***

Monomer **M2** (1.0 g, 3.53 mmol), CTA (5.08 mg, 0.015 mmol), AIBN (0.35 mg, 0.0021 mmol), THF (10 mL). Solvent for purification: hexanes/acetone 4/1. 440 mg of polymer as a lightly yellow powder (44%). M_n = 11300g mol^{-1}, PDI 1.1.

*General Procedure for the RAFT polymerization of the block copolymers **BP1a**, **BP1b**, **BP2a** and **BP2b**.*

Appropriate amount of corresponding homopolymer/macrochain-transfer agent (**bP1a**, **bP1b**, **bP2a** or **bP2b**), pentafluorophenyl acrylate monomer and initiator 2,2′-azibis(2-methylpropionitrile) (AIBN) were dissolved in dry THF and degassed *via* three freeze-pump-thaw cycles. At the end the flask was filled with nitrogen and sealed. Afterward the polymerization solution was immerged into preheated oil bath and left to react at 65°C for 40-72 hours. The reaction solution was rapidly cooled down by immersing the flask into liquid nitrogen for several second. The formed polymer and excess monomer were first precipitated into hexanes. For purification the polymer was repeatedly redissolved in THF and precipitates into hexanes. The remaining solutions containing excess of the monomer were collected and the unreacted monomer recovered for the use in future reactions. The collected polymer was dried at 30°C in vacuum for 24 hours. The polymers were analyzed *via* THF-GPC, ^{1}H NMR and ^{19}F NMR spectroscopies. All polymers exhibit the same signals in ^{19}F NMR and the characteristic C=O band of the aromatic ester at approximately 1784 cm^{-1} in IR spectra. ^{19}F-NMR (282 MHz, $CDCl_3$): δ/ppm -155 (2H), -159 (1H), -1643 (2H).

*Polymer **BP1a***

Homopolymer ***bP1a*** (160 mg, 0.014 mmol), pentafluorophenyl acrylate (197 mg, 0.827 mmol), AIBN (0.28 mg, 0.0017 mmol), THF (3 mL). 170 mg polymer as a lightly yellow powder. M_n = 11100 g mol^{-1}, PDI 1.1.

*Polymer **BP1b***

Homopolymer ***bP1b*** (200 mg, 0.0075 mmol), pentafluorophenyl acrylate (179 mg, 0.75 mmol), AIBN (0.15 mg, 0.001 mmol), THF (3.0 mL), reaction time 47 hours. 200 mg polymer as a lightly yellow powder. M_n = 23300 g mol^{-1}, PDI 1.2.

*Polymer **BP2a***

Homopolymer ***bP2a*** (250 mg, 0.045 mmol), pentafluorophenyl acrylate (865.85 mg, 0.020 mmol), AIBN (0.93 mg, 0.0057 mmol), THF (3.5 mL), reaction time 69 hours. 300 mg polymer as a lightly yellow powder. M_n = 6300 g mol^{-1}, PDI 1.2.

*Polymer **BP2b***

Homopolymer ***bP2b*** (250 mg, 0.022 mmol), pentafluorophenyl acrylate (414 mg, 1.74 mmol), AIBN (0.44 mg, 0.0029 mmol), THF (4.5 mL), reaction time 40 hours. 280 mg polymer as a lightly yellow powder. M_n = 11500 g mol^{-1}, PDI 1.2.

General procedure for the CTA-end group removal

The polymer and 70 eq. of AIBN were dissolved in dry THF and stirred at 75°C for 24 hours. The reaction solution was cooled down and repeatedly precipitated into hexanes/diethyl ether 3/1. The polymer was obtained as colorless powder and dried at 30°C in vacuum for 24 hours.

General procedure for the post-polymerization modification of pentafluorophenyl ester block with 2-methyldithio-ethylamine

The polymer, 100 eq. of 2-methyldithio-ethylamine and 200 eq. of triethylamine were dissolved in dry THF and stirred for 24 hours at 30°C. The reaction solution was repeatedly precipitated into methanol and hexanes. The polymer was obtained as colorless powder and dried at 30°C in vacuum for 24 hours. The successful modification was verified *via* ^{19}F spectroscopy (no signals) and IR spectroscopy. All polymers exhibit the characteristic C=O band of the amide group at approximately 1676 cm^{-1} in IR spectra.

6.4 Synthesis and Characterization of Polymer/Quantum Dot Systems

*General procedure for QD/polymer hybrid **QH1-QH3** synthesis by ligand exchange*

Polymer (5.2 mg) and quantum dots (QD, red, CdSe core, core diameter 4 nm, $Cd_xZn_{1-x}S$ shell, total diameter 16 nm, oleic acid ligands, 5.2 mg) were separately dissolved in toluene (each 50 µL) and subsequently combined. The reaction mixture was sonicated for one hour and ethanol (1.5 mL) was added. The formed sediment was dispersed in toluene (250 µL),

sonicated for one additional hour and left at room temperature for 18 hours. Afterwards ethanol (1.5 mL) was added and the formed sediment was again dispersed in toluene and sonicated for one hour. After addition of ethanol the sediment was dried and dispersed in toluene (600 µL) to obtain QD/polymer hybrid solution (1 wt% polymer, 1 wt% QDs).

*General procedure for the synthesis of QD/polymer hybrids (**H1**-**H4**), blends (**B1**-**B4**) and dual systems (**A1**-**A4**) by ligand exchange*

For the synthesis of hybrids block copolymer **BPS2a** was used, for the synthesis of blend the polymer **P2*** without anchor groups was used and for the synthesis of dual systems the polymer **P2** with one anchor groups was used. Polymer (8.9 mg, 6.7 mg, 4.4 mg or 2.2 mg depending on the sample) and quantum dots (QD, red, CdSe core, core diameter 4 nm, $Cd_xZn_{1-x}S$ shell, total diameter 9 nm, oleic acid ligands, 17.7 mg) were separately dissolved in chlorobenzene (each 100 µL) and subsequently combined. The reaction mixture was sonicated for one hour and ethanol (1.5 mL) was added. The formed sediment was dispersed in chlorobenzene (250 µL), sonicated for one additional hour and left at room temperature for 18 hours. Afterwards ethanol (1.5 mL) was added and the formed sediment was again dispersed in chlorobenzene and sonicated for one hour. After addition of ethanol the sediment was dried and dispersed in the appropriate amount of toluene to obtain QD/polymer hybrid solution with the total concentration of 19.8 mg/mL.

Sample preparation for TEM measurements

QD/polymer hybrid solutions in toluene were spin coated on the freshly cleaved mica substrates (hydrophilic surface) at 3000 rpm for 30 seconds and dried in the oven at 100 °C for 5 minutes. The mica slide was immerged into the water to obtain the free standing hybrid film floating on the water surface. The free standing film was picked up with the carbon coated TEM grid and dried on the air.

Sample preparation for AFM measurements

QD/polymer hybrid solutions in toluene were spin coated on the freshly cleaned glass substrates at 3000 rpm for 30 seconds and dried in the oven at 100 °C for 5 minutes.

6.5 Device Fabrication and Characterization

QLEDs were fabricated on patterned ITO glass substrate. The substrates were cleaned with acetone, isopropanol, deionized water, sequentially. First transparent ZnO nanoparticle solution (25 mg/mL in ethanol) was spin coated on ITO substrate at 2000 rpm for 40 seconds and dried under N_2 at 100℃ for 30 min. With dispersion in toluene (QD@polymer hybrid solution, 1 wt% polymer, 1 wt% QDs), emission layer of hybrid QD layers were similarly cast from solution on top of ZnO/ITO. The CBP, MoO3, and Al were thermally evaporated at a deposition rate of 0.5-1 Å/s for CBP, 0.3 Å/s for MoO3, and 4-5 Å/s for Al electrode. The current-voltage-luminance (I-V-L) characteristics of the devices were measured with a Keithley-236 source-measure unit, a Keithley-2000 multimeter unit, and a calibrated Si photodiode (Hamamatsu S5227-1010BQ). The EL spectra of the device were obtained by using a spectroradiometer (CS-1000A).

6.6 Synthesis of Lipoic Acid-Based Anchor Compounds

*Synthesis of the compound **11***

DL-α-lipoic acid (2.03 g, 9.86 mmol), N,N′-dicyclohexylcarbodiimide (DCC) (2.34 g, 10.85 mmol) and 4-(dimethylamino)pyridine (DMAP) (120 mg, 0.98 mmol) were dissolved in dry DCM (55 mL). 1,3-Diamino-2-propanol (400 mg, 4.44 mmol) was separately dissolved in dry DCM (5 mL) and slowly added to the reaction mixture. The reaction mixture was stirred at room temperature and under protectection from light for 40 hours. The colorless residue formed was separated via filtration through celite. The solvent of the remaining yellow filtrate was removed by rotary evaporation. The residue was purified *via* column chromatography (eluent dichloromethane/methanol) to yield compound **11** as yellow solid (1,23 g, 2.64 mmol, 59 %). ^{1}H-NMR (400 MHz, $CDCl_3$): δ/ppm 6.81 (t, J=6 Hz, 2H), 3.73 (p, J = 5.1 Hz, 1H), 3.57-5.51 (m, 2H), 3.39-3.32 (m, 2H), 3.24-3.05 (m, 6H), 2.47-2.39 (m, 2H), 2.21 (t, J = 7.5 Hz, 4H), 1.92-1.84 (m, 2H), 1.73-1.56 (m, 8H), 1.51-1.36 (m, 4H). ^{13}C NMR (100.6 MHz, $CDCl_3$) δ/ppm 174.71, 69.96, 56.48, 42.53, 40.34, 38.57, 36.36, 34.67, 28.94, 25.48. HRMS (ESI+) m/z calcd 467.1531 [M+H] found 467.1525.

*Synthesis of the compound **12***

Boc-ß-Alanin-OH (446 mg, 2.14 mmol), DCC (531 mg, 2.57 mmol) and DMAP (53 mg, 0.43 mmol) were dissolved in DCM (30 mL). The compound **11** (800 mg, 1.72 mmol) was separately dissolved in DCM (20 mL) and subsequently added to the first solution. The reaction solution was stirred for 48 hours at room temperature and under protection from light. The colorless residue formed was separated *via* filtration through celite. The solvent of the remaining yellow filtrate was removed by rotary evaporation. The residue was purified *via* column chromatography (eluent dichloromethane/acetone) to yield compound **12** as yellow solid (1.02 mg, 1.60 mmol, 75 %). ^{1}H-NMR (400 MHz, $CDCl_3$): δ/ppm 6.96 (s, 2H), 5.05 (s, 1H), 4.84-4.79 (m, 1H), 3.67-3.47 (m, 6H), 3.20-3.07 (m, 6H), 2.49-2.41 (m, 4H), 2.25 (t, J = 7.5 Hz, 4H), 1.94-1.86 (m, 2H), 1.77-1.61 (m, 8H), 1.54-1.42 (m, 13H). ^{13}C NMR (100.6 MHz, $CDCl_3$) δ/ppm 174.15, 170.80, 156.50, 80.01, 71.36, 56.54, 40.39, 38.61, 38.38, 36.53, 34.75, 29.03, 28.50, 25.57. HRMS (ESI+) m/z calcd 638.2426 [M+H] found 638.2415.

*Synthesis of the compound **14***

Tris(hydroxymethyl)-BOC-aminomethane (BOC-TRIS) (0.91 g, 4.09 mmol) and DL-α-lipoic acid (3.80 g, 18.42 mmol) were dissolved in dry DMF (20mL). DCC (3.80 g, 4.95 mmol) DMAP (450 mg, 3.68 mmol) and 1-hydroxybenzotriazole hydrate (HOBt hydrate) (83 mg, 0.61 mmol) were separately dissolved in dry DMF and subsequently added to the first solution. The reaction was stirred at room temperature and under protection from light for 90 hours. The colorless residue formed was separated *via* filtration through celite. The solvent of the remaining yellow filtrate was removed by rotary evaporation. The residue was purified *via* column chromatography (eluent hexanes/ethyl acetate) to yield compound **14** as a yellow waxy oil (3.16 g, 4.02 mmol, 98 %). ^{1}H-NMR (400 MHz, $CDCl_3$): δ/ppm 4.35 (s, 6H), 3.60-3.53 (m, 3H), 3.21-3.53 (m, 6H), 2.50-2.43 (m, 3H), 2.35 (t, J = 7.5 Hz, 6H), 1.95-1.87 (m, 3H), 1.74-1.60 (m, 12H), 1.55-1.43 (m, 15H). ^{13}C NMR (100.6 MHz, $CDCl_3$) δ/ppm 173.11, 156.26, 62.50, 58.44, 56.46, 40.40, 38.63, 34.68, 33.95, 28.84, 28.57, 28.51, 24.68. HRMS (ESI+) m/z calcd 808.2156 [M+Na] found 808.2158.

*Synthesis of the compound **15***

The compound **14** (3.16 g, 4.02 mmol) was dissolved in DCM (90 mL) and trifluoroacetic acid (TFA) (9 mL) was slowly added to reaction solution. After stirring for three hours at room temperature 1M Na_2CO_3 solution (90 mL) was added to the reaction solution. The phases were separated and the organic phase was extracted once with 1M Na_2CO_3 solution, twice with water and once with brine. Finally, the organic phase was dried with Mg_2SO_4 and the solvent was removed by rotary evaporation. The remaining crude product (compound **15**, 2.90 g,) was used in the next step without further purification. ^{1}H-NMR (400 MHz, $CDCl_3$): δ/ppm 4.03 (s, 6H), 3.60-3.53 (m, 3H), 3.21-3.08 (m, 6H), 2.50-2.40 (m, 3H), 2.35 (t, J = 7.4 Hz, 6H), 1.95-1.86 (m, 3H), 1.72-1.41 (m, 18H). ^{13}C NMR (100.6 MHz, $CDCl_3$) δ/ppm 173.04, 65.50, 56.45, 54.21, 40.38, 38.63, 34.71, 34.00, 28.86, 24.73. HRMS (ESI+) m/z calcd 686.1800 [M+H] found 686.1798.

*Synthesis of the compound **16***

Boc-ß-Alanin-OH (1.01 g, 5.33 mmol) was dissolved in DCM (60 mL) and DCC (1.21 g, 5.87 mmol), DMAP (44 mg, 0.36 mmol) and HOBt hydrate (24 mg, 0.18 mmol) were added. The compound **15** (2.44 g, 3.56 mmol) was separately dissolved in DCM (40 mL) and subsequently added to the first solution. The reaction solution was stirred for 65 hours at room temperature and under protection from light. The colorless residue formed was separated *via* filtration through celite. The solvent of the remaining yellow filtrate was removed by rotary evaporation. The residue was purified *via* column chromatography (eluent hexanes/ethyl acetate) to yield compound **16** as yellow waxy oil (664 mg, 0.77 mmol, 22 %). ^{1}H-NMR (400 MHz, $CDCl_3$): δ/ppm 6.09 (s, 1H), 5.14 (t, J = 6.2 Hz, 1H), 4.41 (s, 6H), 3.60-3.53 (m, 3H), 3.38-3.34 (m, 2H), 3.21-3.08 (m, 6H), 2.50-2.42 (m, 3H), 2.39-2.33 (m, 8H), 1.95-1.86 (m, , 3H), 1.74-1.59 (m, 12H), 1.53-1.39 (m, 15H). ^{13}C NMR (100.6 MHz, $CDCl_3$) δ/ppm 173.12, 171.88, 156.26, 77.16, 62.50, 58.44, 56.46, 40.39, 38.63, 37.15, 34.68, 33.95, 28.84, 28.57, 28.50, 24.67.

*Synthesis of the bidentate anchor compound **DL-NH$_2$***

The compound **12** (180 mg, 0.28 mmol) was dissolved in DCM (12 mL) and TFA (1.2 mL) was slowly added to reaction solution. After stirring for three hours at room temperature 1M Na_2CO_3 solution (15 mL) was added to the reaction solution. The phases were separated and the organic phase was extracted once with 1M Na_2CO_3 solution, twice with

water and once with brine. Finally, the organic phase was dried with Mg_2SO_4 and the solvent was removed by rotary evaporation. The remaining crude product **DL-NH$_2$**, (145 mg, 0.27 mmol, 96 %) was used in the next step without further purification. ^{1}H-NMR (300 MHz, $CDCl_3$): δ/ppm 6.78 (t, J = 6.4 Hz, 2H), 4.87 (p, J = 5.4 Hz, 1H), 3.65- 3.43 (m, 4H), 3.39-3.30 (m, 2H), 3.22-3.08 (m, 4H), 3.06-2.99 (m, 2H), 2.50-2.40 (m, 4H), 2.20 (t, J = 7.4 Hz, 4H), 1.97-1.86 (m, 2H), 1.81 (s, 2H), 1.75- 1.59 (m, 8H), 1.50-1.38 (m, 4H).

*Synthesis of the bidentate anchor compound **TL-NH$_2$***

The compound **16** (250 mg, 0.29 mmol) was dissolved in DCM (8 mL) and TFA (0.8 mL) was slowly added to reaction solution. After stirring for three hours at room temperature 1M Na_2CO_3 solution (10 mL) was added to the reaction solution. The phases were separated and the organic phase was extracted once with 1M Na_2CO_3 solution, twice with water and once with brine. Finally, the organic phase was dried with Mg_2SO_4 and the solvent was removed by rotary evaporation. The remaining crude product **TL-NH$_2$** (210 mg, 0.28 mmol, 95 %) was used in the next step without further purification. ^{1}H-NMR (400 MHz, $CDCl_3$): δ/ppm 4.43 (s, 6H), 3.61-3.54 (m, 3H), 3.22-3.09 (m, 8H), 2.51-2.43 (m, 5H), 2.36 (t, J = 7.47, 6H), 1.96-1.88 (m, 3H), 1.81-1.56 (m, 12H), 1.56-1.38 (m, 6H).

Synthesis of 6-azidohexanoic acid

6-bromohexanoic acid (2.0 g, 10.26 mmol) was dissolved in DMF (50 mL) and sodium azide (2.13 g, 32.82 mmol) was added. The reaction mixture was stirred at 60 °C for 6 hours and at room temperature for the additional 12 hours. DCM (50 mL) was added and the reaction mixture was was extracted twice with 1M HCl solution, twice with water and once with brine. Finally, the organic phase was dried with Mg_2SO_4 and the solvent was removed by rotary evaporation to yield 6-azidohexanoic acid (1.55 g, 9.86 mmol, 96 %). ^{1}H-NMR (400 MHz, $CDCl_3$): δ/ppm 8.96 (s, 1H), 3.27 (t, J = 6.9 Hz, 2H), 2.37 (t, J = 7.4 Hz, 2H), 1.73-1.55 (m, 4H), 1.49-1.37 (m, 2H). ^{13}C NMR (100.6 MHz, $CDCl_3$) δ/ppm 179.44, 51.33, 33.93, 28.67, 26.29, 24.31.

*Synthesis of the bidentate anchor compound **DL-N$_3$***

6-Azidohexanoic acid (298 mg, 1.89 mmol) was dissolved in DCM (30 mL) and DCC (426 mg, 2.06 mmol) and DMAP (42 mg, 0.34 mmol) were added. The compound **11** (800 mg, 1.72 mmol) was separately dissolved in DCM (30 mL) and subsequently added

to the first solution. The reaction solution was stirred for 30 hours at room temperature and under protection from light. The colorless residue formed was separated *via* filtration through celite. The solvent of the remaining yellow filtrate was removed by rotary evaporation. The residue was purified *via* column chromatography (eluent dichloromethane/acetone) to yield compound **DL-N$_3$** as yellow solid (930 mg, 1.54 mmol, 90 %). ^{1}H-NMR (400 MHz, $CDCl_3$): δ/ppm 6.40 (t, J = 6.5 Hz, 2H), 4.92-4.76 (m, 1H), 3.60-3.52 (m, 2H), 3.51-3.45 (m, 2H), 3.37-3.32 (m, 2H), 3.29 (t, J = 6.8 Hz, 2H), 3.20-3.07 (m, 4H), 2.45 (dtd, J = 13.1, 6.6, 5.4 Hz, 2H), 2.32 (t, J = 7.4 Hz, 2H), 2.23 (t, J = 7.5 Hz, 4H), 1.90 (dtd, J = 13.1, 6.6, 5.4 Hz, 2H), 1.75-1.57 (m, 12H), 1.53-1.37 (m, 6H). ^{1}H NMR (400 MHz, DMSO-d6) δ 7.87 (t, J = 6.0 Hz, 2H), 4.81- 4.76 (m, 1H), 3.63-3.56 (m, 2H), 3.31 (t, J = 6.8 Hz, 2H), 3.29-3.25 (m, 2H), 3.21-3.05 (m, 6H), 2.44-2.37 (m, 2H), 2.26 (t, J = 7.4 Hz, 2H), 2.05 (t, J = 7.3 Hz, 4H), 1.90-1.82 (m, 2H), 1.70-1.43 (m, 12H), 1.38-1.27 (m, 6H). ^{13}C NMR (100.6 MHz, $CDCl_3$) δ 173.88, 172.75, 71.11, 56.54, 51.34, 40.39, 39.01, 38.61, 36.51, 34.72, 34.13, 28.97, 28.63, 26.29, 25.49, 24.40. HRMS (ESI+) m/z calcd 606.2276 [M+H] found 606.2287.

*Synthesis of the tridentate anchor compound **TL-N$_3$***

6-Azidohexanoic acid (367 mg, 2.33 mmol) was dissolved in DMF (20 mL) and DCC (451 mg, 2.19 mmol), DMAP (36 mg, 0.29 mmol) and HOBt hydrate (20 mg, 0.15 mmol) were added. The compound **15** (1.00 g, 1.46 mmol) was separately dissolved in DMF (20 mL) and subsequently added to the first solution. The reaction solution was stirred for 50 hours at room temperature and under protection from light. The colorless residue formed was separated *via* filtration through celite. The solvent of the remaining yellow filtrate was removed by rotary evaporation. The residue was purified *via* column chromatography (eluent dichloromethane/cyclohexanes/acetone) to yield compound **TL-N$_3$** as yellow waxy oil (580 mg, 0.70 mmol, 48 %). ^{1}H-NMR (400 MHz, $CDCl_3$): δ/ppm 5.93 (s, 1H), 4.42 (s, 6H), 3.60-3.53 (m, 3H), 3.27 (t, J = 6.8 Hz, 2H), 3.1-3.08 (m, 6H), 2.46 (dtd, J = 13.1, 6.6, 5.4 Hz, 3H), 2.35 (t, J = 7.4 Hz, 6H), 2.17 (t, J = 7.5 Hz, 2H), 1.91 (dtd, J = 13.0, 6.7, 5.4 Hz, 3H), 1.74-1.57 (m, 16H), 1.52-1.38 (m, 8H). ^{1}H-NMR (400 MHz, DMSO-d_6): δ/ppm 7.74 (s, 1H), 4.27 (s, 6H), 3.63-3.56 (m, 3H), 3.30 (t, J = 6.9 Hz, 2H), 3.21-3.08 (m, 6H), 2.41 (dtd, J = 12.8, 6.5, 5.5 Hz, 3H), 2.31 (t, J = 7.3 Hz, 6H), 2.08 (t, J = 7.3 Hz, 2H), 1.86 (dtd, J = 12.7, 6.5, 5.4 Hz, 3H), 1.71-1.44 (m, 16H), 1.40-1.24 (m, 8H). ^{13}C NMR (100.6 MHz, $CDCl_3$) δ/ppm 173.16, 173.03, 62.67, 58.45, 56.46, 51.33, 40.39, 38.63,

37.01, 34.69, 33.97, 28.85, 28.72, 26.32, 25.05, 24.69. HRMS (ESI+) m/z calcd 847.2371 [M+Na] found 847.2355.

6.7 Synthesis of PCarb-based Multidentate Polymeric Ligands.

General procedure of post-polymerization modification reaction of end functionalized PCarb with amine modified anchor compounds ***DL-NH$_2$*** *and* ***TL-NH$_2$****.*

PCarb (40 mg, 0.0078 mmol, 1 eq.), the respective amine modified anchor compound (0.159 mmol, 20 eq.) and triethyl amine (31 mg, 66 µL, 0.314 mmol, 60 eq.) were dissolved in 3 mL THF and stirred at 30 °C for 24 hours. The polymer was precipitated in methanol and dried at 30°C in vacuum for 24 hours. The modified polymers were analyzed *via* IR, ^{1}H and DOSY NMR spectroscopies.

6.8 Synthesis of P3HT-Based Multidentate Polymeric Ligands.

General procedure of copper catalyzed azide-alkyne Huisgen cycloaddition between ethynyl-P3HT and azide modified anchor compounds ***DL-N$_3$*** *and* ***TL-N$_3$****.*

Azides were incorporated as polymer end groups according to a modified literature procedure.[180] Under a dry nitrogen atmosphere ethynyl-terminated P3HT (150 mg, 0.029 mol, M_n=5200 g/mol, 1 eq.) was dissolved in 20 mL of dry chloroform. The respective azide (0.288 mmol, 10 eq.), 2,6-lutidine (309 mg, 0.34 mL, 2.88 mmol, 100 eq.) and $[Cu(NCCH_3)_4][PF6]$ (54 mg, 0.144 mmol, 5 eq.) were added. The reaction solution was stirred at room temperature for 64 hours. The reaction mixture was concentrated under reduced pressure and P3HT was precipitated in methanol. The polymer was purified by the repeated precipitation of the polymer dissolved in a small amount of DCM into methanol. The product was obtained as a violet solid and dried in vacuum. The modified P3HT were analyzed via MALDI TOF MS, THF-GPC and ^{1}H NMR spectroscopy.

6.9 Synthesis of Polysarcosine-Based Multidentate Polymeric Ligands

Amine end group modification with biotine.

Polysarcosine (60.0 mg, 0.0039 mmol), (+)-biotin N-hydroxysuccinimide ester (13.2 mg, 0.0387 mmol) and triethyl amine (7.83 mg, 11.0 µL, 0.077 mmol) were dissolved in DMF (1 mL) and stirred at 25 °C for 24 hours. Subsequently, the polymer was precipitated in diethyl ether, redissolved in water and lyophilized.

Amine end group modification with acetic acid ester anhydride.

Polysarcosine (48.0 mg, 0.0031 mmol), acetic anhydride (3.16 mg,3.0 µL 0.0309 mmol) and triethyl amine (6.27 mg, 8.6 µL, 0.062 mmol) were dissolved in DMF (1 mL) and stirred at 25 °C for 24 hours. Subsequently, the polymer was precipitated in diethyl ether, redissolved in water and lyophilized.

General procedure of dibenzocyclooctyl end group modification via strain-promoted azide-alkyne cycloaddition (SPAAC).

1 eq. of polysarcosine and 3 eq. of azide modified anchor compounds (**DL-N$_3$** or **TL-N$_3$**) were dissolved in DMF (polymer concentration ca 0.001 mmol/mL) and stirred for 24 hours at 25 °C. Subsequently, the polymer was dialyzed against methanol and water and lyophilized. Samples were analyzed by HFIP-GPC, ^{1}H NMR and DOSY NMR.

6.10 Synthesis of Water Soluble QDs with PSar-Based Ligands

PSar-based hydrophilic polymeric ligand **PSar-DL** or **PSar-TL** (3 mg) and quantum dots (QD, red, CdSe core, core diameter 4 nm, $Cd_xZn_{1-x}S$ shell, total diameter 16 nm, oleic acid ligands, 1 mg) were separately dissolved in chloroform (each 100 µL) and subsequently combined. The reaction mixture was sonicated for two hour and water (1.0 mL) was added. The water-soluble quantum dots were extracted from the organic to the aqueous phase. The aqueous phase was separated and the extraction repeated 2 more times. The excess polymer was removed by repeated centrifugation with Amicon® Ultra centrifugal filters (100K MWCO).

Alternative work up: The reaction mixture was sonicated for two hour and water (1.0 mL) was added. The water-soluble quantum dots were extracted from the organic to the aqueous phase. The nitrogen was bubbled through the reaction mixture to remove the chloroform. The excess polymer was removed by repeated centrifugation with Amicon® Ultra centrifugal filters (100K MWCO).

7 References

(1) Holder, E.; Tessler, N.; Rogach, A. L. *J. Mater. Chem.* **2008**, *18* (10), 1064.

(2) Medintz, I. L.; Uyeda, H. T.; Goldman, E. R.; Mattoussi, H. *Nat. Mater.* **2005**, *4* (6), 435–446.

(3) Reiss, P.; Couderc, E.; De Girolamo, J.; Pron, A. *Nanoscale* **2011**, *3* (2), 446–489.

(4) Alivisatos, A. P. *Science (80-.).* **1996**, *271* (5251), 933–937.

(5) Reiss, P.; Protière, M.; Li, L. *Small* **2009**, *5* (2), 154–168.

(6) Murray, C. B.; Norris, D. J.; Bawendi, M. G. *J. Am. Chem. Soc.* **1993**, *115* (19), 8706–8715.

(7) Peng, Z. A.; Peng, X. *J. Am. Chem. Soc.* **2001**, *123* (1), 183–184.

(8) Reiss, P.; Bleuse, J.; Pron, A. *Nano Lett.* **2002**, *2* (7), 781–784.

(9) Peng, X.; Schlamp, M. C.; Kadavanich, A. V.; Alivisatos, A. P. *J. Am. Chem. Soc.* **1997**, *119* (30), 7019–7029.

(10) Lim, J.; Jeong, B. G.; Park, M.; Kim, J. K.; Pietryga, J. M.; Park, Y.-S.; Klimov, V. I.; Lee, C.; Lee, D. C.; Bae, W. K. *Adv. Mater.* **2014**, *26* (47), 8034–8040.

(11) Kim, S.; Fisher, B.; Eisler, H.-J.; Bawendi, M. *J. Am. Chem. Soc.* **2003**, *125* (38), 11466–11467.

(12) Yin, Y.; Alivisatos, A. P. *Nature* **2005**, *437* (7059), 664–670.

(13) Li, G.; Zhu, R.; Yang, Y. *Nat. Photonics* **2012**, *6* (3), 153–161.

(14) Facchetti, A. *Chem. Mater.* **2011**, *23* (3), 733–758.

(15) Heeger, A. J. *Chem. Soc. Rev.* **2010**, *39* (7), 2354–2371.

(16) Helgesen, M.; Søndergaard, R.; Krebs, F. C. *J. Mater. Chem.* **2010**, *20* (1), 36–60.

(17) Allard, S.; Forster, M.; Souharce, B.; Thiem, H.; Scherf, U. *Angew. Chem. Int. Ed. Engl.* **2008**, *47* (22), 4070–4098.

(18) *Handbook of Conducting Polymers. Conjugated Polymers:Theory, Synthesis, Properties and Characterization*, Third Edit.; Skotheim, T. A., Reynolds, J., Eds.; CPR Press, 2006.

(19) Chiang, C.; Fincher, C.; Park, Y.; Heeger, A.; Shirakawa, H.; Louis, E.; Gau, S.; MacDiarmid, A. *Phys. Rev. Lett.* **1977**, *39* (17), 1098–1101.

(20) Shirakawa, H.; Louis, E. J.; MacDiarmid, A. G.; Chiang, C. K.; Heeger, A. J. *J. Chem. Soc. Chem. Commun.* **1977**, No. 16, 578.

(21) Osaka, I.; Takimiya, K. *Polymer (Guildf).* **2015**, *59*, A1–A15.

(22) Sirringhaus, H.; Brown, P. J.; Friend, R. H.; Nielsen, M. M.; Bechgaard, K.; Langeveld-Voss, B. M. W.; Spiering, A. J. H.; Janssen, R. A. J.; Meijer, E. W.; Herwig, P.; de Leeuw, D. M. *Nature* **1999**, *401* (6754), 685–688.

(23) Heeger, A. J. *Angew. Chem. Int. Ed. Engl.* **2001**, *40* (14), 2591–2611.

(24) McCullough, R. D.; Lowe, R. D.; Jayaraman, M.; Anderson, D. L. *J. Org. Chem.* **1993**, *58* (4), 904–912.

(25) Robert S. Loewe; Paul C. Ewbank; Jinsong Liu; Lei Zhai, and; McCullough*, R. D. **2001**.

(26) Bao, Z.; Dodabalapur, A.; Lovinger, A. J. *Appl. Phys. Lett.* **1996**, *69* (26), 4108.

(27) Li, G.; Shrotriya, V.; Huang, J.; Yao, Y.; Moriarty, T.; Emery, K.; Yang, Y. *Nat. Mater.* **2005**, *4* (11), 864–868.

(28) Ma, W.; Yang, C.; Gong, X.; Lee, K.; Heeger, A. J. *Adv. Funct. Mater.* **2005**, *15* (10), 1617–1622.

(29) Park, S. H.; Roy, A.; Beaupré, S.; Cho, S.; Coates, N.; Moon, J. S.; Moses, D.; Leclerc, M.; Lee, K.; Heeger, A. J. *Nat. Photonics* **2009**, *3* (5), 297–302.

(30) Mühlbacher, D.; Scharber, M.; Morana, M.; Zhu, Z.; Waller, D.; Gaudiana, R.; Brabec, C. *Adv. Mater.* **2006**, *18* (21), 2884–2889.

(31) Chen, H.-Y.; Hou, J.; Zhang, S.; Liang, Y.; Yang, G.; Yang, Y.; Yu, L.; Wu, Y.; Li, G. *Nat. Photonics* **2009**, *3* (11), 649–653.

(32) Burroughes, J. H.; Bradley, D. D. C.; Brown, A. R.; Marks, R. N.; Mackay, K.; Friend, R. H.; Burns, P. L.; Holmes, A. B. *Nature* **1990**, *347* (6293), 539–541.

(33) Bernius, M. T.; Inbasekaran, M.; O'Brien, J.; Wu, W. *Adv. Mater.* **2000**, *12* (23), 1737–1750.

(34) *Organic Optoelectronics*; Hu, W., Ed.; Wiley-VCH Verlag GmbH & Co. KGaA: Weinheim, Germany, 2013.

(35) Shirota, Y. In *Organic Light-Emitting Devices*; Müllen, K., Scherf, U., Eds.; Wiley-VCH, 2006; pp 245–264.

(36) Fitzner, R.; Reinold, E.; Mishra, A.; Mena-Osteritz, E.; Ziehlke, H.; Körner, C.; Leo, K.; Riede, M.; Weil, M.; Tsaryova, O.; Weiß, A.; Uhrich, C.; Pfeiffer, M.; Bäuerle, P. *Adv. Funct. Mater.* **2011**, *21* (5), 897–910.

(37) Sun, Y.; Welch, G. C.; Leong, W. L.; Takacs, C. J.; Bazan, G. C.; Heeger, A. J. *Nat. Mater.* **2012**, *11* (1), 44–48.

(38) Liu, J.; Li, L.; Pei, Q. *Macromolecules* **2011**, *44*, 2451–2456.

(39) Park, J. H.; Yun, C.; Koh, T.-W.; Do, Y.; Yoo, S.; Lee, M. H. *J. Mater. Chem.* **2011**, *21* (14), 5422.

(40) Yeh, S.-J.; Wu, M.-F.; Chen, C.-T.; Song, Y.-H.; Chi, Y.; Ho, M.-H.; Hsu, S.-F.; Chen, C. H. *Adv. Mater.* **2005**, *17* (3), 285–289.

(41) Sano, N.; Banzai, K.; Naka, S.; Okada, H.; Sanda, F. *J. Polym. Sci. Part A Polym. Chem.* **2015**, DOI: 10.1002/pola.27557.

(42) Kanbara, T.; Yokokawa, Y.; Hasegawa, K. *Polymer (Guildf).* **1999**, No. 1, 28–34.

(43) Chen, M.; Häussler, M.; Moad, G.; Rizzardo, E. *Org. Biomol. Chem.* **2011**, *9* (17), 6111–6119.

(44) Mori, H.; Takano, K.; Endo, T. *Macromolecules* **2009**, *42* (19), 7342–7352.

(45) Sommer, M.; Lang, A. S.; Thelakkat, M. *Angew. Chem. Int. Ed. Engl.* **2008**, *47* (41), 7901–7904.

(46) Karon, K.; Lapkowski, M. *J. Solid State Electrochem.* **2015**, *19* (9), 2601–2610.

(47) Schrögel, P.; Tomkevičienė, A.; Strohriegl, P.; Hoffmann, S. T.; Köhler, A.; Lennartz, C. *J. Mater. Chem.* **2011**, *21* (7), 2266–2273.

(48) Zhang, Y.-D.; Hreha, R. D.; Jabbour, G. E.; Kippelen, B.; Peyghambarian, N.; Marder, S. R. *J. Mater. Chem.* **2002**, *12* (6), 1703–1708.

(49) Evanoff, D. D.; Carroll, J. B.; Roeder, R. D.; Hunt, Z. J.; Lawrence, J. R.; Foulger, S. H. *J. Polym. Sci. Part A Polym. Chem.* **2008**, *46* (23), 7882–7897.

(50) Häussler, M.; Lok, Y. P.; Chen, M.; Jasieniak, J.; Adhikari, R.; King, S. P.; Haque, S. A.; Forsyth, C. M.; Winzenberg, K.; Watkins, S. E.; Rizzardo, E.; Wilson, G. J. *Macromolecules* **2010**, *43* (17), 7101–7110.

(51) Ha Park, J.; Koh, T.-W.; Do, Y.; Hyung Lee, M.; Yoo, S. *J. Polym. Sci. Part A Polym. Chem.* **2012**, *50* (12), 2356–2365.

(52) Klinker, K.; Barz, M. *Macromol. Rapid Commun.* **2015**, DOI: 10.1002/marc.201500403.

(53) Klinker, K.; Holm, R.; Heller, P.; Barz, M. *Polym. Chem.* **2015**, *6* (25), 4612–4623.

(54) Holm, R.; Klinker, K.; Weber, B.; Barz, M. *Macromol. Rapid Commun.* **2015**, DOI: 10.1002/marc.201500402.

(55) Kwak, J.; Bae, W. K.; Zorn, M.; Woo, H.; Yoon, H.; Lim, J.; Kang, S. W.; Weber, S.; Butt, H.-J.; Zentel, R.; Lee, S.; Char, K.; Lee, C. *Adv. Mater.* **2009**, *21* (48), 5022–5026.

(56) Wright, M.; Uddin, A. *Sol. Energy Mater. Sol. Cells* **2012**, *107*, 87–111.

(57) Ehlert, S.; Taheri, S. M.; Pirner, D.; Drechsler, M.; Schmidt, H.-W.; Förster, S. *ACS*

Nano **2014**, *8* (6), 6114–6122.

(58) Ji, X.; Copenhaver, D.; Sichmeller, C.; Peng, X. *J. Am. Chem. Soc.* **2008**, *130* (17), 5726–5735.

(59) Morris-Cohen, A. J.; Vasilenko, V.; Amin, V. A.; Reuter, M. G.; Weiss, E. A. *ACS Nano* **2012**, *6* (1), 557–565.

(60) Mathias, F.; Fokina, A.; Landfester, K.; Tremel, W.; Schmid, F.; Char, K.; Zentel, R. *Macromol. Rapid Commun.* **2015**, *36* (11), 959–983.

(61) Zorn, M.; Meuer, S.; Tahir, M. N.; Khalavka, Y.; Sönnichsen, C.; Tremel, W.; Zentel, R. *J. Mater. Chem.* **2008**, *18* (25), 3050.

(62) Brittain, W. J.; Minko, S. *J. Polym. Sci. Part A Polym. Chem.* **2007**, *45* (16), 3505–3512.

(63) Supran, G. J.; Shirasaki, Y.; Song, K. W.; Caruge, J.-M.; Kazlas, P. T.; Coe-Sullivan, S.; Andrew, T. L.; Bawendi, M. G.; Bulović, V. *MRS Bull.* **2013**, *38* (09), 703–711.

(64) Kim, T.-H.; Jun, S.; Cho, K.-S.; Choi, B. L.; Jang, E. *MRS Bull.* **2013**, *38* (09), 712–720.

(65) Colvin, V. L.; Schlamp, M. C.; Alivisatos, A. P. *Nature* **1994**, *370* (6488), 354–357.

(66) Dabbousi, B. O.; Bawendi, M. G.; Onitsuka, O.; Rubner, M. F. *Appl. Phys. Lett.* **1995**, *66* (11), 1316.

(67) Coe, S.; Woo, W.-K.; Bawendi, M.; Bulović, V. *Nature* **2002**, *420* (6917), 800–803.

(68) Anikeeva, P. O.; Halpert, J. E.; Bawendi, M. G.; Bulović, V. *Nano Lett.* **2009**, *9* (7), 2532–2536.

(69) Stouwdam, J. W.; Janssen, R. A. J. *Adv. Mater.* **2009**, *21* (28), 2916–2920.

(70) Kwak, J.; Bae, W. K.; Lee, D.; Park, I.; Lim, J.; Park, M.; Cho, H.; Woo, H.; Yoon, D. Y.; Char, K.; Lee, S.; Lee, C. *Nano Lett.* **2012**, *12* (5), 2362–2366.

(71) Mashford, B. S.; Stevenson, M.; Popovic, Z.; Hamilton, C.; Zhou, Z.; Breen, C.; Steckel, J.; Bulovic, V.; Bawendi, M.; Coe-Sullivan, S.; Kazlas, P. T. *Nat. Photonics* **2013**, *7* (5), 407–412.

(72) Qian, L.; Zheng, Y.; Xue, J.; Holloway, P. H. *Nat. Photonics* **2011**, *5* (9), 543–548.

(73) Kwak, J.; Bae, W. K.; Lee, D.; Park, I.; Lim, J.; Park, M.; Cho, H.; Woo, H.; Yoon, D. Y.; Char, K.; Lee, S.; Lee, C. *Nano Lett.* **2012**, *12* (5), 2362–2366.

(74) Park, W.-Y.; Kwon, Y.; Lee, C.; Whang, K.-W. *Opt. Express* **2014**, *22 Suppl 7* (107), A1687–A1694.

(75) Yang, J. P.; Bao, Q. Y.; Xu, Z. Q.; Li, Y. Q.; Tang, J. X.; Shen, S. *Appl. Phys. Lett.* **2010**, *97* (22), 223303.

(76) Mueller, A. H.; Petruska, M. A.; Achermann, M.; Werder, D. J.; Akhadov, E. A.; Koleske, D. D.; Hoffbauer, M. A.; Klimov, V. I. *Nano Lett.* **2005**, *5* (6), 1039–1044.

(77) Anikeeva, P.; Madigan, C.; Halpert, J.; Bawendi, M.; Bulović, V. *Phys. Rev. B* **2008**, *78*, 1–8.

(78) Bae, W. K.; Brovelli, S.; Klimov, V. I. *MRS Bull.* **2013**, *38* (09), 721–730.

(79) Anikeeva, P. O.; Madigan, C. F.; Coe-Sullivan, S. A.; Steckel, J. S.; Bawendi, M. G.; Bulović, V. *Chem. Phys. Lett.* **2006**, *424* (1-3), 120–125.

(80) Coe-Sullivan, S.; Woo, W.-K.; Steckel, J. S.; Bawendi, M.; Bulović, V. *Org. Electron.* **2003**, *4* (2-3), 123–130.

(81) Cho, K.-S.; Lee, E. K.; Joo, W.-J.; Jang, E.; Kim, T.-H.; Lee, S. J.; Kwon, S.-J.; Han, J. Y.; Kim, B.-K.; Choi, B. L.; Kim, J. M. *Nat. Photonics* **2009**, *3* (6), 341–345.

(82) Bae, W. K.; Park, Y.-S.; Lim, J.; Lee, D.; Padilha, L. a; McDaniel, H.; Robel, I.; Lee, C.; Pietryga, J. M.; Klimov, V. I. *Nat. Commun.* **2013**, *4*, 2661.

(83) Leck, K. S.; Divayana, Y.; Zhao, D.; Yang, X.; Abiyasa, A. P.; Mutlugun, E.; Gao, Y.; Liu, S.; Tan, S. T.; Sun, X. W.; Demir, H. V. *ACS Appl. Mater. Interfaces* **2013**, *5* (14), 6535–6540.

(84) Dai, X.; Zhang, Z.; Jin, Y.; Niu, Y.; Cao, H.; Liang, X.; Chen, L.; Wang, J.; Peng, X. *Nature* **2014**, *515* (7525), 96–99.

(85) Li, Y.; Rizzo, A.; Mazzeo, M.; Carbone, L.; Manna, L.; Cingolani, R.; Gigli, G. *J. Appl. Phys.* **2005**, *97* (11).

(86) Kwak, K.; Cho, K.; Kim, S. *Appl. Phys. Lett.* **2014**, *104* (10), 1–5.

(87) Zhou, J.; Tang, W. Q.; Wang, C. F.; Chen, L.; Chen, Q.; Chen, S. *J. Polym. Sci. Part A Polym. Chem.* **2012**, *50* (18), 3736–3742.

(88) Jung, H.; Chung, W.; Lee, C. H.; Kim, S. H. *J. Nanosci. Nanotechnol.* **2012**, *12* (7), 5407–5411.

(89) Chin, P. T. K.; Hikmet, R. a. M.; Janssen, R. a. J. *J. Appl. Phys.* **2008**, *104* (1), 013108.

(90) Zhao, L.; Zhou, Z.-L.; Guo, Z.; Gibson, G.; Brug, J. A.; Lam, S.; Pei, J.; Mao, S. S. *J. Mater. Res.* **2012**, *27* (04), 639–652.

(91) Park, J. Y.; Advincula, R. C. *Phys. Chem. Chem. Phys.* **2014**, *16* (18), 8589–8593.

(92) Zorn, M.; Bae, W. K.; Kwak, J.; Lee, H.; Lee, C.; Zentel, R.; Char, K. *ACS Nano* **2009**, *3* (5), 1063–1068.

(93) Zhou, R.; Xue, J. *Chemphyschem* **2012**, *13* (10), 2471–2480.

(94) Thompson, B. C.; Fréchet, J. M. J. *Angew. Chem. Int. Ed. Engl.* **2008**, *47* (1), 58–

77.

(95) Wienk, M. M.; Kroon, J. M.; Verhees, W. J. H.; Knol, J.; Hummelen, J. C.; van Hal, P. A.; Janssen, R. A. J. *Angew. Chem. Int. Ed. Engl.* **2003**, *42* (29), 3371–3375.

(96) Lee, J.-S.; Kovalenko, M. V; Huang, J.; Chung, D. S.; Talapin, D. V. *Nat. Nanotechnol.* **2011**, *6* (6), 348–352.

(97) Zhou, R.; Stalder, R.; Xie, D.; Cao, W.; Zheng, Y.; Yang, Y.; Plaisant, M.; Holloway, P. H.; Schanze, K. S.; Reynolds, J. R.; Xue, J. *ACS Nano* **2013**, *7* (6), 4846–4854.

(98) Ren, S.; Chang, L.-Y.; Lim, S.-K.; Zhao, J.; Smith, M.; Zhao, N.; Bulović, V.; Bawendi, M.; Gradecak, S. *Nano Lett.* **2011**, *11* (9), 3998–4002.

(99) Kochemba, W. M.; Pickel, D. L.; Sumpter, B. G.; Chen, J.; Kilbey, S. M. *Chem. Mater.* **2012**, *24* (22), 4459–4467.

(100) Liu, J.; Tanaka, T.; Sivula, K.; Alivisatos, A. P.; Fréchet, J. M. J. *J. Am. Chem. Soc.* **2004**, *126* (21), 6550–6551.

(101) Sun, B.; Marx, E.; Greenham, N. C. *Nano Lett.* **2003**, *3* (7), 961–963.

(102) Chen, H.-C.; Lai, C.-W.; Wu, I.-C.; Pan, H.-R.; Chen, I.-W. P.; Peng, Y.-K.; Liu, C.-L.; Chen, C.; Chou, P.-T. *Adv. Mater.* **2011**, *23* (45), 5451–5455.

(103) Wu, Y.; Zhang, G. *Nano Lett.* **2010**, *10* (5), 1628–1631.

(104) Lim, J.; Lee, D.; Park, M.; Song, J.; Lee, S.; Kang, M. S.; Lee, C.; Char, K. *J. Phys. Chem. C* **2014**, *118* (8), 3942–3952.

(105) Bokel, F. A.; Sudeep, P. K.; Pentzer, E.; Emrick, T.; Hayward, R. C. *Macromolecules* **2011**, *44* (7), 1768–1770.

(106) Brinkmann, M.; Aldakov, D.; Chandezon, F. *Adv. Mater.* **2007**, *19* (22), 3819–3823.

(107) Qian, L.; Yang, J.; Zhou, R.; Tang, A.; Zheng, Y.; Tseng, T.-K.; Bera, D.; Xue, J.; Holloway, P. H. *J. Mater. Chem.* **2011**, *21* (11), 3814.

(108) Noone, K. M.; Strein, E.; Anderson, N. C.; Wu, P.-T.; Jenekhe, S. A.; Ginger, D. S. *Nano Lett.* **2010**, *10* (7), 2635–2639.

(109) Stalder, R.; Xie, D.; Zhou, R.; Xue, J.; Reynolds, J. R.; Schanze, K. S. *Chem. Mater.* **2012**, *24* (16), 3143–3152.

(110) Michalet, X.; Pinaud, F. F.; Bentolila, L. A.; Tsay, J. M.; Doose, S.; Li, J. J.; Sundaresan, G.; Wu, A. M.; Gambhir, S. S.; Weiss, S. *Science* **2005**, *307* (5709), 538–544.

(111) Bruchez Jr., M. *Science (80-.).* **1998**, *281* (5385), 2013–2016.

(112) Howes, P. D.; Chandrawati, R.; Stevens, M. M. *Science (80-.).* **2014**, *346* (6205),

1247390–1247390.

(113) Resch-Genger, U.; Grabolle, M.; Cavaliere-Jaricot, S.; Nitschke, R.; Nann, T. *Nat. Methods* **2008**, *5* (9), 763–775.

(114) Blanco-Canosa, J. B.; Wu, M.; Susumu, K.; Petryayeva, E.; Jennings, T. L.; Dawson, P. E.; Algar, W. R.; Medintz, I. L. *Coord. Chem. Rev.* **2014**, *263-264* (1), 101–137.

(115) Palui, G.; Aldeek, F.; Wang, W.; Mattoussi, H. *Chem. Soc. Rev.* **2014**, *44*, 193–227.

(116) Wang, W.; Ji, X.; Na, H. Bin; Safi, M.; Smith, A.; Palui, G.; Perez, J. M.; Mattoussi, H. *Langmuir* **2014**, *30* (21), 6197–6208.

(117) Parak, W. J.; Gerion, D.; Pellegrino, T.; Zanchet, D.; Micheel, C.; Williams, S. C.; Boudreau, R.; Gros, M. A. Le; Larabell, C. A.; Alivisatos, A. P. *Nanotechnology* **2003**, *14* (7), R15–R27.

(118) Mattoussi, H.; Mauro, J. M.; Goldman, E. R.; Anderson, G. P.; Sundar, V. C.; Mikulec, F. V.; Bawendi, M. G. *J. Am. Chem. Soc.* **2000**, *122* (49), 12142–12150.

(119) Uyeda, H. T.; Medintz, I. L.; Jaiswal, J. K.; Simon, S. M.; Mattoussi, H. *J. Am. Chem. Soc.* **2005**, *127* (11), 3870–3878.

(120) Zhan, N.; Palui, G.; Safi, M.; Ji, X.; Mattoussi, H. *J. Am. Chem. Soc.* **2013**, *135* (37), 13786–13795.

(121) Chen, X.; Lawrence, J.; Parelkar, S.; Emrick, T. *Macromolecules* **2013**, *46*, 119–127.

(122) Muro, E.; Pons, T.; Lequeux, N.; Fragola, A.; Sanson, N.; Lenkei, Z.; Dubertret, B. *J. Am. Chem. Soc.* **2010**, *132* (13), 4556–4557.

(123) Tomczak, N.; Liu, R.; Vancso, J. G. *Nanoscale* **2013**, *5* (24), 12018–12032.

(124) Stewart, M. H.; Susumu, K.; Mei, B. C.; Medintz, I. L.; Delehanty, J. B.; Blanco-Canosa, J. B.; Dawson, P. E.; Mattoussi, H. *J. Am. Chem. Soc.* **2010**, *132* (28), 9804–9813.

(125) Viswanath, A.; Shen, Y.; Green, A. N.; Tan, R.; Greytak, A. B.; Benicewicz, B. C. *Macromolecules* **2014**, *47* (23), 8137–8144.

(126) Viswanath, A.; Paudel, P.; Kittikhunnatham, P.; Green, A. N.; Greytak, A. B.; Benicewicz, B. C. *Polym. Chem.* **2015**.

(127) Liu, W.; Greytak, A. B.; Lee, J.; Wong, C. R.; Park, J.; Marshall, L. F.; Jiang, W.; Curtin, P. N.; Ting, A. Y.; Nocera, D. G.; Fukumura, D.; Jain, R. K.; Bawendi, M. G. *J. Am. Chem. Soc.* **2010**, *132* (2), 472–483.

(128) Wang, M.; Felorzabihi, N.; Guerin, G.; Haley, J. C.; Scholes, G. D.; Winnik, M. A. *Macromolecules* **2007**, *40* (17), 6377–6384.

(129) Moad, G.; Rizzardo, E.; Thang, S. H. *Aust. J. Chem.* **2005**, *58* (6), 379.

(130) Braunecker, W. A.; Matyjaszewski, K. *Prog. Polym. Sci.* **2007**, *32* (1), 93–146.

(131) Georges, M. K.; Veregin, R. P. N.; Kazmaier, P. M.; Hamer, G. K. *Macromolecules* **1993**, *26* (11), 2987–2988.

(132) Moad, G.; Chen, M.; Häussler, M.; Postma, A.; Rizzardo, E.; Thang, S. H. *Polym. Chem.* **2011**, *2* (3), 492–519.

(133) Semsarilar, M.; Perrier, S. *Nat. Chem.* **2010**, *2* (10), 811–820.

(134) McLeary, J. B.; Calitz, F. M.; McKenzie, J. M.; Tonge, M. P.; Sanderson, R. D.; Klumperman, B. *Macromolecules* **2005**, *38* (8), 3151–3161.

(135) Perrier, S.; Takolpuckdee, P. *J. Polym. Sci. Part A Polym. Chem.* **2005**, *43* (22), 5347–5393.

(136) Mayadunne, R. T. A.; Rizzardo, E.; Chiefari, J.; Chong, Y. K.; Moad, G.; Thang, S. H. *Macromolecules* **1999**, *32* (21), 6977–6980.

(137) Mayadunne, R. T. A.; Rizzardo, E.; Chiefari, J.; Krstina, J.; Moad, G.; Postma, A.; Thang, S. H. *Macromolecules* **2000**, *33* (2), 243–245.

(138) Han, S.-Y.; Kim, Y.-A. *Tetrahedron* **2004**, *60* (11), 2447–2467.

(139) *Functional Polymers by Post-Polymerization Modification*; Theato, P., Klok, H.-A., Eds.; Wiley-VCH, 2013.

(140) Anderson, G. W.; Zimmerman, J. E.; Callahan, F. M. *J. Am. Chem. Soc.* **1964**, *86* (9), 1839–1842.

(141) Ferruti, P.; Bettelli, A.; Feré, A. *Polymer (Guildf).* **1972**, *13* (10), 462–464.

(142) Batz, H.-G.; Franzmann, G.; Ringsdorf, H. *Angew. Chemie Int. Ed. English* **1972**, *11* (12), 1103–1104.

(143) Eberhardt, M.; Théato, P. *Macromol. Rapid Commun.* **2005**, *26* (18), 1488–1493.

(144) Eberhardt, M.; Mruk, R.; Zentel, R.; Théato, P. *Eur. Polym. J.* **2005**, *41* (7), 1569–1575.

(145) Mohr, N.; Barz, M.; Forst, R.; Zentel, R. *Macromol. Rapid Commun.* **2014**, *35* (17), 1522–1527.

(146) Nilles, K.; Theato, P. *J. Polym. Sci. Part A Polym. Chem.* **2010**, *48* (16), 3683–3692.

(147) Rostovtsev, V. V; Green, L. G.; Fokin, V. V; Sharpless, K. B. *Angew. Chem. Int. Ed. Engl.* **2002**, *41* (14), 2596–2599.

(148) Tornøe, C. W.; Christensen, C.; Meldal, M. *J. Org. Chem.* **2002**, *67* (9), 3057–3064.

(149) Kolb, H. C.; Finn, M. G.; Sharpless, K. B. *Angew. Chem. Int. Ed. Engl.* **2001**, *40* (11), 2004–2021.

(150) Agard, N. J.; Prescher, J. A.; Bertozzi, C. R. *J. Am. Chem. Soc.* **2004**, *126* (46), 15046–15047.

(151) Wittig, G.; Krebs, A. *Chem. Ber.* **1961**, *94* (12), 3260–3275.

(152) Meier, H.; Petersen, H.; Kolshorn, H. *Chem. Ber.* **1980**, *113* (7), 2398–2409.

(153) Baskin, J. M.; Prescher, J. A.; Laughlin, S. T.; Agard, N. J.; Chang, P. V; Miller, I. A.; Lo, A.; Codelli, J. A.; Bertozzi, C. R. *Proc. Natl. Acad. Sci. U. S. A.* **2007**, *104* (43), 16793–16797.

(154) Debets, M. F.; van Berkel, S. S.; Schoffelen, S.; Rutjes, F. P. J. T.; van Hest, J. C. M.; van Delft, F. L. *Chem. Commun. (Camb).* **2010**, *46* (1), 97–99.

(155) Jin, L.; Tolentino, D. R.; Melaimi, M.; Bertrand, G. *Sci. Adv.* **2015**, *1* (5), e1500304–e1500304.

(156) Yang, Y.; Zheng, Y.; Cao, W.; Titov, A.; Hyvonen, J.; Manders, J. R.; Xue, J.; Holloway, P. H.; Qian, L. *Nat. Photonics* **2015**, *9* (4), 259–266.

(157) Shirasaki, Y.; Supran, G. J.; Bawendi, M. G.; Bulović, V. *Nat. Photonics* **2013**, *7* (December 2012), 933–933.

(158) Bae, W. K.; Lim, J.; Zorn, M.; Kwak, J.; Park, Y.-S.; Lee, D.; Lee, S.; Char, K.; Zentel, R.; Lee, C. *J. Mater. Chem. C* **2014**, *2* (25), 4974.

(159) Borg, L. zur; Lee, D.; Lim, J.; Bae, W. K.; Park, M.; Lee, S.; Lee, C.; Char, K.; Zentel, R. *J. Mater. Chem. C* **2013**, *1* (9), 1722.

(160) Tao, Y.; Yang, C.; Qin, J. *Chem. Soc. Rev.* **2011**, *40* (5), 2943–2970.

(161) Yook, K. S.; Lee, J. Y. *Adv. Mater.* **2014**, *26* (25), 4218–4233.

(162) Gong, S.; Yang, C.; Qin, J. *Chem. Soc. Rev.* **2012**, *41* (14), 4797–4807.

(163) Bansal, A. K.; Sajjad, M. T.; Antolini, F.; Stroea, L.; Gečys, P.; Raciukaitis, G.; André, P.; Hirzer, A.; Schmidt, V.; Ortolani, L.; Toffanin, S.; Allard, S.; Scherf, U.; Samuel, I. D. W. *Nanoscale* **2015**, *7* (25), 11163–11172.

(164) Park, J. H.; Koh, T. W.; Chung, J.; Park, S. H.; Eo, M.; Do, Y.; Yoo, S.; Lee, M. H. *Macromolecules* **2013**, *46* (Iii), 674–682.

(165) Guo, Z.-S.; Zhao, L.; Pei, J.; Zhou, Z.-L.; Gibson, G.; Brug, J.; Lam, S.; Mao, S. S. *Macromolecules* **2010**, *43* (4), 1860–1866.

(166) Zhang, Q.; Chen, J.; Cheng, Y.; Wang, L.; Ma, D.; Jing, X.; Wang, F. *J. Mater. Chem.* **2004**, *14* (5), 895.

(167) Kwak, J.; Lyu, Y.-Y.; Lee, H.; Choi, B.; Char, K.; Lee, C. *J. Mater. Chem.* **2012**, *22* (13), 6351.

(168) Iraqi, A.; Pickup, D. F.; Yi, H. *Chem. Mater.* **2006**, *18* (4), 1007–1015.

(169) Kawamura, Y.; Yanagida, S.; Forrest, S. R. *J. Appl. Phys.* **2002**, *92* (1), 87.

(170) Mathias, F.; Tahir, M. N.; Tremel, W.; Zentel, R. *Macromol. Chem. Phys.* **2014**, *215* (7), 604–613.

(171) Fokina, A.; Lee, Y.; Chang, J. H.; Braun, L.; Bae, W. K.; Char, K.; Lee, C.; Zentel, R. *Polym. Chem.* **2016**, DOI: 10.1039/C5PY01492A.

(172) Tsai, M.-H.; Hong, Y.-H.; Chang, C.-H.; Su, H.-C.; Wu, C.-C.; Matoliukstyte, A.; Simokaitiene, J.; Grigalevicius, S.; Grazulevicius, J. V.; Hsu, C.-P. *Adv. Mater.* **2007**, *19* (6), 862–866.

(173) Roth, P. J.; Kim, K.-S.; Bae, S. H.; Sohn, B.-H.; Theato, P.; Zentel, R. *Macromol. Rapid Commun.* **2009**, *30* (14), 1274–1278.

(174) Lim, J.; Jeong, B. G.; Park, M.; Kim, J. K.; Pietryga, J. M.; Park, Y.-S.; Klimov, V. I.; Lee, C.; Lee, D. C.; Bae, W. K. *Adv. Mater.* **2014**, *26* (47), 8034–8040.

(175) Palui, G.; Avellini, T.; Zhan, N.; Pan, F.; Gray, D.; Alabugin, I.; Mattoussi, H. *J. Am. Chem. Soc.* **2012**, *134* (39), 16370–16378.

(176) Aldeek, F.; Hawkins, D.; Palomo, V.; Safi, M.; Palui, G.; Dawson, P. E.; Alabugin, I.; Mattoussi, H. *J. Am. Chem. Soc.* **2015**, 150211140421009.

(177) Fronk, S. L.; Mai, C.-K.; Ford, M.; Noland, R. P.; Bazan, G. C. *Macromolecules* **2015**, *48* (17), 6224–6232.

(178) Jeffries-El, M.; Sauvé, G.; McCullough, R. D. *Macromolecules* **2005**, *38* (25), 10346–10352.

(179) Kaplánek, R.; Bříza, T.; Havlík, M.; Martásek, P.; Král, V. *J. Fluor. Chem.* **2007**, *128* (3), 179–183.

(180) Weymiens, W.; Hartl, F.; Lutz, M.; Slootweg, J. C.; Ehlers, A. W.; Mulder, J. R.; Lammertsma, K. *European J. Org. Chem.* **2012**, *2012* (34), 6711–6721.

8 List of Abbreviations

A

A ampere

AFM atomic force microscopy

AIBN 2,2′-azobis(2-methylpropionitrile)

Al aluminum

ATRP atom-transfer radical polymerization

B

Boc tert-butyloxycarbonyl

C

CBP 4,4′-bis(N-carbazolyl)-1,1′-biphenyl

cd candela

CdS cadmium sulfide

CdSe cadmium selenide

cm centimeter

COSY correlation spectroscopy (NMR)

CRP controlled radical polymerization

CTA chain transfer agent

CTL charge transport layer

CuAAC copper-catalyzed azide-alkyne cycloaddition

CV cyclic voltammetry

D

DBCO dibenzocyclooctyl

DCC N,N′-dicyclohexylcarbodiimide

DCM dichloromethane

DHLA dihydrolipoic acid

DMAP 4-(dimethylamino)pyridine

DMF dimethylformamide

DMSO dimethyl sulfoxide

DOSY diffusion ordered spectroscopy

DSC differential scanning calorimetry

δ chemical shift (NMR)

E

EL electroluminescence

EOD electron only device

eq. equivalent

EQE external quantum efficiency

ESI electrospray ionization

et al. and others (Latin)

ETL electron transport layer

F

Fc ferrocene

FWHM full width at half maximum

G

GPC gel permeation chromatography

GRIM Grignard metatheses

H

HOBt 1-hydroxybenzotriazole hydrate

HOMO highest occupied molecular orbital

HRMS high resolution mass spectroscopy

HTL hole transport layer

HTM hole transport material

I

IR infrared

ITO indium tin oxide

J

J current

K

KI potassium iodide

L

LA lipoic acid

LED light emitting diode

LUMO lowest unoccupied molecular orbital

λ wavelength

M

m meter

MALDI matrix-assisted laser desorption ionization

mCP 1,3-bis(N-carbazolyl)benzene

MEH-PPV poly(2-methoxy-5-(2-ethylhexyloxy)-1,4-phenylenevinylene)

$MgSO_4$ magnesium sulfate

Mn number average molecular weight (GPC)

MoOx molybdenum oxide

MS mass spectroscopy

MWCO molecular weight cut-off

N

Na_2CO_3 sodium carbonate

NHS N-hydroxysuccinimide ester

NMP nitroxide-mediated polymerization

NMR nuclear magnetic resonance

O

OFET organic field effect transistor

OH hydroxy group

OLED organic light emitting diode

OPV organic photovoltaic

ORTEP Oak Ridge Thermal Ellipsoid Plot

P

P3HT poly(3-hexylthiophene)

PCBM 1-(3-(Methoxycarbonyl)propyl)-1-phenyl-[6.6]C61

PCDTBT Poly(N-9′-heptadecanyl-2,7-carbazole-alt-5,5-(4′,7′-di-2-thienyl-2′,1′,3′-benzothiadiazole))

$Pd(PPh_3)_4$ Tetrakis(triphenylphosphine) palladium(0)

PDI polydispersity

PL photoluminescence

ppm parts per million

PPV poly(1,4-phenylenevinylene)

PSar poly(N-methyl glycine

PVK poly(9-vinylcarbazole)

Q

QD quantum dot

QLED quantum dot-based light emitting diodes

R

RAFT reversible addition fragmentation chain transfer

RMS root-mean-squared

S

S siemens

SarNCA N-methyl glycine N-carboxyanhydride

SNU Seoul National University

SPAAC strain-promoted azide-alkyne cycloaddition

STEM: scanning transmission electron microscopy

T

TBAPF6 tetrabutylammonium hexafluorophosphate

TCTA tris(4-carbazoyl-9-ylphenyl)amine

TEM transmission electron microscopy

TFA trifluoroacetic acid

Tg glass transition temperature

TGA thermo-gravimetric analysis

THF tetrahydrofuran

TOF time of flight

U

UPS ultraviolet photoelectron spectroscopy

UV ultraviolet

V

V voltage, volt

vs. versus

W

wt% weight percent

Z

ZnO zink oxide

9 Appendix. ^{1}H NMR Spectra

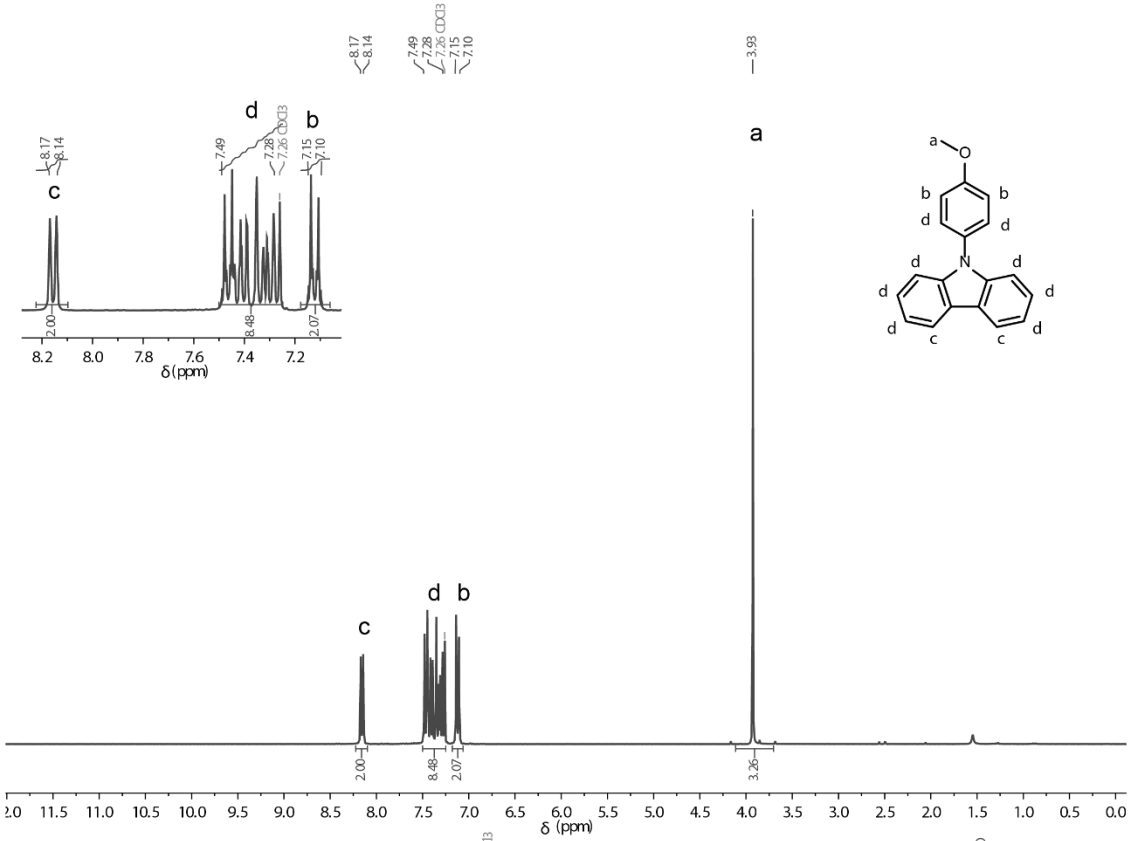

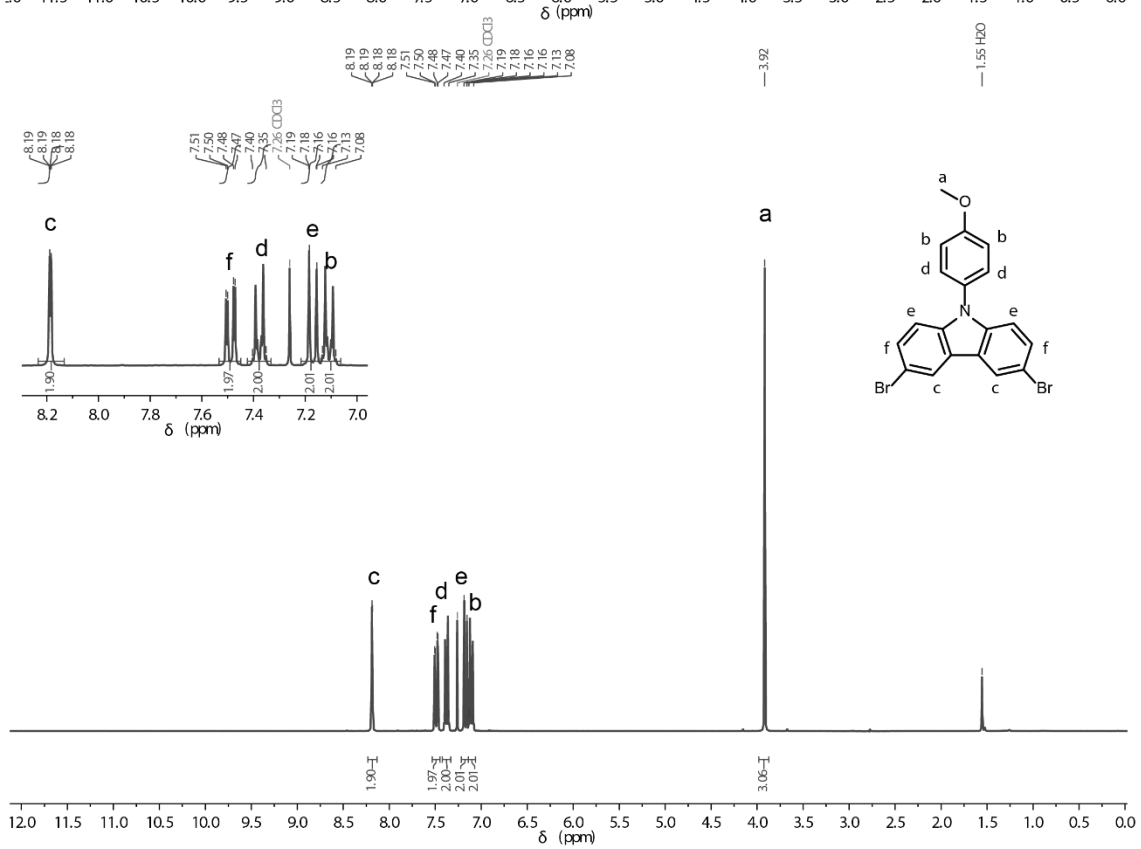

*Figure A 1. ^{1}H NMR spectra of compound **1** (top) and compound **2** (bottom).*

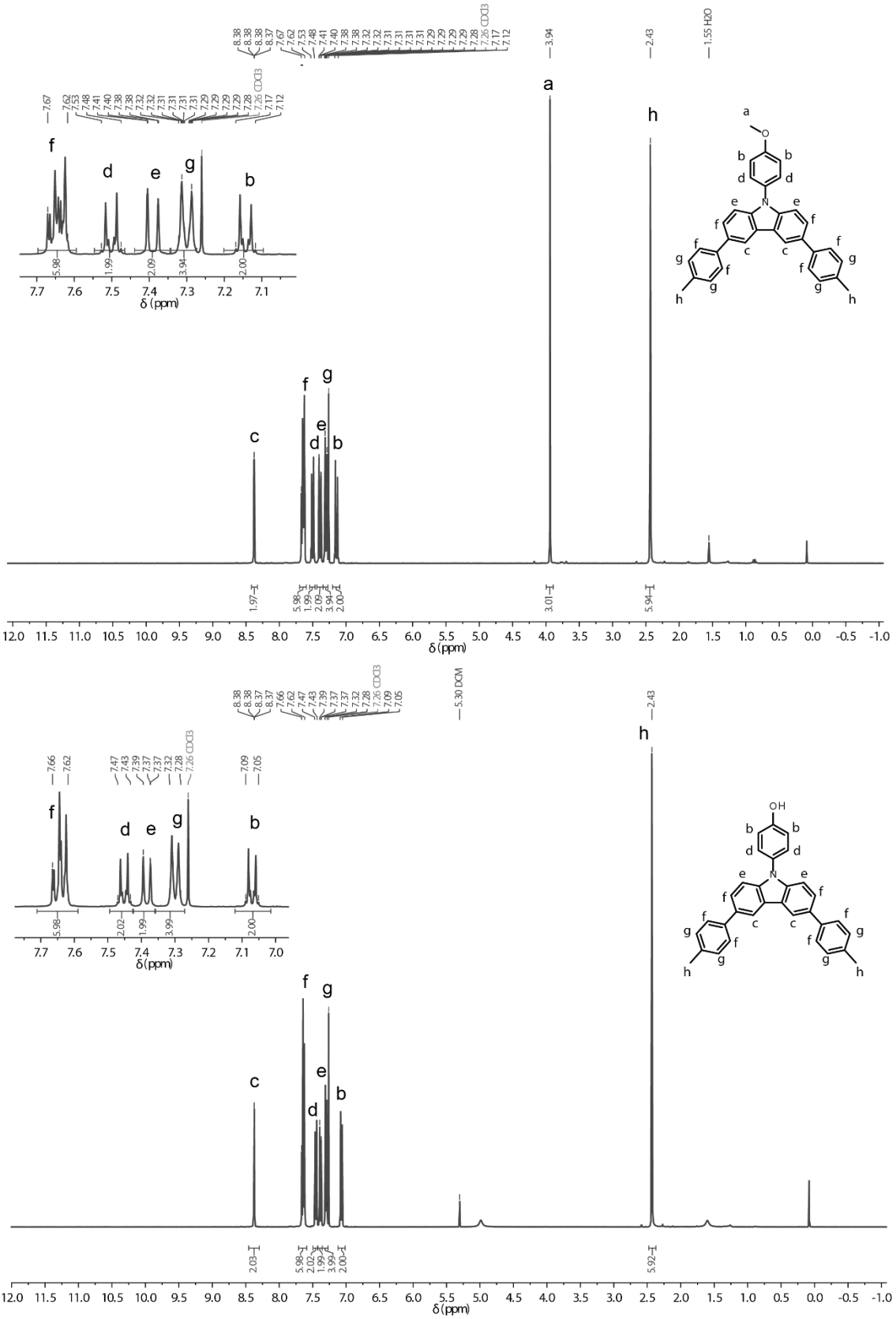

*Figure A 2. [1]H NMR spectra of compound **3** (top) and compound **4** (bottom).*

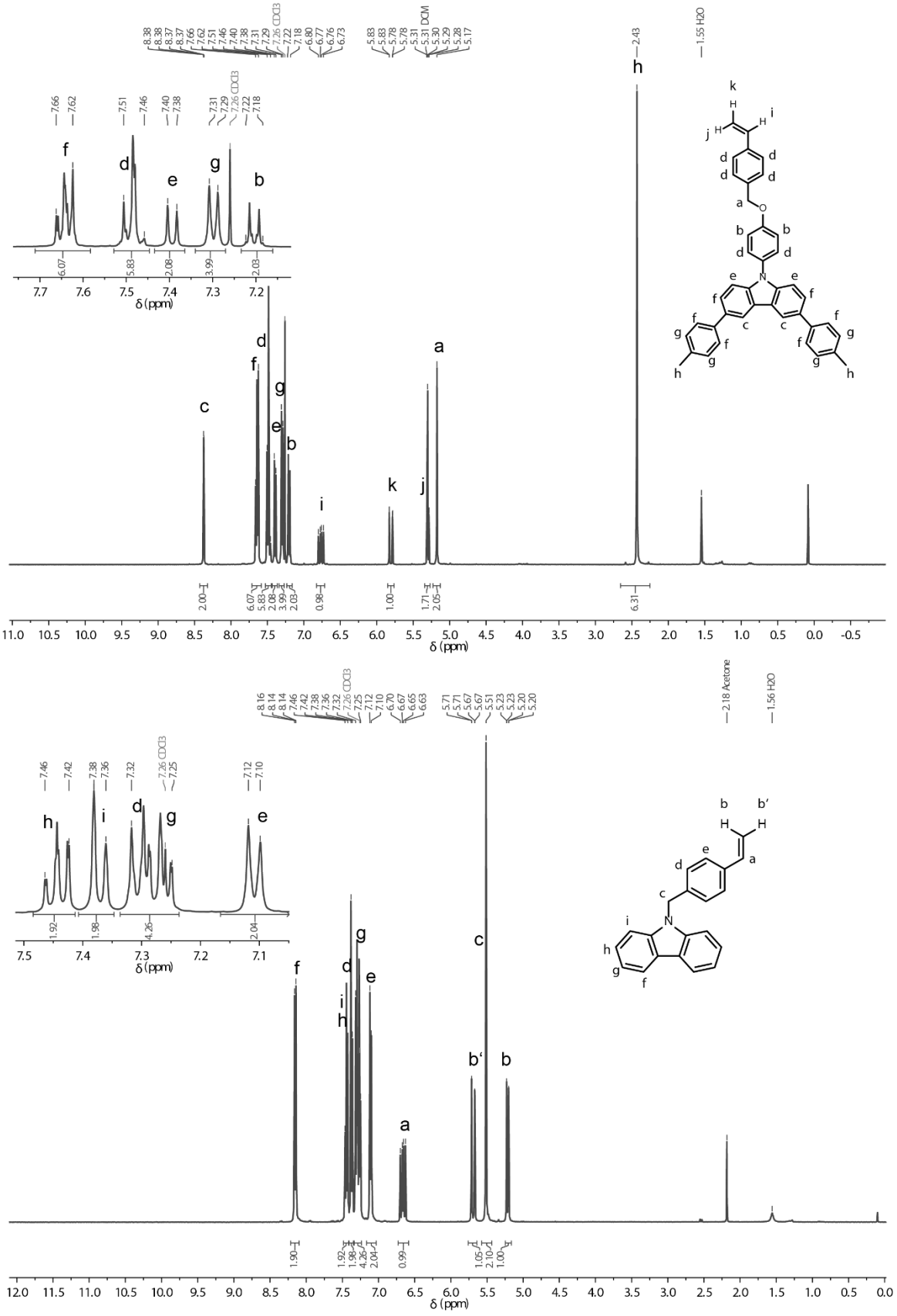

*Figure A 3. [1]H NMR spectra of monomer **M1** (top) and monomer **M2** (bottom).*

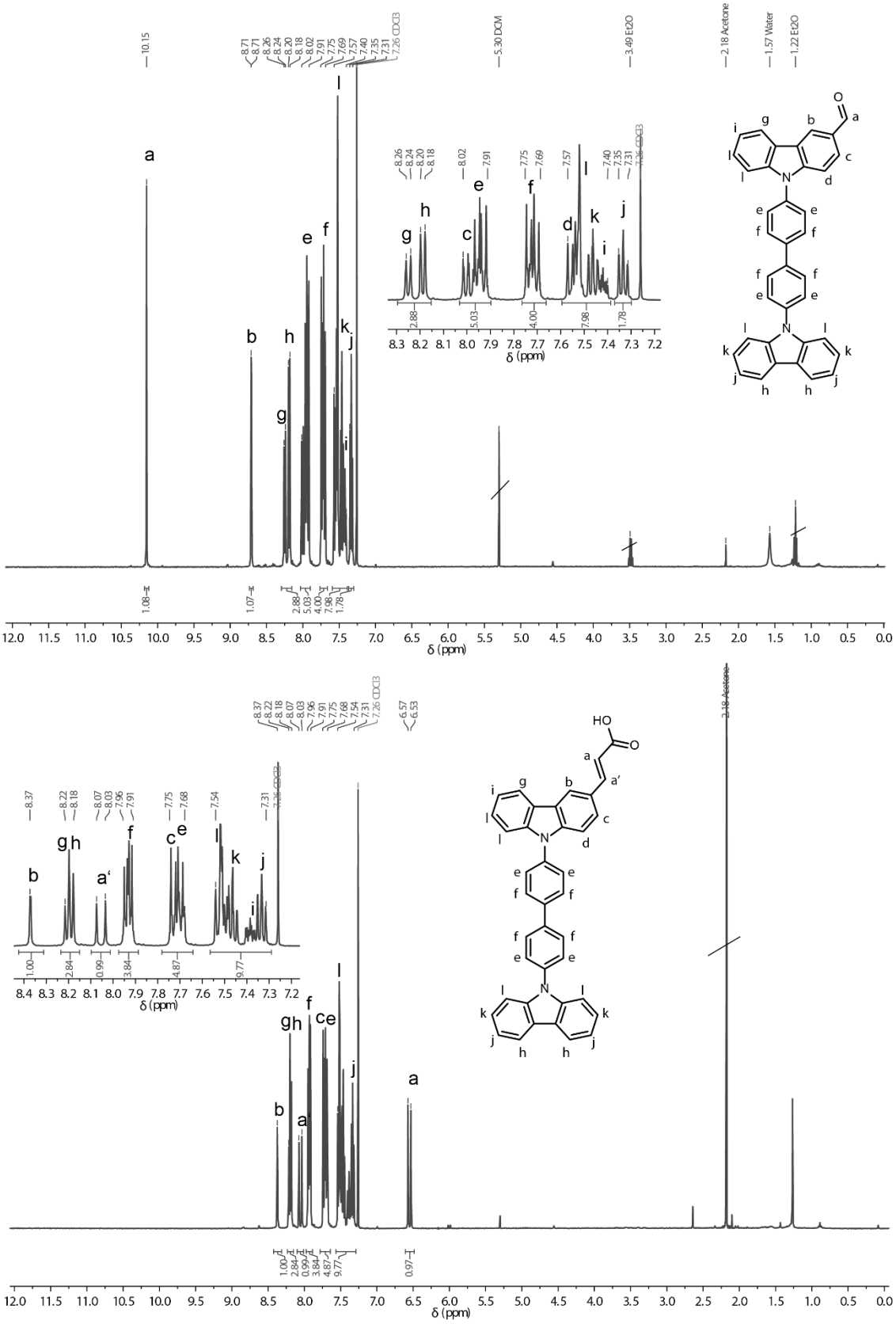

*Figure A 4. ^{1}H NMR spectra of compound **7** (top) and compound **8** (bottom).*

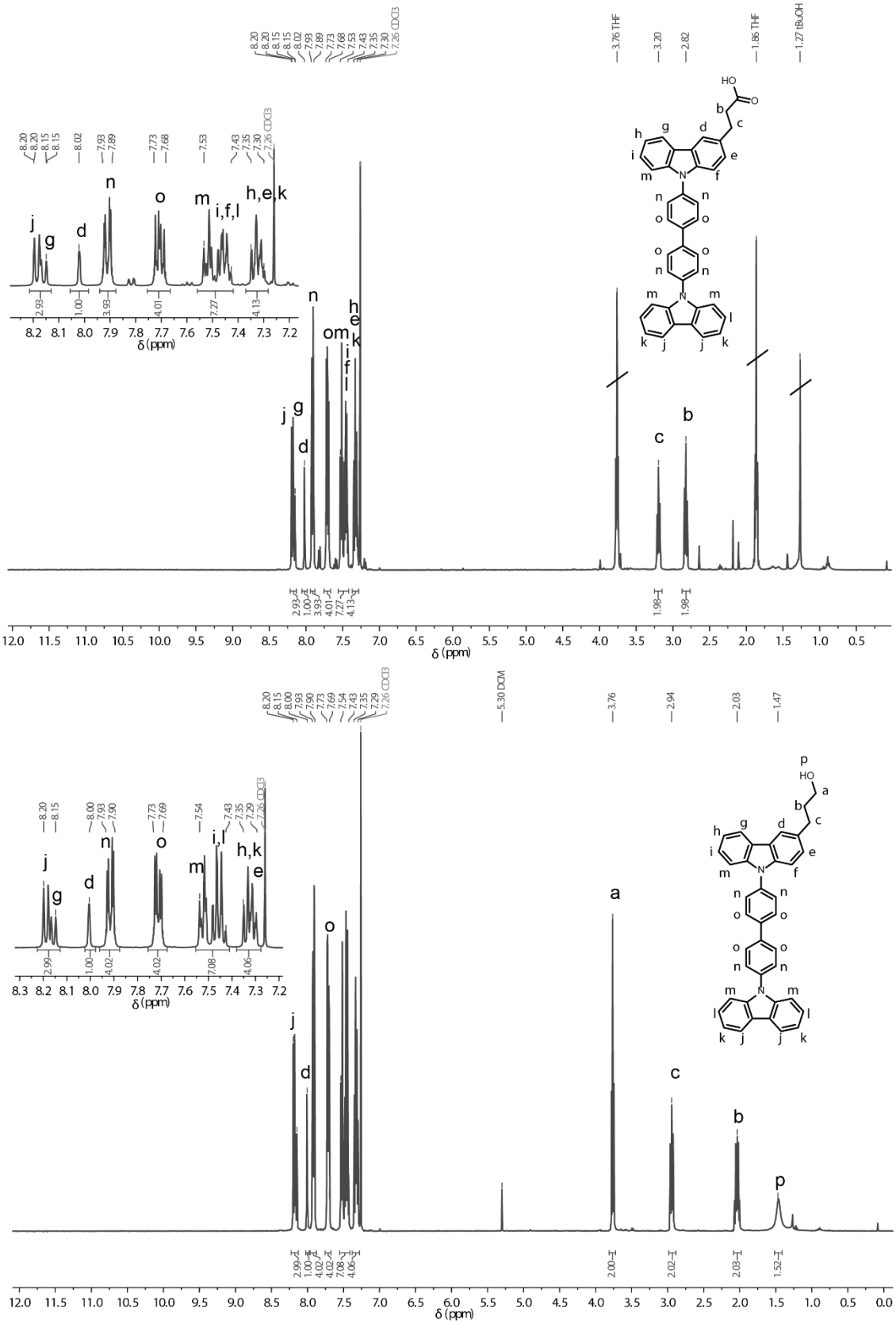

*Figure A 5. [1]H NMR spectra of compound **9** (top) and compound **10** (bottom).*

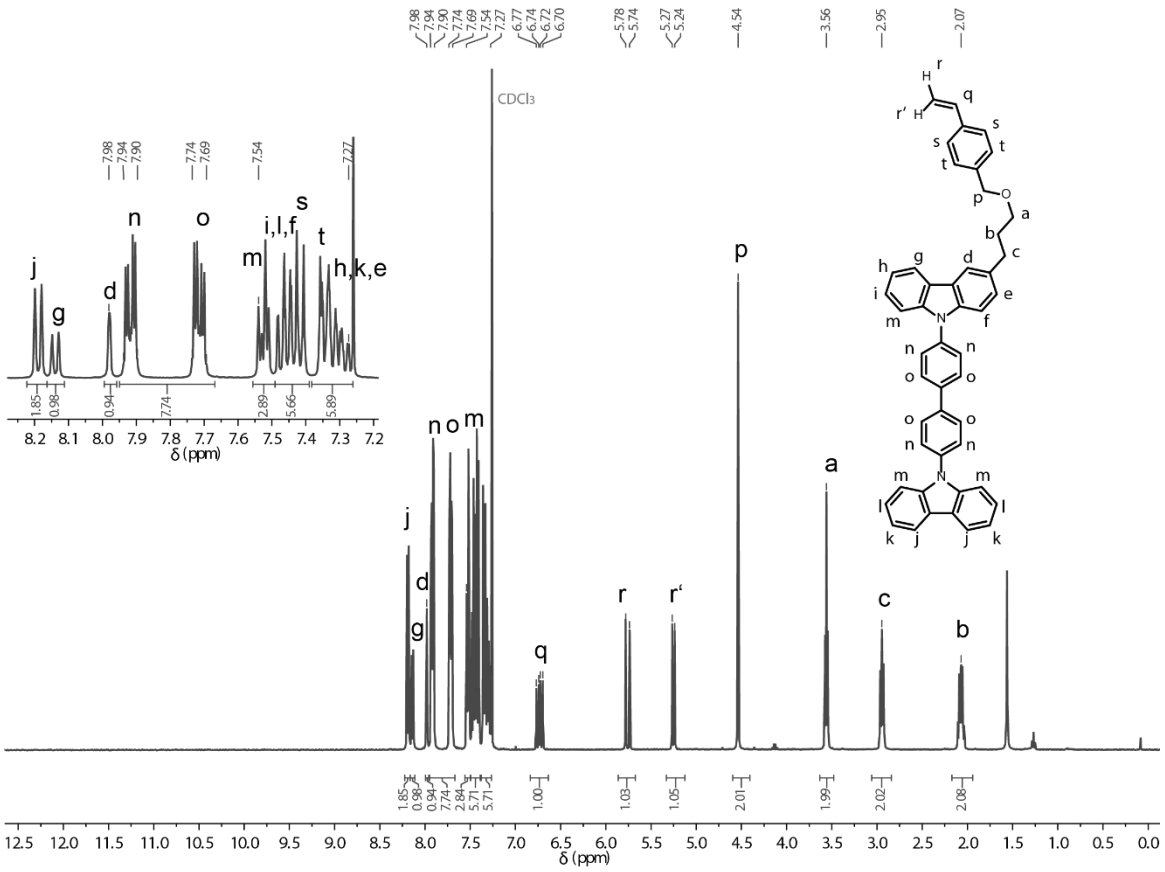

*Figure A 6. [1]H NMR spectrum of monomer **M3**.*

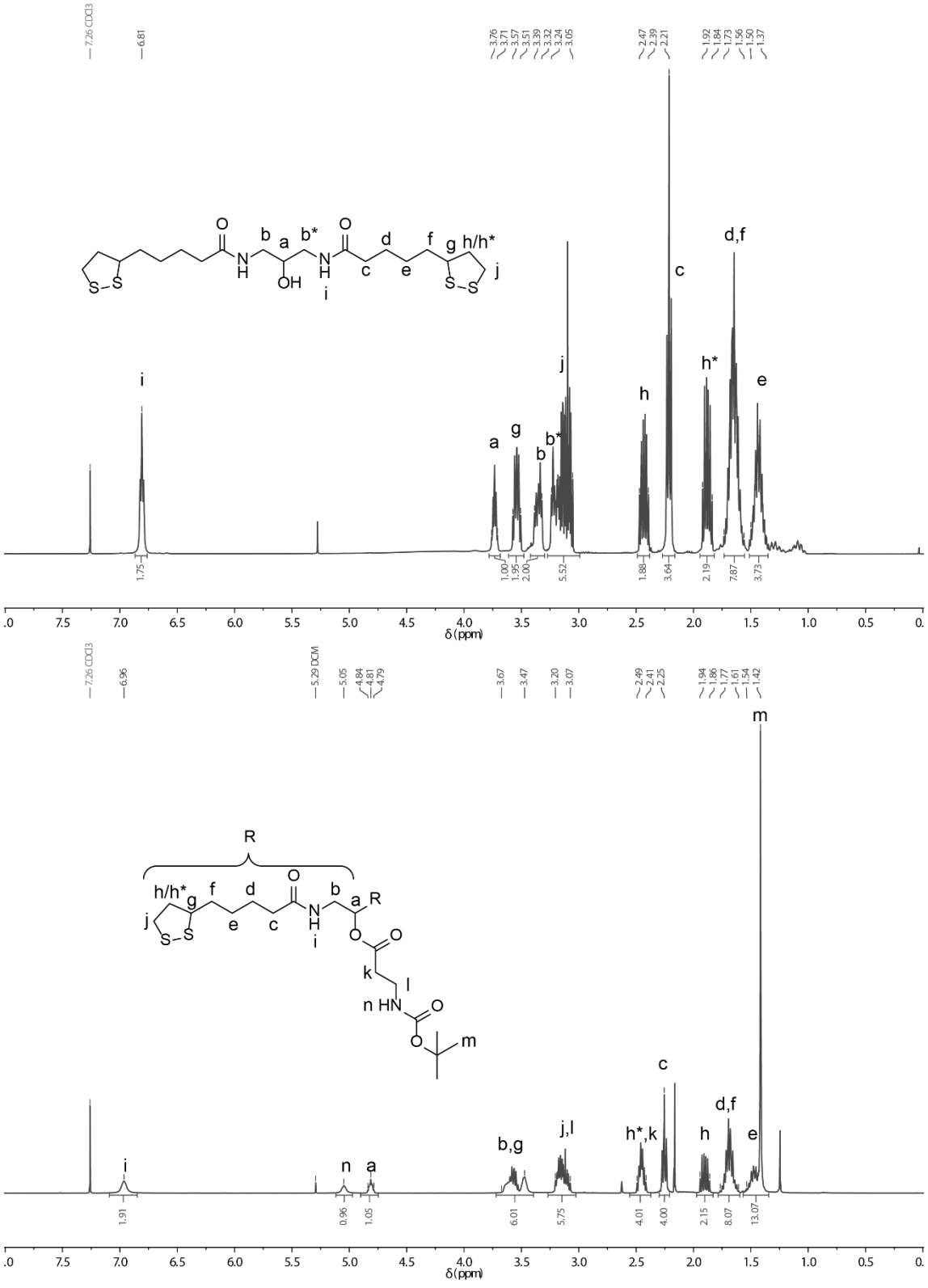

*Figure A 7. [1]H NMR spectra of compound **11** (top) and compound **12** (bottom).*

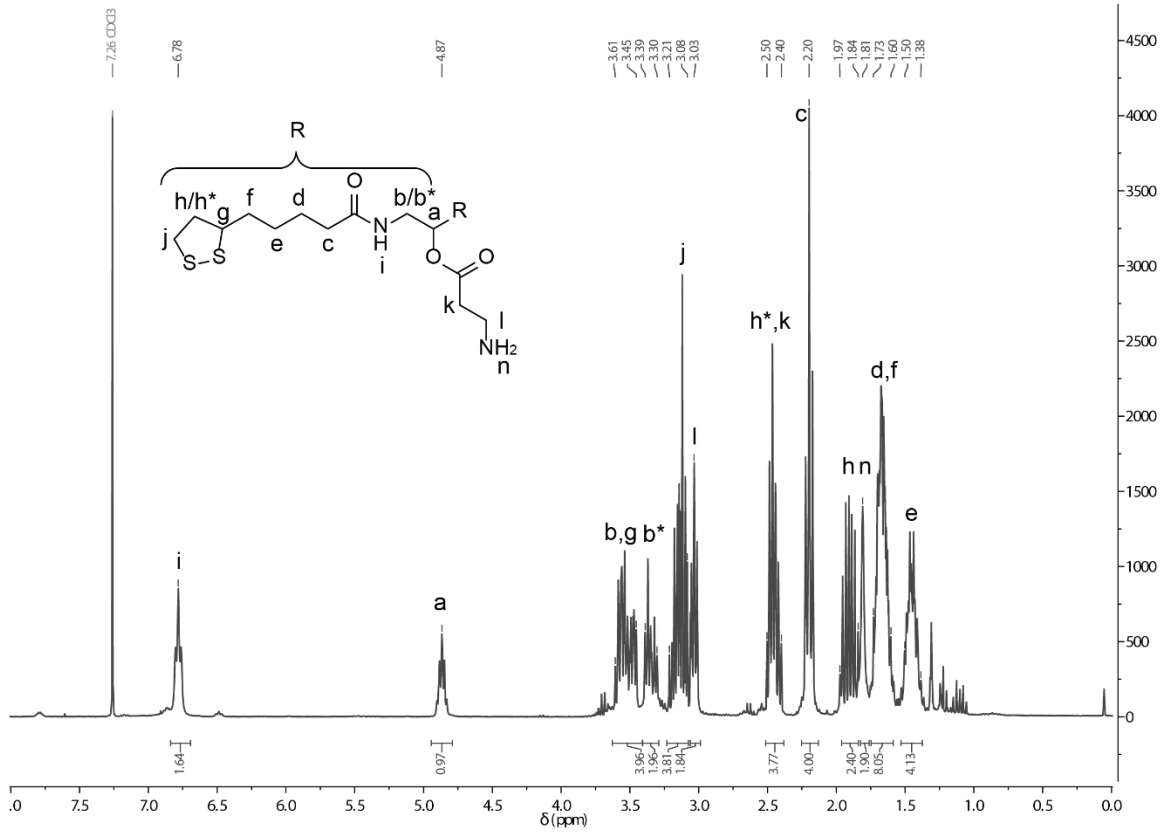

Figure A 8. ^{1}H NMR spectra of anchor compound ***DL-NH₂.***

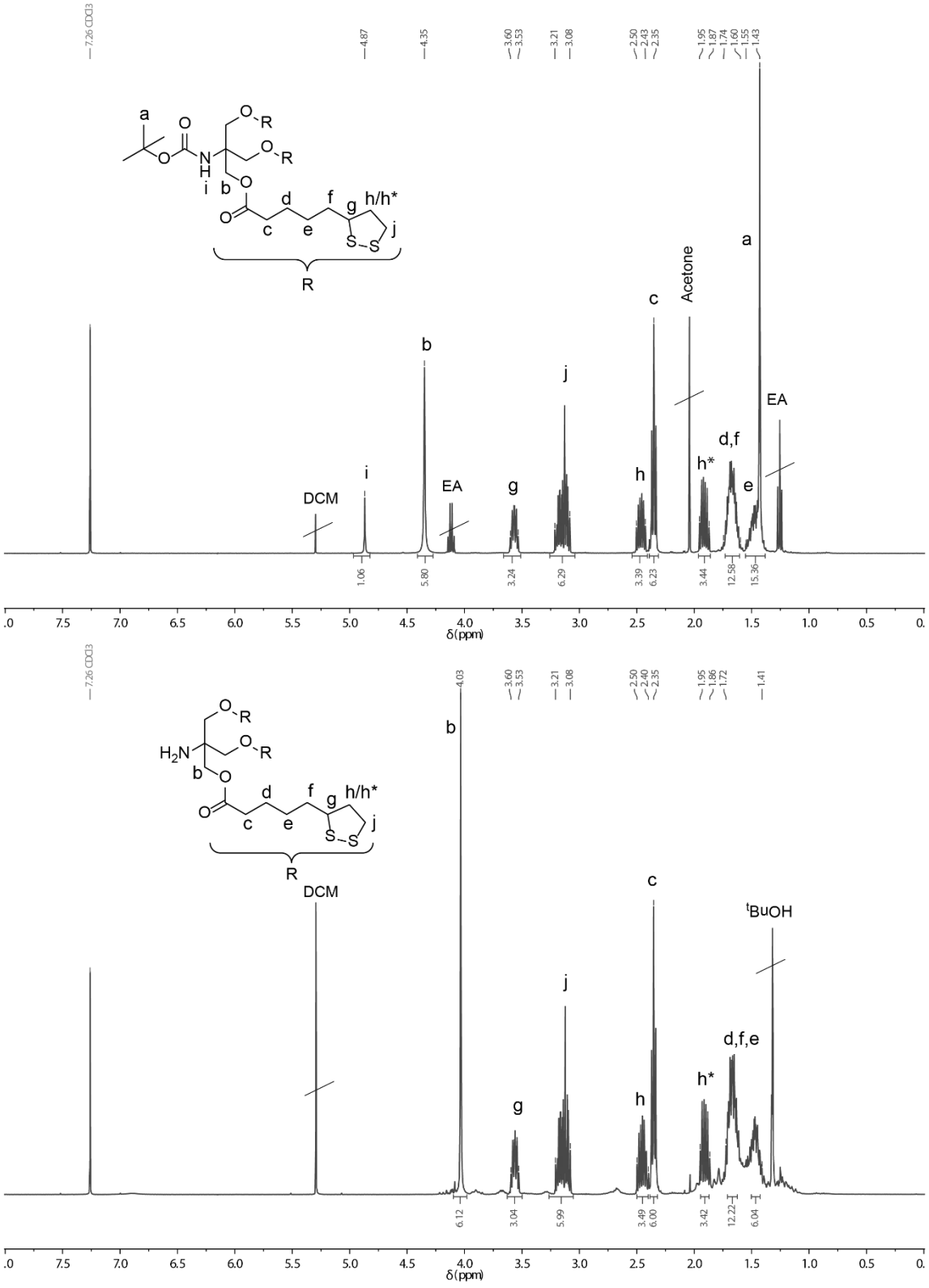

*Figure A 9. [1]H NMR spectra of compound **14** (top) and compound **15** (bottom).*

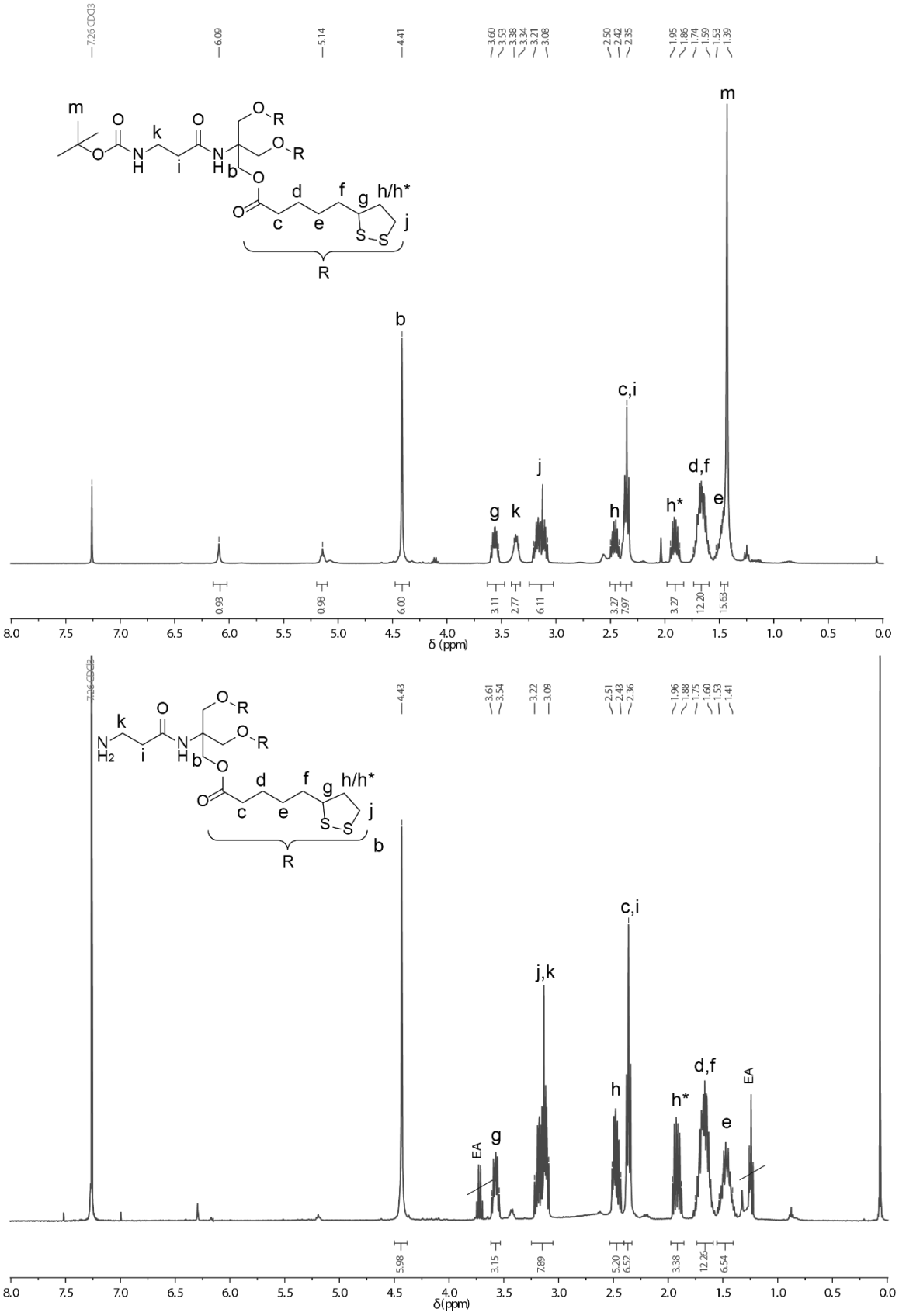

*Figure A 10. [1]H NMR spectra of compound **16** (top) and anchor compound **TL-NH₂** (bottom).*

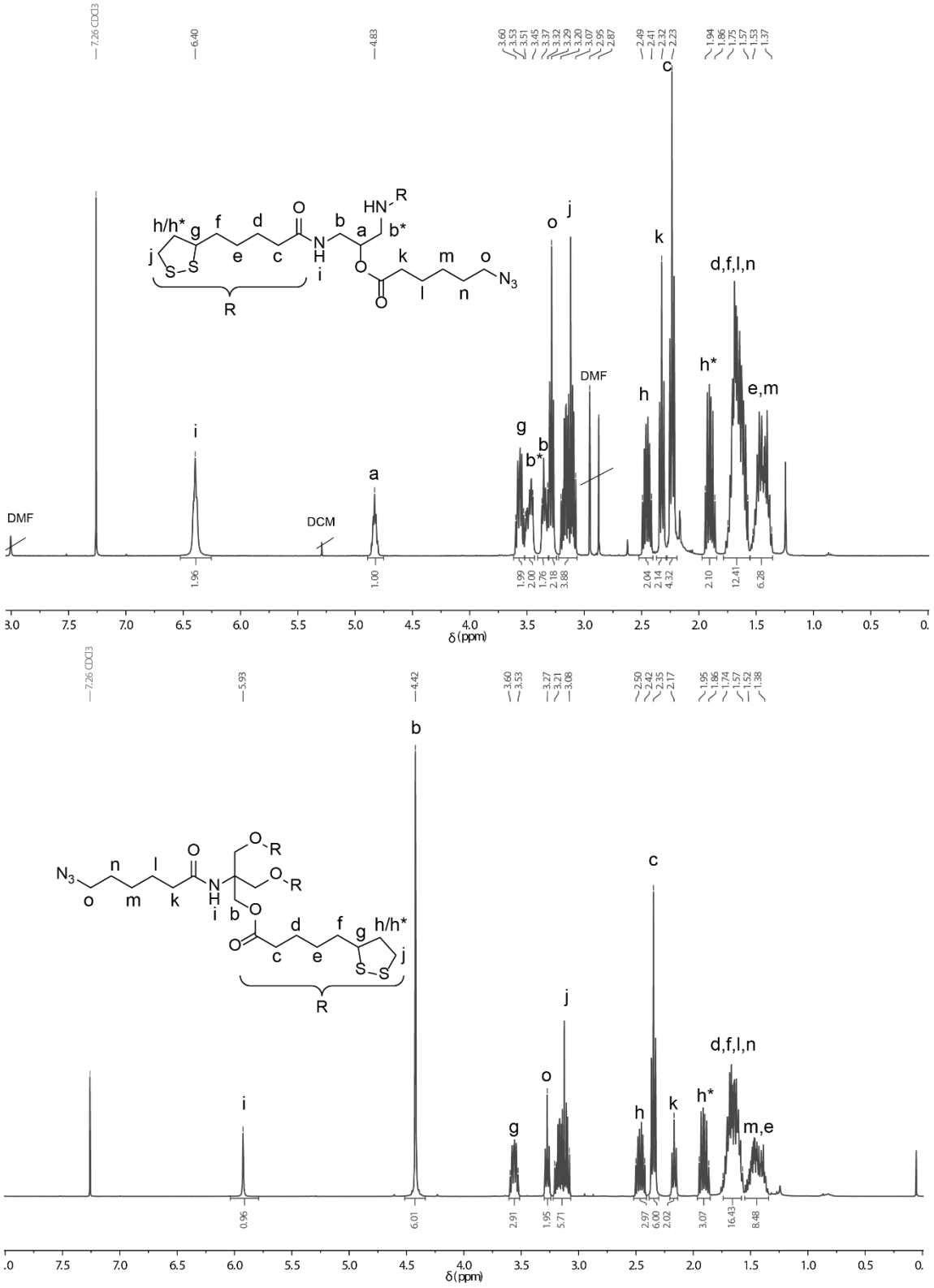

Figure A 11. [1]H NMR spectra of anchor compound ***DL-N₃*** *(top) and anchor compound* ***TL-N₃*** *(bottom) in* $CDCl_3$.

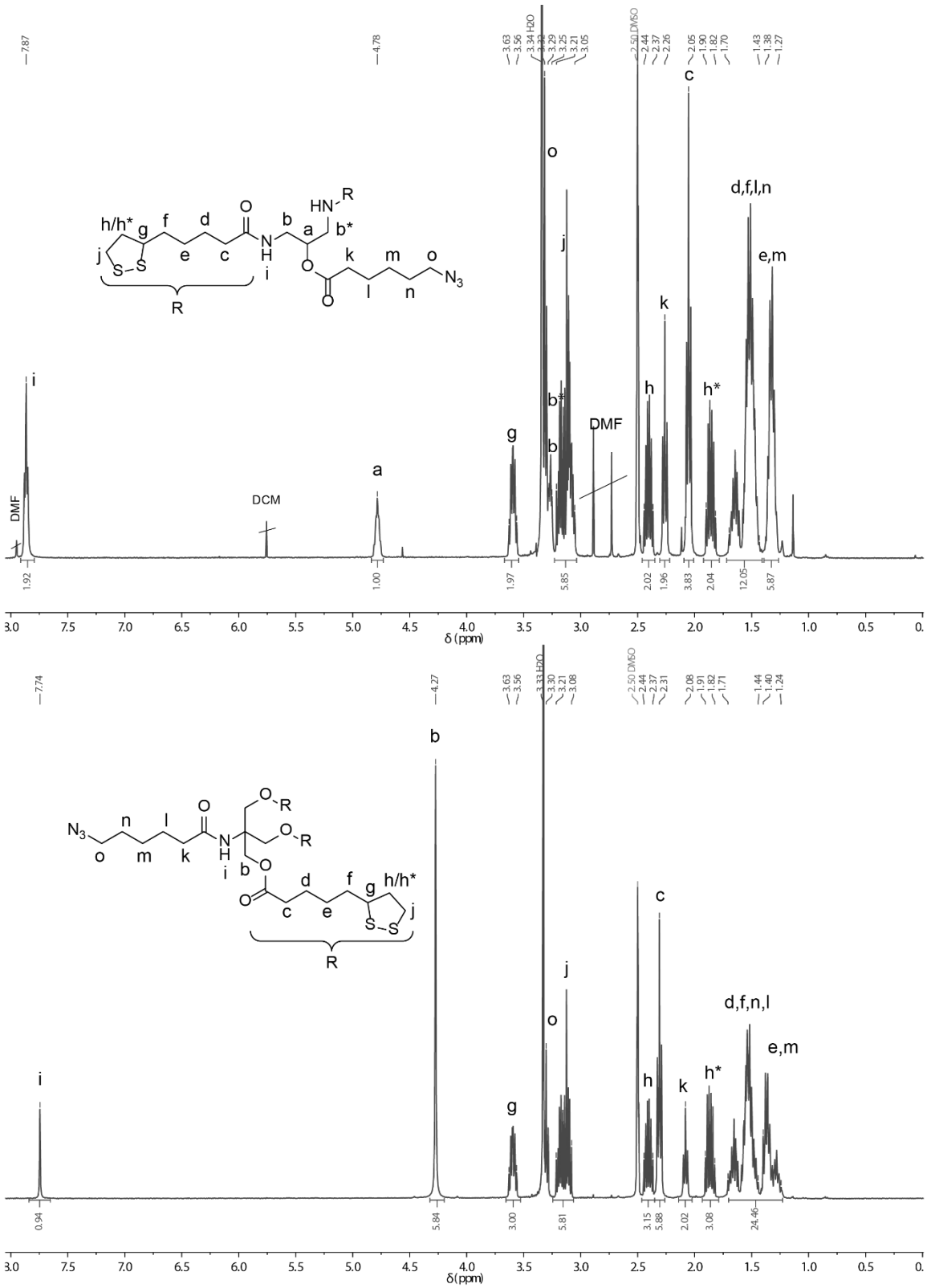

*Figure A 12. ^{1}H NMR spectra of anchor compound **DL-N_3** (top) and anchor compound **TL-N_3** (bottom) in DMSO-d_6.*